A PROACTIVE SAFETY ENHANCEMENT METHODOLOGY FOR GENERAL AVIATION USING A SYNTHESIS OF AIRCRAFT PERFORMANCE MODELS AND FLIGHT DATA ANALYSIS

A Dissertation
Presented to
The Academic Faculty

By

Sanggyu Min

In Partial Fulfillment
of the Requirements for the Degree
Doctor of Philosophy in the
School of Aerospace Engineering

Georgia Institute of Technology

December 2018

A PROACTIVE SAFETY ENHANCEMENT METHODOLOGY FOR GENERAL AVIATION USING A SYNTHESIS OF AIRCRAFT PERFORMANCE MODELS AND FLIGHT DATA ANALYSIS

Approved by:

Dr. Dimitri Mavris, Advisor
School of Aerospace Engineering
Georgia Institute of Technology

Dr. Daniel Schrage
School of Aerospace Engineering
Georgia Institute of Technology

Dr. Simon Briceno
School of Aerospace Engineering
Georgia Institute of Technology

Dr. Karen Marais
School of Aeronautics and Astronautics
Purdue University

Dr. Angela Campbell
Aviation Research Division
Federal Aviation Administration

Date Approved: October 31st, 2018

This dissertation is dedicated to my family.

ACKNOWLEDGEMENTS

At the end of my long journey through graduate programs, I would like to thank many people who supported me during this journey. My sincere gratitude goes first to Professor Dimitri Mavris who provided me with many valuable opportunities and expertly guided me through my research. Without his support and guidance, this accomplishment could not have been achieved. I also would like to express my appreciation to the committee members, Professor Daniel Schrage, Dr. Simon Briceno, Professor Karen Marais, and Dr. Angela Campbell. Their invaluable advice and direction on my research have enriched my knowledge and made my research more meaningful. Thank you all again for sharing your valuable time with me and steering my way to the right direction.

It is a pleasure acknowledging my gratitude to my friends and colleagues who made the long graduate school life become a great asset of my life. Among various great opportunities that I have had in the Aerospace Systems Design Laboratory, I was greatly honored to be a member of the amazing SAGA team. The late Hernando Jimenez, Imon Chakraborty, Evan Harrison, and Tejas Puranik have inspired me with innovative idea throughout the project. Thank you for being great co-workers and friends. Also, I was able to have memorable experiences in the graduate school because of many other friends. I cannot mention all their names here, but I sincerely appreciate all the current and the former members of the Korean-aerospace community at Georgia Tech, the FAA fellowship buddies, and other close companions who made my graduate life happier. In addition, I would like to thank the flight safety team at Delta Air Lines for understanding and supporting me at the final stage of my Ph.D. journey.

My acknowledgement would be incomplete without thanking the biggest source of my strength, my family. My achievements would not be possible without the support and love of my wife, Myoungmo An. I also would like to thank my little kids, Soyee, Ehan, and Jeyee, who have brought me the biggest happiness in my life. The blessings of my parents

and parents in law, the love and care of my sister and her husband, the encouragement from my brother-in-law and his wife, and the joys from my lovely nephews all made a tremendous contribution in helping me reach this accomplishment. This would not have been possible without their unwavering and endless love and prayers for me at all times. I thank you and love you all with all my heart.

Lastly but most importantly, I thank the Lord for all the blessings and I give all the glory to Him.

"So whether you eat or drink or whatever you do, do it all for the glory of God"

1 Corinthians 10:31

TABLE OF CONTENTS

LIST OF TABLES

LIST OF FIGURES

NOMENCLATURE

AGL	Above Ground Level
ALAR	Approach and Landing Accident Reduction
AOA	Angle of attack
AOPA	Aircraft Owners and Pilots Association
ASAP	Aviation Safety Action Program
ASIAS	Aviation Safety Information Analysis and Sharing
CAST	Commercial Aviation Safety Team
CFD	Computational Fluid Dynamics
CFIT	Controlled Flight Into Terrain
CLASS	Cumulative Landing and Approach Safety Score
DFT	Discrete Fourier Transform
EMD	Empirical Mode Decomposition
ESDU	Engineering Sciences Data Unit
FAA	Federal Aviation Administration
FDA	Flight Data Analysis
FDM	Flight Data Monitoring
FDR	Flight Data Recorder
FEV	Filtering Effectiveness Value
FFT	Fast Fourier Transform
FGFS	Flight Gear Flight Simulator
FOQA	Flight Operational Quality Assurance
FSF	Flight Safety Foundation

GA	General Aviation
GA-ASI	General Aviation Air Safety Investigator
GAARD	General Aviation Airborne Recording Device
GAJSC	General Aviation Joint Steering Committee
GAMA	General Aviation Manufacturers Association
GPS	Global Positioning System
HADaR	Hybrid Approach for Data-noise Reduction
ICAO	International Civil Aviation Organization
KCAS	Knots Calibrated Air Speed
KEAS	Knots Equivalent Air Speed
KIAS	Knots Indicated Air Speed
KTAS	Knots True Air Speed
LOC	Loss of Control
MSL	Mean Sea Level
NASA	National Aeronautics and Space Administration
NTSB	National Transportation Safety Board
PEGASAS	Partnership to Enhance General Aviation Safety, Accessibility and Sustainability
POH	Pilot's Operating Handbook
QMS	Quality Management System
RMSE	Root-Mean-Square Error
SD	Standard Deviation
SI	System Identificatoin
SMS	Safety Management Systems
SNR	Signal to Noise Ratio
SNRdB	Signal to Noise Ratio in Decibel
SOP	Standard Operating Procedure

TBA	The Bootstrap Approach
USDOT	The United Sates Department of Transportation
VSO	Stall Speed with Landing Configuration, that is flaps out and landing gear down
$(\alpha_{C_{Lmax}})_A$	Angle of attack for maximum lift coefficient for aircraft
$(\alpha_{C_{Lmax}})_W$	Angle of attack for maximum lift coefficient for 3-D wing
$(C_{l_\alpha})_{theory}$	Theoretical airfoil section lift-curve slope
$(C_{L_{\alpha_A}})_\delta$	Lift-curve slope change for aircraft due to flap deflection
$(C_{L_{\alpha_W}})_\delta$	Lift-curve slope change for wing due to flap deflection
$(C_{l_\alpha})_\delta$	Lift-curve slope change for airfoil due to flap deflection
$(d\varepsilon/d\alpha)_\delta$	Flaps-down downwash gradient
α	Angle-of-attack
α^*	Angle of attack linearity limit for 2-D airfoil
α_A^*	Angle of attack linearity limit for 3-D aircraft
α_{0L_A}	Zero lift angle of attack 3-D aircraft
α_{0L_W}	Zero lift angle of attack for 3-D Wing
α_{0l}	Zero lift angle of attack for 2-D Airfoil
α_0	Angle of attack at zero lift
$\alpha_{\delta_{C_L}}$	3-D flap-effectiveness parameter
α_δ	Airfoil lift effectiveness parameter
$\alpha_{C_{l_{max}}}$	Angle of attack for maximum lift coefficient for 2-D airfoil
α_i	Angle of attack for design lift coefficient
β	Prandtl-Glauert compressibility correction factor
$\Delta\varepsilon_f$	Tail downwash angle increment due to flap deflection
$\Delta C_{D_{flap}}$	Drag change due to flap
$\Delta C_{D_{int}}$	Interference drag change due to flap
ΔC_{D_i}	Induced drag change due to flap

ΔC_{D_p}	Parasite drag change due to flap
$\Delta C_{L_{flap}}$	Lift coefficient increment due to flap
$\Delta\alpha_{stall}$	Angle of attack increment factor
$\Delta\alpha_{W/C}$	Difference between angles of attack for a carnard stall and a wing stall
δ_{C_l}	2-D flap-effectiveness parameter
δ_f	Flap deflection angle
$\dot{V}_{abs}$	Absolut acceleration
η_h	Ratio of horizontal tail to wing dynamic pressure
γ	Path angle
γ_{bg}	Best glide angle
κ	Ratio of 2-D lift-curve slope to 2π
$\Lambda_{C/2}$	Sweepback of wing mid-chord
μ	Mean
Φ	Atmospheric power or torque lapse factor
ϕ_w	Roll in the wind frame
ψ	Yaw angle
ρ	Air density
ρ_0	Standard MSL air density
σ	Standard Deviation
σ_{air}	Relative air density
θ	Pitch angle
θ_w	Pitch in the wind frame
ε_{0_h}	Horizontal tail downwash angle
ε_t	Wing twist angle
AR	Aspect ratio
b	Propeller polar intercept
c	Airfoil chord length

$c^{'}$	Flapped airfoil chord length
C_{D_0}	Parasite drag coefficient
$C_{D_{L\&P}}$	Leakage and protuberance drag coefficient
$C_{D_{min}}$	Parasite drag coefficient
$C_{D_{misc}}$	Miscellaneous components drag coefficient
C_D	Drag coefficient for aircraft
C_{f_e}	Equivalent skin friction coefficient
C_f	Flat-plate skin-friction drag coefficient
$C_{L_{0_A}}$	Zero angle of attack lift coefficient for aircraft
$C_{L_{0_{Wf}}}$	Wing-fuselage zero angle of attack lift coefficient
$C_{L_{\alpha_A}}$	Lift-curve slope for aircraft
$C_{L_{\alpha_h}}$	Horizontal tail lift-curve slope
$C_{L_{\alpha_{Wf}}}$	Wing-fuselage lift-curve slope
$C_{L_{\alpha_W}}$	Lift-curve slope for 3-D wing
C_{l_α}	Lift-curve slope for 2-D airfoil
$C_{L_{BG}}$	Lift coefficient for best glide
C_{l_i}	Design lift coefficient
$C_{L_{max_A}}$	Maximum lift coefficient for aircraft
$C_{L_{max_W}}$	Maximum lift coefficient for 3-D wing
$C_{l_{max}}$	Maximum lift coefficient for 2-D airfoil
C_L	Lift coefficient for aircraft
C_P	Power coefficient
C_T	Thrust coefficient
D	Drag
d	Propller diameter
$d\eta/d\alpha$	Downwash gradient at the horizontal tail
e	Oswald efficiency factor

F	Fuselage lift factor
FF	Form factor
g	Gravity acceleration
$GndSpd$	Ground speed
h	Height
i_h	Horizontal tail incidence angle
i_W	Wing incidence angle
J	Advance ratio
K	Induced drag factor
k	Ratio of 2D lift-curve slope to 2
k_Δ	Planform correction factor
k_b	Flap-span factor
K_{int}	Flap interference factor
k_{wh}	Wing-on-horizontal-tail interference factor
KE	Kinetic Energy
L	Lift
L/D_{max}	Maximum lift to drag ratio
M	Touque
m	Propeller polar slope
M_0	Rated MSL touque
n	Propeller revolutions per second
n_0	Rated maximum propeller revolutions per second
P	Power
P_0	Rated MSL power
PE	Potential Energy
Q	Component interference factor
q	Pitch rate

q_w	Pitch rate in the wind frame
S	Reference wing area
S_c	Leading edge suction weighting factor
S_h	Horizontal tail area
S_{W_f}	Flapped wing area
S_{wet}	Aircraft total wetted area
STE	Specific Total Energy
T	Thrust
TE	Total Energy Height
TER	Total Energy Height Rate
V	Speed
V_{abs}	Absolute velocity
V_{bg}	Speed for best glide
V_M	Speed for maximum level flight
V_{spdG}	Vertical speed (GPS)
V_x	Speed for largest climb angle
V_y	Speed for best rate of climb
W	Aircraft weight

SUMMARY

As general aviation (GA) industry and its operations have grown along with the aviation industry development, improving aircraft safety has been a key interest in the GA industry. According to the U.S. Department of Transportation, GA in the U.S. has been suffering higher fatal accident rate compared to that of scheduled airline flights. This statistic indicates that safety enhancement effort is inevitable and reduction of GA aircraft fatality rate needs to be a prioritized goal in the GA community.

The increasing pervasiveness of data-driven-safety programs such as flight data monitoring (FDM) in commercial aviation has permeated GA, giving rise to a growing body of quantitative safety analysis opportunities. FDM and other data-driven programs such as flight operations quality assurance (FOQA) feature a retrospective analysis of flight data records that identify potential safety-critical phenomena and the formulation and implementation of corrective actions. Thus, quantitative aircraft performance modeling emerges as a critical enabler for safety analysis, particularly when coupled with flight data records that produce a rich and meaningful picture of operational safety.

However, the intended application of the operational safety analysis imposes essential requirements on GA aircraft models and flight data records to be used by safety analysts. First, models must provide predictive capabilities with high flexibility and accuracy over the wide range of operational conditions. Also, to maximize the benefits of data-driven safety analysis, securing tidy data that is ready to be analyzed is as important as the ongoing collection and analysis of flight data records. Thus, the objective of this study is to develop a proactive operational safety analysis method by introducing a realistic and accurate performance modeling method and an efficient data noise removal technique for a fixed-wing GA aircraft. This fundamental goal leads to the following sub-goals. First, this research aims to develop a realistic and accurate aerodynamic performance model that is computationally affordable and compositionally flexible so that this modeling method can

be utilized by any GA aircraft users capturing the characteristics of each aircraft. Also, this study proposes an effective noise removal technique for the purpose of obtaining clean and credible flight information for the operational safety assessment process. Finally, using the developed reliable aerodynamic performance model and filtered clean flight data, this work suggests an idea of evaluating flight performance safety of a GA fixed-wing aircraft using flexible standard performance envelopes and a quantitative safety assessment metric.

For achieving the first research goal, this study suggests a data-driven aerodynamic modeling methodology for a GA fixed-wing aircraft. As the first step for developing an accurate aerodynamic model, this study introduces an improved theoretical modeling approach that evaluates, compares, and combines all the possible theoretical performance modeling methods. Based on the developed theoretical model, this study enhances the accuracy of the aerodynamic model by fitting the model curves to the actual flight data which is collected from a test flight. The necessary accuracy of the aerodynamic model can be satisfied when the model is able to estimate the flap activity during flight. The developed aerodynamic model in this study can be used to indicate the aircraft's proximity to stall which is one of the unsafe aerodynamic events.

The second goal of this study is to develop a methodology that can effectively remove data noise and improve the quality of the flight data records. As the role of flight data in aviation safety enhancement programs becomes increasingly important, this study ensures clean flight data. This study introduces the HADaR (Hybrid Approach for Data-noise Reduction) method that examines various data noise filtering techniques in both time and frequency domains to suggest an affordable and effective data cleaning process while preserving true aircraft behavior. The HADaR method identifies and categorizes important data parameters considering the measuring methods. In this method, three data noise filtering techniques in the time domain, and two data noise filtering techniques in the frequency domain are utilized with two different levels of filtering intensity factors for each technique. Based on the selected parameters and data noise filtering techniques, this method

investigates the filtering effect of each combination then selects the most effective data noise filtering method. The developed HADaR method can improve the credibility of the data-driven analysis result of further flight data analysis.

Lastly, this research suggests a flight safety assessment procedure that utilizes flexible standard performance envelopes and a quantitative safety assessment metric for the safety evaluation. This research suggests a statistical approach of defining flexible performance envelopes by observing normal operations in a large number of flight data records. Also, this study introduces a quantitative safety evaluation metric, the Cumulative Landing and Approach Safety Score (CLASS), to measure the abnormality of the data parameters of the flight. Finally, this study demonstrates a safety quantification process using the developed performance envelope and the CLASS metric.

In summary, this study reveals that the suggested data-driven aerodynamic modeling method and the HADaR method are capable of providing more credible information toward the GA safety assessment work. For the aviation safety enhancement efforts to be more successful, precise aircraft performance models and clean flight data have to be appropriately obtained and utilized. Furthermore, a proper data noise filtering method that is specific to GA flight data and an appropriate data collection procedure is required for improving the reliability of data-driven safety analysis programs. Finally, this study harmonizes the accurate performance model and the noise-filtered flight data to satisfy the requirements of the GA safety enhancement programs. Therefore, this research is expected to positively contribute to GA safety enhancement by introducing a quantitative safety assessment and monitoring methodology for GA safety improvement.

CHAPTER 1
INTRODUCTION

1.1 General Aviation

1.1.1 Definition of General Aviation

General aviation (GA) is a sometimes ambiguous concept. The federal aviation administration (FAA) defines GA as "That portion of civil aviation that does not include scheduled or unscheduled air carriers or commercial space operations [1]." The General Aviation Manufacturer's Association (GAMA) has a similar definition: "All aviation other than commercial and military aviation [2]." The International Civil Aviation Organization (ICAO) defines GA as "All civil aviation operations other than scheduled air services and non-scheduled air transport operations for remuneration or hire [3]." The Aircraft Owners and Pilots Association (AOPA) uses a much more specific definition in their annual accident analysis. "GA is all flight activity of every kind except that done by the uniformed armed services and the scheduled airlines. In addition to personal and recreational flying, it includes public-benefit missions such as law enforcement and fire suppression, flight instruction, freight hauling, and passenger charters, crop-dusting, and other types of aerial work that range from news reporting to helicopter sling loads [4]." As stated in the above definitions, all aircraft operations that are not categorized as commercial, cargo, or military operations can be defined as GA operations. Thus, GA operations can range from personal or recreational activities to instructional, medical, and touristic operations. Actively operating GA aircraft in the U.S. and their primary use are summarized in Table 1.1. In this study, GA is defined as any small fixed-wing aircraft for non-scheduled, on-demand, and non-commercial operations.

Table 1.1: Active U.S. GA Aircraft by Primary Use and Aircraft Type [2]

Aircraft Type	Total	Personal	Business	Instructional	Aerial Apps.	Air Taxi	Tour	Medical	Other
Fixed-Wing	164,293	107,469	25,360	12,529	6,112	5,790	525	876	5,631
Piston	141,141	104,669	13,920	12,182	3,775	1,567	509	425	4,092
Turboprop	9,712	1,263	3,579	162	2,236	1,548	16	252	657
Turbojet	13,440	1,537	7,861	185	101	2,675	0	199	882
Rotorcraft	10,506	1,277	976	1,603	3,302	684	424	1,498	743
Other Aircraft	4,941	3,723	13	518	0	0	635	2	50
Gliders	1,870	1,455	8	360	0	0	40	0	15
Lighter-than-Air	3,071	2,268	13	158	0	0	595	2	35
Experimental	27,922	25,284	770	697	209	19	102	27	816
Special Light-Sport	2,369	1,948	45	320	26	2	0	0	28
All Aircraft	**210,030**	**139,700**	**27,163**	**15,667**	**9,650**	**6,494**	**1,685**	**2,403**	**7,267**

1.1.2 General Aviation Industry

The GA industry, as an essential part of the air transportation system, takes an important role in the aviation industry in the United States. Taking into consideration manufacturing and visitor expenditures, GA accounted for an economic contribution of USD 76.5 billion. According to AOPA, GA aircraft is the mainspring of a $20 billion a year industry, and it can generate more than $150 billion in economic activity [5]. Also, GA contributed USD 38.8 billion in economic output and created 496,000 jobs in 2009 [6]. Despite a rapid decrease in GA operation caused by the effects of the 9/11 terror attack, increasing fuel prices, and worldwide economic recession, the GA industry strived for invigorating the GA economy and the GA airplane shipment and billings rebounded in 2010. The active GA fleet is projected to increase at an average annual rate of 0.2 percent over the 21-year forecast period, with turbine-powered and jet-propulsion aircraft portion increasing at 2.1 and 2.5 percent a year respectively. In an actual flight operation point of view, the total number of GA hours flown will increase by 1.2 percent yearly, and turbine and jet GA aircraft are

forecast to increase 2.6 percent and 3.1 percent per year respectively over the forecast period, which is from 2015 to 2036 [7]. As the aforementioned statistics have indicated, GA takes an indispensable and essential role not only in the aviation industry but also in the economy nationwide.

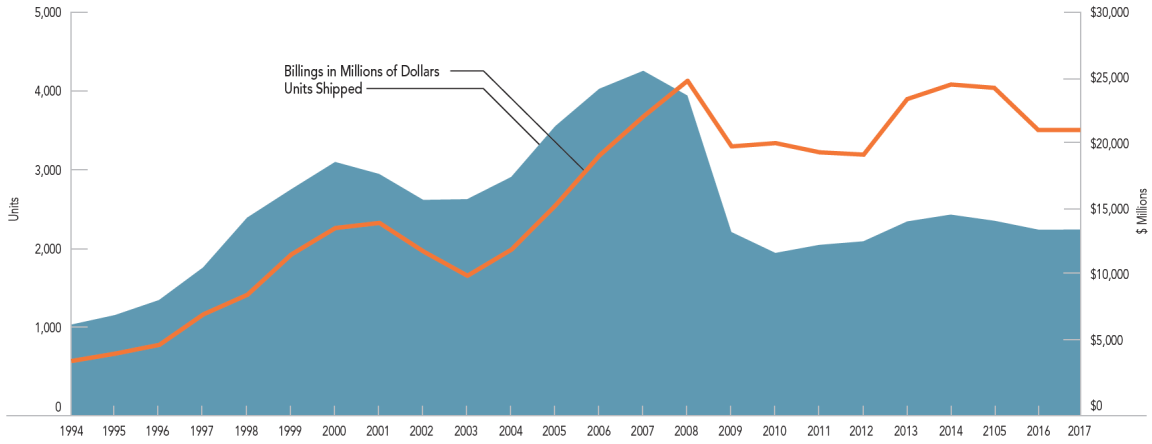

Figure 1.1: GA Airplane Shipments and Billings Worldwide (1994 – 2017) [2]

1.2 Aviation Safety

Aviation is one of the safest means of transportation. According to FAA, the total aviation accident rate in the U.S. has been reduced by 57% since 2001 [8]. Although aviation safety record indicates that aviation safety has been improved over decades, aviation safety has always been fundamental ongoing considerations in the aviation community because of the significant impact. Safety is defined by ICAO as "The state in which the possibility of harm to persons or of property damage is reduced to, and maintained at or below, an acceptable level through a continuing process of hazard identification and risk management [9]." Under the ultimate goal of improving aviation safety, numerous safety enhancement programs have been established.

1.2.1 Safety Management System (SMS)

To maximize opportunities for continuous and effective improvement of the overall aviation system safety, safety management system (SMS) framework has been developed. SMS is the formal, top-down, organization-wide approach to managing safety risk and assuring the effectiveness of safety risk controls. It includes systematic procedures, practices, and policies for the management of safety risk [10]. In other words, SMS is a dynamic risk management system based on quality management system (QMS) principles in a structure scaled appropriately to the operational risk, applied in a safety culture environment. ICAO defines SMS as "A systematic approach to managing safety, including the necessary organizational structures, accountabilities, policies and procedures [9]." The principal idea of SMS is to provide a systematic approach for achieving acceptable levels of safety risk. SMS is comprised of four functional components and Table 1.2 summarizes important components of the SMS framework.

Table 1.2: Safety Management System Framework [9]

Safety Policy and Objectives	**Safety Risk Management**	**Safety Assurance**	**Safety Promotion**
• Management Commitment & Responsibioity • Safety Accountabilities • Appointment of Key Safety Personnel • SMS Implementation Plan • Coordination of Emergency Response Planning • SMS Documentation	• Hazard Identification • Risk Assessment & Mitigation	• Safety Performance Monitoring & Measurement • The Management of Change • Continuous Improvement of the SMS	• Training and Education • Safety Communication

1.2.2 Flight Data and Aviation Safety Enhancement Programs

Aircraft flight data that is collected using onboard data measurement and recording devices enable various data-driven flight safety analysis. The flight data monitoring (FDM) or Flight Operations Quality Assurance (FOQA) programs are representative examples of the safety improvement efforts using flight data records. The primary purpose of FDM or FOQA program is to improve operational safety and efficiency by regularly recording and analyzing flight data [11]. The Aviation Safety Action Program (ASAP) is another form of data-driven safety enhancement program which focuses on encouraging voluntary reporting of safety issues and events [12]. In addition, FAA and aviation industry developed the Aviation Safety Information Analysis and Sharing (ASIAS) program which is for monitoring known risks, evaluating the effectiveness of deployed mitigations, and detecting emerging risks by sharing a wide variety of safety data and information across the aviation industry [13]. The aforementioned data analysis and sharing programs are typical examples of safety enhancement program which is well established and widely used for large commercial aircraft.

1.3 General Aviation Safety

1.3.1 Aviation Safety Statistics

As GA industry and its operations have grown along with the aviation industry development, improving aircraft safety has been a critical interest in the GA industry because safety is generally attributed by the industry to be the major hurdle for higher utilization of GA aircraft in the transportation system. According to the U.S. Department of Transportation (USDOT), GA in the year of 2014 suffered 1.40 fatal accidents for every 100,000 hours of flying in the United States compared to zero fatal accident rate for scheduled airline flights [14]. The historical accident rates of air carrier and GA aircraft are compared in Figure 1.2 and Figure 1.3. As shown in the figures, GA has higher accident rates and fatality rates than

air carriers. This statistical data indicates that GA operational safety enhancement effort is inevitable and reduction in GA aircraft accident rates needs to be set as a common goal in the GA community.

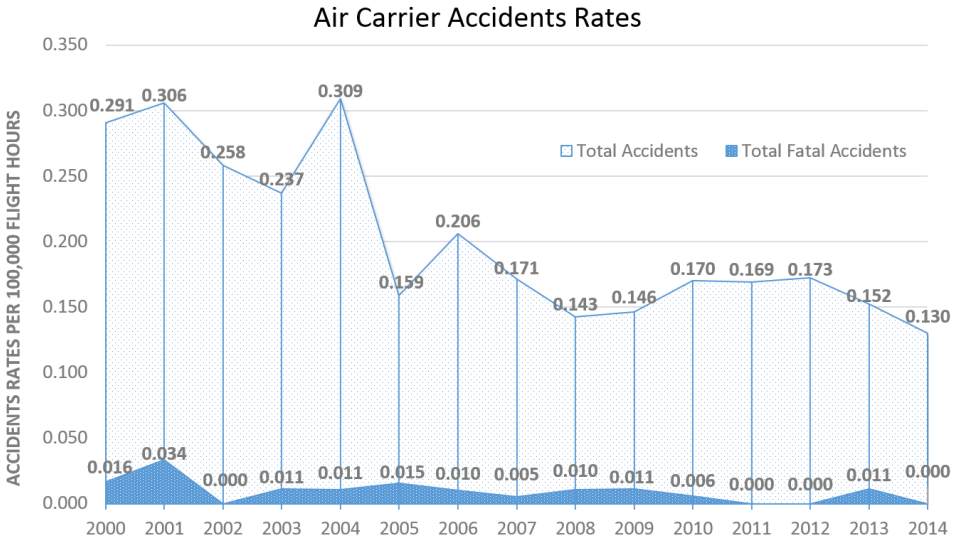

Figure 1.2: U.S. Air Carrier Accident Rate History [14]

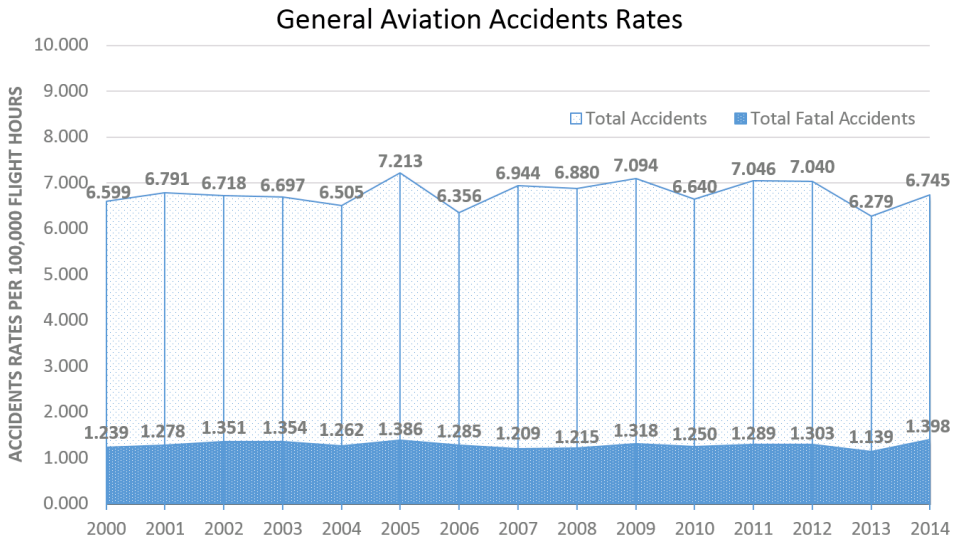

Figure 1.3: U.S. General Aviation Accident Rate History [14]

1.3.2 Safety Enhancement Efforts for General Aviation

In order to improve GA safety, numerous efforts have been made by the GA community. For example, one of the main goals of the National Aeronautics and Space Administration (NASA) is to develop technologies to reduce aircraft safety risks substantially [15]. Also, the Federal Aviation Administration (FAA) has set a target to reduce GA fatal accident rate of less than 1.02 fatal accidents per 100,000 flight hour [16]. The General Aviation Joint Steering Committee (GAJSC) analyzes aviation safety data to identify emerging issues and develop mitigation strategies to address and prioritize safety issues [17]. In addition, many organizations such as General Aviation Air Safety Investigators (GA-ASI) of GAMA and Air Safety Institute of AOPA Foundation hold workshops or training programs with a goal of helping all pilots fly safer by sharing, discussing, and educating current safety-related information [18][19]. Furthermore, FAA has constantly been striving to improve GA safety. One of the FAA's effort is Partnership to Enhance General Aviation Safety, Accessibility and Sustainability (PEGASAS) which is partnering with a national network of world-class researchers, educators and industry leaders for the mission of GA safety enhancement [20]. Although these safety programs for GA have been contributing to GA safety improvement, the accidents rate of GA is still much higher than that of the air carrier. Thus, the uniqueness of GA has to be well acknowledged by aviation safety stakeholders, and it has to be considered when GA safety enhancement efforts are pursued.

1.3.3 Approach and Landing Safety

According to Flight Safety Foundation (FSF), approach-landing phase is one of the riskiest phase of flight [21]. A review of accident statistics indicates that more than 45 percent of GA accidents occur during the approach and landing phases [22]. Among the identified cases of the accidents, the pilot related issue is the biggest contributing factor that takes over 90 percent of the accidents. Also, 33 percent of the accidents were caused by the loss of control (LOC) issue according to the FAA. Various accidents can happen during the

approach and landing phase of flight and controlled flight into terrain (CFIT) and runway excursions are the most common types of GA accidents during approach and landing phase. Because the approach and landing is a high risk phase of flight, a lot of safety enhancement efforts for this phase of flight have been conducted to address the risks. For example, Fala et al. developed algorithms to detect safety events during the approach phase using the flight data generated by a Cirrus SR-20 aircraft which is one of the widely used GA aircraft [23]. The algorithms developed by Fala et al. detects and categorizes the safety events in the approach and landing phase. Also, Rao et al. investigated historical GA accident data from the National Transportation Safety Board (NTSB) and revealed the main causes for unstable approaches in GA operations [24]. The FSF suggested the specific criteria for defining stabilized approach that can provide useful insight to approach and landing safety assessment efforts [25]. When an aircraft is not satisfying requirements for a safe landing during approach and landing phase, the aircraft should perform a go-around. A go-around is a standard aircraft maneuver which is a procedure of discontinuing an approach to landing flight to avoid potentially dangerous situations. To maximize the benefits of the go-around maneuver, Campbell et al. conducted an experiment to develop more realistic go-around criteria for transport category aircraft [26]. The information provided by the Campbell et al. can be used to revise and improve the stabilized approach criteria for commercial airline aircraft by relating the flight parameters during approach and landing performance parameters. This strategy can be applied to the GA field to improve the safety of GA approach and landing operations. Based on observations of the studies mentioned above, concentrating on safety of approach and landing phase of flight has a high impact on improving overall GA safety. This effort can be supported by developing quantitative methods to understand safety of approach and landing operations. Pilots can use the identified and quantified safety information to develop their proper skills for stable approach and landing, and they can follow established procedures to reduce the chance of an accident caused by a pilot-related mishap.

1.3.4 Uniqueness of General Aviation

Since GA is different from regular commercial aviation regarding not only aircraft type but also its operation concept, it is indispensable to understand the uniqueness of GA to improve its safety. First of all, GA aircraft are heterogeneous and usually smaller than commercial aviation aircraft or military aircraft. Also, GA aircraft are operated by various types of pilots such as private pilots, flight instructors, student pilots and so on. That means each GA pilot's experience level is diverse compared to airline pilots, and as a result, the GA flight operations and its safety characteristics are also different. Besides, GA operations and its flight profiles are more flexible than airliners or military operations because it is non-scheduled flight. GA operations range from personal or recreational flight to instructional flight, and GA aircraft operate in various airports. In the U.S., around 5,200 airports are available for GA aircraft while scheduled flights operate in approximately 530 airports in the U.S. [27] Thus, each GA mission profile is unique and corresponding flight performance characteristics are also different from each other. Another unique characteristic of GA is its lack of data logging capability. Flight data recording device is not mandatory for GA aircraft, so many GA aircraft do not have data recording capability. However, FAA developed a smartphone application named GAARD which is designed to collect flight data and enhance aviation safety. Using this application, GA pilots can record and monitor the flight data by collecting GPS position and attitude information [28].

Considering the characteristics of GA aircraft and operations, a more flexible approach of GA safety assessment and enhancement is required. For example, aircraft performance characteristics can vary depending on the pilot's experience level, the age of aircraft, or operation type. Thus, safety enhancement effort has to be made considering the uniqueness of GA mentioned above, and realistic and credible GA flight data is one of the critical element of this safety improvement approach.

1.4 Summary

GA safety is an essential part of the aviation industry in the U.S. and has been contributing positively to the community in numerous ways. However, GA has been suffering from a relatively high rate of accident and fatality, so various aviation safety programs are developed to improve GA safety. The benefits of aviation safety management and enhancement programs described in the above section can be maximized when the programs are flexible enough to reflect the uniqueness of GA operations properly. For the aviation safety enhancement efforts to be flexible, precise aircraft performance models and clean flight data have to be appropriately obtained and used. For this reason, an aircraft performance modeling method that can generate a not only flexible but also accurate performance model is necessary for predicting and capturing aircraft behavior in any operational conditions. Furthermore, a data noise filtering technique that is specific to GA flight data and its collection procedure is required for improving the reliability of data-driven safety analysis programs. Finally, the harmonization of accurate performance models and clean flight data is expected to positively contribute to GA safety enhancement by enabling flexible and reliable operational safety assessment and monitoring.

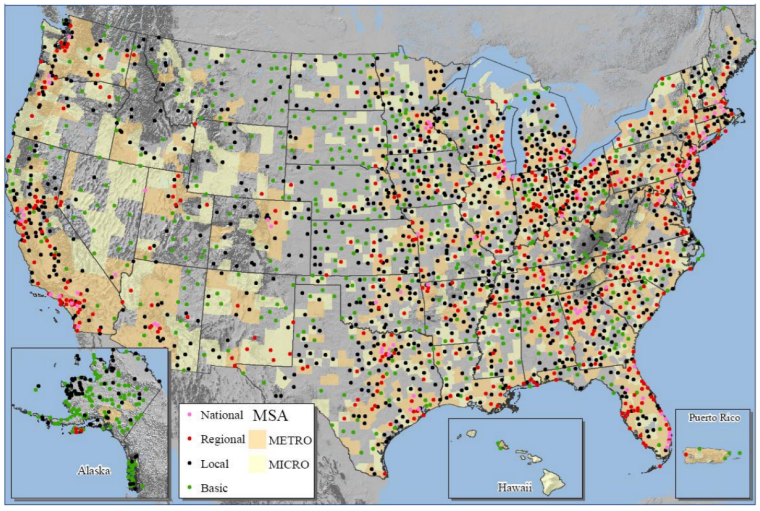

Figure 1.4: Map of the General Aviation Airports [29]

CHAPTER 2
BACKGROUND AND LITERATURE REVIEW

This chapter focuses on the literature review of existing aircraft performance modeling methods and flight data analysis program and how they have been applied to not only GA but also overall aviation safety improvement. The first section of this chapter explains various programs and efforts for improving aviation safety that has been done by multiple aviation industry stakeholders. The next part discusses how flight data is applied to aviation safety improvement programs and introduces different types of flight data analysis methods and their applications. Also, the following section addresses the importance of data quality, then provides a brief overview of various noise filtering methods that are commonly used in the data analysis field. The last part explains existing aerodynamic modeling methods for a fixed-wing aircraft with different levels of model fidelity, then discusses their applicability to GA aviation safety assessment.

2.1 Aviation Safety Enhancement Efforts

Safety means that "the state in which the possibility of harm to persons or of property damage is reduced to, and maintained at or below, an acceptable level through a continuing process of hazard identification and safety risk management" [9]. Based on the definition of "safety", aviation safety means that the state in which risks of an aircraft or an aviation system are reduced and controlled to an acceptable level. To improve aviation safety, there have been many studies and programs in the aviation field and it is still ongoing efforts. This section intends to provide some examples of aviation safety enhancement programs.

2.1.1 Flight Operational Quality Assurance (FOQA)

FOQA is the most representative use of flight data for aircraft safety enhancement program. This program is a voluntary safety program that is intended to make commercial aviation safer by providing commercial airlines and pilots for sharing every possible information that is related to aviation safety. [30]. In this program, FAA can monitor overall trends in aircraft operations and take actions to address operational risk issues. The fundamental goal of this program is to allow all related parties to identify and reduce or eliminate safety risks, as well as minimize deviations from the regulations[9]. In order to achieve this objective and gain helpful information, the airlines, pilots, and the FAA agree to participate in this program under the ultimate goal of making aviation safer. A FOQA program is used to reveal operational situations in which risk is increased to enable early corrective action before that risk results in an incident or accident [30].

2.1.2 Aviation Safety Assurance Program (ASAP)

ASAP are the most important part of the safety management system that aviation service providers or aircraft operators shall implement in order to meet ICAO SARPS and regulatory requirements [31]. Safety assurance includes systematic processes for continuous monitoring and recording of the organization's safety performance, as well as the evaluation of the safety management processes. Safety assurance demonstrates that organizational arrangements and processes for safety achievement are correctly applied and continue to achieve their intended goals [30].

2.1.3 Aviation Safety Information Analysis and Sharing (ASIAS)

ASIAS is a collaborative government and industry initiative on data sharing and analysis to proactively discover safety concerns before accidents or incidents occur, leading to timely mitigation and prevention [32]. ASIAS works as a primary channel for the sharing of safety information among its stakeholders, contributing an important resource for the

aviation community. The goal of ASIAS the establishment of a broad network of safety information sources shared by stakeholders. ASIAS program has connected a wide variety of safety data and information sources across government and industry, including voluntarily provided safety data [33]. The ASIAS program works closely with the Commercial Aviation Safety Team (CAST) and the General Aviation Joint Steering Committee (GAJSC) to monitor known risk, evaluate the effectiveness of deployed mitigations, and detect emerging risk.

2.1.4 Partnership to Enhance General Aviation Safety, Accessibility and Sustainability (PEGASAS)

The main purpose of PEGASAS is to enhance GA safety, accessibility, and sustainability by collaborating with the FAA, universities, researchers, and industry leaders [34]. In order to achieve the goal, PEGASAS has established an extended network of relevant aviation-related organizations and industry partners such as not only industrial companies, but also government agencies, and airport operators. This program has been devoted to conducting various researches in collaboration with the stakeholders for enhancing GA safety.

2.2 Flight Data in Aviation Safety Programs

2.2.1 Flight Data Analysis

Data is defined as the values or qualitative or quantitative variables, belonging to a set of items. Flight data analysis (FDA) is a generic term for gathering and analyzing data recorded during routine flights to improve flight crew performance, operating procedures, flight training, air traffic control procedures, air navigation services, or aircraft maintenance and design [35]. FDA and flight data monitoring (FDM) technique was enabled by the development of flight data recorders (FDR). The main purpose of FDR was to assist accident investigators in determining the cause of aviation accidents. Repeatedly gathering and an-

alyzing flight data from the flight recorders reveals meaningful information and provides the aircraft operators deep understanding of what constituted a safe envelope for the flight operations. It also provides performance information on airframes and engines.

FDA is an essential element to SMS in the aviation field. FDA programs and FDM techniques are used for monitoring and analysis of flight operations and performance data. In addition, they can also detect adverse trends in any part of the flight regime which can be mitigated by revision of Standard Operating Procedures (SOP), Air Traffic Control (ATC) procedures or understanding anomalies in aircraft performance [36]. FDA/FDM is very useful in identifying exceedances of flight parameters that either indicate an underlying systemic issue or improper operating technique. This is established by comparing the specific flight record to the nominal profile developed based on the fleet profile. For example, a flight maneuver can be detected as an unstable approach when it is detected as an isolated event [37].

A core element in the successful application of FDA/FDM in SMS is securing informative flight data. This can be achieved by continuously collecting flight data and ensuring that the collected flight data is clean and has no inherent noise. When it is observed that the collected flight data has a significant noise, the noise must be removed by applying appropriate data noise filtering techniques.

2.2.2 Data Noise

As mentioned earlier, ensuring clean flight data is an essential requisite for flight-data-driven safety management. Therefore, this section is dedicated to overviewing what kind of noise filtering methods are existing in the aviation field.

Time Domain Filtering Methods

• *Kalman Filter-Based Methods*

One of the well-known noise filtering methods in the time domain is the Kalman filtering method. The Kalman filter has as objective the minimization of the estimation square error of a nonstationary signal buried in noise. This noise filtering technique deals with random processes described using state–space modeling which generates signals that can be measured and processed utilizing time recursive estimation formulas. The Kalman filter is a recursive estimator. This means that only the estimated state from the previous time step and the current measurement are needed to compute the estimate for the current state. In contrast to batch estimation techniques, no history of observations and/or estimates is required [38]. Figure 2.1 describes the basic concept of the discrete-time Kalman filter method. In addition to the discrete-time Kalman filter, The Kalman filtering method has been developed and transformed into various forms such as extended Kalman filter, frequency-weighted Kalman filter, Unscented Kalman filter, Kalman-Bucy filter, and so on.

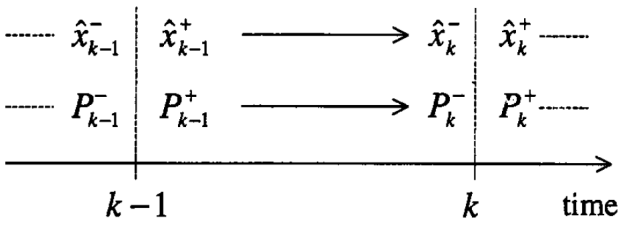

Figure 2.1: Timeline Showing a Priori and a Posteriori State Estimates and Estimation-Error Covariances [39]

Frequency Domain Filtering Methods

• *Fourier Transformation Filtering*

Another way of removing data noise is investigating the data in the frequency domain by applying the Fourier transformation method. The Fourier Transform is extensively used

in the field of Signal Processing in many applications. Flight data is also a kind of signal which is logged in the time domain. Thus, the Fourier transform (FT) decomposes the data into frequency components. In signal processing, the FT can reveal important characteristics of a signal including noise components. The TF has two main categories: Discrete Fourier transform (DFT) and fast Fourier transform (FFT).

The Fourier transform is a mathematical formula that relates a signal sampled in time or space to the same signal sampled in frequency. For a vector that has uniformly sampled points, the following Equation 2.1 defines the DFT of x where i is the imaginary unit, $w = e^{-2\pi i/n}$ is one of n complex roots of unity. j and k are indices that run from 0 to n-1 [40]. Also, Equation 2.2 is the inverse Fourier transform that converts a signal in frequency domain back to time domain.

$$y_{k+1} = \sum_{j=0}^{n-1} w^{jk} x_{j+1} \tag{2.1}$$

$$x_{j+1} = \frac{1}{n} \sum_{k=0}^{n-1} w^{-jk} y_{k+1} \tag{2.2}$$

The FFT is a variation of DFT that is more efficient computationally. While a one-dimensional DFT requires on the order of n^2 floating-point operations for a vector of n data points, the FFT requires on the order of $n \log n$ operations, a significant reduction in computational complexity [40].

Observations

In the previous sections, the most prominent noise filtering concepts are reviewed in both time and frequency domain. Since flight data consists of various types of parameters measured with different types of measuring instrument, the types of data noise that are embedded in the recorded flight data can be grouped into some categories according to the inherent characteristics caused by the nature of measuring instrument. For example,

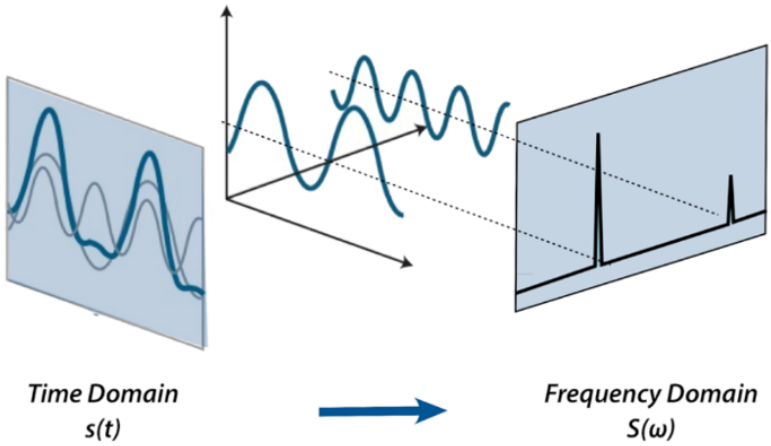

Figure 2.2: Data Noise in Frequency Domain [41]

speed-related parameters are measured using pitot tube which is a tool to measure the total pressure. Angle-related parameters such as pitch and bank angles are measured using a gyroscope. Positions of an aircraft such as latitude/longitude and altitude are measured using GPS and barometer respectively. Therefore, different noise removal techniques may be required for a certain type of noise in each parameter and a tactical approach for minimizing possible errors in FDA caused by data noise is necessary.

2.3 Fixed-Wing Aircraft Performance Models

Among various types of performance models for predicting and defining the behavior of the aircraft when performing different kinds of maneuvering, an aerodynamic model is one of the most primary models for capturing fundamental behaviors of aircraft. Many modeling methods for developing aerodynamic models have been introduced from low fidelity to high fidelity depending on the purpose of the model. This section summarizes the review of the aerodynamic modeling methods.

2.3.1 Physics-Based Modeling Method

Aerodynamic modeling for aircraft performance consists of two main parts: lift-curve modeling and drag polar modeling. Figure 4.2 shows the typical shapes of lift curve and drag polar of a fixed-wing aircraft. The lift-curve model is used for predicting variation in the lift coefficient with a change in the angle of attack, and the drag polar model provides the relationship between the lift of an aircraft and its drag. Various theoretical aerodynamic modeling methods for estimating the aerodynamic performance of an aircraft using key aerodynamic parameter were surveyed and explained.

Lift-Curve Modeling

An aerodynamic model (a lift-curve) that provides the fully defined relationship between the lift coefficient and the angle of attack for an aircraft was created by evaluating in three stages that include all the aspects of the aircraft: the 2-D wing airfoil, the 3-D wing, including the 3-D effect, and complete aircraft. The lift curve for each stage that governs the shape of the curve is defined by five parameters: the zero-lift angle of attack, the lift-curve slope, the angle of attack limit for a linear range, the angle of attack for the maximum lift coefficient, and the maximum lift coefficient [42]. Creating the linear range of the lift curve using zero the lift angle of attack, the lift-curve slope, and the angle of attack limit for the linear range is straightforward. In other words, the lift curve can be expressed by a simple straight-line equation. The non-linear part near the stall point can be modeled using a quadratic equation, and it can be defined by the lift-curve slope, the angle of attack for the maximum lift coefficient, and the maximum lift coefficient given a requirement that the slope of the linear and nonlinear parts $(dC_L/d\alpha)$ is identical where the two parts meet. The combination of these two equations of the linear and non-linear area completes basic lift performance modeling for an aircraft in a clean configuration.

When an aircraft is required to use high lift devices in a specific operation such as takeoff or landing operation, the lift characteristics change because of the effect of high-lift

device deployment. This effect causes a lift increment, a lift-curve slope change, and a maximum lift coefficient increment [42]. Figure 4.5 notionally describes how the lift-curve varies in flaps-deplyed configuration. The amount of the lift increment or the slope change depends on the amount of flap deflection.

Drag Polar Modeling

The drag polar is the aerodynamic characteristic that is most relevant for modeling or assessing the aircraft's performance capabilities/characteristics. The drag coefficient can be presented as a function of the angle of attack, but another effective plot that can provide the aerodynamic performance of an aircraft is the drag polar, which shows the drag coefficient as a function of the lift coefficient. The drag polar of an aircraft contains almost all information required for analyzing its aerodynamic performance. Aircraft drag is mainly composed of parasite drag and induced drag. Equation 2.3 is a general expression of drag coefficient for an aircraft in a clean configuration with a parasite drag term and an induced drag term [43].

Parasite drag, also called zero-lift drag, consists of mostly skin-friction drag and small separation pressure drag [44]. Induced drag is drag resulting from the lift that is proportional to the square of the lift coefficient with a proportionality factor K, shown in Equation 2.3. The skin-friction method and the component buildup method [44] are methods for parasite drag estimation. In addition, induced drag factor K can be estimated by the Oswald span efficiency method and the leading-edge suction method [44]. A detailed description of each estimation method for parasite drag and induced drag will be provided in the next subsequent sections.

$$C_D = C_{D_{min}} + \frac{{C_L}^2}{\pi ARe} = C_{D_{min}} + K{C_L}^2 \tag{2.3}$$

$$\Delta C_{D_{flap}} = \Delta C_{D_p} + \Delta C_{D_i} + \Delta C_{D_{int}} \tag{2.4}$$

Drag characteristic, as well as lift characteristic, is highly dependent on the flap deployment of an aircraft. The drag increment can be estimated from the sum of the flap profile drag increment, the induced drag increment, and the interference drag increment [42]. The total aircraft drag coefficient in the flap-down condition can be expressed as the sum of the drag coefficient of a clean configuration aircraft and drag coefficient increment caused by the flap deflection. For flap-deployed configuration, the drag increment caused by deflected flap can be estimated using Equation 2.4, where $(\Delta C_D)_{flap}$ is total drag change and ΔC_{Dp}, ΔC_{Di}, and ΔC_{Dint} are parasite, induced, and interference drag change respectively.

2.3.2 The Bootstrap Approach

The Bootstrap Approach (TBA) is a simple flight-data-driven performance modeling method for a fixed-pitch propeller-driven aircraft. In addition to the original TBA, Extended TBA was also developed for variable pitch propeller aircraft [45]. The fundamental idea of TBA is that a set of simple equations with nine aircraft parameters plus aircraft weight and density can generate the drag polar and propeller polar, which represents a relation between power and thrust, of an aircraft. The aircraft weight and air density are the variables that need to be identified by the pilot. The pilot may find the aircraft weight by directly measuring them or adding the weights of fuel, oil, crew, passengers, and baggage to the empty weight. In addition, the pilot can obtain air density during flight using pressure altitude and the outside air temperature information. The nine aircraft parameters that are essential to this method are listed in Table 2.1 [45].

The first five parameters in Table 2.1 – wing reference area, wing aspect ratio, rated mean-sea-level (MSL) torque, altitude drop-off parameters (power lapse parameter), and propeller diameter – are given in the POH or the engine manual. Wing reference area, wing aspect ratio, and propeller diameter are cleared indicated in POH. The altitude drop off parameter, which is the proportion of internal engine losses not responsive to atmospheric density, may be inferred from in the engine manual or it also can be computed by conduct-

ing a simple experiment to see how engine power or torque drops off with altitude. For most internal combustion aircraft engines, this number is about 0.12 and it is substantially correct [46]. The rated MSL torque M_0 can be calculated using Equation 2.5 whare P_0 is the full throttle power, n_0 is the rated maximum propeller revolutions per second. The other four parameters – parasite drag coefficient, aircraft efficiency factor, propeller polar slope, propeller polar intercept – should be computed from multiple glides and climb maneuvers, which is describing the basic concepts of obtaining the input parameters for TBA.

$$M = \frac{P}{2\pi n} \quad or \quad M_0 = \frac{P_0}{2\pi n_0} \tag{2.5}$$

Table 2.1: Bootstrap Data Plate Items

Bootstrap Data Plate Item	**Symbol**	**Aircraft**
Wing Reference Area	S	Airframe
Wing Aspect Ratio	AR	Airframe
Rated MSL Torque	M_0	Engine
Altitude Dropoff Parameter	C	Engine
Propeller Diameter	d	Propeller
Parasite Drag Coefficient	C_{D_0}	Airframe
Aircraft Efficiency Factor	e	Airframe
Prepeller Polar Slope	m	Propeller
Propeller Polar Intercept	b	Propeller

Among the nine parameters listed in Table 2.1, the parasite drag coefficient and the aircraft efficiency factor can be computed from multiple glide test data using Equation 2.6 and 2.7 [45]. A pilot conducts glide flight repeatedly over the same vertical interval until the best glide angle γ_{bg}, and the best glide speed V_{bg} are identified. The glide test must be conducted for each flap setting to obtain the drag polar parameters for flap-deflected

aerodynamic performance estimation.

$$C_{D_0} = \frac{W \sin \gamma_{bg}}{\rho_0 {V_{Cbg}}^2 S} \tag{2.6}$$

$$e = \frac{4W \cos \gamma_{bg}}{\pi AR \tan \gamma_{bg} \rho_0 {V_{Cbg}}^2 S} \tag{2.7}$$

Similarly, the propeller polar slope m and propeller polar intercept b can be obtained from multiple climb flight test data. The basic form of a propeller polar is shown in Equation 2.8 where C_T is thrust coefficient and C_P is power coefficient. This equation is empirically supported by the assumption of linearity between C_T/J^2 and C_P/J^2 [47].

$$\frac{C_T}{J^2} = m\frac{C_P}{J^2} + b \tag{2.8}$$

During repeated climb maneuvers, speed for largest climb angle V_x and speed for best rate of climb V_y are identified. Then the pilot or user is able to calculate the intercept of the linearized propeller polar, b using Equation 2.9. Also, the propeller polar slope can be computed using Equation 2.10. Alternatively, the pilot can simply make a level full-speed flight to find V_M and use Equation 2.11 to calculate the propeller polar slope, m [45].

$$b = \frac{SC_{D_0}}{2d^2} - \frac{2W^2}{\rho^2 d^2 S \pi e AR {V_x}^4)} \tag{2.9}$$

$$m = \frac{2n_0 dW^2}{\Phi(\sigma_{air}) P_0 \rho S \pi e AR} \left(\frac{3{V_y}^2}{{V_x}^4} + \frac{1}{{V_y}^2} \right) \tag{2.10}$$

$$m = \frac{2n_0 dW^2}{\Phi(\sigma_{air}) P_0 \rho S \pi e AR} \left(\frac{1}{{V_M}^2} + \frac{{V_M}^2}{{V_x}^4} \right) \tag{2.11}$$

Once the nine parameters for TBA are all identified, the pilot can compute the aircraft performance using the parameters and develop flight performance data table specific to

the aircraft. This chapter is for introducing performance modeling methods, generation of performance data using the TBA method will be discussed later.

In summary, the TBA method is a simple but reliable performance modeling method for an existing fixed-wing light aircraft with fixed-pitch propellers. This modeling method requires basic flight skills to conduct several sets of glide and climb flight test maneuvers.

2.3.3 System Identification and Parameter Estimation

System identification is the process of determining an adequate mathematical model, usually containing differential equations, with unknown parameters that have to be determined indirectly from measured data [48]. It is mainly focusing on the determination of the mathematical or performance model structure representing the dynamic system, which is in general unknown and not unique. Zadeh defines system identification as ”the determination, on the basis of observation of input and output, of a system within a specified class of systems to which the system under test is equivalent [49].”

In the flight vehicle development phase, system identification is useful because it enables the development of adequately accurate and validated mathematical models of the flight vehicle. More specifically, system identification provides an overall understanding of the flight vehicle's dynamics by observing the inputs and its response to them. Furthermore, system identification yields an accurate and comprehensive database for flight simulators which is extremely useful for realistic pilot training. Although the system identification method provides high fidelity performance models, the measurement of inputs and system response to applied inputs are required to determine the system model.

2.3.4 Computational Fluid Dynamics

Computational Fluid Dynamics (CFD) is a numerical analysis method for predicting the aerodynamic performance of aircraft. This analysis method is used for not only aircraft but also various fluid mechanics-related applications such as fan, wind blades, automobiles

and so on. CFD is widely used in aircraft aerodynamic performance analysis because it allows the aerodynamics performance estimation of an aircraft with extremely high levels of accuracy. In addition, CFD analysis provides the ability to conduct thorough, automated, multi-point design optimization. It is obvious that CFD has many advantages such as high accuracy, reality, and broad applicability, it requires enormous computational requirements and time compared to the classical aerodynamic modeling methods. Furthermore, aircraft geometry is the key requisite for CFD analysis but detailed geometry information of aircraft is usually not available for common GA aircraft users. Also, CFD analysis should be followed by result validation based on experimental data but it is generally not affordable for GA aircraft owners, pilots, or safety analysts. Lastly, modeling cost or CFD analysis tool cost is extremely high.

2.3.5 Experimental Method

The basic idea of wind tunnel test is observing and measuring the effects of air moving past solid objects to identify the object's aerodynamic parameters. A wind tunnel consists of a tubular testing zone with the testing object mounted in the middle. During an experiment, air is made to flow past the model by a powerful fan system while the forces on the object are measured using various types of instrumentation such as sensors to measure aerodynamic forces, pressure distribution, or other aerodynamic-related characteristics of the testing object [50].

Flight testing is for developing and gathering data during actual flight of an aircraft and then analyzes the flight data to evaluate the aerodynamic performance characteristics of the aircraft for in design validation including safety aspects. The main objective of flight test is finding and fixing any design problems and verifying/documenting the vehicle capabilities for certification. The flight test phase can range from the test of a single system such as wing or winglets to the complete development and certification of a new aircraft. Therefore, the duration of a particular flight test program can vary from a few weeks to many years

and the modeling cost as well as modeling time for flight test is tremendously expensive.

2.3.6 Fidelity Spectrum of Aerodynamic Models

In the previous section, the currently existing aerodynamic modeling methods with various levels of fidelity are summarized and explained. Since each modeling method has its own purpose and targeting fidelity, selecting an appropriate aerodynamic modeling method considering the modeling purpose is important to maximize benefits from the model. Thus, it is required to consider the trade-off between accuracy against modeling cost.

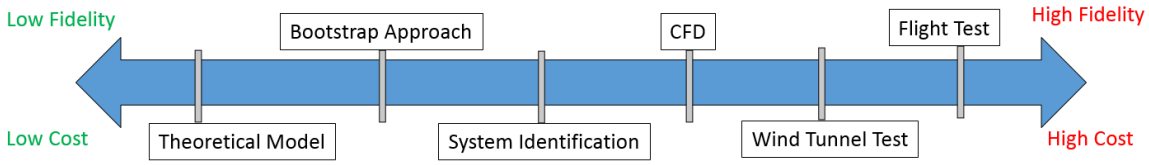

Figure 2.3: Conceptual Fidelity Spectrum of Aerodynamic Modeling Methods

2.4 Summary and Observations

The aviation safety enhancement programs mentioned above have been achieving steady improvement in aviation safety through various efforts and collaborations. From the observations on the programs, it is shown that flight data accounts for a large portion of the programs. However, most of the aviation safety programs mentioned above are aimed at improving the commercial aviation safety which can take full advantage of the data because enough amount of flight data is available. One of the unique characteristics of GA is that GA aircraft do not record flight data, so an extra effort is required to utilize a data-driven safety enhancement program for GA. Furthermore, it is observed that the importance of the flight data is often neglected in the programs. It is certain that the results from data-driven analysis programs are highly dependent on the quality of the data being utilized in the process. Therefore, there is a need for a method that can appropriately remove the noise in the

flight data. Also, it is discovered that there is a lock of the standard to assess the GA aircraft safety quantitatively. Considering the characteristics of the GA, the GA can generate the flight data relatively freely. Therefore, applying this uniqueness of GA to the GA safety improvement effort will maximize the advantage of the flight data and complement the shortcomings of data-driven GA safety program mentioned above. The observations from the survey lead to the research goal of this study which is elaborated in the next chapter.

CHAPTER 3
PROBLEM FORMULATION

The purpose of this chapter is formulating research problem with the given observations from the literature review. In the beginning, the research objective is stated to describe clearly what the aim of this research is. Then, research questions that represent the scope of this research are formulated in the following sections.

3.1 Research Objective

Given the requirements that are reviewed and identified in the literature review, this study seeks to identify more effective methods for evaluating the operational safety of a fixed-wing GA aircraft using an aerodynamic performance model and flight data analysis techniques. To achieve this main research goal, three sub-objectives are derived.

First, this research aims to develop a realistic and accurate aerodynamic performance model that is computationally affordable with adequate fidelity and compositionally flexible so that this modeling method can be used by any GA aircraft users capturing the characteristics of each aircraft. This goal has to be supported by the answer to what constitutes a suitable aerodynamic model for operational safety assessment.

Next, this study intends to suggest an effective noise removal technique to obtain clean and tidy flight data records for the aerodynamic modeling process as well as the operational safety assessment process. To ensure that the flight data to be used in the process is clean, it is required to have a proper way of quantifying the data noise, then establish a method that can reach to the optimal degree of tidiness.

Finally, using a previously obtained reliable aerodynamic performance model and filtered clean flight data, this work develops and tests the idea of evaluating flight performance safety of a GA fixed-wing aircraft. By achieving this goal, this research is able to propose

an effective and practical procedure of identifying and quantifying any unsafe behavior of an aircraft.

The research objective and sub-objectives stated above are summarized in Figure 3.1. Ultimately, this study attempts to provide answers to the following key research questions that are formulated in the next section.

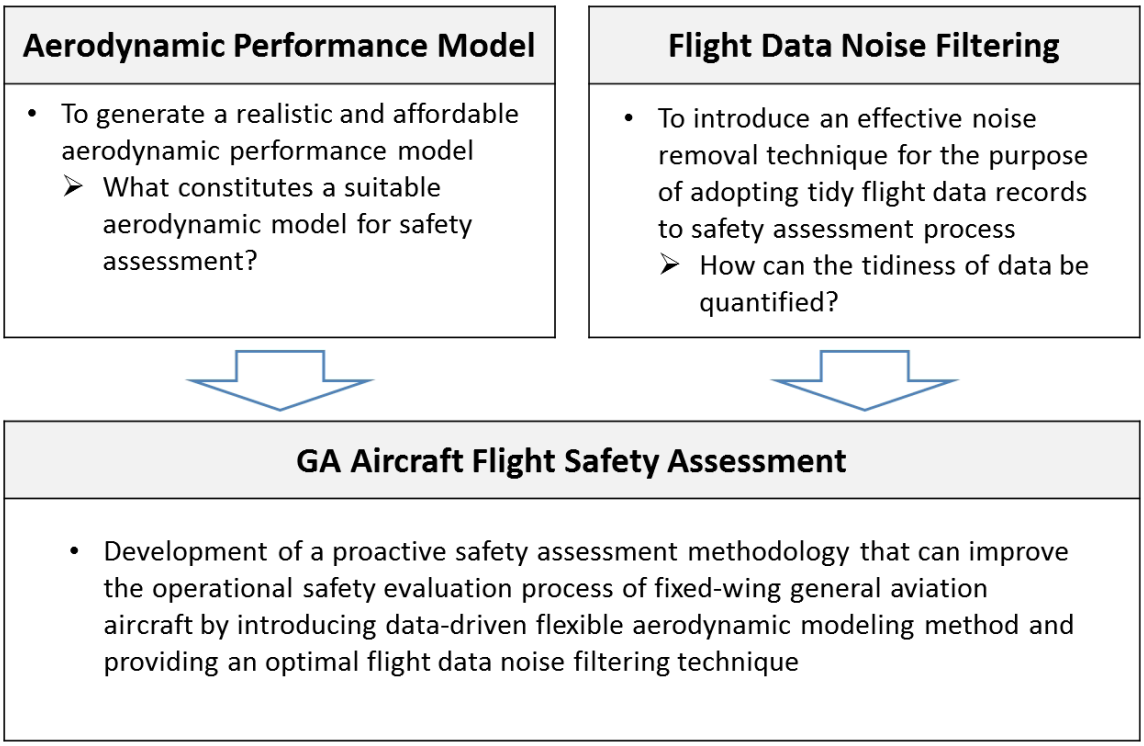

Figure 3.1: Overview of Research Objective

3.2 Research Questions

3.2.1 Aerodynamic Performance Model

In the literature survey, it is observed that an aircraft performance model can introduce more transparency and capability to flight data-driven safety analysis by actually looking at the aircraft behavior and flight data simultaneously. In order to enhance GA safety through successful application of SMS, accurate aircraft performance models are critical requisites

because main requirements of SMS such as hazard identification, risk assessment, and safety performance monitoring must be supported by the ability to capture the behavior of aircraft precisely under any operational conditions. The review of aerodynamic modeling methods for a fixed-wing aircraft provided the general concept of the various modeling methods with advantages and limitations. For example, Pilot's operating handbook (POH), which is a document developed by the airplane manufacturer and approved by the FAA, lists essential information regarding the design, operation, and limitations of the aircraft, as well as its performance characteristics. Although the performance information in POH is accurate under specifically indicated conditions, it should be able to flexibly adapt to other operating conditions that are not stated in POH. Given the needs of performance predictability using an aerodynamic model for flight data analysis, it is essential to generate an aerodynamic model with an appropriate level of fidelity. In other words, flexible performance models that are able to capture realistic flight characteristics under any operating condition are required for aviation safety management. Thus, this study attempts to answer the following research question to generate an aerodynamic model for a fixed-wing GA aircraft for the purpose of GA operational performance envelope identification. The hypothesis to that is established to provide the answer to the research question 1 is also described below.

Research Question 1

What is a more effective way of developing an aerodynamic model that has a necessary level of fidelity to adequately predict aerodynamic performance and capture unsafe aerodynamic behaviors of a fixed-wing GA aircraft?

Hypothesis 1

An aerodynamic model that is accurate enough to estimate flap usage during flight can capture unsafe behaviors of a fixed-wing GA aircraft, and the necessary accuracy can be achieved with the combination of a theoretical model and flight data.

It is important to note that requisite information for the development of models should be publicly available and provided by reputable or authoritative sources such as a pilot's operating handbook and published flight/ground test data. The is a significant and recurring issue in aircraft model development and calibration process because much of the requisite information is not typically available to the public. By answering the research question, it is expected that this study identifies and introduces a better way to find a reasonable trade-off between model accuracy and modeling cost with given reference data and ability to obtain or generate any required data.

3.2.2 Data Noise Filtering

The advantages of flight data analysis are well acknowledged in the aviation industry and tremendous data-driven safety enhancement programs have been developed and widely used. As noted in the literature review section, FDM is the representative flight data analysis program focusing on aviation safety enhancement. However, such data-driven safety programs have limitations to be used for GA operations because GA aircraft are not obligated to flight data record and the majority of GA aircraft currently in service are not equipped with devices capable of recording flight data. Although FAA developed a free app named GAARD for pilots to contribute their flight data to a national database for safety monitoring [28], providing the flight data using this app is voluntary and non-enforceable. Thus, there is an inevitable limit to the use of flight data for improving GA safety.

Although flight data perform highly important roles in safety analysis by providing the behavioral information of aircraft, flight data itself contain unavoidable noise. That

being said, even if GA flight data is secured, it is difficult to extract accurate information because of inherent noise in the flight data collected by an app or other recording devices. Therefore, ensuring clean and tidy flight data that is ready to be analyzed is crucial in the use of that data in aircraft safety assessment work. In other words, it is essential to be able to "clean up" recorded flight data in order to develop performance models using voluntarily self-recorded flight data and also perform retrospective flight safety analysis.

While various types of noise filtering methods have been introduced in the data analytics fields, the inherent characteristics of data noise in different types of data parameters have not been examined thoroughly. To be more specific, there is no explicit information whether a certain noise filtering method performs better with a specific type of data parameters. Therefore, the focus of this study is an examination of the effects of different filtering methods applied to each data parameters which are measured in different measuring method. The benefits of noise filtering method and flight data-driven safety analysis can be maximized by answering research question 2. Based on the research question, the following hypothesis for research question 1 is as follows.

Research Question 2

What kind of noise filtering techniques or data cleaning methods are suitable for effectively detecting and removing existing noise in flight data while preserving true aircraft behaviors?

Hypothesis 2

Specific flight parameters require noise removal techniques that can capture the characteristics of the parameters. Applying a filtering method that is identified considering inherent noise characteristics to corresponding parameters will ensure the necessary level of filtering result.

3.2.3 Flight Safety Assessment

As discussed earlier, in aircraft operational safety analysis, it is important to have precise information about the aircraft performance. The true aircraft performance information can be estimated using an accurate aircraft performance model and reliable flight data. The two components are the most important sources of the aircraft performance information because they can be used to predict or analyze the behavior of an aircraft and the flight capabilities of an aircraft.

For assessing the flight capabilities of an aircraft, flight envelopes provide meaningful information about operational limits of the aircraft. Thus, by looking at the aircraft behavior in those flight envelopes, we can determine if certain flight operation is dangerous so that a pilot must avoid that kind of operation. Although POH is the official flight manual which contains proven performance data in certain conditions and publicly available primary source of that performance information, POH has some limitations that can hamper performance envelope identification. For example, most speeds in POH are not cited for various gross weights and density altitudes. Moreover, the rate of climb and best glide information are only for one gross weight. In addition to the drawbacks mentioned above, there are many other limitations of POH performance data. Thus, identifying more flexible operational limits or flight envelopes of an aircraft strategically using actual flight data has to be an essential step during flight safety assessment efforts.

Moreover, detecting unsafe events of flight requires consideration of not only the predefined flight envelopes but also frequency and likelihood of that events. In this safety assessment process, quantitative safety metrics are required that can indicate both aircraft performance characteristics and abnormality of the flight. Statistical data analysis method using enough number of sample flights can support this quantitative safety evaluation process.

Therefore, this research will address the following research questions and proposes an effective way of assessing operational performance safety of an aircraft by answering the following questions. The requirements as mentioned earlier can be satisfied by answering the research questions shown below and proving the following hypothesis can support the answer.

Research Question 3

How can flight performance safety of a fixed-wing GA aircraft be analyzed using a synthesis of an accurate aerodynamic performance model and clean flight data?

- How can operational performance limits or flight envelopes for a fixed-wing GA aircraft be identified using performance models and flight data?
- How can the generated performance envelopes be used for quantitatively judging or determining that an aircraft is in a dangerous or safe state?

Hypothesis 3

Using a synthesis of a realistic aircraft performance model and clean flight data will reduce the chance of misidentifying or failing to identify abnormal flight operations.

3.3 Research Scope

3.3.1 Fixed-Wing General Aviation Aircraft

Among various types of GA aircraft, Cessna Skyhawk (C172S) aircraft is selected for providing answers to the research questions stated in the previous section. One of the main reason why this aircraft can be a good sample aircraft for this study is that C172 is the most

popular fixed-wing propeller-driven aircraft consistently in the GA community. According to NASA statistics, the C172 aircraft accounted for 13.5% of all aircraft, and it is the largest number of aircraft models in 1999 [51]. In 2017, 129 airplanes are shipped by manufacturer worldwide for the C172S aircraft, and it is the highest number in the year among other comparable piston-engine fixed-wing aircraft [2]. Another reason is that C172S belongs to the aircraft type that has been most frequently contributing to the GA accident records. AOPA's study has shown that non-commercial fixed-wing GA flights were responsible for 82% of all the GA accidents in 2014, and more than 70% of the accident aircraft were single-engine fixed-gear (SEF), including 60% of those involved in fatal accidents [52]. Also, personal flights resulted in 76.1% of the GA accidents in 2014 and 82.5% of fatal accidents. Table 3.1 and Table 3.2 show the statistics in detail. For this reason, the Cessna C172S model is the most suitable GA aircraft for achieving the goal of this study. The example picture of C172S and its three-view are shown in Figure 3.2 and Figure 3.3.

Figure 3.2: Cessna Skayhawk (C172S) [53]

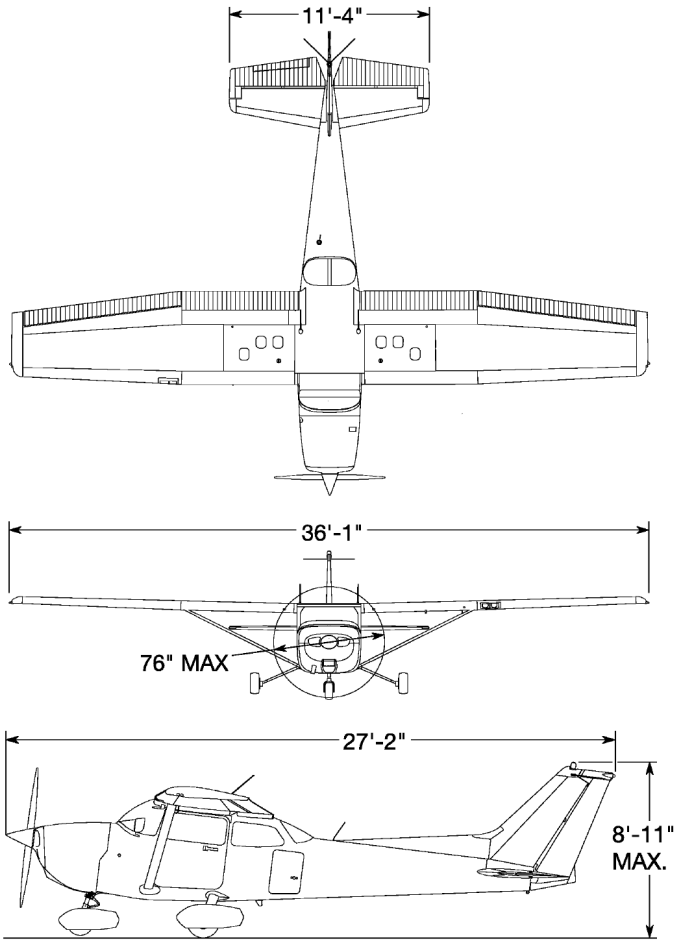

Figure 3.3: Cessna Skayhawk (C172S) Three-View (Normal Ground Attitude) [54]

Table 3.1: General Aviation Accidents in 2014 [52]

	Non-Commercial		**Commercial**	
	Fixed-Wing	**Helicopter**	**Fixed-Wing**	**Helicopter**
Number of Accidents	952	108	68	36
Number of Aircraft	959	108	68	36
Number of Fatal Accidents	196	14	11	8
Lethality (percent)	20.6	13.0	16.2	22.2
Fatalities	300	24	17	13

Table 3.2: GA Accidents: Type of Operation [52]

Type of Operation	Accidents		Fatal Accidents		Fatalities	
Personal	730	76.1%	165	82.5%	246	82.0%
Instructional	132	13.8%	17	8.5%	32	10.7%
Public Use	8	0.8%	1	0.5%	1	0.3%
Positioning	16	1.7%	4	2.0%	4	1.3%
Aerial Observation	5	0.5%	2	1.0%	2	0.7%
Business	22	2.3%	2	1.0%	2	0.7%
Executive / Corporate	1	0.1%	0	0.0%	0	0.0%
Other Work Use	25	2.6%	4	2.0%	5	v1.7%
Other or Unknown	20	2.1%	5	2.5%	8	2.7%

3.3.2 Phases of Flight

The final stage of this study is to evaluate the operational safety of the flight using the flight data records. The flight data is a record of all the data parameters from the start of the flight until landing, and each flight contains multiple phases of flight. As discussed earlier, approach and landing phases of flight are considered as one of the most riskiest flight. According to the AOPA's report, pilot-related causes consistently account for about 75 percent of non-commercial fixed-wing accidents [52], and landing related accidents are the most frequent accidents as described in Figure 3.4. Although various safety enhancement effort for these risky phases of flight have been performed by many safety programs, GA operations have a lot of variabilities during these phases and safety performance of an aircraft needs to be properly measured. Thus, this study focuses on quantifying GA operation safety during approach and landing phase for improving flight safety of GA fixed-wing aircraft because this final phase of flight is often considered as one of the most dangerous parts during flight.

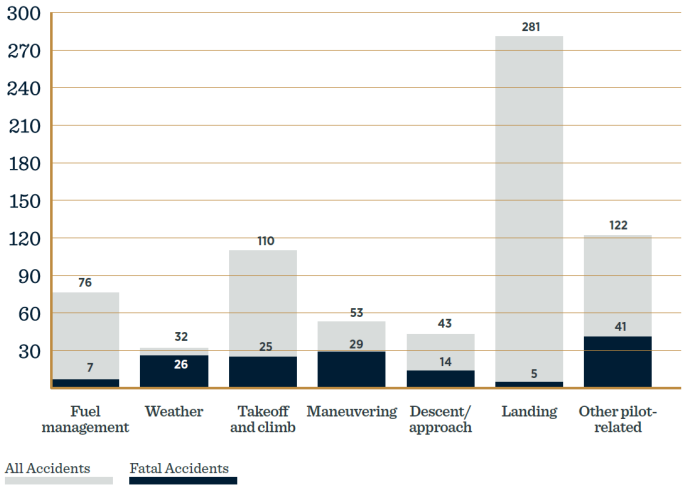

Figure 3.4: Types of Pilot-Related GA Accidents [52]

3.3.3 Flight Data

As explained in the previous sections, flight data takes the critical role in this research. Thus, obtaining real flight data records is the most important requirement of this work. For this study, more than 1,500 training or regular flight data records flown by C172S aircraft are acquired with the help of a flight school. These records are for research purpose only and have been provided without any detailed information such as the tail number or the name of the pilot or student. The flight data parameters in the records are time series data which are logged in Garmin G1000 data recorder format. The logged data contains basic aircraft state information as well as basic position, speed, GPS data, and so on. The parameters recorded by the G1000 system are listed in Table 3.3. In this study, a subset of the logged parameters are selected and they are considered as a raw data set. Using these raw data parameters, These flight data records are the main source of this study and will be used for data-driven aerodynamic performance model development, the data noise removal process, and GA operational safety assessment.

Table 3.3: The List of Data Parameters in G1000 Logging System [55]

Date	Longitude (degrees; geodetic; +East)	GPS fix
Time	Magnetic Heading (degrees)	GPS horizontal alert limit
GPS altitude (MSL)	HSI source	GPS vertical alert limit
GPS altitude (WGS84 datum)	Selected course	SBAS GPS horizontal protection level
Baro-Corrected altitude (feet)	Com1/Com2 frequency	SBAS GPS vertical protection level
Baro Correction (in/Hg)	Nav1/Nav2 frequency	Fuel Qty (right & left)(gals)
Indicated airspeed (kts)	CDI deflection	Fuel Flow (gph)
Vertical speed (fpm)	VDI/GP/GS deflection	Fuel Pressure (psi)
GPS vertical speed (fpm)	Wind Direction (degrees)	Voltage 1 and/or 2
OAT (degrees C)	Wind Speed (knots)	Amps 1 and/or 2
True airspeed (knots)	Active Waypoint Identifier	Engine RPM
Pitch Attitude Angle (degrees)	Distance to next waypoint (nm)	Oil Pressure (psi)
Roll Attitude Angle (degrees)	Bearing to next waypoint (degrees)	Oil Temperature (deg. F)
Lateral and Vertical G Force (g)	Magnetic variation (degrees)	TIT (deg. F)
Ground Speed (kts)	Autopilot On/Off	Manifold Pressure (in. Hg)
Ground Track (degrees magnetic)	AFCS roll/pitch modes	CHT
Latitude (degrees; geodetic; +North)	AFCS roll/pitch commands	EGT

CHAPTER 4

AERODYNAMIC PERFORMANCE MODEL DEVELOPMENT

This chapter explains the developed flexible aerodynamic modeling methodology that can provide a solution to the first research question formulated in the previous chapter. The first section in this chapter provides an overview of the aerodynamic modeling methodology which consists of the physics-based modeling process and data-driven modeling process. Then, the suggested aerodynamic modeling process is described in detail in the following section. Finally, the experiment which provides answers to the research questions is elaborated with the modeling result.

4.1 Methodology Development

4.1.1 Overview

The primary purpose of this aerodynamic modeling methodology development for a fixed-wing GA aircraft is to ensure that the obtained aerodynamic model is flexible enough to capture the aerodynamic performance characteristics of an aircraft with high fidelity and affordable modeling efforts. To accomplish this goal, this chapter aims to provide a methodology for successfully answering the research question below which was formulated in the previous chapter.

Research Question 1

What is a more effective way of developing an aerodynamic model that has a necessary level of fidelity to adequately predict aerodynamic performance and capture unsafe aerodynamic behaviors of a fixed-wing GA aircraft?

As the first step toward answering the question, an aerodynamic model will be developed starting with the lowest fidelity method then increase its fidelity by introducing actual flight data into the modeling process. Among various aerodynamic performance modeling methods introduced in the previous chapters, selecting an accurate as well as the computationally affordable aerodynamic model is the main goal of this proposed method. In the beginning, this study first uses a physics-based modeling approach to develop a theoretical model that will be used as a basis for the next data-driven modeling process. For developing a theoretical aerodynamic model, several aerodynamic modeling and calibration methods are surveyed, examined, and compared in this study. Then, an aerodynamic model will be established in multiple flap settings and validated against not only the data published in reliable sources such as the pilots operating handbook, historical data, and wind tunnel experiment but also the best combination of the sources.

Next, this study will develop a data-driven modeling method that improves accuracy and flexibility of the previously obtained theoretical aerodynamic model using actual flight data which is strategically generated and collected for this modeling process. This study suggests several simple flight maneuvers with different flap activities for generating a set of reference flight data which will be used for improving the fidelity of the developed theoretical aerodynamic model. Using the reference flight data record from the sample flight maneuvers, this study will develop a data-driven aerodynamic model by determining the optimized set of shape modification factors that can alter the shape of the lift curve and the drag polar of the aerodynamic model.

Finally, the fidelity of the aerodynamic model will be evaluated to see if this model meets the pre-defined requirements for the model fidelity. The requirement for an acceptable model fidelity is that the aerodynamic model has to be able to capture the aerodynamic performance variance caused by different flap settings. The fidelity of the obtained aerodynamic model will be evaluated and tested in the last section of this chapter. The overall process flow of the proposed aerodynamic modeling method is described in Figure 4.1. As

shown in the flowchart, the final outcome of this modeling process is a data-driven aerodynamic model for a fixed-wing GA aircraft, which is C172S aircraft in this research scope. It is important to note that the proposed flexible aerodynamic modeling method in this study is applicable to any other aircraft models.

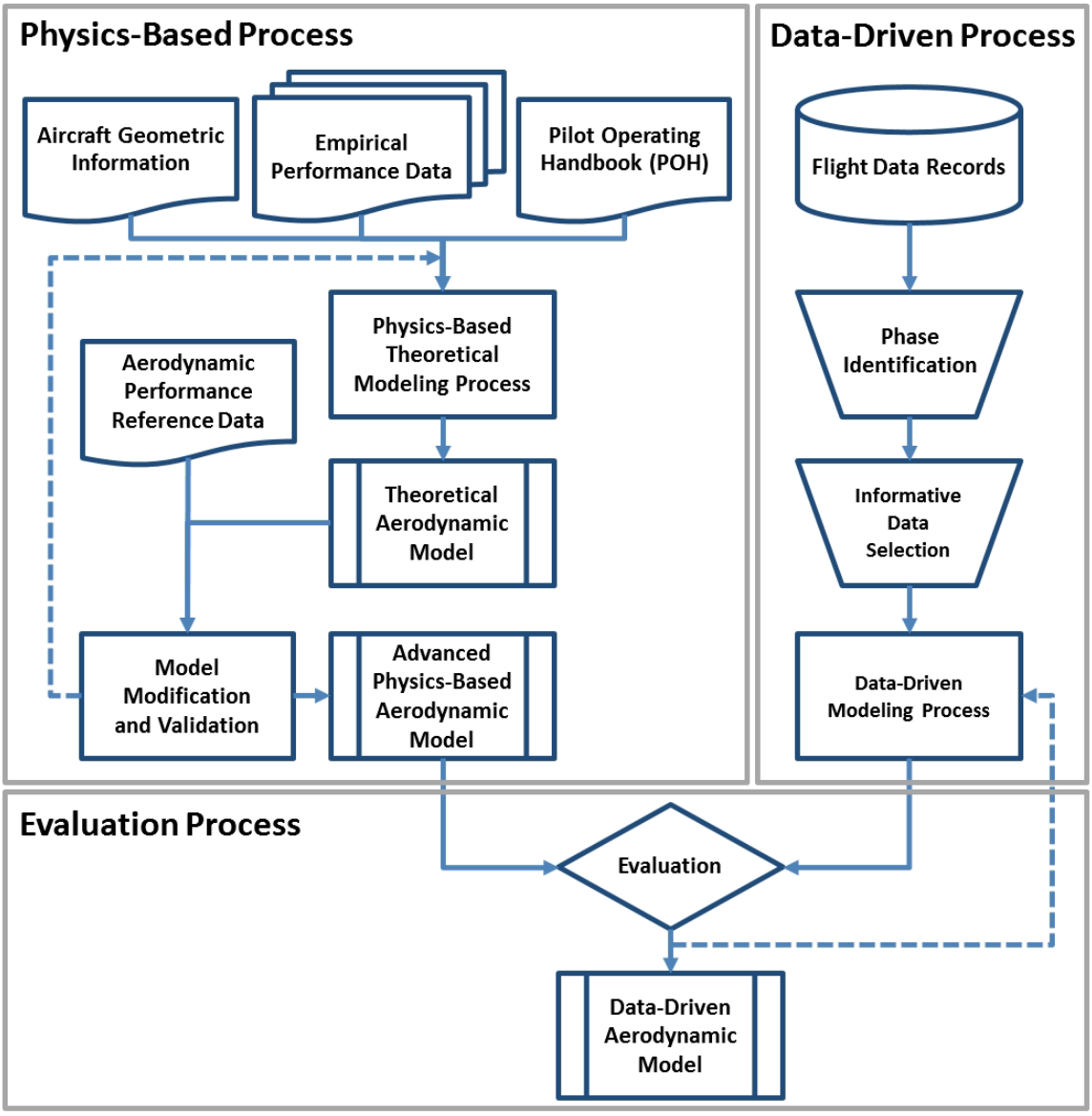

Figure 4.1: Overview of Aerodynamic Modeling Process

4.1.2 Experiment Setup

Ultimately, this aerodynamic performance model is for evaluating GA operational safety. For this purpose, the following hypothesis for the first research question is established in the previous chapter. Thus, the rest of this chapter is mainly about proving the hypothesis to answer the first research question and to achieve the research goal.

Hypothesis 1

An aerodynamic model that is accurate enough to estimate flap usage during flight can capture unsafe behaviors of a fixed-wing GA aircraft, and the necessary accuracy can be achieved with the combination of a theoretical model and flight data.

Given the hypothesis stated above, the fidelity of the developed aerodynamic model will be tested to examine if this model is credible enough to capture the aircraft's flap activity during the flight. Although the flap setting is the most important factor in predicting the aerodynamic performance of an aircraft, most of the GA aircraft do not have flap activity record during flight. Therefore, the criterion for determining the accuracy of the aerodynamic model to be developed in this study is that the model is able to predict flap activity using given flight data parameters. The flight data record provides sufficient information of angle-of-attack (AOA) during the flight, and the aerodynamic coefficient can be obtained by inputting the AOA into the aerodynamic model. The aerodynamic model will output lift and drag coefficients for different flap settings which will be compared to the data-driven lift and drag coefficients. These data-driven aerodynamic coefficients are calculated using the following Equation 4.1 and Equation 4.2 assuming that aircraft weight is known and the thrust information is given by the propulsion model of the C172S aircraft. The data parameters other than the aircraft weight and thrust can be provided by the flight record.

This equations and parameters will be explained in detail in the following chapter.

$$L = W\cos\theta_w\cos\phi_w - \frac{W}{g}V_{abs}q_w \tag{4.1}$$

$$D = T - W\sin\theta_w - \frac{W}{g}\dot{V}_{abs} \tag{4.2}$$

Once the desired fidelity of the aerodynamic model is achieved, the model will be used to detect unsafe flight behavior of the aircraft. Among many unsafe flight maneuvers, a stall is the most representative unsafe flight maneuver and this research will test whether a stall behavior can be detected using this aerodynamic model.

4.2 Advanced Physics-Based Model

4.2.1 Overview

Aerodynamic modeling for aircraft performance consists of two main parts: lift-curve modeling and drag polar modeling. Figure 4.2 shows the typical shapes of lift curve and drag polar of a fixed-wing aircraft. The lift-curve model is used for predicting variation in the lift coefficient with a change in the angle of attack, and the drag polar model provides the relationship between the lift of an aircraft and its drag. In this modeling process, various theoretical aerodynamic modeling methods for estimating the aerodynamic performance of an aircraft using the key aerodynamic parameter were surveyed and explained. The final outcome of this modeling process will be lift curve and drag polar for clean configuration and three different flap-down configurations of C172S aircraft. Figure 4.3 describes the scope of this aerodynamic modeling process.

Lift Curve Modeling

An aerodynamic model (a lift-curve) that provides the fully defined relationship between the lift coefficient and the angle of attack for an aircraft was created by evaluating in

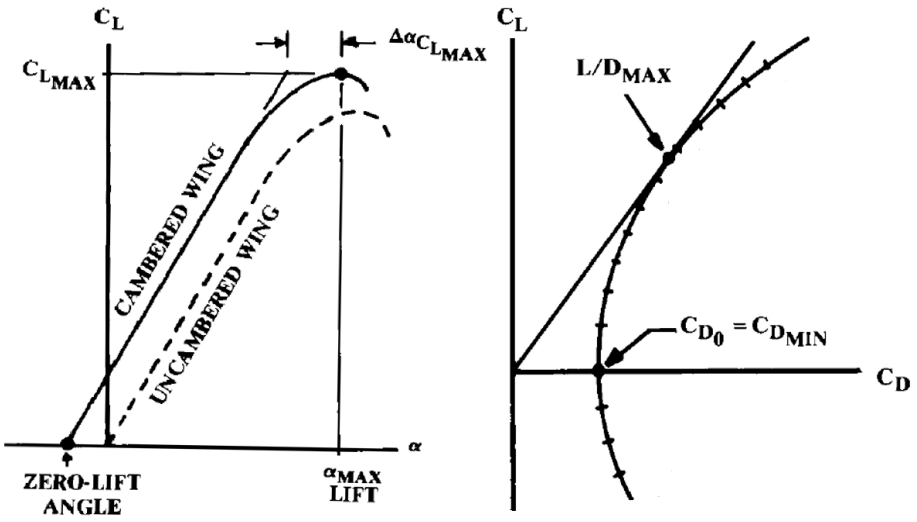

Figure 4.2: Generic Lift Curve and Drag Polar [44]

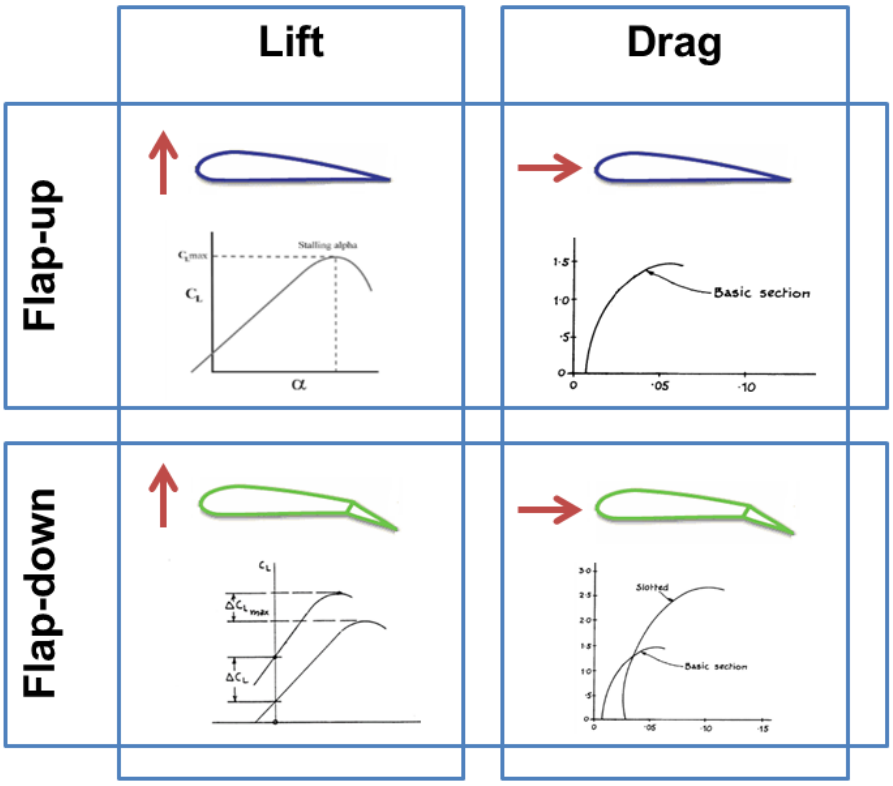

Figure 4.3: Aerodynamic Modeling Scope

three stages that include all the aspects of the aircraft: the 2-D wing airfoil, the 3-D wing, including the 3-D effect, and complete aircraft. The lift curve for each stage that governs the shape of the curve is defined by five parameters: the zero-lift angle of attack, the lift-curve slope, the angle of attack limit for a linear range, the angle of attack for the maximum lift coefficient, and the maximum lift coefficient [42]. Figure 4.4 show how these parameters define the lift curve for the aerodynamic modeling stage of the complete aircraft. Creating the linear range of the lift curve using zero the lift angle of attack, the lift-curve slope, and the angle of attack limit for the linear range is straightforward. In other words, the lift curve can be expressed by a simple straight-line equation. The non-linear part near the stall point can be modeled using a quadratic equation, and it can be defined by the lift-curve slope, the angle of attack for the maximum lift coefficient, and the maximum lift coefficient given a requirement that the slope of the linear and nonlinear parts $(dC_L/d\alpha)$ is identical where the two parts meet. The combination of these two equations of the linear and non-linear area completes basic lift performance modeling for an aircraft in a clean configuration.

When an aircraft is required to use high lift devices in a specific operation such as takeoff or landing operation, the lift characteristics change because of the effect of high-lift device deployment. This effect causes a lift increment, a lift-curve slope change, and a maximum lift coefficient increment [42]. Figure 4.5 notionally describes how the lift-curve varies in flaps-deployed configuration. The amount of the lift increment or the slope change depends on the amount of flap deflection.

Drag Polar Modeling

The drag polar is the aerodynamic characteristic that is most relevant for modeling or assessing the aircraft's performance capabilities/characteristics. The drag coefficient can be presented as a function of the angle of attack, but another effective plot that can provide the aerodynamic performance of an aircraft is the drag polar, which shows the drag coefficient as a function of the lift coefficient. The drag polar of an aircraft contains

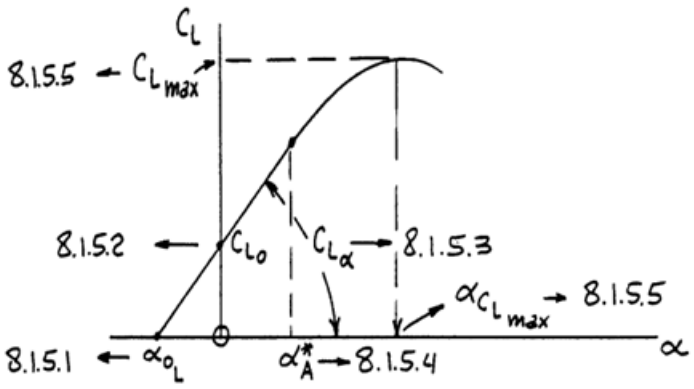

Figure 4.4: Construction of Aircraft Lift-Curve [42]

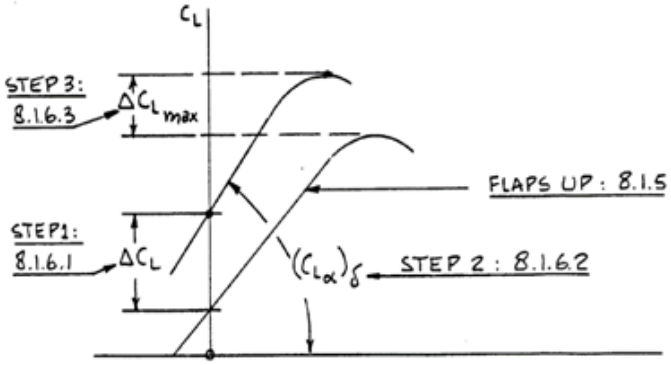

Figure 4.5: Construction of Aircraft Lift-Curve with Flap Down [42]

almost all information required for analyzing its aerodynamic performance. Aircraft drag is mainly composed of parasite drag and induced drag. Equation 4.3 is a general expression of drag coefficient for an aircraft in a clean configuration with a parasite drag term and an induced drag term [43]. Parasite drag, also called zero-lift drag, consists of mostly skin-friction drag and small separation pressure drag [44]. Induced drag is drag resulting from the lift that is proportional to the square of the lift coefficient with a proportionality factor K, shown in Equation 4.3. The skin-friction method and the component buildup method [44] are methods for parasite drag estimation. In addition, induced drag factor K can be estimated by the Oswald span efficiency method and the leading-edge suction method [44]. A detailed description of each estimation method for parasite drag and induced drag will

be provided in the next subsequent sections.

$$C_D = C_{D_{min}} + \frac{{C_L}^2}{\pi ARe} = C_{D_{min}} + K{C_L}^2 \tag{4.3}$$

$$\Delta C_{D_{flap}} = \Delta C_{D_p} + \Delta C_{D_i} + \Delta C_{D_{int}} \tag{4.4}$$

During flight, drag characteristic, as well as lift characteristic, is highly dependent on the flap deployment of an aircraft. The drag increment can be estimated from the sum of the flap profile drag increment, the induced drag increment, and the interference drag increment [42]. The total aircraft drag coefficient in the flap-down condition can be expressed as the sum of the drag coefficient of a clean configuration aircraft and drag coefficient increment caused by the flap deflection. For flap-deployed configuration, the drag increment caused by deflected flap can be estimated using Equation 4.4, where $\Delta C_{D_{flap}}$ is total drag change and ΔC_{Dp}, ΔC_{Di}, and ΔC_{Dint} are parasite, induced, and interference drag change respectively.

4.2.2 Lift Curve Construction

Zero Lift Angle-of-Attack

Zero Lift Angle-of-Attack is the angle of attack at which the lift coefficient is zero.

• *2-D Airfoil*

Airfoil databases or airfoil performance analysis tools provide the aerodynamic performance of a specific airfoil. A NASA technical report titled "Summary of Airfoil Data" [56] contains a vast collection of airfoil experimental data and aerodynamic characteristics of various airfoils. Whenever possible, one study recommended using actual airfoil experimental data or numerical analysis data to find the zero lift angle of attack of an airfoil [42]. If such data are not available, the zero lift angle of attack can be calculated using Equation

4.5, suggested by the United States Air Force Stability and Control Digital DATCOM [57]. Factor k is an empirical factor that depends on the airfoil series. In Equation 4.5, C_{l_i} is the design lift coefficient and α_i is the angle of attack for the design lift coefficient. Reference [57] provides design lift coefficients and the angle of attack for the coefficients in tabular form.

$$\alpha_{0l} = k(\alpha_i - \frac{57.3}{2\pi} C_{l_i}) \tag{4.5}$$

• *3-D Wing*

In terms of the aerodynamic performance of a 3-D wing, wing geometry such as the aspect ratio, the sweep angle, the taper ratio, and the incidence angle has a significant effect on aerodynamic performance. For wings with constant airfoil sections and linear twist distributions, the wing zero lift angle of attack can be estimated from Roskam's equation, Equation 4.6 [42], which requires the airfoil lift-curve slope, also obtained above. In addition, the twist angle and the change in the angle of attack caused by the wing twist are used to estimate the zero lift angle of attack of a wing. A book written by Snorri Gudmundsson suggests another method using the zero lift angle of attack of an airfoil for that of 3-D wing [58].

$$\alpha_{0L_W} = \left\{ \alpha_{0l} + \left(\frac{\Delta\alpha_0}{\varepsilon_t} \right) \varepsilon_t \right\} \left\{ \frac{(\alpha_{0l})_{atM}}{(\alpha_{0l})_{atM=0.3}} \right\} \tag{4.6}$$

• *Complete Aircraft*

The zero lift angle of attack of a complete aircraft in a clean configuration can be estimated from Equation 4.7 using the zero angle of attack lift coefficient and the slope of the aircraft lift curve, which need to be obtained before this step. To find the zero lift angle of attack for an entire aircraft, one must first define the lift coefficient at the zero angle of attack. Obtaining this lift coefficient first is a small difference between the first and

second stage procedures. The lift coefficient at the zero angle of attack can be estimated from Equation 4.8. The variable ε_{0_h} is the horizontal tail downwash angle for the zero aircraft angle of attack. Setting this value zero is typically acceptable according to reference [42]. Variables iW and ih are the incidence angle of the wing and the horizontal tail, respectively. Finally, $C_{L_{0_{Wf}}}$ is the wing-fuselage interference factor, which depends on the fuselage geometry.

$$\alpha_{0L_A} = -\frac{C_{L_{0A}}}{C_{L_{\alpha A}}} \tag{4.7}$$

$$C_{L_{0_A}} = C_{L_{0_{Wf}}} + C_{L_{\alpha_h}} \eta_h \frac{S_h}{S} \left(i_h - \varepsilon_{0_h}\right) \tag{4.8}$$

Lift-Curve Slope

Lift-Curve Slope defines the slope of the straight line in the linear range of the curve.

• *2-D Airfoil*

The lift-curve slope of an airfoil can be obtained from airfoil databases or technical reports. Actual airfoil data should be used for determining the slope whenever these data are available. Equation 4.9 in the DATCOM method [57] provides a way of estimating the airfoil lift curve for arbitrary airfoils. Here, $(C_{l_\alpha})_{theory}$ is the theoretical airfoil section lift-curve slope, which has been presented as a function of only the airfoil thickness ratio. The ratio of C_{l_α} to $(C_{l_\alpha})_{theory}$ is an empirical correction factor that accounts for the development of the boundary layer that extends to the airfoil trailing edge. β is the Prandtl-Glauert compressibility correction factor.

$$C_{l_\alpha} = \frac{1.05}{\beta} \left(\frac{C_{l_\alpha}}{(C_{l_\alpha})_{theory}} \right) (C_{l_\alpha})_{theory} \tag{4.9}$$

• *3-D Wing*

The lift-curve slope of a 3-D wing can be estimated using Equation 4.10. This equation is accurate up to the drag-divergent Mach number and reasonably accurate up to Mach 1 for a swept wing [44][42][58]. In this equation, AR is the wing aspect ratio, β is the Prandtl-Glauert correction factor, κ is the ratio of the two-dimensional lift-curve slope to 2π, and $\Lambda_{C/2}$ is the sweepback of the mid-chord of the wing. John Anderson suggests a slightly different equation shown in the Equation 4.11 [43]. This equation, Helmbold's equation, is accurate for wings with an aspect ratio smaller than four and in the incompressible air condition.

$$C_{L_{\alpha_W}} = \frac{2\pi AR}{2 + \sqrt{(\frac{AR\beta}{\kappa})^2(1 + \frac{(\tan\Lambda_{C/2})^2}{\beta^2}) + 4}} \tag{4.10}$$

$$C_{L_{\alpha_W}} = \frac{C_{l_\alpha}}{\sqrt{1 + \frac{C_{l_\alpha}}{(\pi AR)^2}} + \frac{C_{l_\alpha}}{\pi AR}} \tag{4.11}$$

• *Complete Aircraft*

The first method for estimating the lift-curve slope for a complete aircraft clean configuration is shown in Equation 4.12 [42]. Wing-fuselage lift-curve slope $C_{L_{\alpha_{wf}}}$ is estimated using the wing-fuselage interference factor and the clean wing lift-curve slope. η_h is the dynamic pressure ratio of the horizontal tail, and $d\eta/d\alpha$ is the downwash gradient at the horizontal tail. Another expression for the complete aircraft lift-curve slope is given in Equation 4.13 [58]. This equation is similar to Equation 4.12 but uses the wing lift-curve slope instead of the wing-fuselage lift-curve slope and the dynamic pressure ratio. Equation 4.14 is a semi-empirical formula for a complete aircraft lift-curve slope [44]. This lift-curve slope can be estimated from the exposed wing planform area and fuselage lift factor F, which accounts for the fact that the fuselage creates some lift caused by a spillover of

lift from the wing.

$$C_{L_{\alpha_A}} = C_{L_{\alpha_{Wf}}} + C_{L_{\alpha_h}} \eta_h \left(\frac{S_h}{S}\right)\left(1 - \left(\frac{d\varepsilon}{d\alpha}\right)\right) \tag{4.12}$$

$$C_{L_{\alpha_A}} = C_{L_{\alpha_W}} + C_{L_{\alpha_h}} \left(\frac{S_h}{S}\right)\left(1 - \left(\frac{d\varepsilon}{d\alpha}\right)\right) \tag{4.13}$$

$$C_{L_{\alpha_A}} = C_{L_{\alpha_W}} \left(\frac{S_{exposed}}{S_{ref}}\right) F \tag{4.14}$$

Linearity Limit Angle

Linearity Limit Angle is the angle-of-attack limit for the linear range, which means that this angle is the upper limit of the linear range of the lift curve. After this angle, the lift coefficient does not increase proportionally to angle-of-attack.

• *2-D Airfoil*

This angle of attack should be obtained from experimental data. Additionally, Roskam provides a summary of basic airfoil data [42]. The airfoil lift-curve plot from other airfoil data sources can be used to determine the point at which the graph starts to lose its linearity. The Engineering Sciences Data Unit (ESDU) suggests a method of estimating the angle of attack limit for an arbitrary airfoil [59]. Equation 4.15 shown below defines the linearity limit with the information for the maximum sectional lift coefficient and the lift-curve slope.

$$\alpha^* = \alpha_0 + \frac{C_{l_{max}} - 0.3}{C_{l_\alpha}} \left(\frac{180}{\pi}\right) \tag{4.15}$$

• *3-D Wing*

Estimating the angle of attack at which the lift-curve deviates from linear variation for a wing cannot be accomplished by a specific method. However, using the angle of attack

linear limit of an airfoil instead of that of a 3-D wing, which was found in the previous stage, is acceptable in a preliminary design [42].

• *Complete Aircraft*

The angle of attack limit for the linear lift curve range of an aircraft can be expressed as Equation 4.16 , where i_W is the incidence angle of the wing [42]. This equation is often acceptable in the preliminary design stage.

$$\alpha_A^* = \alpha_W^* - i_W \tag{4.16}$$

Angle-of-Attack for the Maximum Lift Coefficient

Angle-of-Attack for the Maximum Lift Coefficient is the angle at which the maximum lift coefficient occurs. This angle is known as the stall angle because stall occurs beyond this angle.

• *2-D Airfoil*

This information is an essential characteristic of an airfoil because it is the point at which stall occurs. Thus, this value should be found in the airfoil database or other aerodynamic sources. Also, this angle can be found in a lift curve graph obtained from experiments. ESDU proposes an equation that can define the angle of attack for the maximum lift coefficient using the lift curve slope and the linear range limit of an airfoil [59], as shown in Equation 4.17.

$$\alpha_{C_{l_{max}}} = \alpha^* + \frac{0.39}{C_{l_\alpha}} \left(\frac{180}{\pi} \right) \tag{4.17}$$

• *3-D Wing*

The angle of attack at which maximum lift coefficient is located can be calculated using Equation 4.18, which is from DATCOM method 2 [57]. $C_{L_{(\alpha_W}}$ is the wing lift curve slope obtained in the previous step, $C_{L_{max_W}}$ the maximum lift coefficient of a wing, α_{0L_W} the wing zero lift angle, and $\Delta\alpha_{stall}$ the angle of attack increment factor, a function of the leading edge parameter and the leading edge sweep angle.

$$(\alpha_{C_{Lmax}})_W = \frac{C_{L_{max_W}}}{C_{L_{\alpha_W}}} + \alpha_{0L_W} + \Delta\alpha_{stall} \tag{4.18}$$

• *Complete Aircraft*

The angle of attack for the maximum lift coefficient of an aircraft can be estimated from Equation 4.19 [42]. $\Delta\alpha_{W/C}$ is the difference between the angles of attack for a carnard stall and for the wing stall of a complete aircraft. This term can be neglected for the aircraft without a carnard wing.

$$(\alpha_{C_{Lmax}})_A = (\alpha_{C_{Lmax}})_W - i_W - \Delta\alpha_{W/C} \tag{4.19}$$

Maximum lift coefficient

The maximum lift coefficient is the highest lift coefficient of the airfoil, the wing, and the aircraft without high lift devices.

• *2-D Airfoil*

The maximum lift coefficient can be obtained from an airfoil database or experimental data and estimated. The airfoil maximum lift coefficient depends on the following parameters[42][57]:

- The leading edge shape quantified by the Δy parameter

- The maximum thickness and the position of the maximum thickness
- The maximum camber and the position of the maximum camber
- The Reynold's number
- The Mach number

Given information about the parameters, we can estimate the maximum lift coefficient of an airfoil by adding the camber, the thickness, the Reynold's number, the airfoil roughness, and the Mach number effect to the basic airfoil maximum lift coefficient, which is a function of the airfoil geometry, as shown in Equations 4.20[42][57].

$$C_{l_{max}} = C_{l_{max_{base}}} + C_{l_{max_{camber}}} + C_{l_{max_{thickness}}} + C_{l_{max_{Reynolds}}} + C_{l_{max_{roughness}}} + C_{l_{max_{Mach}}} \tag{4.20}$$

• *3-D Wing*

The subsonic maximum lift coefficient for an untwisted-, constant-section, a high aspect-ratio wing can be estimated using the expression below [57]. The ratio of the maximum lift coefficient of the wing to that of the airfoil, the Mach number correction factor, and $\Delta C_{L_{max_W}}$ are obtained from a data plot, a function of the Mach number and the leading edge shape factor. The sectional maximum lift coefficient, estimated above, is used in Equation 4.21.

$$C_{L_{max_W}} = \frac{C_{L_{max_W}}}{C_{l_{max}}} C_{l_{max}} + \Delta C_{L_{max_W}} \tag{4.21}$$

• *Complete Aircraft*

The maximum lift coefficient of an aircraft can be calculated from Equation 4.22[42]. In this equation, most of the terms, except the horizontal tail downwash angle for the zero

angle of attack for an aircraft, ε_{0_h}, are obtained from the previous steps. Reference [42] indicates that using zero for that angle is acceptable for this parameter.

$$C_{L_{max_A}} = C_{L_{max_W}} - C_{L_{\alpha_{Wf}}} \Delta\alpha_{W/C} + C_{L_{\alpha_h}} \left(\frac{s_h}{s}\right) \left\{ \left(\alpha_{C_{L_{max}}}\right)_A \left(1 - \frac{d\varepsilon}{d\alpha} - \varepsilon_{0_h}\right) + i_h \right\} \tag{4.22}$$

Lift with Flaps Down

The way to estimate the effect of high lift device deployment highly depends on the types of lift device. There are various types of trailing edge flaps and leading edge flaps, and the aerodynamic modeling method for each type of device is explained in [42]. In this study, single-slotted flap type is chosen to estimate the aerodynamic effect on the performance model. The main effects of flaps are lift increment, lift-curve slope change, and maximum lift coefficient increment. Each effect needs to be calculated separately in three different stages: 2-D airfoil, 3-D wing, and complete aircraft level.

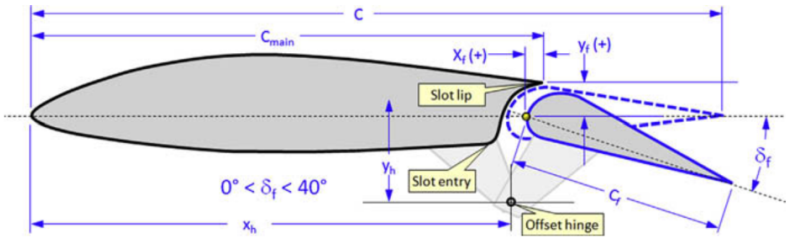

Figure 4.6: Schematic of the Single Slotted Flap [58]

• *Lift Increment*

The airfoil incremental lift coefficient due to single-slotted flap deflection, ΔC_l is obtained using Equation 4.23 [42]. The airfoil lift-curve slope, C_{l_a} is from previous flap-up lift-curve. α_δ and δ_f is the airfoil lift effectiveness parameter and flap deflection, respectively.

The wing lift increment can be estimated from Equation 4.24 [42], where k_b is the flap-span factor and $\alpha_{\delta_{C_L}}/\delta_{C_l}$ is the ratio of the 3-D flap-effectiveness parameter to the 2-D flap-effectiveness parameter, which is a function of aspect ratio and flap-chord ratio. The aircraft lift increment due to flap deflection can be obtained from Equation 4.25 [42]. k_{wh} is the wing-on-horizontal-tail interference factor and it is acceptable to use a value of one in early design. $\Delta\varepsilon_f$ is the increase in tail downwash angle due to wing flap deflection.

$$\Delta C_l = C_{l_\alpha}\alpha_\delta\delta_f \tag{4.23}$$

$$\Delta C_{L_W} = k_b\Delta C_l\left(\frac{C_{L_{\alpha_W}}}{C_{l_\alpha}}\right)\left(\frac{\alpha_{\delta_{C_L}}}{\delta_{C_l}}\right) \tag{4.24}$$

$$\Delta C_{L_A} = \Delta C_{L_W} + k_{Wh}\frac{S_h}{S}\Delta C_{L_h} - C_{L_{\alpha_h}}\eta_h\frac{S_h}{S}\Delta\varepsilon_f \tag{4.25}$$

• *Lift-Curve Slope Change*

The flapped airfoil lift-curve slope is changed because the flapped airfoil chord, c' is normally more significant than the unflapped airfoil chord, c. For this reason, the lift-curve slope with flap deflection is given in Equation 4.26. The wing lift curve slope with flap deflection may be shown as Equation 4.27, where S_{W_f} is the flapped wing area. The aircraft lift curve slope with the flap deflection can be estimated using Equation 4.28 [42]. $(d\varepsilon/d\alpha)_\delta$ is the flaps-down downwash gradient at the horizontal tail.

$$(C_{l_\alpha})_\delta = \frac{c'}{c}C_{l_\alpha} \tag{4.26}$$

$$(C_{L_{\alpha_W}})_\delta = C_{L_{\alpha_W}}\left\{1 + \left(\frac{c'}{c} - 1\right)\frac{S_{W_f}}{S}\right\} \tag{4.27}$$

$$(C_{L_{\alpha_A}})_\delta = k_{Wh}(C_{L_{\alpha_W}})_\delta + C_{L_{\alpha_h}}\eta_h\frac{S_h}{S}\left\{1-(\frac{d\varepsilon}{d\alpha})_\delta\right\} \tag{4.28}$$

• *Maximum Lift Coefficient Increment*

The maximum lift coefficient change of an airfoil can be calculated using Equation 4.29. The k's are correction factors which accounts for the flap-chord ratio, flap angle difference, and flap motion. Equation 4.30 is the estimation of the maximum wing incremental lift coefficient due to flaps. k_Δ is a planform correction factor which accounts for the wing sweep effect. The aircraft maximum lift coefficient increment due to flap deflection can be obtained from Equation 4.31 [42]. This estimation method uses the information of previous wing lift increment and horizontal tail aerodynamic and geometric characteristics.

$$\Delta C_{l_{max}} = k_1 k_2 k_3 (\Delta C_{l_{max}})_{base} \tag{4.29}$$

$$\Delta C_{L_{max_W}} = \Delta C_{l_{max}}\frac{S_{W_f}}{S}k_\Delta \tag{4.30}$$

$$\Delta C_{L_{max_A}} = (\Delta C_{L_{max_W}}) + C_{L_{\alpha_h}}\frac{S_h}{S}\left\{(1-\frac{d\varepsilon}{d\alpha}) + i_h - \Delta\varepsilon_f\right\} \tag{4.31}$$

4.2.3 Drag Polar Construction

Parasite Drag (Zero-Lift Drag)

• *Equivalent Skin-Friction Method*

The equivalent skin-friction method is based on the fact that an aircraft in clean configuration will have parasite drag which is mostly skin-friction drag and small separation drag. This method uses the concept of an equivalent skin friction coefficient, C_{f_e} which includes both skin-friction and separation drag. The parasite drag can be estimated by Equation 4.32

[44][42]. S_{wet} is the aircraft total wetted area that is the sum of each component's wetted area.

$$C_{D_0} = C_{D_{min}} = C_{f_e} \left(\frac{S_{wet}}{S_{ref}} \right) \tag{4.32}$$

• *Component Buildup Method*

The component buildup method estimates the subsonic parasite drag of each component using a flat-plate skin-friction drag coefficient, C_f and form factor, FF [44]. The form factor estimates the pressure drag due to viscous separation. Also, the interference effect of the component drag is calculated as a factor, Q. Then the total component drag is obtained using Equation 4.33. $C_{D_{misc}}$ is the drag coefficient which accounts for the additional drag contributions due to aircraft component such as fuselage upsweep. $C_{D_{L\&P}}$ is the drag coefficient that is caused by leakage and protuberance drag.

$$C_{D_0} = C_{D_{min}} = \frac{\sum \left(C_{f_c} F F_c Q_c S_{wet_c} \right)}{S_{ref}} + C_{D_{misc}} + C_{D_{L\&P}} \tag{4.33}$$

• *Extracting Drag from L/D_{max} Information*

The parasite drag coefficient can be estimated using the aircraft performance data such as the best gliding speed. Pilot's operating handbooks (POH) usually provides the best gliding speed. Since the best gliding condition means that the parasite drag is minimum at this point, the parasite drag can be estimated using Equation 4.34 [58]. The maximum lift-to-drag ratio, aspect ratio, Oswald span efficiency factor, and other operating condition such as gliding altitude and gross weight are required for this estimation.

$$C_{D_0} = C_{D_{min}} = \frac{C_{L_{BG}}}{(L/D)_{max}} - \frac{(C_{L_{BG}})^2}{\pi A R e} \tag{4.34}$$

Induced Drag

• *Oswald Span Efficiency Method*

The induced drag of an aircraft is proportional to the square of the lift coefficient with a factor, K, which is expressed as Equation 4.35 [44]. The Oswald efficiency factor, e, is typically between 0.7 and 0.85 and it is the best if the Oswald factor is known for a specific aircraft. Otherwise, it is possible to estimate the Oswald factor, and there are numerous estimation methods for this factor. This factor accounts for the extra drag due to the non-elliptical lift distribution and the flow separation.

$$K = \frac{1}{\pi A R e} \tag{4.35}$$

• *Leading Edge Suction Method*

This method is a semi-empirical method for estimation of K. If there is no viscous separation or induced downwash, it is the ideal case that is called 100% leading-edge suction and Oswald factor, e, is 1 in this case. When e is 1, the K equals the inverse of the aspect ratio times π. On the other hand, when the leading edge suction is 0%, which is the case of a zero-thickness flat-plate airfoil, all pressure forces cause high drag. In this case, the K value is the inverse of the lift-curve slope. The actual K can be estimated using weighting factor S_c as shown in Equation 4.36. For a subsonic wing with large leading-edge radius and moderate sweep, the S_c value is usually between 0.85 and 0.95 [44].

$$K = S_C K_{100} + (1 - S_C) K_0 \tag{4.36}$$

Drag with Flaps Down

The flap deflection will cause additional drag and the drag coefficient due to flap deflection may be expressed as the total sum of flap profile drag increment, induced drag

increment, and interference drag increment [44]. The total aircraft drag coefficient in flaps-down condition is a summation of the clean configuration drag coefficient and this flap drag coefficient. The flap profile drag increment, the induced drag increment, the interference drag increment due to flaps, and the total aircraft drag increment due to flap deflection may be found from the following equations 4.37 $\sim$ 4.40.

$$\Delta C_{D_p} = \Delta C_{d_p} \cos(\Lambda_{c/4}) \left(\frac{S_{wf}}{S} \right) \tag{4.37}$$

$$\Delta C_{D_i} = K^2 \left(\Delta C_{L_{flap}} \right)^2 \cos(\Lambda_{c/4}) \tag{4.38}$$

$$\Delta C_{D_{int}} = K_{int} \Delta C_{D_p} \tag{4.39}$$

$$\Delta C_{D_{flap}} = \Delta C_{D_p} + \Delta C_{D_i} + \Delta C_{D_{int}} \tag{4.40}$$

4.2.4 Result Summary

The previous sections have shown that the five parameters for construction of the lift curve for an aircraft can be obtained from various methods. The sequences of evaluation and the flow of lift-curve shape parameters are summarized and shown in Figure 4.7.

Lift Curve Modeling Result: Flaps Up

• *2-D Airfoil Lift-Curve Parameters*

The five parameters that are required fully construct the lift-curve can be estimated using various methods. However, DATCOM suggest that it is encouraged to use actual wind- tunnel test data if it is available [57]. The C172S aircraft uses NACA2412 airfoil for the main wing [58], and the aerodynamic characteristic of this airfoil are available from

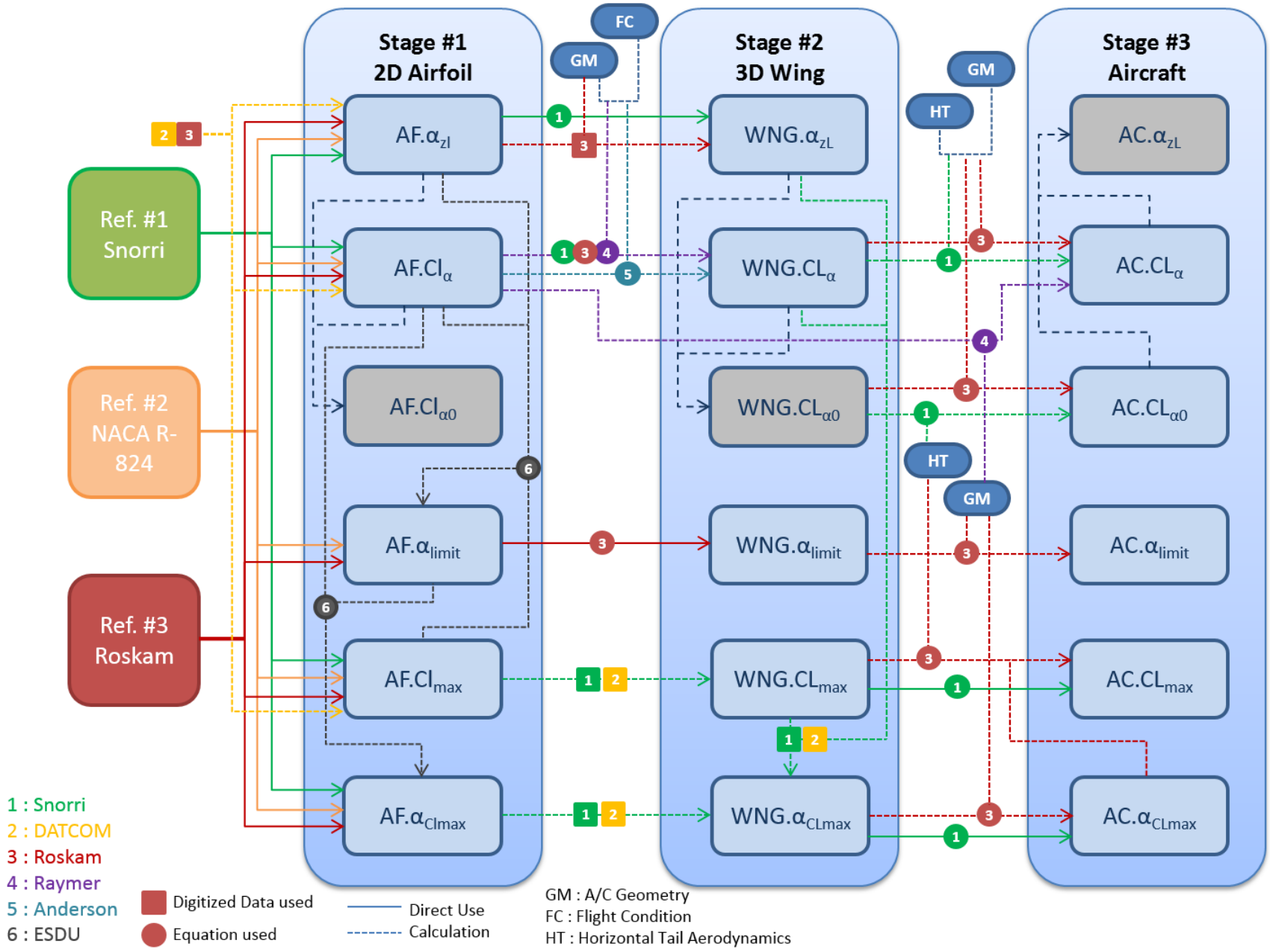

Figure 4.7: Lift-Curve Modeling Stages and Parameters Flow Chart

various source as shown in Table 4.1.

Table 4.1: Summary of 2-D Airfoil Lift-Curve Parameters

Lift-Curve Parameters	**Modeling Result**		**Reference Values**		
	DATCOM	**ESDU**	**Cudmundsson**	**Roskam**	**NACA R-824**
Zero lift angle of attack, α_{0l} [deg]	-1.9192		-1.8	-2	-1.938
Lift-curve slope, C_{l_α} [1/deg]	0.017		0.101	0.105	0.1054
AOA limit for curve linearity, α^* [deg]		10.398		9.5	9.814
AOA for max lift coefficient, $\alpha_{C_{lmax}}$ [deg]		14.0989	16	16.8	16.6261
Maximum lift coefficient, $C_{l_{max}}$	1.4156		1.62	1.671	1.6713

• *3-D Wing Lift-Curve Parameters*

The lift-curve parameters for 3-D wing aerodynamic performance are obtained using several different modeling methods considering the wing geometry of the C172S aircraft. It is to be noted that some references share the same estimation methods. As stated above and shown in Figure 4.7, some of these parameters use the result of previous 2-D airfoil's result, and the combinations of selected parameters in this stage will affect the result of the next stage, which is for the entire aircraft performance modeling. Since the comparable reference for the wing only is not available in the public domain, the validation of these results will be performed in the next stage along with the complete aircraft aerodynamic modeling results.

• *Complete Aircraft Lift-Curve Parameters*

The five parameters for the lift-curve of complete aircraft are slightly different than the parameters for 2-D airfoil or 3-D wing lift curve. In this stage, the lift coefficient at zero

Table 4.2: Summary of 3-D Wing Lift-Curve Parameters [42][56][58]

Lift-Curve Parameters	**Gudmundsson**	**DATCOM**	**Roskam**	**Raymer**	**Anderson**
Zero lift angle of attack, α_{0L_W} [deg]	-1.938		-0.6776		
Lift-curve slope, $C_{L_{\alpha_W}}$ [1/deg]	0.0829		0.0829	0.0829	0.0835
AOA limit for curve linearity, ${\alpha^*}_W$ [deg]			9.8140		
AOA for max lift coefficient, $(\alpha_{C_{L_{max}}})_W$ [deg]	18.5825	18.5825			
Maximum lift coefficient, $C_{L_{max_W}}$	1.4944	1.4944			

angle of attack, rather than zero lift angle of attack, is used to determine the linear line of lift-curve. The reason is that it is easier to estimate the lift change due to the fuselage and horizontal tail than to estimate the angle of attack at which the aircraft produces zero lift. The modeling results are compared to the reference data in Table 4.3 which is from the University of Illinois at Urbana-Champaign (UIUC) [60].

Table 4.3: Summary of Complete Aircraft Lift-Curve Parameters

Lift-Curve Parameters	**Gudmundsson**	**Roskam**	**Raymer**	**Reference Data** [60]
Zero Angle of Attack Lift Coefficient,α_{0L_A}[deg]	0.0433	0.1639		0.155
Lift curve slope,$C_{L_{\alpha_A}}$ [1/deg]	0.0910	0.0866	0.0961	0.093
AOA limit for curve linearity, ${\alpha^*}_A$ [deg]		8.3140		9.657
AOA for max. lift coefficient,$(\alpha_{C_{Lmax}})_A$ [deg]		17.0825		16.5
Maximum lift coefficient, $C_{L_{max_A}}$	1.6	1.5735		1.5404

• *Lift Curve Validation*

The lift-curve for the C172S were developed for the pre-stall and post-stall regime using the aerodynamic modeling methods presented above. The pre-stall lift curve buildup was implemented using the method proposed separately by Roskam and Raymer, having compared it to all other methods reviewed and finding that they provide the best fit to the known aerodynamic properties of the C172S. Among the estimated results using various modeling methods for each parameter in different stages, the combination of methods which provides the closest lift-curve model to the reference data was selected and is summarized in Table 4.4. Although it is shown that Roskam's method is used for all parameters in Stage 3, the results are highly dependent on the previously chosen parameters. In other words, it is important to choose the best combination of parameters among various resources even though the reference values of the airfoil are all from a reliable document. The reference values used are somewhat different from each other, as shown in the 4.1, and this small difference causes loss of validity in the end. Thus every possible resource should be evaluated and considered in the aerodynamic modeling process in advance. The plot shown in Figure 4.8 illustrates the value of $C_{L_{max}}$ (dotted horizontal line) derived from the POH stall data in flap-up configuration, which matches values published in a variety of sources including Jane's All the World's Aircraft [61]. The plot also depicts the lift curve slope here developed with the method by Roskam and Raymer in the linear (solid) and non-linear (dotted) regime. Also shown is published data for the C172S (circles) generated with the Flight Gear Flight Simulator (FGFS) aerodynamic model. This data is initially developed for the Smart Icing System Project at the University of Illinois at Urbana-Champaign, using tunnel data to develop a linear and nonlinear aircraft model. This reference data was adjusted here to match the known and empirically validated value of $C_{L_{max}}$ (stars). Results show good agreement between the developed model, general trends of the adjusted data from higher fidelity methods, and the empirical value of $C_{L_{max}}$.

Table 4.4: Selected Combinations of Lift Curve Parameters for C172S

Lift-Curve Parameters	Stage 1 2-D Airfoil		Stage 2 3-D Wing		Stage 3 Complete Aircraft	
	Selected Method	Value	Selected Method	Value	Selected Method	Value
Zero lift angle of attack	NACA R-824	-1.938	Roskam	-0.6776		
Lift curve slope	NACA R-824	0.1054	Raymer	0.0829	Gudmundsson	0.0910
Zero AOA lift coefficient					Roskam	0.1805
AOA limit for curve linearity	NACA R-824	9.814	Roskam	9.814	Roskam	8.3140
AOA for max. lift coefficient	NACA R-824	16.626	DATCOM	18.5825	Roskam	17.0825
Maximum lift coefficient	NACA R-824	1.6713	DATCOM	1.4944	Roskam	1.5735

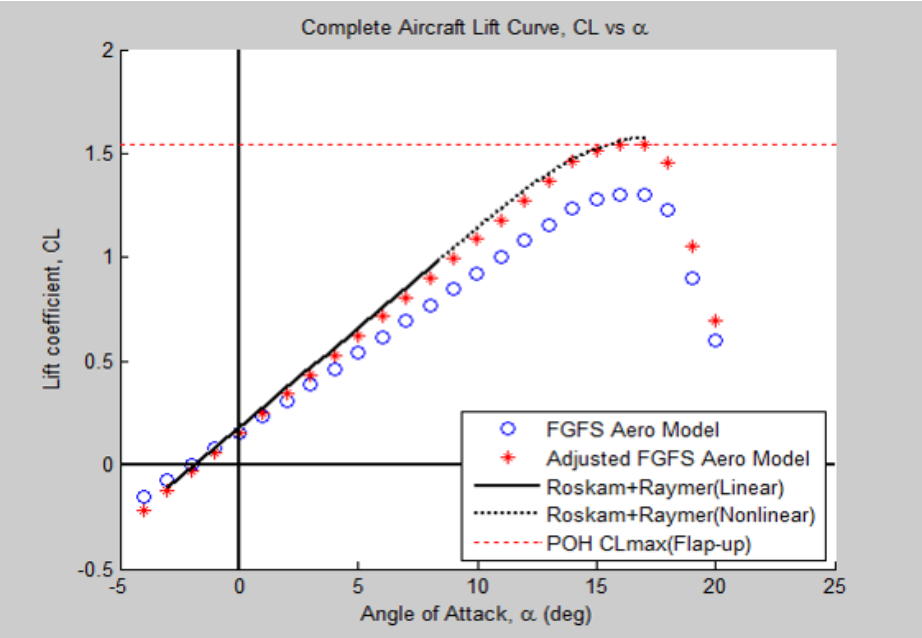

Figure 4.8: C172S Lift-Curve Model with Selected Combination of Parameters

Lift Curve Modeling Result: Flaps Down

The flap effects on the lift characteristics are obtained for each stage as shown in Table 4.5. C172S has single-slotted flaps, and the result is obtained under the assumption of

30-degree flap deflection. It is shown that the effect of the flap is smaller on the complete aircraft configuration compared to the 3-D wing or 2-D airfoil. The lift-curve slope change is shown to be very small, and the flap deflection mainly changes overall and maximum lift coefficient of the aircraft.

Table 4.5: Summary of Lift-curve Parameters with Flaps Down

Flap Effects	**2-D Airfoil**	**3-D Wing**	**Complete Aircraft**
Lift Increment	0.5711	0.2104	0.1648
Lift-Curve Slop Change	0.1111	9.7895e-04	9.7492e-04
Maximum Lift Coeff. Change	0.2464	0.0920	0.0130

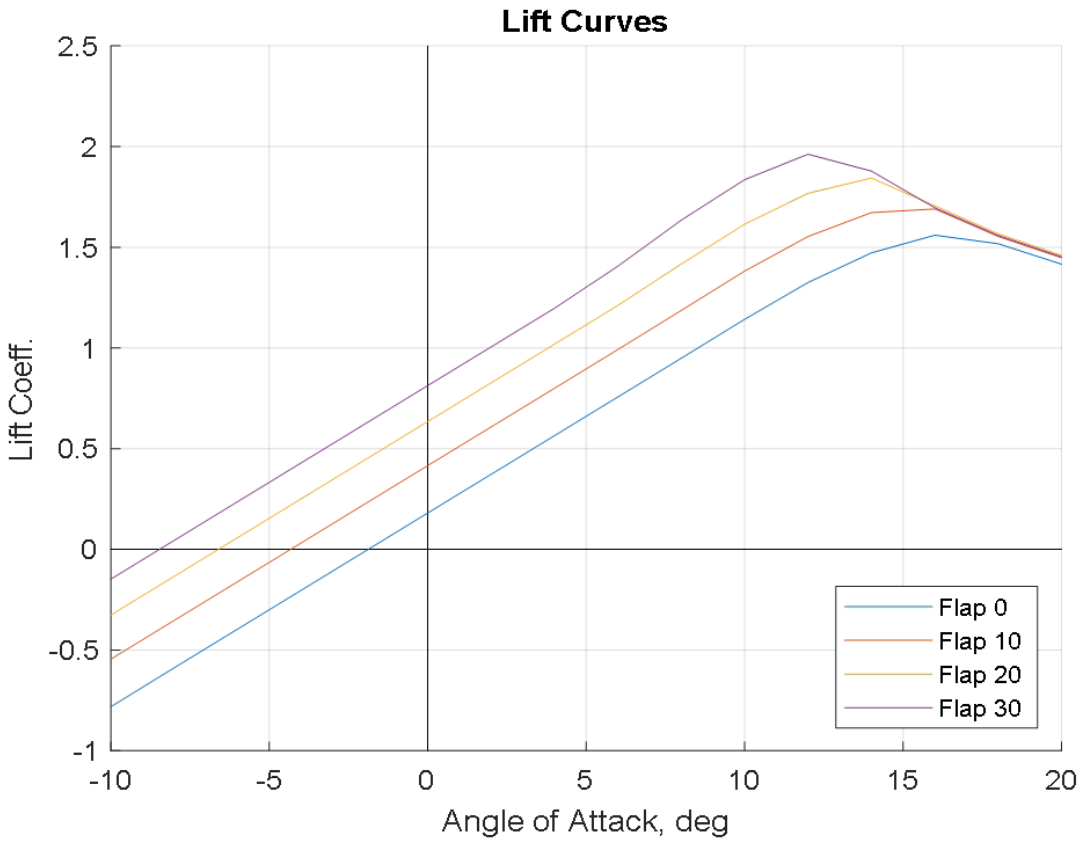

Figure 4.9: Lift Curves of C172S Aircraft with and without Flap Effect

The lift curves for different flap settings shown in Figure 4.9 are valid up to the stall point. The shape of the lift curves are defined by the five parameters for complete aircraft shown in Table 4.4. One lift curve consists of two parts: a linear line and a curve. The lift curve slope and zero angle-of-attack lift coefficient determines the linear line, and the other three factors define the shape of the remaining part. The curve part connects the end point of the straight line and the maximum lift point. Even though the shape of the curvature expresses lift coefficients beyond the maximum lift point, they are the outcome of the generated curve that satisfies given constraints, and they do not provide actual modeled lift information. Thus, the developed aerodynamic model can only provide lift coefficients that correspond to angle-of-attack less than the maximum lift angle-of-attack.

Drag Polar Modeling Result: Flaps Up

• *Parasite Drag*

The results of three different parasite drag estimation methods are summarized and compared in Table 4.6. As shown in the table, the minimum drag extracting method from the best gliding speed gives the highest value of parasite drag which is the closest value to the reference data.

• *Induced Drag*

Oswald span efficiency method and leading-edge suction method are investigated, and the results are compared in Table 4.7. The Oswald span efficiency factor, e, was estimated using Kroo's method [62] using C172S wing geometry and its value is 0.7469. The Oswald span efficiency method yields the closest K value to the reference data.

Table 4.6: Parasite Drag Modeling Result

Estimation Methods	C_{D_0}
Equivalent Skin-friction Method	0.0229
Component Buildup Method	0.0207
Minimum Drag Extracting from Best Gliding Speed	0.0344
Flight Gear Aerodynamic Model [60]	0.0355
NASA Historical Data [63]	0.0319

Table 4.7: Induced Drag Modeling Result

Estimation Methods	K
Oswald Span Efficiency Method	0.0562
Leading Edge Suction Method	0.0709
Flight Gear Aerodynamic Model	0.05499

• *Drag Polar Validation*

The pre-stall drag polar for C172S aircraft was obtained using the combination of extracting parasite drag from the best gliding speed method and Oswald span efficiency method. The results are shown in Table 4.8 and Figure 4.11. This drag polar was developed using Equation 2.3 for the set of C_L vs. α values in the linear regime where the flow is attached and no degradations of C_L or additional increase in C_D due to separation phenomena are observed. It is known that C_D as a function of α is well behaved as a quadratic relationship up to the stall point. Accordingly, a quadratic C_D vs. α relationship was readily developed using the lift curve (C_L vs. α), and the drag polar for the linear regime (C_D vs C_L). The relationship was extended up to the stall point. The resulting drag polar up to the stall point is shown in Figure 4.11 where the linear and non-linear regions of the lift curve are differentiated. The reference data (circles) is the FGFS aerodynamics model data,

here adjusted (stars) to match the validated $C_{L_{max}}$ and known $(L/D)_{max}$ value from NASA historical report [63]. In general, good agreement is observed, between the model and the FGFS data for the linear lift regime and up to the midpoint of the non-linear regime. Good agreement is further noted for the adjusted FGFS data.

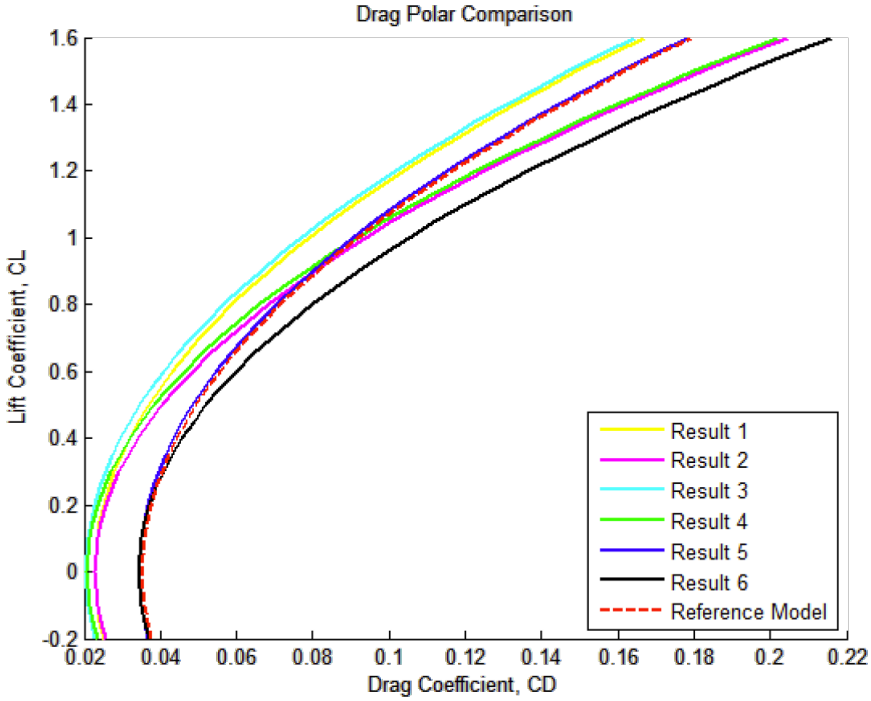

Figure 4.10: Comparison of Drag Polar Estimation Results

Table 4.8: Selected Combinations of Drag Polar Parameters for C172S

Drag Polar Parameters	**Selected Method**	**Value**
Parasite Drag, C_{D_0}	Extracting from Best Gliding Speed (POH)	0.0344
Induced Drag Coeff. K	Oswald Span Efficiency Method	0.0568

• *Drag Polar Modeling Result: Flaps Down*

The drag increment due to flap deflection is estimated, and the results are shown in Table 4.9. As explained earlier, the drag variation caused by flap deflection can be estimated

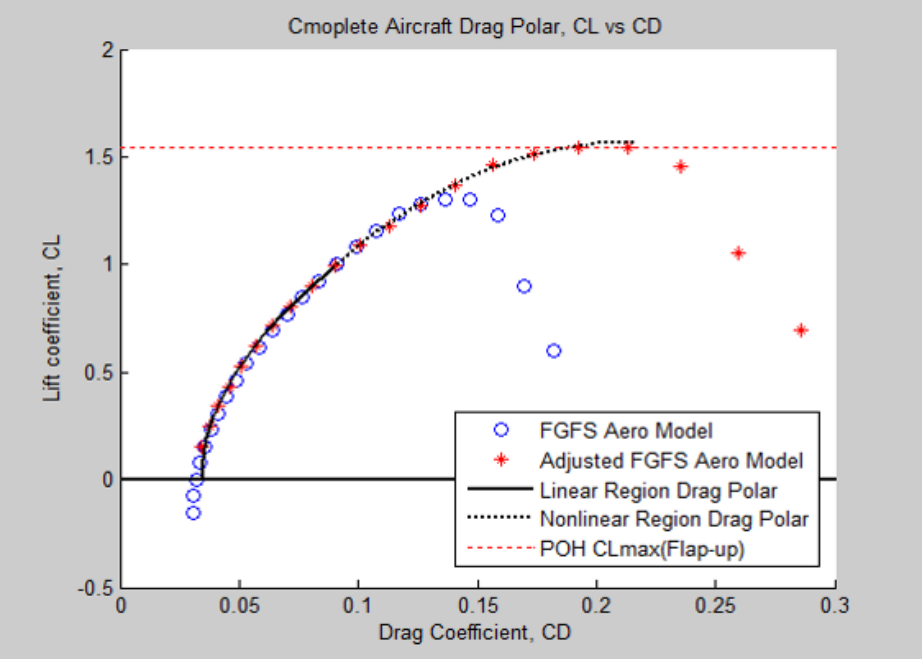

Figure 4.11: C172S Drag Polar Model with Selected Combination of Parameters

in three aspects: profile drag change, induced drag change, and interference drag change. Among three flap-deflected configurations, the modeling result of the maximum flap deflection is shown here as an example. The 30 degree of flap deflection causes a total drag increment, and the amount of induced drag increment depends on the angle of attack as shown in 4.12. It is shown that smaller deflection adds smaller drag into the aircraft drag characteristic. The results below are under the condition of 30-degree flap deflection. The total drag variation can be obtained by summing the three different drag components.

Table 4.9: Drag Increment due to Flap Deflection: 30 degree

Drag Increment due to Flap (30 degree)	***K***
Profile Drag Increment	0.0028
Induced Drag Increment	Shown in Figure 4.12
Interference Drag Increment	0.0011
Total Drag Increment	Shown in Figure 4.12

Similar to the lift curves for different flap settings developed in the previous section,

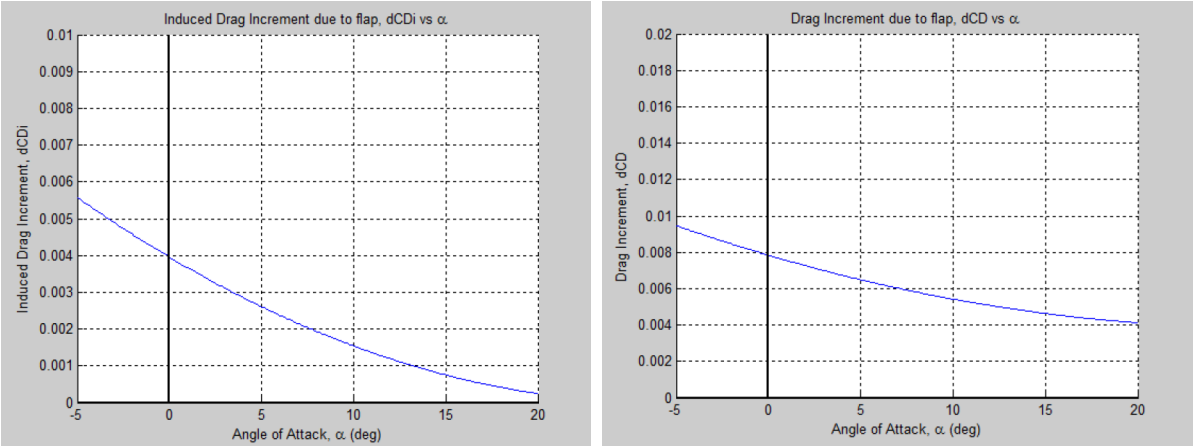

(a) Induced Drag Increment (b) Total Drag Increment

Figure 4.12: Drag Increment due to Flap: 30 Degree Deflection

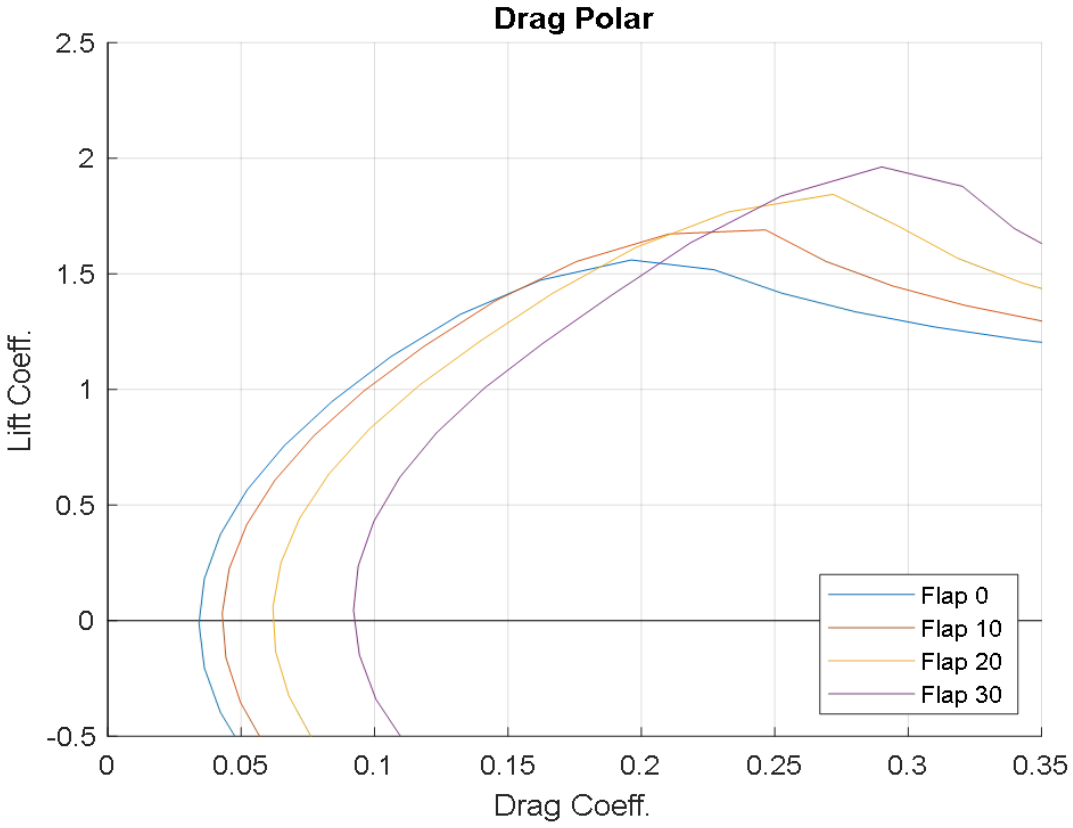

Figure 4.13: Drag Polar Change due to Flap Deflection: 30 degree

drag polars for different flap settings also consists of two parts. Instead of having one quadratic equation for one drag polar, two different curves for the linear part and non-linear

part were obtained. The drag polar up to the linearity limit of the lift curve can be expressed using the modeled parameters. For the non-linear part, the modeled drag coefficients can be expressed as a function of angle-of-attack, and the points are fitted using another curve. By connecting the two curves and plotting them on lift and drag coefficients domain, the drag polar for that flap condition can be obtained as shown in Figure 4.13. Again, even though the shape of the drag polars for each flap setting provide drag information beyond the stall points, that information cannot be trusted because they are defined by the second curves that were designed to pass the given points within non-stall ranges. Thus, the developed drag polars can only provide lift and drag coefficients information that correspond to angle-of-attack less than the maximum lift angle-of-attack.

4.3 Data-Driven Model

This section will provide a detailed explanation about a data-driven aerodynamic modeling method which is to improve the model fidelity by using actual flight data. The advanced theoretical aerodynamic model obtained in the previous physics-based modeling process will be used as a basis for this data-driven modeling process which will be covered in this section. Strategic flight maneuvers for flight data generation have been proposed and described in the following section. The next section explains how the obtained data can be used to improve the fidelity of the aerodynamic model.

4.3.1 Tactical Flight Data Generation

The suggested flight maneuvers for flight data generation consist of five different maneuvers. An overview of this flight data generation plan is shown below in Figure 4.14. It comprised two complete cycles of the flap (0-10-20-30-20-10-0 deg) during cruise flight at two distinct altitudes. Between the two cruise segments, the aircraft climbs from the low cruise altitude to the high cruise altitude with the maximum power setting. After that, the flaps were used during a transition to slow flight followed by a simulated rectangular

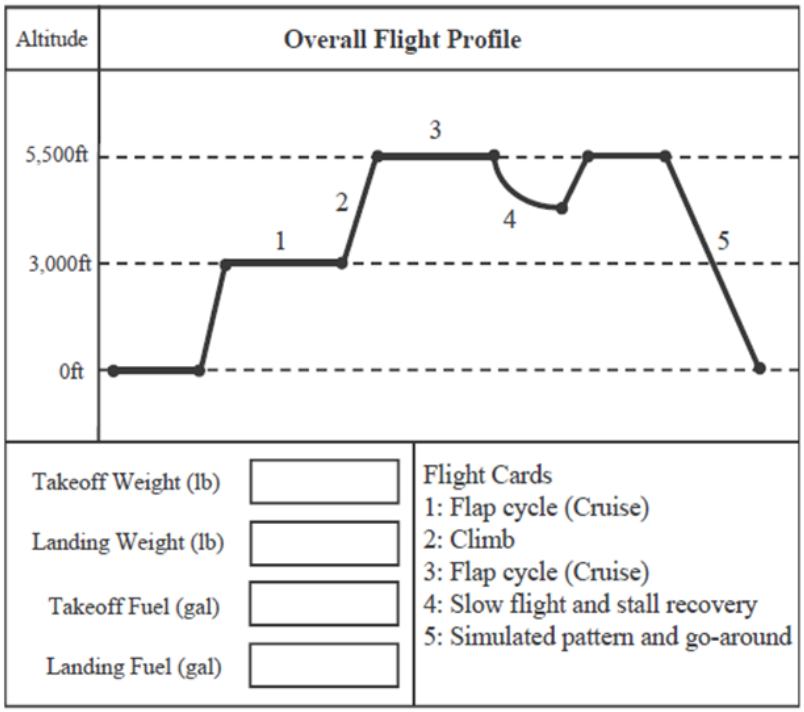

Figure 4.14: Overview of the Suggested Flight Maneuver for Data Collection

pattern entry at the altitude. The Garmin G1000 data log corresponding to this flight has been verified to ensure that the test flight is acceptable. Since the Garmin G1000 does not record flap position, flap operation during the flight was noted by the flight crew using the NAV1 frequency, which is logged by the G1000 system. The original flight cards that contain the detailed explanation of the flight maneuvers are described in the appendix section. The flight cards were provided to partners at Ohio State University and the flight data was generated by them. Figure 4.15 provide an overview of sample flight parameters generated from the suggested flight maneuvers.

4.3.2 Data-Driven Modification Strategy

Lift Curve and Drag Polar Shape Variation

The aerodynamic model consists of lift curve and drag polar, and the basic idea of the data-driven aerodynamic model is to find the best shape of the lift curve and drag polar which minimize the errors between the reference data points and the aerodynamic model.

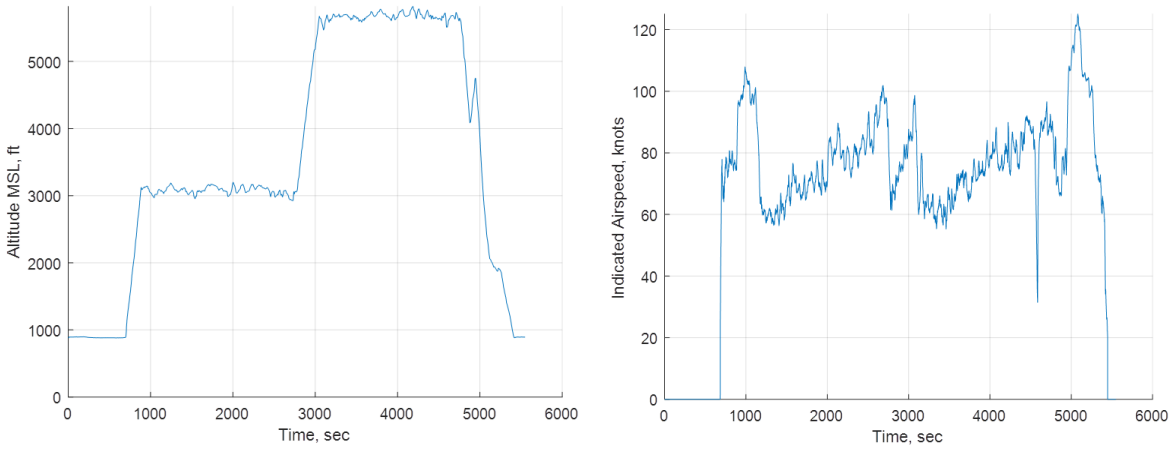

(a) Altitude (MSL)

(b) Indicated Airspeed

Figure 4.15: Sample Flight Data Parameters from the Suggested Flight Maneuvers

In order to vary the shape of the lift curve and drag polar, it is necessary to parameterize the shape of both lift curve and drag polar. For this purpose, shape modification factors were introduced, and they can add flexibility to the model by altering the shape of the lift curve and drag polar for both clean configuration and flap deployed configuration. To be more specific, the shape modification factors changes the lift curve shape factors, drag polar coefficients, lift increment due to flap deflection, and drag increment due to flap deflection. The relationship between the introduced shape modification factors and the shape of the lift curve and drag polar is described in Figure 4.16. As shown in Figure 4.16, the shape modification factors can vary the values of modeling factors that defines the lift curve shapes and the drag polar shapes for both clean configuration and flap-deflected configurations.

Possible ranges of the defined shape modeling factors were set to the extent that the factors do not violate physics constraints. Figure 4.17 describes the variation of clean configuration lift curve and drag polar with different shape modification factors applied within the pre-defined ranges. To be more specific, shape modification factor settings within the given ranges change the shape of the baseline lift curve or the baseline drag poalr, but some of them may distort the basic characteristics of the model. Considering the physics of the

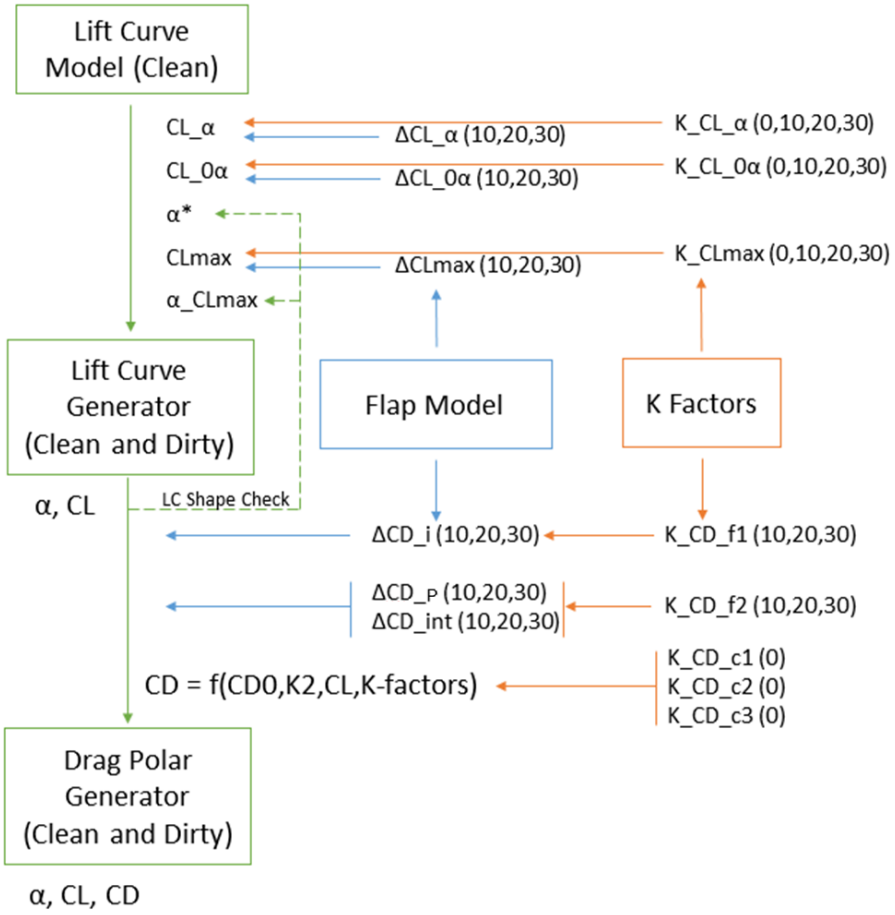

Figure 4.16: Model Modification Strategy using Shape Modification Factors

aerodynamic model, the shape factor settings that are not physically possible were removed from the possible combinations of the factors. As shown in the figure, the shape modification factors can cover the entire range of possible lift curve and drag polar shapes. Thus, the final goal of this process is to find the best fitting lift curve and drag polar that minimizes the errors between the modeled aerodynamic coefficients and the flight data-driven aerodynamic coefficients.

Reference Data

The recorded data during the suggested flight maneuvers contains a rich set of information with different flap activities that can be used for the data-driven aerodynamic modeling method. Assuming that aerodynamic characteristics of an aircraft do not change signifi-

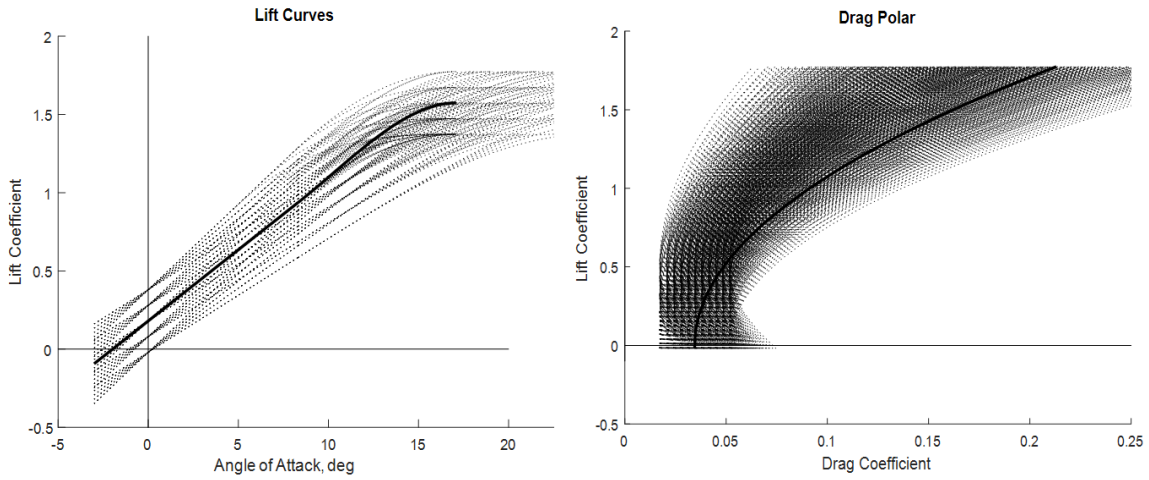

Figure 4.17: Lift Curve and Drag Polar Variation using Shape Modification Factors

cantly during the entire flight, the flight data parameters from the two cruise maneuvers were selected and used in this modeling process.

First of all, the flight data provides angle-of-attack information which is an essential input for the aerodynamic model. However, the Garmin G1000 does not directly record the angle-of-attack data. Therefore, angle-of-attack needs to be calculated using other given parameters such as pitch angle and flight path angle because angle-of-attack is the angle between pitch angle and flight path angle of an aircraft as shown in Figure 4.18. The flight path angle also needs to be calculated using vertical speed and ground speed data because the flight path angle is not one of the data parameters that G1000 records. The equations for calculating those values are shown in the below equations where α is angle-of-attack, θ is pitch angle, and γ is flight path angle.

$$\alpha = \theta - \gamma \tag{4.41}$$

$$\gamma = \arctan\left[\frac{V_{spdG}}{GndSpd}\right] \tag{4.42}$$

Once the angle-of-attack during the flight is calculated using Equations 4.41 and 4.42, the aerodynamic coefficients during the flight also can be obtained from the aerodynamic

model. The lift coefficients and drag coefficients are the values that will be compared to the data-driven lift and drag coefficients.

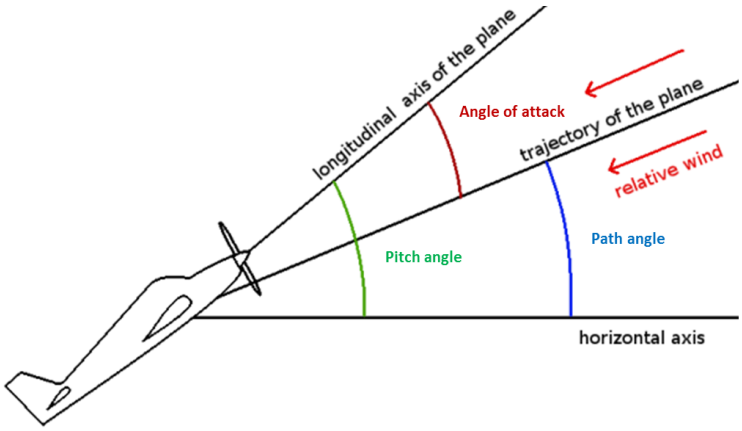

Figure 4.18: Angle-of-Attack, Pitch Angle, and Path Angle

As shown in the Equations 4.1 and 4.2 earlier, the aerodynamic forces, lift and drag, during flight can be calculated using logged flight parameters such as pitch rate, absolute velocity, roll angle, and so on. Each parameter that is required for calculating lift and drag can be obtained directly from the flight data record or calculation using other logged parameters. The equations for calculating the parameters that cannot be obtained directly from the flight data record are listed below [43][44][64].

$$q = \dot{\theta}\cos\phi + \dot{\psi}\cos\theta\sin\phi \tag{4.43}$$

$$\theta_w = \gamma \tag{4.44}$$

$$V_{abs} = \sqrt{V_{spdG}^2 + GndSpd^2} \tag{4.45}$$

Once lift and drag during the flight are obtained using the logged or calculated data parameters listed above, the calculated lift and drag are converted into aerodynamic coef-

ficients using Equations 4.46 and 4.47, where S is the given wing area, V is airspeed, ρ is air density.

$$C_L = \frac{2L}{\rho V^2 S} \tag{4.46}$$

$$C_D = \frac{2D}{\rho V^2 S} \tag{4.47}$$

When modeled aerodynamic coefficients and data-driven aerodynamic coefficients are both obtained from the equations above, optimal shapes of lift curve and drag polar can be obtained by selecting shape modification factors that minimize the errors between the modeled values and data-driven values. In other words, the lift curve and drag polar shapes that minimize the root-mean-square error (RMSE) between modeled and data-driven aerodynamic coefficients are considered as the aerodynamic model which is accurate enough to predict flap activity. This level of model fidelity meets the goal of this study as stated earlier. The result of this data-driven aerodynamic modeling is discussed in the following section, and the fidelity of this model will be tested.

4.3.3 Modeling Result

Lift Curve

As explained in the previous section, lift curve shapes for different flap settings are optimized using shape modification factors and data-driven aerodynamic coefficients. The result of lift curves for each flap settings are shown in Figure 4.20. The reference data points which are calculated lift coefficients using a subset of the generated flight data shown as circles in the figure. The dotted lines are the previously obtained physics-based model and the solid lines are the data-driven aerodynamic model. Figure 4.21 shows that the accuracy of the lift curve has been improved by data-driven modeling process regarding not only the magnitude of the errors but also the shape of the error distribution.

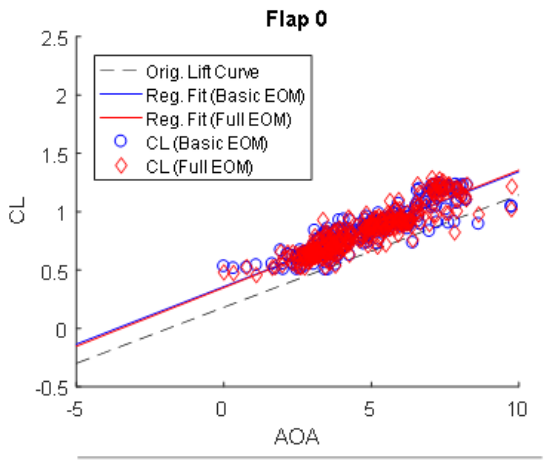

	Basic Equation	Full Equation
Slope, m	0.0986	0.1006
Intercept, b	0.3571	0.3493
R2	0.822	0.8275
RMSE	0.0783	0.0784
Coeff. Corr.	0.9066	0.9097

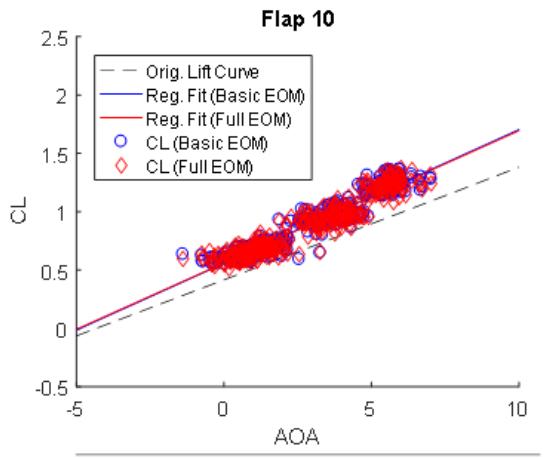

	Basic Equation	Full Equation
Slope, m	0.1146	0.1135
Intercept, b	0.5578	0.5595
R2	0.9203	0.9097
RMSE	0.0683	0.0724
Coeff. Corr.	0.9593	0.9538

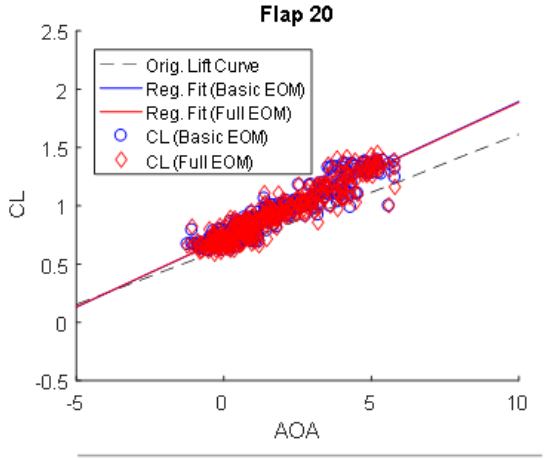

	Basic Equation	Full Equation
Slope, m	0.1176	0.1169
Intercept, b	0.7184	0.718
R2	0.901	0.8794
RMSE	0.0695	0.0772
Coeff. Corr.	0.9492	0.9378

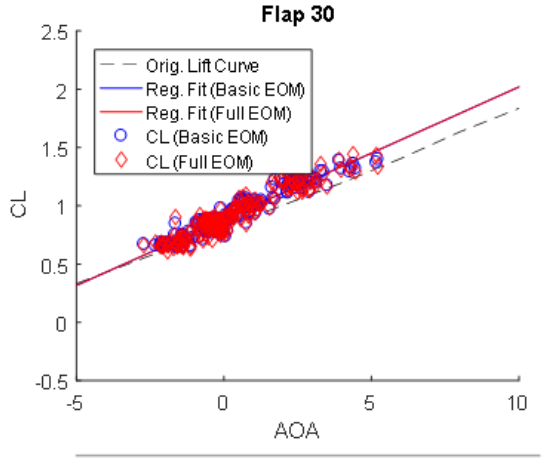

	Basic Equation	Full Equation
Slope, m	0.1136	0.1136
Intercept, b	0.8845	0.884
R2	0.9182	0.9061
RMSE	0.0558	0.0601
Coeff. Corr.	0.9582	0.9519

Figure 4.19: Lift Curve Model Fitting Details

Finally, accurate lift curves for different flap settings are obtained through this data-driven modeling process. In this modeling process, the lift curve shape that minimizes the errors between modeled coefficients and the flight data is considered the best data-driven

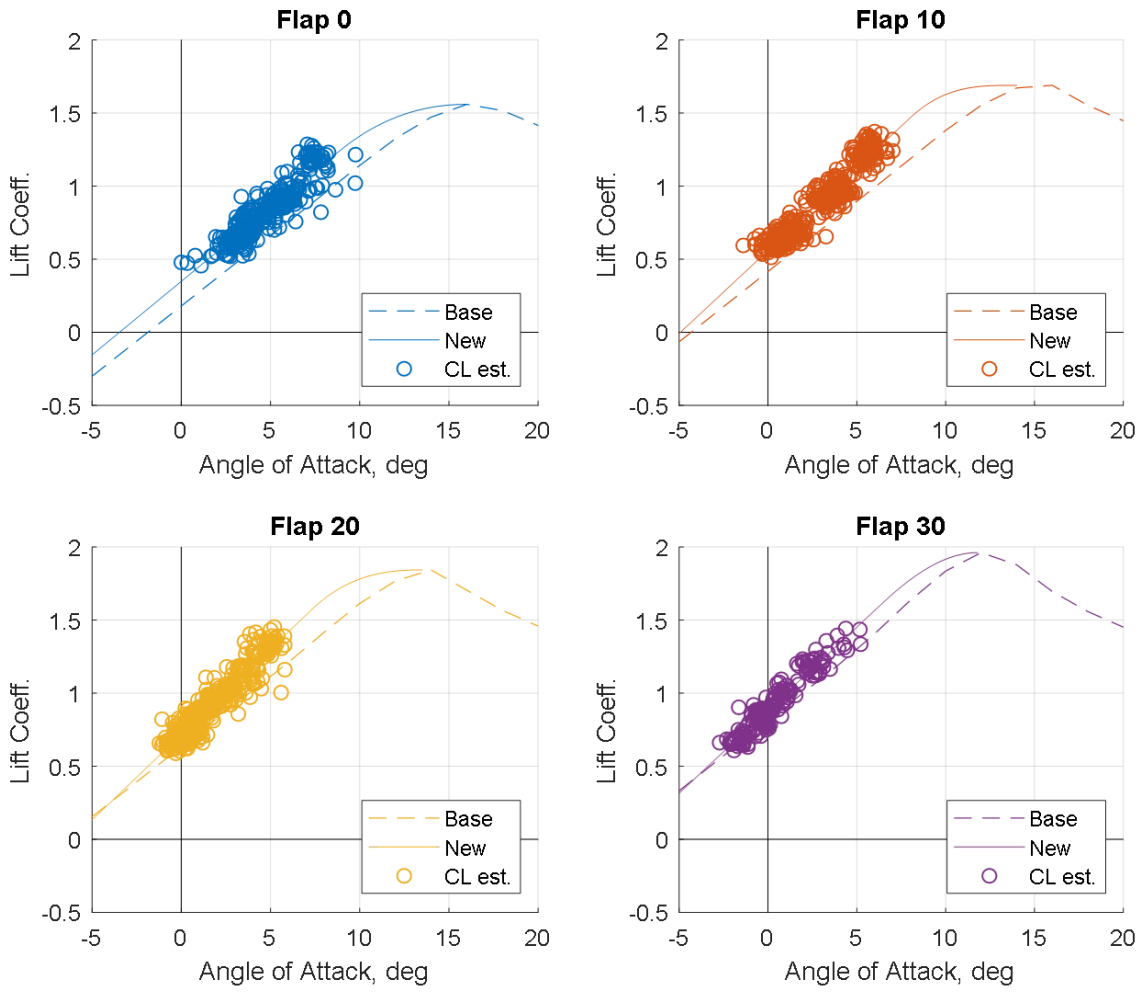

Figure 4.20: Lift Curve Modeling Result for Different Flap Settings

lift curve. In other words, the final lift curve shapes, shown in Figure 4.22, are chosen because these shapes have the minimum RMSE values compared to other lift curve candidates generated using the pre-defined shape factors. It has to be acknowledged here that the amount of error that can be allowed in this step has to be set considering the limitation of this method. The reference data points, the calculated aerodynamic coefficients, are obtained from the flight data, and they may have some uncertainties. Thus, the modeling errors which are the discrepancies between the modeled aerodynamic coefficients and the data-driven estimated coefficients cannot be zero. Instead, all the quantified error-sums of the candidates are compared, then the case that has the minimum error is chosen in this

study as the final lift curve. The final results are shown in Figure 4.22 and compared with the baselines which are the physics-based lift curves.

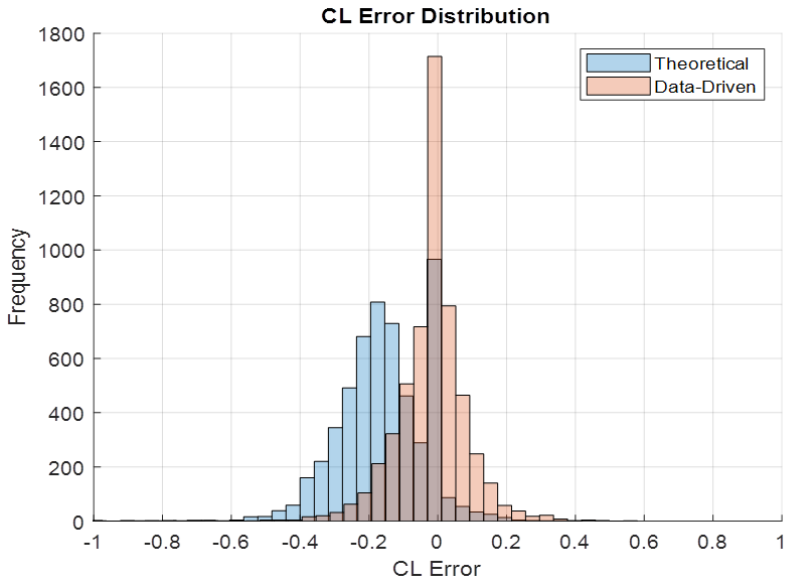

Figure 4.21: Lift Curve - Error Distribution

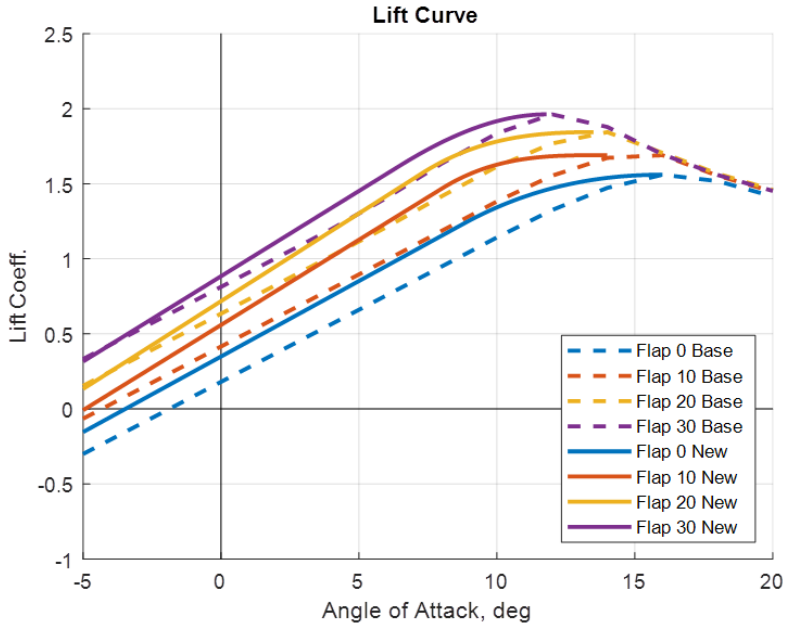

Figure 4.22: Lift Curve Modeling Result

Drag Polar

In the same way as the lift curves are optimized in the above section, drag polar shapes for different flap settings are also optimized using shape modification factors and data-driven drag coefficients. The result of drag polars for each flap settings are shown in Figure 4.23. Same as the lift curves, the circles are representing the data-driven aerodynamic coefficients and dotted and solid lines are physics-based and data-driven drag polars respectively. Also, Figure 4.24 compares errors of theoretical drag polar and the newly obtained data-driven drag polar. It is shown that the drag coefficient errors are reduced after the data-driven model modification process. As discussed in the lift curve modeling part, the modeling error shown in Figure 4.24 is from the case that has the minimum error among many other drag polar candidates populated using the drag polar shape modification factors. Again, the reference data points for fitting the drag polars are from the actual flight data which contains unavoidable uncertainties. That means it is not possible to have perfect reference data set for this data-driven modeling process. Thus, the target error that can be allowed in this modeling process has to be defined, then the results has to satisfy the target. The goal of this data-drive aerodynamic modeling process is to find the shape modification factors that produces the minimum error-sum among the set of shape factors within the pre-defined ranges. The final drag polars for each flap setting described in Figure 4.23 are the best possible outcome of this data-driven aerodynamic modeling method.

Through this data-driven modeling process, a more accurate aerodynamic model which meets the research goal of this study is obtained, and the results are shown in Figure 4.25 as four different drag polars. This aerodynamic model will be examined if it is accurate enough to capture flap activity during flight. Once this aerodynamic model is verified to be sufficiently accurate, it will be used to test if unsafe aerodynamic behavior can be detected using this aerodynamic model.

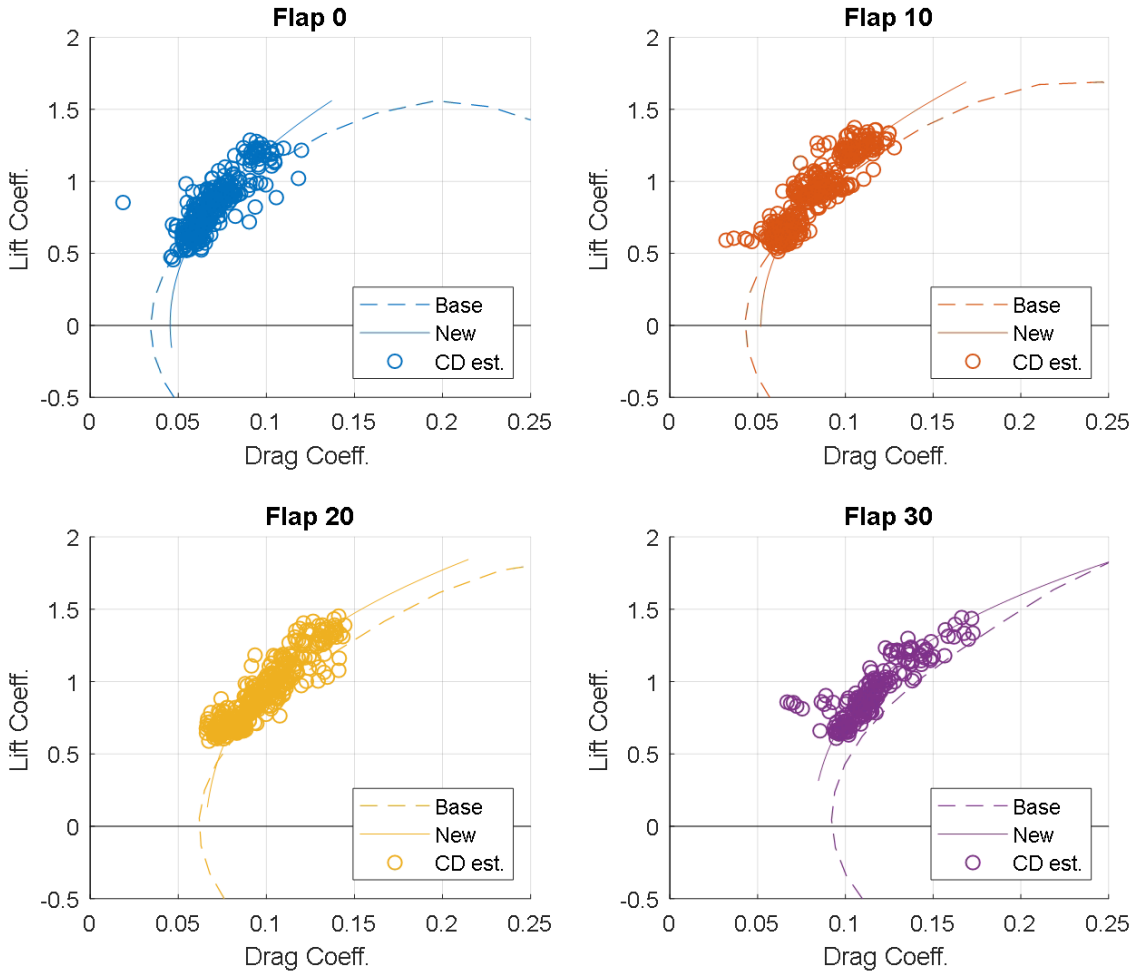

Figure 4.23: Drag Polar Modeling Result for Different Flap Settings

4.4 Experiment and Result

4.4.1 Flap Activity Estimation

Flap deflection is one of the significant factors affecting aerodynamic characteristics of an aircraft. That being said, an accurate aerodynamic model can predict flap activity during flight if sufficient flight data parameters are given. In other words, if an aerodynamic model can accurately predict flap deployment, then the model can be considered a sufficiently accurate model. Therefore, the fidelity of the aerodynamic model will be tested by examining its flap estimation capability.

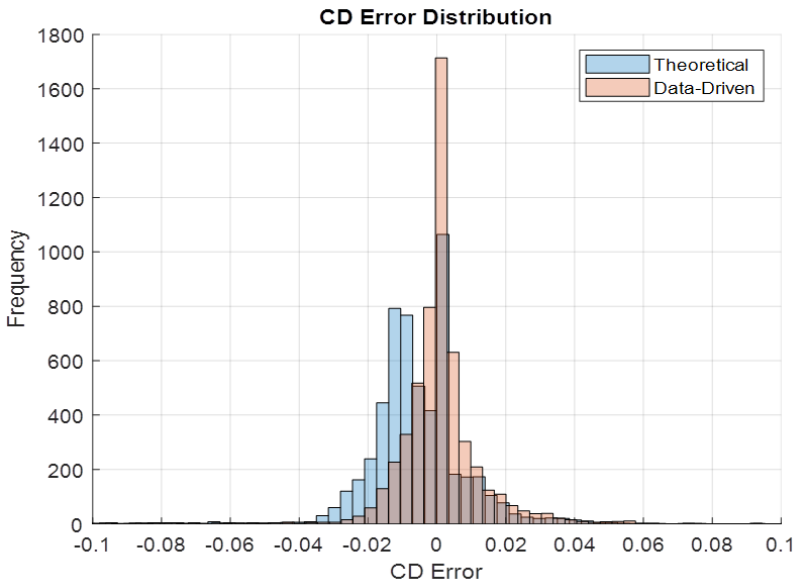

Figure 4.24: Drag Polar - Error Distribution

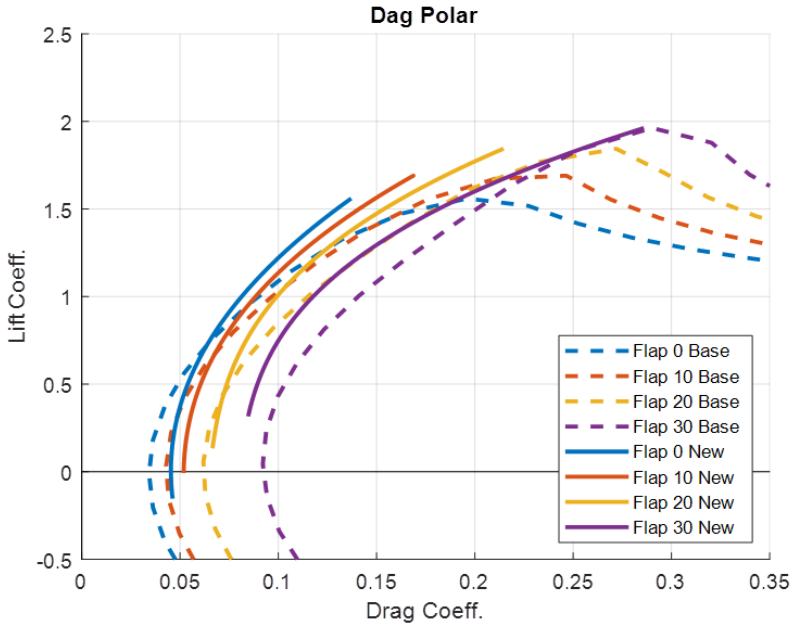

Figure 4.25: Drag Polar Modeling Result

The overall process of estimating flap positions is described in Figure 4.26. As the first step, the calculated angle-of-attack during the entire flight are inputted to the aerodynamic models for different flap settings. The C172S aircraft has four different flap settings: clean

configuration, 10-degree setting, 20-degree setting, and 30-degree setting. By inputting the angle-of-attack derived from the flight data into the four aerodynamic models, four sets of lift and drag coefficients for each flap settings are obtained because each lift curve and drag polar provides different aerodynamic coefficients. Since the flap position is not known yet, these four lift and drag coefficients are possible candidates for the correct aerodynamic coefficients. Based on the information about the data-driven lift and drag coefficients and comparing the with the previously obtained modeled aerodynamic coefficients, the best set of aerodynamic coefficients and the corresponding flap position can be selected.

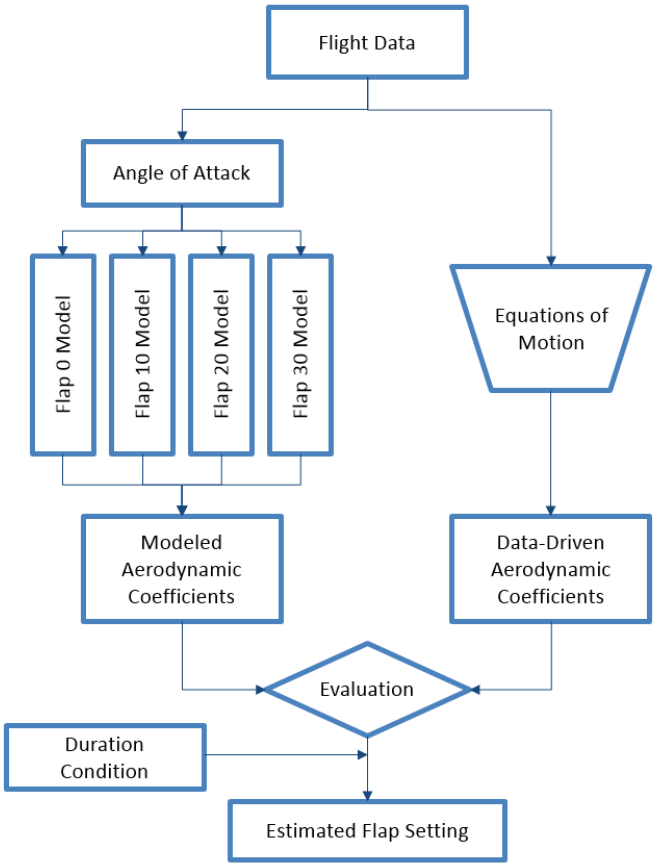

Figure 4.26: Flap Activity Estimation Process using the Aerodynamic Model

Harrison et al. from Georgia Institute Technology developed an algorithm for the estimation of flap deflection using collected flight data [65]. The fundamental idea of this algorithm is based on the concept of the total mechanical energy of an aircraft during flight.

In this algorithm, the specific total energy rates can be calculated using both flight data or estimated forces from aircraft performance models. The airspeed and aircraft weight from flight data and thrust and drag from the performance models can provide the total energy rate [66]. Also, Airspeed, altitude, and gravity acceleration can estimate the total energy rate as shown in Equation 4.48. More detailed information about this algorithm and the energy metrics can be found in [65], [37], and [67].

$$\dot{E} = \frac{(T - D)V}{W} = \dot{h} + \frac{V \times \dot{V}}{g} \tag{4.48}$$

By comparing the total energy rates from two difference sources, this algorithm detects the flap activities during flight. The biggest difference between the flap estimation method in this study and the flap detection algorithm proposed by Harrison et al. is that this method focuses on aerodynamic coefficients only instead of using thrust, drag, and weight information. It is shown in this study that flap estimation using aerodynamic coefficients can detect unknown flap activities during flight with high accuracy.

Figure 4.27 shows the drag coefficients obtained from the four different drag polars with given angle-of-attack information. Also, data-driven aerodynamic coefficients were calculated in the previous chapter and plotted in Figure 4.27. By selecting the modeled line that is closest to the data-driven line, the flap position during the flight can be estimated. To be more specific, by comparing the coefficients obtained from the aerodynamic model and the flight data, the most likely flap setting can be estimated by selecting the closest modeled coefficients to the data-driven coefficients.

To see the difference between modeled and data-driven coefficients more clearly, the errors between the modeled values at each flap setting and data-driven values are shown in Figure 4.28. In this figure, the lowest line represents the smallest error, and the rank of the modeled lines keep changing through the flight. That means the flap position can be estimated by selecting the modeled line that has the lowest rank.

The initial result obtained by the method described above is shown in Figure 4.29 (a).

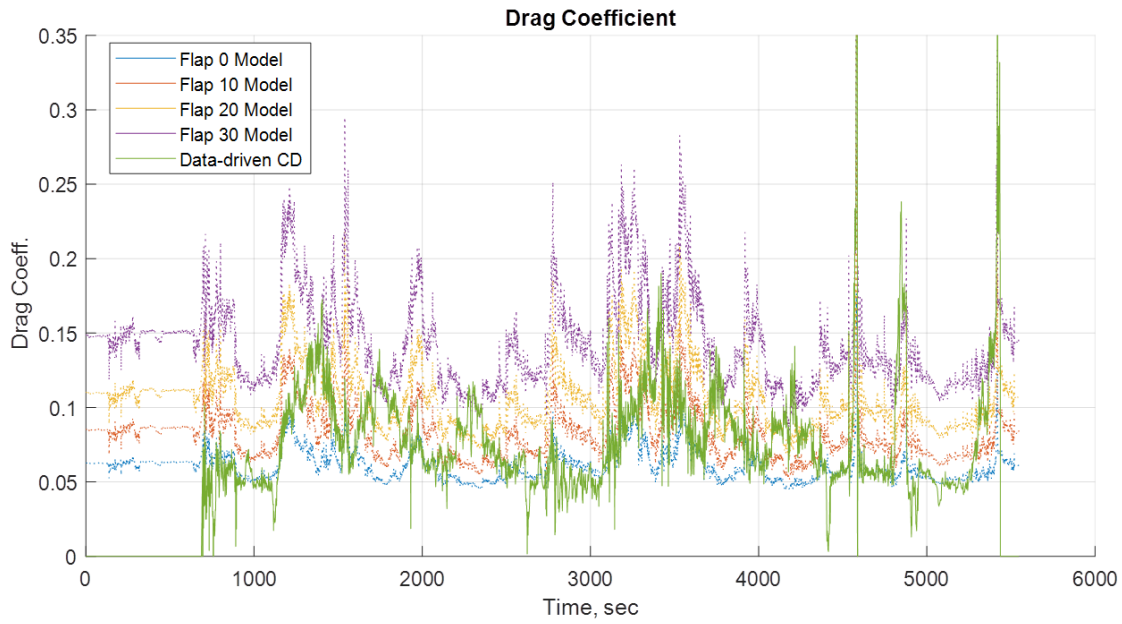

Figure 4.27: Comparison of Modeled and Data-Driven Drag Coefficients

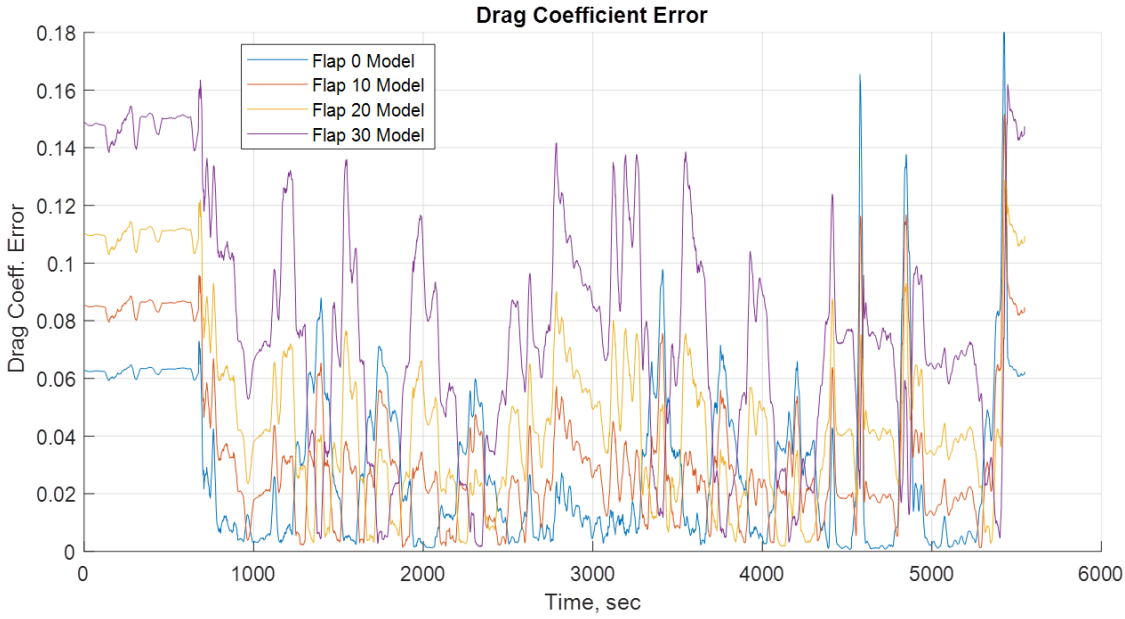

Figure 4.28: Errors Between Modeled and Data-Driven Drag Coefficients

As shown in the figure, it is observed that the initial flap estimation result contains a bunch of non-negligible fluctuation of flap position in a very short period, which is almost impossible. By adding a condition that flap position cannot be changed within a short period, the

erroneous fluctuation in the predicted flap position can be removed. When we consider that the flap position cannot be changed in a very short period of time, the erroneous fluctuations can be removed, then the aerodynamic model-driven flap estimation process provides more reliable result. When the time threshold was set as 10 seconds, almost every short fluctuations are removed as shown in Figure 4.29 (b).

In the flap estimation result, the overall estimation result matches to the logged flap activity almost perfectly while there are two false positives and one true negative. The two false positives are located around 1,000 seconds and 2,500 seconds in flight time. These may be caused by modeling error, but the first false positive and second false positive can be removed when the time threshold is set as 20 seconds and 18 seconds respectively. The true negative is located around 4,600 flight seconds which is when stall occurred. Thus, this true negative cannot be considered as a modeling error. The most notable result of this flap estimation test is that the aerodynamic model is able to predict the flap position change during approach and landing which is not logged by the pilot. According to this aerodynamic model driven flap estimation, the pilot deployed the flap in stages when the aircraft approached for landing, which is a routine procedure for landing. The hypothesis established in this chapter is that an aerodynamic model that is accurate enough to estimate flap usage during flight can capture unsafe behaviors of a fixed-wing GA aircraft, and the necessary accuracy can be achieved with the combination of a theoretical model and flight data. Based on the above result, it can be concluded that the aerodynamic model has reached the necessary fidelity by combining the theoretical modeling method and the data-driven modeling method.

4.4.2 Stall Recognition

In the previous section, it is proven that the aerodynamic model developed in the last section is accurate enough to estimate flap deflections during flight. To answer to the research question and prove that the suggested data-driven modeling method provides a more

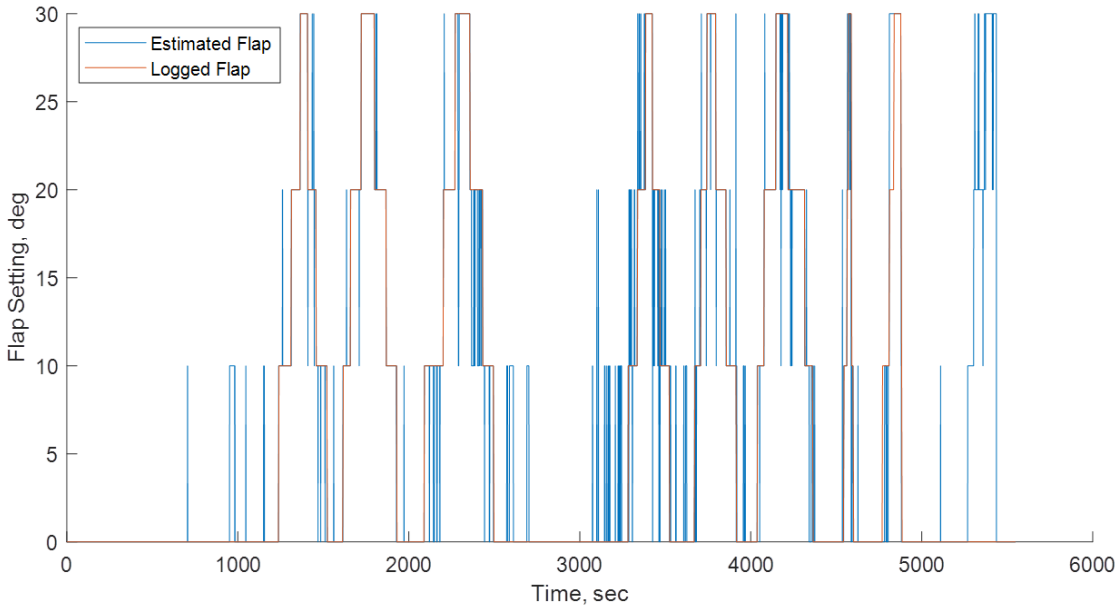

(a) Initial Flap Estimation Result

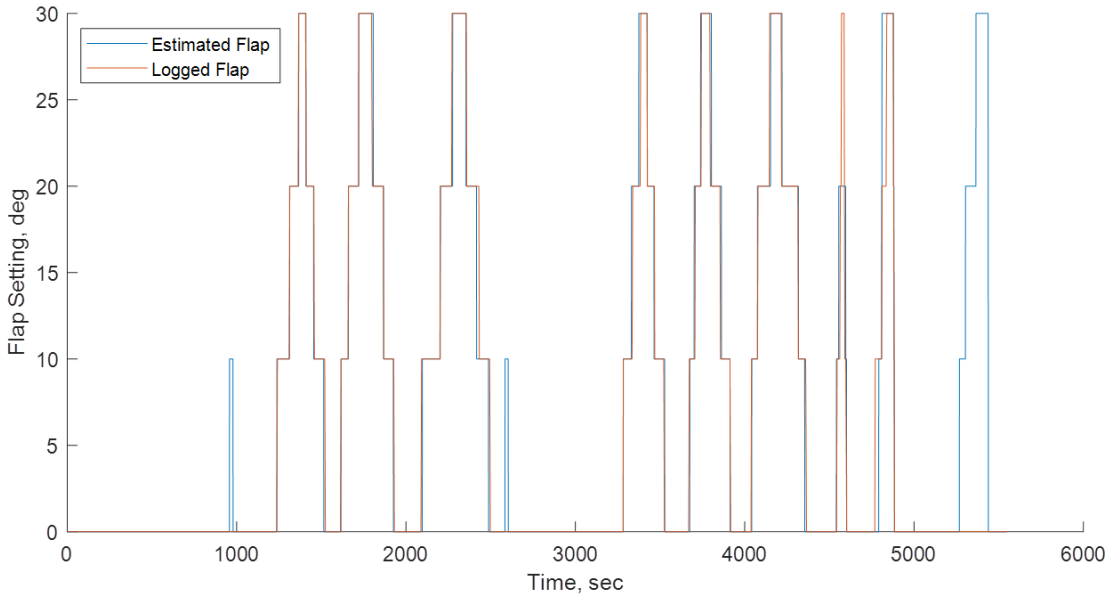

(b) Modified Flap Estimation Result

Figure 4.29: Flap Activity Estimation Result using the Aerodynamic Model

efficient performance model that can detect any unsafe aerodynamic behaviors of an aircraft, this section examines whether the aerodynamic model can identify a stall recovery flight which was a part of the suggested flight maneuver. As proposed, the pilot conducted a constant level flight, then slowly reduced its airspeed maintaining the desired altitude. During the flight, the pilot deployed its flap step by step and stalled with full flap condition, then recovered from the stall. This suggested slow flight and stall maneuver is summarized in Figure 4.30.

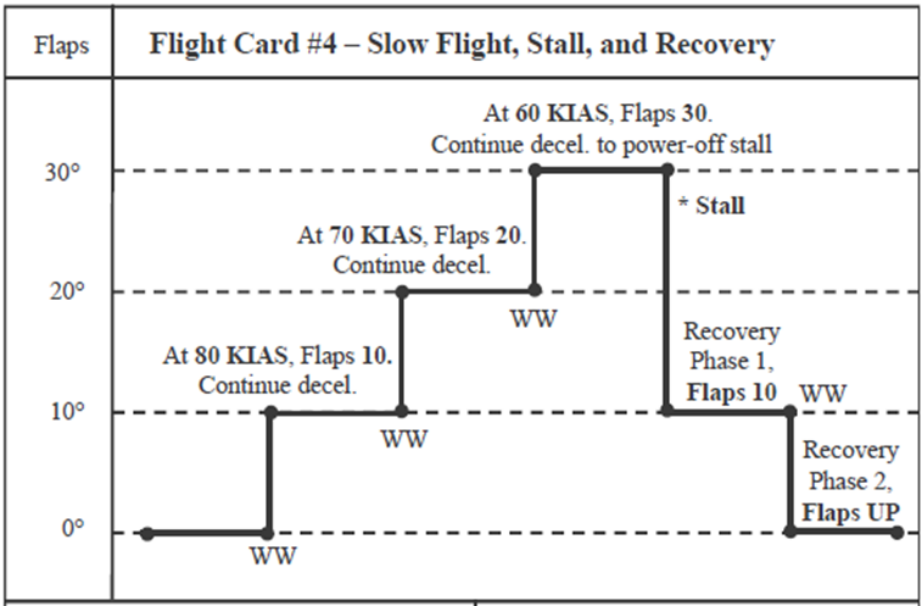

Figure 4.30: Flight Maneuver - Slow Flight, Stall, and Recovery

The flight data during this stall maneuver is shown in Figure 4.31 and marked as red circles. The blue circles are data points from other flight maneuvers such as two cruise flight with flap cycle, maximum power climbing, simulated pattern, and approach and landing. As seen in the figure, many red circles are widely located outside the normal operating region in the lift curve and drag polar domain. At the beginning of this phase of flight, red circles remain in the normal region. However, when the aircraft approaches the stall point, the red circles move toward the outside of the normal operating area. This trend can be more clearly seen in Figure 4.32 which shows lift and drag coefficient errors. The lift and

drag coefficients errors shown in the figure are the minimized error resulted from the data-driven modeling process. As discussed in the modeling process in the previous section, these errors between modeled coefficient and the data are unavoidable errors caused by the inherent uncertainties of the flight data. Thus, these errors are supposed to be close to zero, and any big errors can be considered as the consequences of unexpected events that cannot be estimated by the performance models. In Figure 4.32, it is shown that the modeling errors spike on both lift coefficient and drag coefficient when the aircraft is getting close to stall. Therefore, it can be concluded that the aerodynamic model developed in this study can detect aircraft's unsafe behavior, which is the proximity to stall, by observing the discrepancy between modeled aerodynamic coefficient and actual flight data. This conclusion can only be supported by the fact that the aerodynamic model is accurate, and it is proven in this study that the developed aerodynamic model is accurate enough to detect abnormal behavior of the aircraft and the reliability of the model was supported by showing its capability of flap activity prediction.

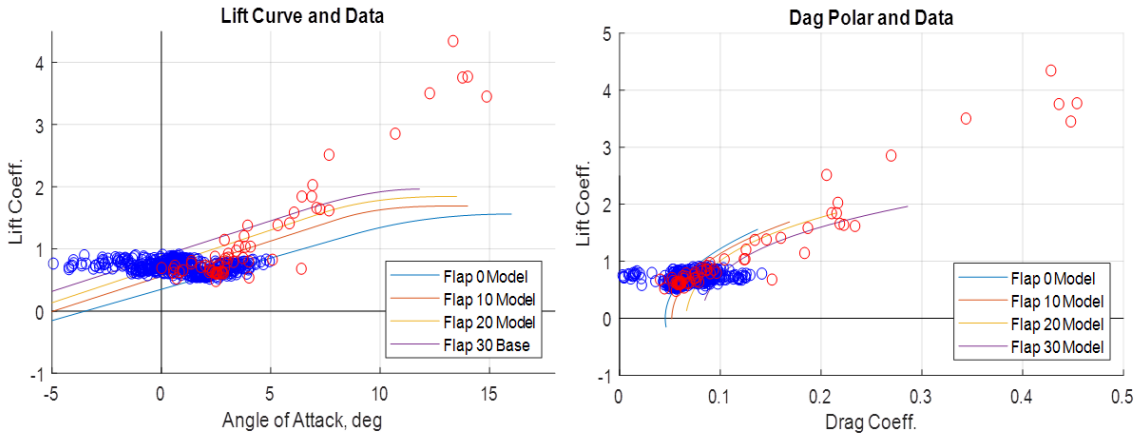

Figure 4.31: Aerodynamic Model and Unsafe Flight Data

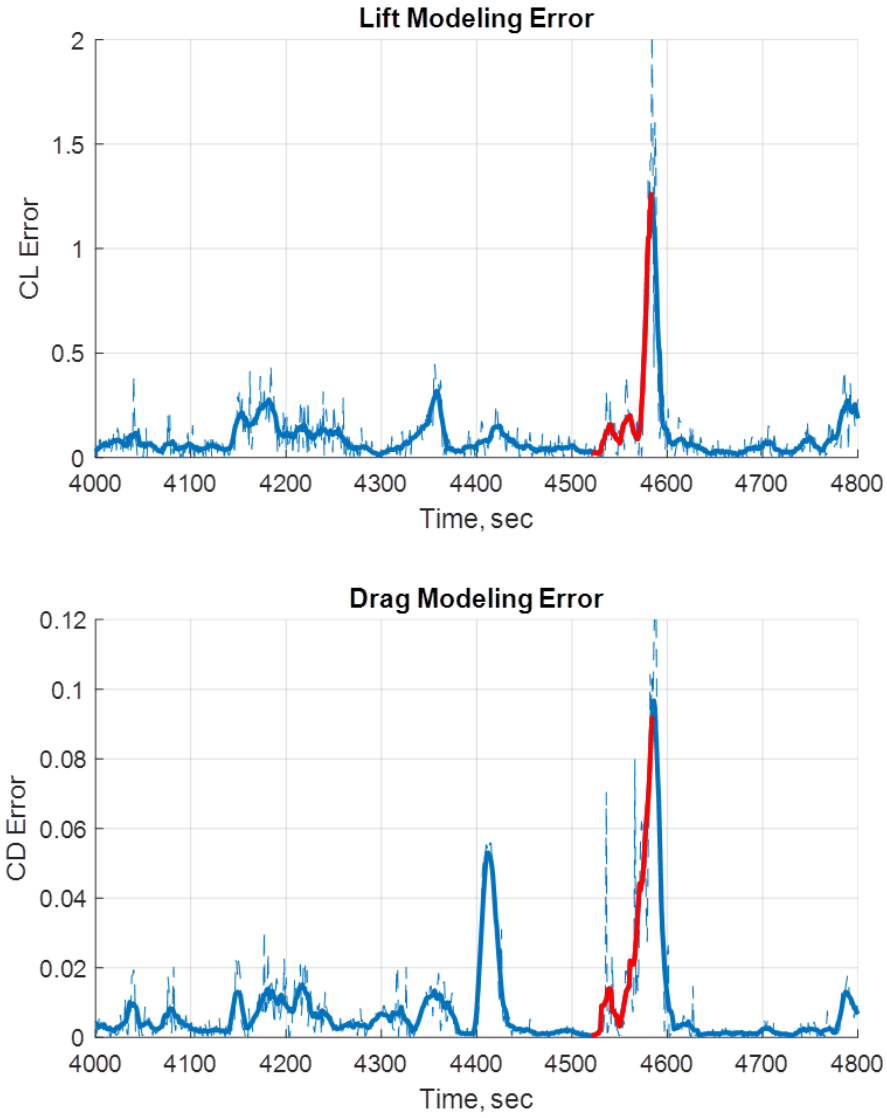

Figure 4.32: Stall Recognition using Aerodynamic Model

4.4.3 Summary

Considering the nature of GA operations, a flexible aerodynamic modeling method for GA fixed-wing aircraft has been elaborated in this chapter. The research goal of this chapter was to generate a realistic and accurate aerodynamic performance model that is computationally affordable with adequate fidelity and compositionally flexible so that this modeling method can be used by any GA aircraft users capturing the characteristics of each aircraft.

To support this goal, the necessary level of the model fidelity was set as the capability of predicting its flap activity in the entire flight. Also, the hypothesis, which is that an unsafe flight of an aircraft can be detected with an accurate performance model and flight data record, was established. For developing an aerodynamic model that meets the necessary level of fidelity, a theoretical model that can serve as the basis model was developed not only using single theoretical modeling method but also evaluating, comparing, and combining all the possible modeling methods. Based on the developed theoretical model, the accuracy of the aerodynamic model was improved by optimizing the shape of the model using shape modification factors and actual flight data. Strategic flight maneuvers were suggested for generating realistic flight data for the modeling process, and the partners at Ohio State University provided the flight data of these maneuvers. It is proven that the final outcome of this data-driven modeling process can estimate the flap activity during flight with high accuracy. Given the accurate aerodynamic model, the proximity to stall can be detected by observing the error which is basically the discrepancy between modeled aerodynamic coefficients and data-driven calculated aerodynamic coefficients.

CHAPTER 5
FLIGHT DATA NOISE FILTERING METHOD DEVELOPMENT

This chapter is devoted to the development of data noise filtering method for GA flight data. Based on the literature survey and the previous data-driven aerodynamic modeling method, it is acknowledged that flight data takes a crucial role in the data-centered GA flight safety enhancement efforts. Thus, improving the quality of flight data by introducing an effective noise removal technique is the primary goal of this chapter. In the beginning, this chapter discusses the proposed methodology and review the research questions and hypothesis that are established in the previous chapter to achieve the research goal. The next section describes the selected data parameters to be filtered and the filtering methods that will be covered in this method. Finally, a quantitative metric that can measure the effectiveness of the filtering method is introduced then the optimal filtering case is selected using the proposed metric.

5.1 Methodology Development

5.1.1 Overview

The main focus of this chapter is to provide a novel approach for noise filtering in the flight data records of GA fixed-wing aircraft. It is noted that flight data record is an irreplaceable factor in assessing and improving GA flight safety. Although ongoing collection and analysis of flight data records takes place an important role in the aviation safety improvement program, one of the most crucial requirements is securing clean and meaningful data that is ready to be analyzed to maximize the benefits of data-driven safety analysis. In other words, removing data noise in the collected data record is as important as collecting and analyzing flight data, and the benefit of using flight data in the process of GA safety

enhancement efforts can be maximized when the data to be used in the process is clean and reliable.

Figure 5.1: Data Analysis Procedure

In addition, as revealed in the previous chapter, flight data can also be used in the data-driven performance modeling process and the accuracy of the performance model can be improved when the flight data is truly providing actual aircraft performance information without data noise. Thus, the objective of this study is to examine various data noise filtering techniques considering inherent characteristics of flight data parameters and to introduce an efficient noise removal method for the purpose of general aviation safety enhancement. This study aims to answer the following research question 2 to achieve the research goal which is ensuring clean flight data to be used in both data-driven GA performance modeling process and GA safety assessment effort.

Research Question 2

What kind of noise filtering techniques or data cleaning methods are suitable for effectively detecting and removing existing noise in flight data while preserving true aircraft behaviors?

One of the most important premises for answering the research question stated above is that the noise filtering technique proposed in this study should not distort the actual behavior of the aircraft. In other words, it is necessary to have a credible metric which represents the true behavior of aircraft. This study suggests the aerodynamic coefficients obtained from the performance model as the metric that can be believed as the factors

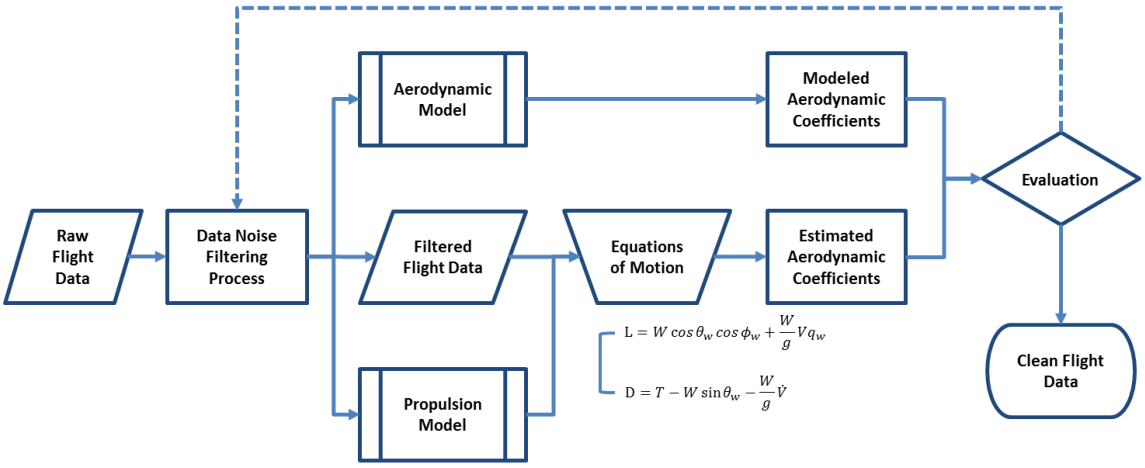

Figure 5.2: Flight Data Noise Filtering Process

which are not affected by data noise. The overall process of the suggested data noise filtering technique is described in Figure 5.2. As shown in the flowchart, the aerodynamic performance coefficients from the previously developed aerodynamic model will serve as the key evaluation metric in this process.

The first approach to answer the research question is to select primary data parameters which will be used in the noise filtering process. As described in the previous chapter for the data-driven aerodynamic modeling process, the data-driven aerodynamic coefficients can be calculated by inputting corresponding flight data parameters into the equations of motion. The logged data parameters cannot be directly used in the equations of motion, so it is necessary to convert the original form of parameters into required input parameters. Thus, proper data noise removal technique has to be applied to the data processing because the parameter converting process can intensify the potential data noise. This study focuses on the original form of data parameters to be converted into the required input parameters for the calculation of data-driven aerodynamic coefficients.

Once the objective data parameters are selected, they are categorized considering the nature of their measurement type. It is assumed that the inherent noise characteristics of logged flight data can differ depending on how the data parameters are measured. For this

reason, flight data measuring devices are surveyed and the selected data parameters are assigned to each category according to the measurement method.

Next step is to apply noise filtering techniques to the categorized data parameters. Among various noise filtering techniques, possibly suitable techniques for flight data parameters are selected in the time domain and the frequency domain filtering methods for capturing a broad range of noise characteristics. The selected filtering techniques are applied to each data categories and the effect of the applied noise filtering method are compared for every combination of the techniques. Finally, this study will suggest a methodology that can select the optimal combination of noise removal techniques by providing answer to the research question Then this methodology will be verified and supported by the suggested experiment described in the next section.

5.1.2 Experiment Setup

Data noise is an unwanted but inevitable presence in the data analysis process. It is certain that data noise is also present in various forms in flight data records. Therefore, the purpose of this research is to remove as much data noise as possible in the flight data. However, since data noise exists in various forms, the effect of noise filtering cannot be maximized using single noise removal technique only. This is because each noise can be effectively removed only by applying a filtering technique that is suitable for its noise characteristics. It is assumed that the noise characteristic is determined by how the data is measured. Therefore, the following hypothesis has been established, and this study attempts to achieve the research purpose which is developing a methodology of effective flight data noise removal by proving this hypothesis.

Hypothesis 2

Specific flight parameters require noise removal techniques that can capture the characteristics of the parameters. Applying a filtering method that is identified considering inherent noise characteristics to corresponding parameters will ensure the necessary level of filtering result.

In order to prove the hypothesis mentioned above, a great number of filtering cases will be developed by combining the pre-selected data noise filtering techniques and the parameters of interest. An important factor to be considered in the case development phase is that the cases should be able to cover the effect of filtering intensity factors used in filtering techniques. For this reason, two levels of filtering intensity factors are chosen for each noise removal technique. In the end, noise filtering cases for the experiment will be technically populated with different types of filtering techniques, different levels of filtering intensity, and different categories of data parameters. The process of developing effective noise filtering cases will be explained in detail in the following sections.

The basic purpose of the filtering cases populated in this study is to find the best combination of filtering techniques with optimal filtering intensity factor applied to appropriate data parameters. To test and select the best way of data noise filtering for flight data analysis, it is required to have a quantitative metric that can measure the effectiveness of each filtering case. This study proposes a metric named "Filtering Effectiveness Value (FEV)" which is a newly developed form of error between noisy data and true data. Thus, the main goal of this test is to find the case that minimizes the suggested FEV. The definition of FEV and how it is calculated will be explained in the following section in detail. Using this evaluation metric, the most effective way of flight data noise filtering will be selected, then the hypothesis will be proved in the end.

5.2 Motivation for Data Noise Filtering

In the data-driven process, it is obvious that the data quality greatly affects the result from data analysis. When some data parameters are cannot be directly obtained from the database, but the unknown parameters are the necessary complement of the data process, they may have to be calculated using given data parameters. Especially in GA aircraft, the acquisition of enough data parameters are limited, so conversion between data parameters frequently occurs. For example, the Garmin G1000 data logging system in C172S aircraft does not provide any angle-of-attack parameter, which is the most critical parameter for aerodynamic models. Angle-of-attack information during flight can be easily obtained when the airspeed parameters in both x-direction and z-direction in wind frame are available. When the flight data record does not have the information of airspeed in the wind frame, and Angle-of-attack can also be calculated using its flight path angle and pitch angle. The flight path angle is also not provided by the G1000 system, and it can be calculated using ground speed and vertical speed. When the ground speed is not available in the data set, it can also be calculated using latitude and longitude information. As can be seen from the above example, many converting steps with a number of data parameters may be needed for obtaining one required parameter. In this situation, the quality of the obtained parameter, angle-of-attack, cannot be trusted when the data quality of the input parameters for the conversion, such as latitude, longitude, vertical speed, and pitch angle is not guaranteed. In fact, the quality of the final outcome of this process can become worse because of the nature of noises. The following test case can support this statement.

Assuming that an aircraft is in a simple cruise condition, its lift coefficient during this maneuver can be calculated using simple equations when its weight, reference area, and flight conditions are given. The necessary data parameters and detailed flight conditions are given below.

- Phase of flight : Constant speed level flight - cruise

- Aircraft weight : 2,200 lbf (constant)
- Reference wing area : 174 ft^2
- Cruise altitude : 4,000 $ft(MSL)$ (constant)
- Air density : 0.0023 $slug/ft^3$ (constant)
- Cruise airspeed : 70 $knots$ (constant)
- Cruise duration : 300 sec

During the sample cruise flight, the lift coefficient can be calculated using the aircraft weight, altitude, air density, and airspeed, known that lift is equal to the aircraft weight. In this situation, the calculated lift coefficient during this flight is also constant. The noise effect on this conversion process is evaluated using normal distributed random noise which is generated and added to each parameter. The clean parameters and noisy parameters are compared in Figure 5.3, and the distribution of the generated noise for each parameter is shown in Figure 5.4. In the figures, the lift coefficient is the calculated parameter using the other three parameters.

In order to quantify noisiness of data, root-mean-squared error (RMSE) and signal-to-noise ratio (SNR) is calculated for each parameter. The RMSE is a metric that measures the differences between true value and noisy value. Smaller RMSE is better because it is basically the sum of squared error. The SNR is one of the most widely-used metrics which compares a level of signal power to a level of noise power. SNR is most often expressed in decibels (dB). When it is required to reduce data noise, higher SNR numbers mean a better specification, since there is more signal power then noise power. That means data with higher SNR has more useful information than unwanted data, the noise. The result of this noise effect test described in Figure 5.5 provides a meaningful motivation for this research. According to the result, the SNR of the calculated parameter, Lift coefficient, has decreased by 19.3% compared to others, which means the noise power has been increased

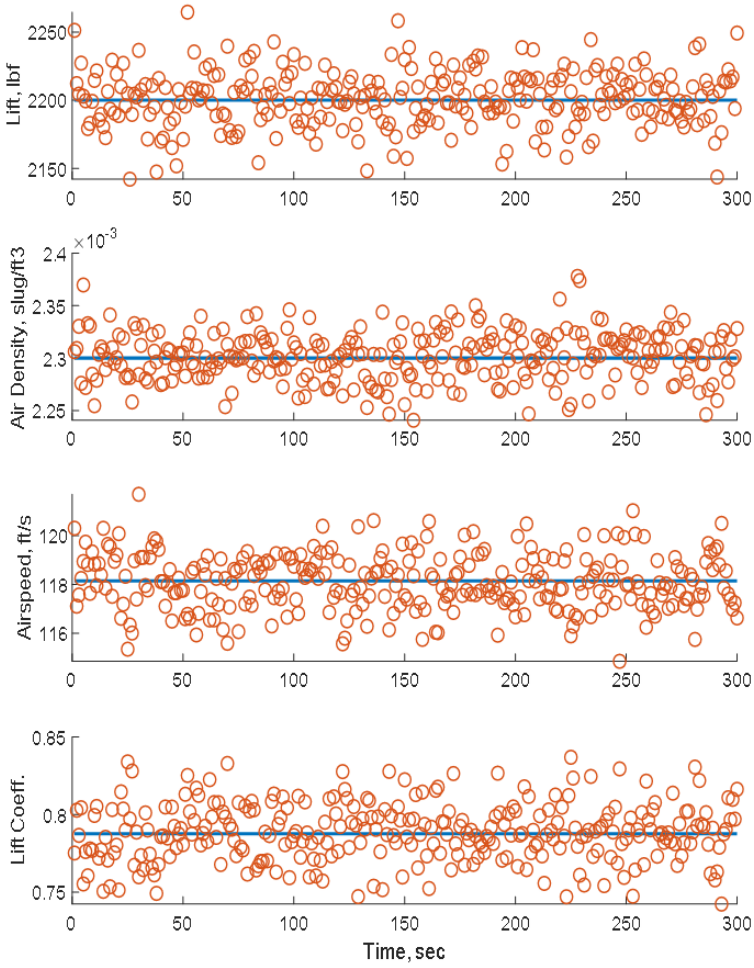

Figure 5.3: Sample Data Parameters with Artificial Noise

after the calculation. The result of RMSE shows a similar result. The RMSEs for each parameter are normalized using their mean value so that they can be compared in the same domain. As shown in Figure 5.5 (b), the normalized RMSE of the estimated lift coefficient is 143% higher than that of the other parameters. The test result leads to the conclusion that data noise removal is an essential step before processing the given data parameters for data analysis tasks to avoid any unwanted situation such as potential data noise is intensified by the parameter converting process. The rest of this chapter will discuss how the unwanted data noise in the flight data can be filtered scientifically.

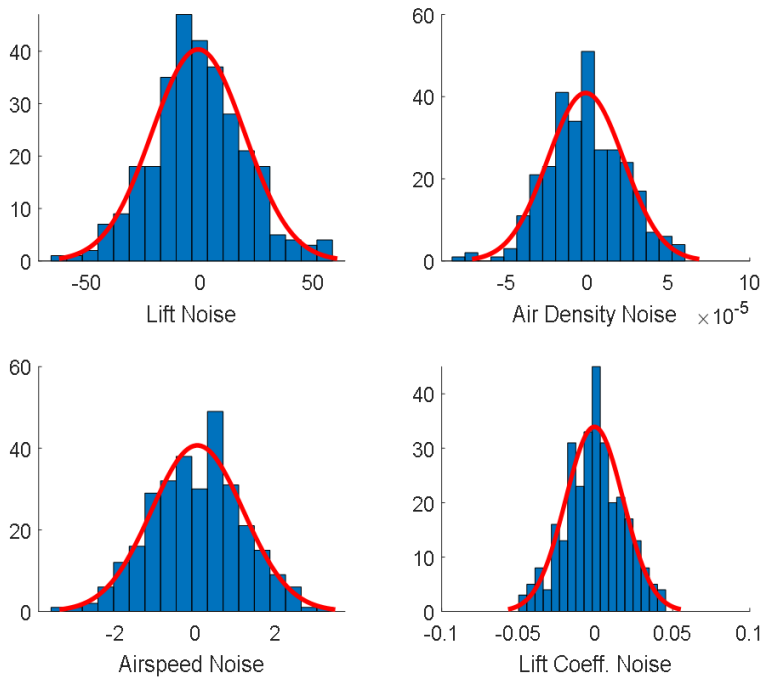

Figure 5.4: Artificial Noise Distribution

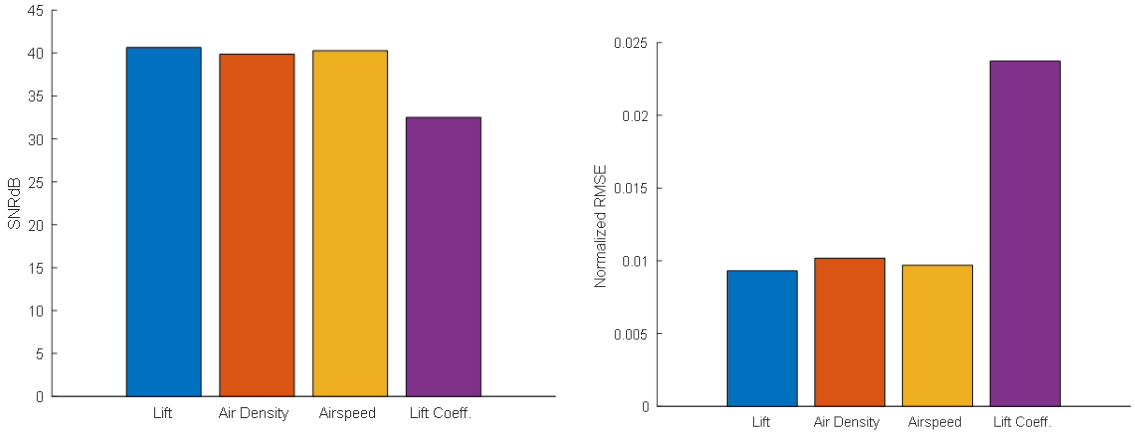

(a) Signal-to-Noise Ratio

(b) Normalized RMSE

Figure 5.5: Noise Comparison between Input Parameters and Calculated Parameter

5.3 Flight Data Parameters

5.3.1 Parameter Selection

Identifying important parameters to be used in this noise filtering effort is the first step to be considered. The equations of motion play the most crucial part by connecting the

data-driven aerodynamic coefficient and modeled aerodynamic coefficients. Among many other data parameters in the logged flight data set, this study focuses on the parameters used in this equations of motion. Equations 5.1 and 5.2 are the equations to be used for the data processing, and Equations 5.3 and 5.4 are the equations for converting the outputs of the equations of motion, lift and drag, to non-sensationalized parameters, aerodynamic coefficients.

$$L = W\cos\theta_w\cos\phi_w - \frac{W}{g}V_{abs}q_w \tag{5.1}$$

$$D = T - W\sin\theta_w - \frac{W}{g}\dot{V}_{abs} \tag{5.2}$$

$$C_L = \frac{2L}{\rho V_{abs}^2 S} \tag{5.3}$$

$$C_D = \frac{2D}{\rho V_{abs}^2 S} \tag{5.4}$$

The equations of motion require multiple parameters as its inputs, and they are primarily from the flight data records. However, the logged flight data parameters need to be pre-processed to be used in the equations above because the flight data record does not log every input parameters for the equations. The input data parameters for the equations can be divided into three groups: Direct parameters, calculated parameters, and given parameters. The direct parameters are the parameters that can be obtained directly from the flight data records. The roll angle is the only parameter that is logged by the data recorder and used in the equations as its original form for the data processing. The calculated parameters are the parameter that is not recorded by the data logging system but can be calculated using other data parameters in the logged dataset or previously given or known parameters. For example, the angle-of-attack parameter can be calculated using ground speed, vertical

speed, and pitch angle as discussed in the previous section for the noise effect test. Other the than angle-of-attack, pitch rate, absolute speed are dynamic pressure are other examples of the calculated parameters. The last group is the given parameters which are obtained from other sources such as the pilot's operating handbook (POH), propulsion model, or standard atmosphere table. The wing area, thrust, and aircraft initial weight the parameters that belong to the given parameters category. Although the thrust parameter is considered as a given parameter, actually the propulsion model is given, so any other logged parameters that are required for the propulsion model need to be included in the target parameters to be filtered. All data parameters needed in this process are listed in Table 5.4 with a brief explanation of how they are obtained and what other parameters are required for getting that particular parameter.

The relations of all the data parameters mentioned above is systematically described in Figure 5.6. As discussed earlier, the data-driven aerodynamic coefficients are calculated using the corresponding flight data parameters into the equations of motions. Also, angle-of-attack information from the flight data record will provide the modeled aerodynamic coefficients which are considered as the reference data points. all the data parameters from the data recorder will be transformed into the inputs of the equations as well as the input for the aerodynamic model. Then, the data-driven and the modeled coefficients are compared to measure the effectiveness of the applied filtering cases. Finally, the parameters that will be filtered in this study are selected and listed in Table 5.1.

As shown in Figure 5.6, This data processing flow includes many calculations, and this implies that this data process can amplify the data noise inherent in the data parameters. Thus, it is highly important to apply proper data noise removal techniques to this data processing steps to prevent the data quality from deteriorating. The next section will discuss the nature of these parameters and how they can be categorized considering their measurement methods.

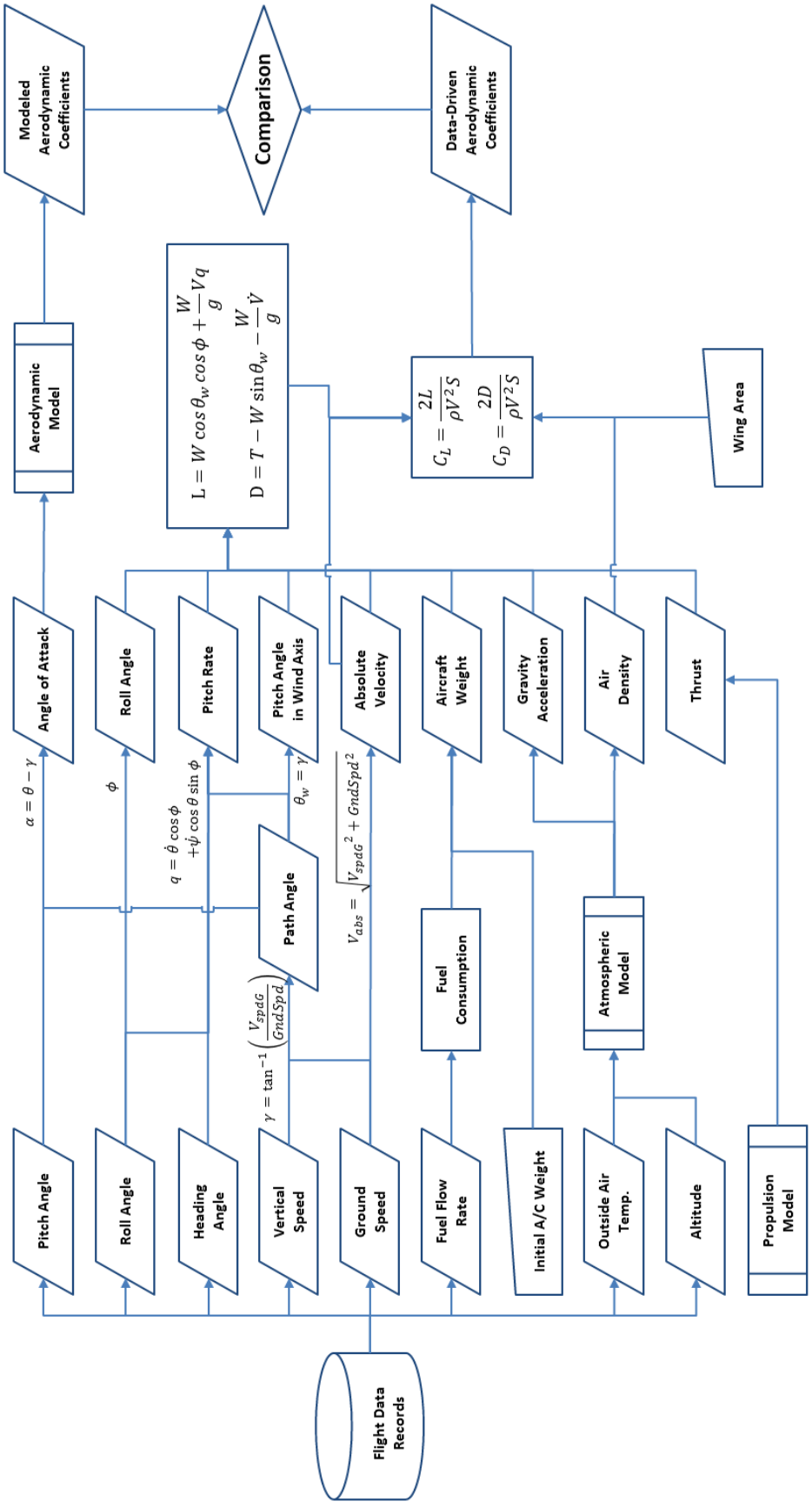

Figure 5.6: Flight Data Processing Flow Chart

Table 5.1: Selected Parameters for Noise Filtering

Parameter	Description	Unit
$AltMSL$	Mean-sea-level altitude	$ftMSL$
IAS	Indicated airspeed	$knots$
TAS	True airspeed	$knots$
$Pitch$	Pitch angle	deg
$Roll$	Roll angle	deg
HDG	Heading	deg
OAT	Outside air temperature	$degC$
$GndSpd$	Ground speed	$knots$
V_{SpdG}	Vertical speed – GPS	fpm
RPM	Engine revolution per minute	rpm
F_{Flow}	Engine fuel flow	gph

5.3.2 Parameter Categorization

The data parameters mentioned above are measured in many different ways using different measuring devices. Because the main purpose of this study is to remove noise from the flight data parameters, a sufficient understanding of how the data parameters are measured is necessary for this study. This is because the nature of the inherent noise of the data parameters depends on the way how they are measured, and noise removal techniques should be applied differently depending on the nature of the noise. Therefore, this section will describe the principles of how the above-mentioned data parameters are measured, then classify the selected parameters to be filtered in this study according to the corresponding measurement methods.

Flight Instruments

To understand the nature of data noise in the flight data parameters, flight instruments for measuring the flight data are surveyed and explained in this section. The flight instruments for measuring flight data can be classified into six groups: Pitot-static system, gyroscopic system, magnetic system, thermometric system, global positioning system, and engine system. The principles of each measuring system and their basic concept will be discussed in the following sections.

• *Pitot-Static System*

The pitot-static system is a combined system which measures airspeed, altitude, and vertical speed. This system uses the static air pressure and the dynamic pressure caused by the motion of the aircraft during flight. The static air pressure, or ambient pressure, is simply the barometric pressure in the air where the aircraft is present. The dynamic pressure is a pressure due to the motion of the aircraft. These two pressures measured by the pitot tube in this system are transferred to the airspeed indicator, vertical speed indicator, and altimeter. The components of this pitot-static system are described in Figure 5.7. This system sends the measured airspeed, altitude, and vertical speed from the air pressure to the flight data recorder.

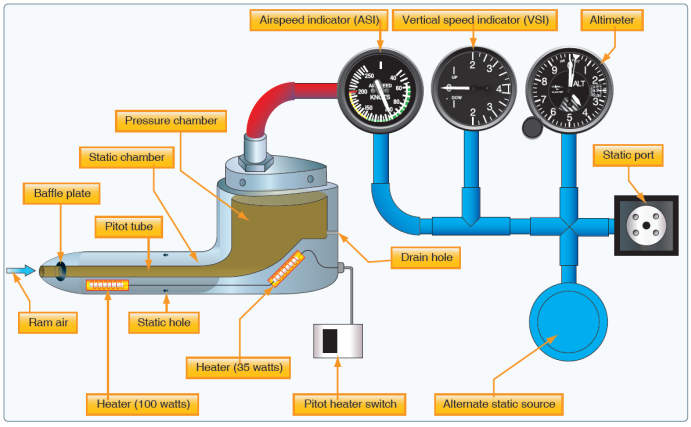

Figure 5.7: Pitot-static system[68]

• *Gyroscopic System*

The gyroscopic system is the instrument that measures the attitude of the aircraft. Among various flight instruments utilize the properties of a gyroscope for their operation, the attitude indicator is the most common instrument containing gyroscopes. A gyroscope is a wheel that is mounted on the instrument to capture the motion of any spinning object. By mounting this wheel on a set of gimbal rings, the gyro is able to rotate freely in any direction. Thus, if the gimbal rings are tilted or twisted, the gyro remains in the plane in which it was originally spinning. The attitude of the aircraft attitude such as pitch and roll angle is measured based on this principle. The attitude indicator shown in Figure 5.8 (a) is the device that displays a picture of the attitude of the aircraft, and this device indicates the changes in attitude instantaneously.

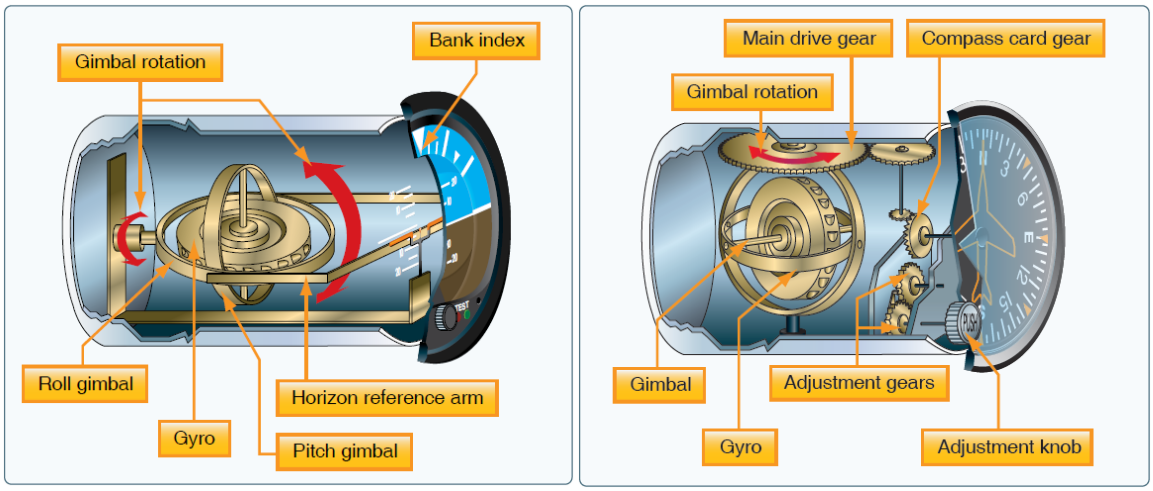

(a) Attitude Indicator (b) Heading Indicator

Figure 5.8: Gyroscopic System and Magnetic System [68]

• *Magnetic System*

The magnetic system is basically the compass system that shows direction relative to the geographic directions. The heading indicator shown in Figure 5.8 (b) is fundamentally a mechanical instrument designed to facilitate the use of the magnetic compass. Although

this device utilizes the gimbal rotation same as the gyroscopic system, heading indicator is separated from the gyroscopic system because errors in the magnetic compass may cause a different type of data noise. The magnetometer in the G1000 provides the magnetic north reference and the heading parameter can be obtained from this information.

• *Thermometric System*

The thermometric system is the device that measures the outside air temperature. The temperature sensor consists of a bimetallic-type thermometer in which two different materials are combined together in a single strip and twisted into a helix [68]. The outside temperate measured by this sensor is transmitted to the flight data recorder and logged as a parameter named OAT which will provide meaningful information for the condition of the atmosphere. This information is also an input for the propulsion model which provides the estimated thrust during the flight.

• *Global Positioning System*

The global positioning system, known as GPS, is a satellite-based radio-navigation system. This system in the aircraft is actually a receiver of the GPS signal from four or more GPS satellites. The Garmin G1000 GPS receiver receives not only latitude and longitude information but also geometric height above Mean Sea Level which can vary significantly from the altitude information from the pressure altimeter. The ground speed and vertical speed parameters are based on this GPS signal. Thus, it is considered that the potential noises in these two parameters have similar characteristics.

• *Engine System*

The flight data parameters which are related to the aircraft engine is the fuel flow rate and the RPM. The fuel flow rate provides information about fuel consumption, so the weight changes during flight can be measured. The RPM is an important parameter that

indicates the throttle setting set by the pilot. This information is a crucial element for the propulsion model for estimating the thrust. The fuel flow rate and the RPM use different sensors to measure the values, but they are considered as one category in the study. The assumption that the engine itself is the most contributing factor that causes data noise in the two parameters is the main reason why the parameters fall into this engine system category together.

Categorized Data Parameters

Based on the measuring method explained in the previous sections, the target parameters to be used in this noise filtering study are grouped by six categories and they are summarized below. It is assumed that the data parameters in the category have similar nature of noise in them, thus the same noise filtering technique is required for the parameters in the category.

- Pitot-Static System : Mean-sea-level altitude, Indicated airspeed, True airspeed
- Gyroscopic System : Pitch angle, Roll angle
- Magnetic System : Heading
- Thermometric System : Outside air temperature
- Global Positioning System : Ground speed, Vertical speed
- Engine System : Engine revolution per minute, Engine fuel flow

5.4 Noise Filtering Techniques

5.4.1 Overview of Noise Filtering Methods

Flight data quality enhancement is a fundamental topic of this chapter as discussed earlier. Depending on the mechanism that generates the flight data, the noise can be classified

into different categories, and the selected data parameters for this study were categorized in the previous chapter considering the measuring mechanism. Data noise reduction can be performed in two domains: Time-domain and frequency-domain. Frequency-domain approaches are usually preferred in real-time applications because they can be implemented efficiently compared to the time-domain approaches. However, frequency-domain approaches cannot efficiently remove a certain type of noise such as residual noise [69]. The time-domain noise reduction approach does not have this problem, but they are computationally more complex. The research question in this chapter is stated here again.

Research Question 2

What kind of noise filtering techniques or data cleaning methods are suitable for effectively detecting and removing existing noise in flight data while preserving true aircraft behaviors?

In order to answer the question, multiple data noise filtering techniques are surveyed in both time and frequency domain to effectively remove various types of noise stored in the flight data parameters. Based on the surveyed filtering methods, proper filtering techniques are selected for the research goal which is developing an efficient methodology of flight data noise filtering specifically for data-driven flight safety assessment effort.

5.4.2 Time-Domain Noise Reduction Techniques

Moving Average Method

The moving average method is the most well-known filtering method especially for digital signal processing because it is the easiest filtering method to understand and use. This method is optimal for reducing random noise while retaining a sharp step response. However, the moving average is the worst filter for frequency domain signals, with little ability to separate one band of frequencies from another [70].

This filtering method smooths data by substituting each data point with the average of the adjacent data points within the span which is set by users. This filtering process requires an input called "span" which is the sample size of the data points they are averaged by the filter at a time. When the span size is given, the moving average filter calculates the average of the data points within the span size and produces a single output. This averaging process is expressed in Equation 5.5 where x is the input, y is the output, and M is the span size, As the span increases, the filtering intensity becomes higher, and this means the smoothness of the output increases.

$$y_i = \frac{1}{M} \sum_{j=0}^{M-1} x_{i+j} \tag{5.5}$$

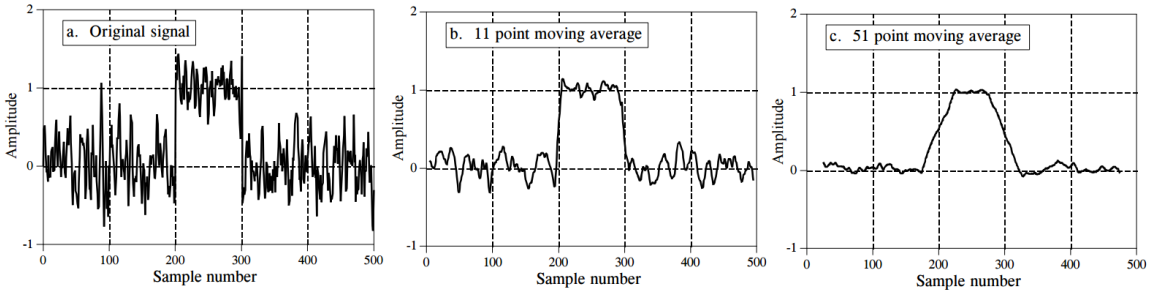

Figure 5.9: Example of a Moving Average Filter with Different Number of Points [71]

Local Regression Method

The local regression method is a type of generalized moving average and polynomial regression method [72]. This method fits a smooth curve between two variables or a smooth surface between an outcome and the predictor variable [73]. Figure 5.10 shows the basic concept of the local regression method. At each point, this technique utilizes a regression function to fit nearest neighbors of that point. The most common techniques of this method are LOESS (locally estimated scatterplot smoothing) and LOWESS (locally weighted scatterplot smoothing) filter. Both are non-parametric regression methods that combine multiple regression models in a k-nearest-neighbor-based meta-model [73]. These techniques

use a robust weight function so this process is resistant to outliers [74]. The biggest difference between the two techniques is the model used in the regression. LOWESS uses a linear polynomial model and LOESS uses a quadratic polynomial model. This method extends the idea of fitting a line over variable bin-widths but it is a weighted regression line. The process is weighted because a regression weight function is defined for the data points contained within the span. This span is the input variable for this filtering method defined by users. Like the moving average method, the smoothness of the output increases as the span increases. This study will apply the LOESS method which is more suitable for non-linear signals.

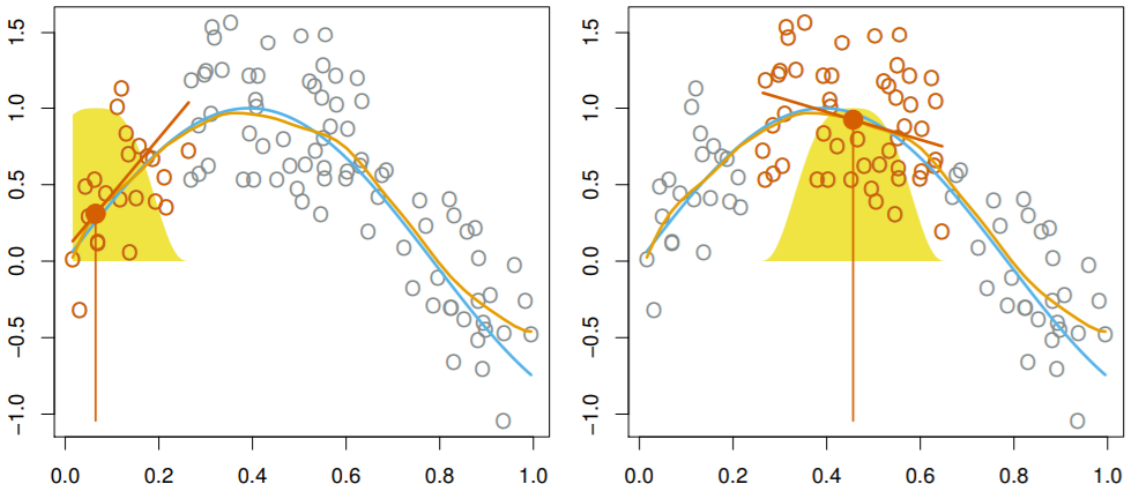

Figure 5.10: Example of Weighted Local Regression [75]

Smoothing Spline Method

The smoothing spline is a method of fitting a smooth curve to a data set which may contain noise using a spline function, and it provides a flexible way of estimating the underlying regression function. The basic definition of the spline function is that it is a curve created from polynomial sections that are subject to conditions or continuity at their joints [76]. Spline interpolation method gives a good trade-off between the smoothness of the data and its closeness to the data points. [77]. This method minimizes the following value,

where p is the specified smoothing parameter and W_i is the specified weights.

$$p\sum_i w_i(y_i - s(x_i))^2 + (1-p)\int(\frac{d^2s}{dx^2})^2 dx \tag{5.6}$$

In Equation 5.6, when the smoothing factor p becomes one, it generates a cubic spline interpolant while it creates a least-squares line fit when p equals zero. This study will investigate the effect of the smoothing spline filtering method with two different levels of the smoothing factor.

5.4.3 Frequency-Domain Noise Reduction Techniques

Fast-Fourier Transform Method

The Fast Fourier Transform (FFT) is a method for calculating the discrete Fourier transform to sample signals in time-series and to divide them to their frequency components. In other words, the FFT is a converting process for a signal from time domain to frequency domain. The baseline of this filtering method is that actual data and noise data have their frequencies, so by looking at the signals in the frequency domain, the noise can be efficiently distinguished then removed. The basic concept of this signal transformation is illustrated in Figure 5.11.

While it produces the same result as the other approaches, it is incredibly more efficient,

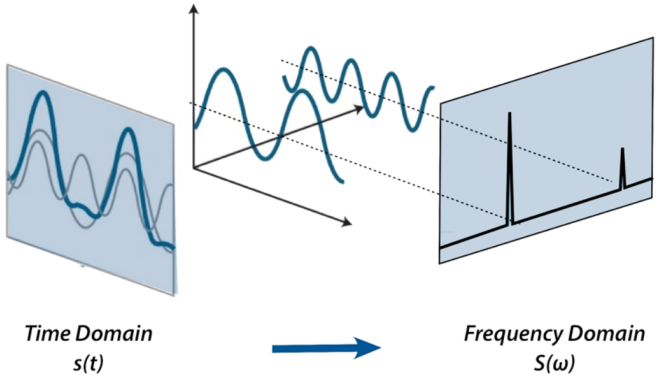

Figure 5.11: Signals in Time Domain and Frequency Domain [78]

often reducing the computation time by hundreds. As shown in Figure 5.12, FFT consists of three steps. The first step is to decompose an N point time domain signal into N signals each containing a single point. The next step is to find the spectrum of each of the N point signals. The final step is to synthesize the N frequency spectra into a single frequency spectrum [70] . During the FFT filtering process, the target data points can be filtered using a sum of weighted sine and cosine terms of increasing frequency.

The FFT filter has very good smoothing procedures, and users can choose cutoff frequency which controls its filtering intensity. Also, this filter is computationally efficient because it stores the coefficients rather than the data points. Adding FFT terms with higher frequency components improves the quality of the fit of areas containing rapid changes. In this study, the FFT filtering effect will be investigated with different levers of the cutoff frequency.

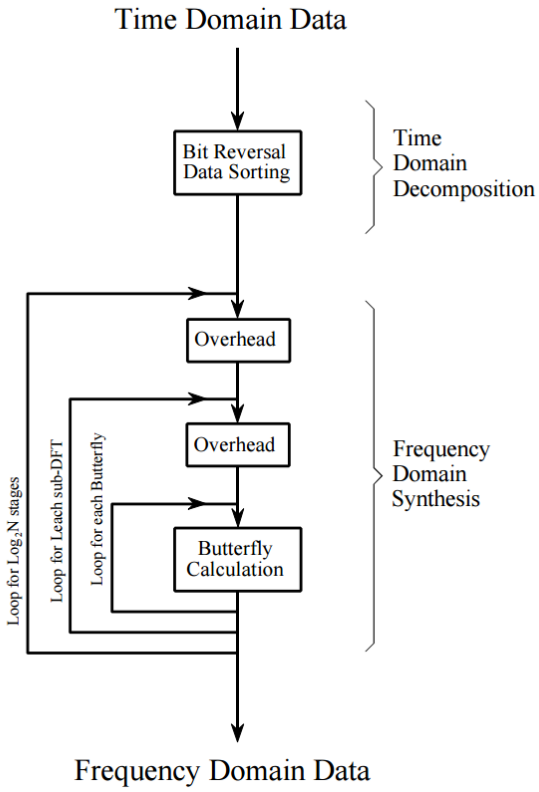

Figure 5.12: Flow Diagrom of the FFT [70]

Empirical Mode Decomposition Method

The empirical mode decomposition (EMD) is an adaptive method in which a given discrete signal is decomposed into a set of oscillating components through a transformation process [79]. The EMD method is inherent to the Hilbert-Huang Transform (HHT) which is a transformation algorithm for decomposing the given data in time domain into its oscillatory modes named intrinsic mode functions (IMF) in the frequency domain. This transformation process is called the "sifting process," and the steps of this process are summarized as listed below [80].

- Determine the location of local maxima and minima of given signal $X(t)$ to construct an upper envelope $s_+(t)$, and a lower envelope $s_-(t)$.
- Calculate the mean envelope of the spline curves at i^{th} iteration, $m_{k,i}(t)$.

$$m_{k,i}(t) = \frac{1}{2}[s_+(t) + s_-(t)] \tag{5.7}$$

- With $c_k(t) = X(t)$ for the first iteration, subtract mean envelope from residual signal. The procedure is iterated again at step 1 with the new value of $C_k(t)$.

$$C_k(t) = C_k(t) - m_{k,i}(t) \tag{5.8}$$

- If $C_k(t)$ matches the criteria of an IMF, a new residual is computed. To update the residual signal, subtract the k^{th} IMF from the previous residual signal.

$$r_k(t) = r_{k-1}(t) - c_k(t) \tag{5.9}$$

- Then begin from step 1, using the residual obtained as a new signal $r_k(t)$, and store $c_k(t)$ as an intrinsic mode function.

- For N intrinsic mode functions, the original signal is represented as,

$$X(t) = \sum_{i=1}^{N} c_i(t) + r_N(t) \tag{5.10}$$

Once IMFs are obtained, they yield instantaneous frequencies as functions of time that give sharp identifications of embedded structures. Thus, this filtering method provides meaningful information about instantaneous frequency information. Another advantage of this EMD method is its high efficiency that can be gained from the adaptive process. Also, since the decomposition is based on the local characteristic time scale of the data, it is applicable to nonlinear and non-stationary processes. For the purpose of the noise filtering work, the EMD filtering method will be implemented to the selected flight data parameters and its filtering effectiveness will be examined.

5.5 Experiment and Result

5.5.1 Case Development

The primary purpose of this experiment is to effectively apply various noise reduction techniques to the selected flight data parameters. As stated earlier, it is assumed that there exist various types of noise in the flight data; thus different ways of noise removal technique are required to maximize the benefits of this noise filtering process. For this experiment, a total of 11 data parameters that take the main role in the process of flight data analysis are selected. The selected data parameters are grouped by six categories considering how they are collected in terms of measuring devices. Then, various data noise filtering techniques and their characteristics are surveyed and summarized. Among many noise filtering methods, three filtering techniques in time-domain and two techniques in frequency-domain are chosen for this study. The focus of this noise-filtering study is to investigate the effect of different filtering techniques with varying factors of intensity. The larger the filtering factor, the more data is filtered. Conversely, the smaller the filtering factor, the less data is

filtered. Figure 5.13 shows an example of the effect of filtering intensity factors applied to a sample indicated airspeed parameter.

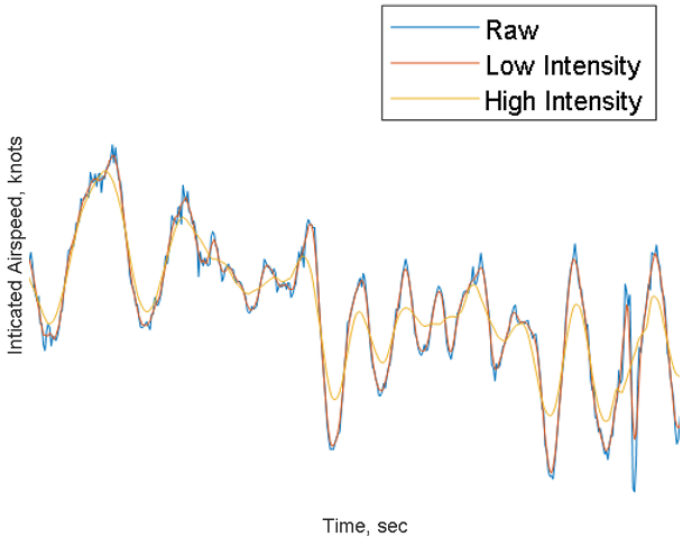

Figure 5.13: The Effect of Filtering Intensity Factor Levels

Since each noise filtering technique has its own filtering intensity factor which affects the filtering result significantly, two levels - high and low - of the intensity factors for each technique were defined. The two different levels of intensity factors can be used to detect the effect of intensity factors on the data noise filtering result. The high and low-intensity levels are chosen based on the observations from the preliminary filtering effect tests. The selected noise filtering methods and their intensity factor settings for this data noise filtering study are summarized in Table 5.2.

Table 5.2: Selected Noise Filtering Methods and Intensity Factor Settings

Filtering Methods	**Intensity Factor**	**High**	**Low**
Moving Average (MA)	Span	20	5
Robust Loess (RL)	Span	20	5
Smoothing Splines (SS)	Smoothing Parameter	0.5	0.1
Fast-Fourier Transform (FFT)	Cutoff Frequency	0.25	0.0625
Empirical Mode Decomposition (EMD)	Tolerance	0.02	0.98

Given the categorized data parameters, the selected data noise removal techniques, and the defined intensity factors, this study attempts to evaluate the noise filtering effectiveness of all the possible combinations of filtering techniques and data parameters. Therefore, total 1,000,000 noise filtering cases are populated with six data categories and five noise filtering techniques with two levels of each filtering intensity factor. Figure 5.14 illustrates the overall process of this case development. Among the developed filtering cases, the most effective filtering combination will be selected with a suggested quantitative metric which will be explained in the next section.

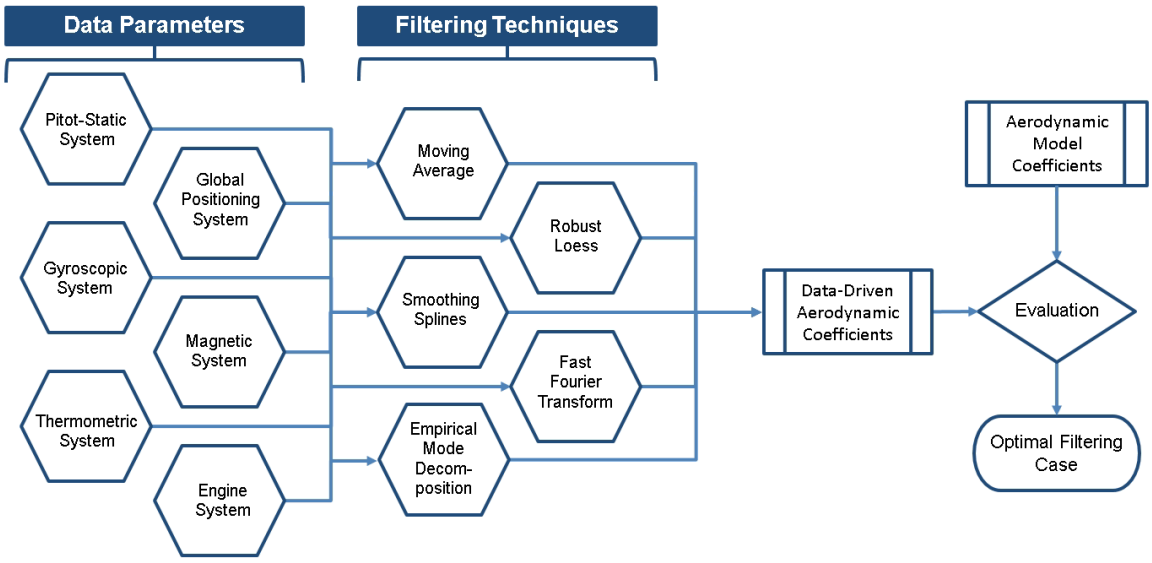

Figure 5.14: Noise Filtering Case Development and Evaluation Process

5.5.2 Filtering Effectiveness Evaluation

Evaluation Strategy

To maximize the effect of the data noise removal process, the effectiveness of noise filtering methods has to be quantitatively defined first. As shown in Figure 5.14, the filtered data parameters will be converted into aerodynamic coefficients then compared to the aerodynamic coefficients obtained from the aerodynamic model. The most important aspect during the flight data noise removal process is that the noise filtering process should

remove data noise only while maintaining the true behavior of the aircraft. If the noise filtering process is not appropriately applied, the noise filtering result of this process is against the research purpose because the true information can be lost. The aerodynamic coefficients provided by the accurate model can be trusted as the true information when the model is accurate, and that is why the modeled aerodynamic coefficients are considered as reference data points. Therefore, the outcome of each noise filtering case will be compared to the modeled aerodynamic coefficient and the difference between them will be measured using a quantitative metric. This quantitative metric represents the effectiveness of the noise filtering case and the best case will be selected in the end.

Evaluation Metrics

This section suggests several quantitative a metric that can be used for the evaluation process discussed in the previous section. Since the goal is to minimize the errors between the data-driven aerodynamic coefficients and modeled aerodynamic coefficients, this study will measure the magnitude and dispersion of the errors using root-mean-squared error and standard deviation respectively. Also, the signal-to-noise ratio (SNR) will compare the desired data and filtered data noise. Finally, this study will suggest a combined metric named filtering effectiveness value (FEV) which has to be minimized to obtain the best result. In this experiment, the FEV for each filtering case will be calculated, then the case which has the minimum FEV will be considered as the best combination of data parameters and data noise filtering techniques.

• *Root-Mean-Squared Error (RMSE)*

One of the most common metric used to measure errors is the root mean square error (RMSE) [81]. The RMSE is defined as the sum of the square root of the errors, and it can be calculated using Equation 5.11, where $\hat{y}_i$ is reference data, y_i is estimated data, and n is a number of data points. This metric provides information about the magnitude of the

errors. Thus, lower RMSE value means the error between reference data and estimated or filtered data is small.

$$RMSE = \sqrt{\frac{\sum_{i=1}^{n}(\hat{y}_i - y_i)^2}{n}} \tag{5.11}$$

• *Standard Deviation (SD)*

The standard deviation (SD) is another common metric that represents a characteristic of errors. The SD is used to quantify the variation or dispersion of a set of reference data and estimated data, and it can be calculated using Equation 5.12. In the equation, $\bar{e_i}$ is the mean of errors, e_i is the errors at each data point. When this value is small, it indicates that the data points are close to the mean of the data points. Therefore, it is required to have the smallest SD in this experiment because it means that the errors between the modeled aerodynamic coefficients and data-driven coefficients tend to be close to the mean which is desired to be zero.

$$SD = \sqrt{\frac{\sum_{i=1}^{n}(\bar{e_i} - e_i)^2}{n-1}} \tag{5.12}$$

• *Signal-to-Noise Ratio (SNR)*

The signal-to-noise ratio (SNR) is a measurement which compares the desired signal and the background noise. This value is a proportion of desired signal power to noise power, and it is often expressed as decibels: Signal-to-noise ratio in decibel (SNRdB). The SNRdB can be expressed as shown in Equation 5.13, where P_{signal} is signal power and P_{noise} is noise power [82]. When the SNRdB is higher than 0, it means there is more signal power then noise power. Thus, a higher SNRdB value is desired because that means the data contains more powerful signal information compared to noise information. This study seeks to find the case which has the maximum SNRdB value because in this case, the noise

power has the minimum effect in the data compared to other cases.

$$SNRdB = 10log_{10}\frac{P_{signal}}{P_{noise}} \tag{5.13}$$

• *Filtering Effectiveness Value (FEV)*

The evaluation metrics mentioned previously all have meaningful information about the characteristics of the error. Based on the definition of the metrics, it is desired to have minimum RMSE, minimum SD, and maximum SNRdB. In order to examine whether the noise filtering process improves the result compared to the baseline, the metrics mentioned above can be normalized using the baseline values which is the metrics of the raw data. The normalized metrics are calculated using the following Equations 5.14 - 5.16, where i indicates the case number and the metrics with the bar on top means the metrics obtained from the raw data without noise filtering applied. According to their definition, the noise filtering process improves the result when the normalized metrics are greater than one, and worsens the result when they are less than one.

$$nRMSE(i) = \frac{RMSE(i)}{\overline{RMSE}} \tag{5.14}$$

$$nSD(i) = \frac{SD(i)}{\overline{SD}} \tag{5.15}$$

$$nSNRdB(i) = \frac{SNRdB(i)}{\overline{SNRdB}} \tag{5.16}$$

In this experiment, it is desired to have a single metric that can combine all three metrics to have more robust results of the data noise filtering process by considering all three aspects of the errors mentioned above. Thus, this study suggests another metric named FEV which can be obtained from Equation 5.17. By this definition, the effectiveness of data noise filtering can be judged as improved if it is smaller than one and worsened if it is

greater than one. The FEV will be the metric for evaluating the effectiveness of data noise filtering cases in this experiment.

$$FEV(i) = \frac{nRMSE(i) \times nSD(i)}{nSNRdB(i)} \tag{5.17}$$

5.5.3 The Optimal Filtering Method

This section provides the result of the data noise filtering experiment. The goal of this experiment is to prove the following hypothesis:

- **Hypothesis 2**: Specific flight parameters require noise removal techniques that can capture the characteristics of the parameters. Applying a filtering method that is identified considering inherent noise characteristics to corresponding parameters will ensure the necessary level of filtering result.

The case that provides the minimum FEV is the case that successfully reduces the noise in the flight data. Since the aerodynamic model provides two different reference data, lift and drag coefficients, the FEV values in terms of both lift and drag coefficients are investigated. From the 1,000,000 cases with different data noise filtering methods and data parameters assigned, the same number of sets containing two FEVs of the "filtered" data-driven lift and drag coefficient for each case were obtained. The obtained FEVs are plotted in the lift coefficient and the drag coefficient domain as shown in Figure 5.15.

In the figure, the baseline point which is the FEV value of "non-filtered" data is spotted as a red circle. Since the FEV is the value normalized by the baseline error metrics, both the FEV of lift coefficient and the FEV of drag coefficient are one as described. By definition of the FEV, the points located inside the box defined by the FEV number of one for both are the results that have improved noise filtering effect, which means that the data noise in the data parameters is removed by this process. It is also shown that a large number of points are located outside the desired box. This indicates that data noise filtering process

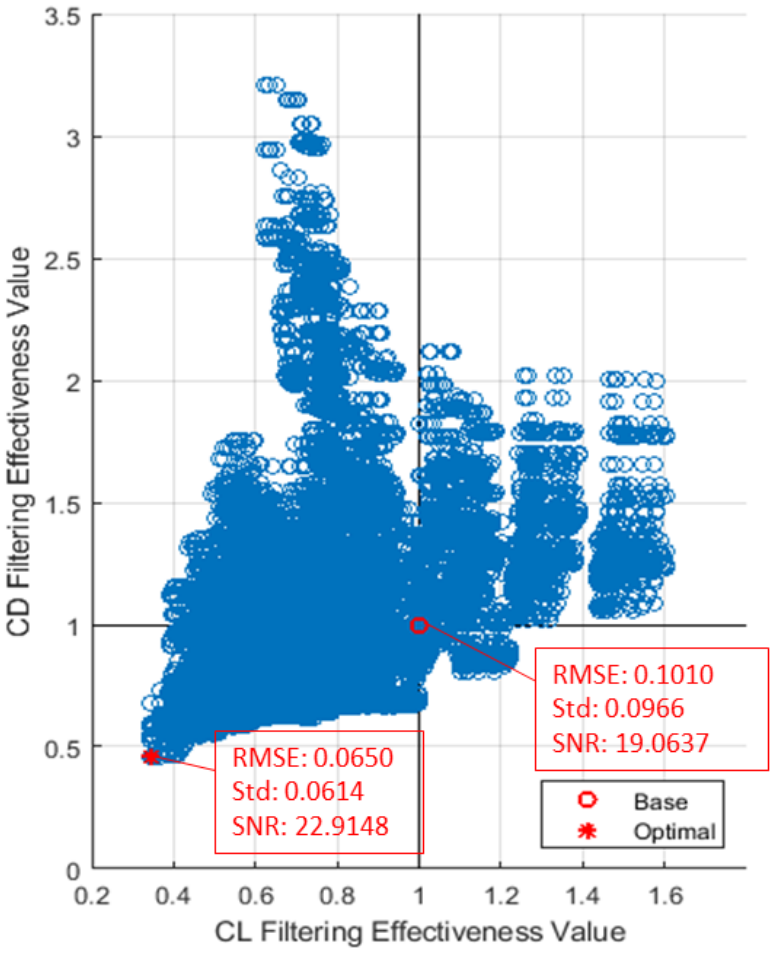

Figure 5.15: Data Noise Filtering Result with the Baseline and the Optimal Filtering Effectiveness Value

can worsen the result by over-filtering the data and possibly distorting the true behavior of the aircraft. Among the obtained results, the optimal point is chosen and highlighted in Figure 5.15 at the bottom left. This point is the optimal case that minimizes the FEV of both lift and drag coefficients, and the data parameters and applied noise filtering techniques are shown in Table 5.3. According to the result, it is shown that the moving average method with high span setting worked best for the pitot-static system, the gyroscopic system, and a global positioning system. For the thermometric system, the robust Loess method with high span setting resulted in the best filtering effect while the smoothing spline technique with high smoothing parameter setting resulted in the best effect. The magnetic system is the only parameter category that was filtered best in the frequency domain. The empirical mode

Table 5.3: The Optimal Filtering Case

		Moving Average (MA)		Robust Loess (RL)		Smoothing Splines (SS)		Fast-Fourier Transform (FFT)		Empirical Mode Decomposition (EMD)	
		High	Low	High	Low	High	Low	High	Low	High	Low
Pitot-Static System	Altitude	O									
	Indicated Airspeed										
	True Airspeed										
Gyroscopic System	Pitch Angle	O									
	Roll Angle										
Magnetic System	Heading Angle										O
Thermometric System	Outside Air Temp.			O							
Global Positioning System	Ground Speed	O									
	Vertical Speed										
Engine System	Fuel Flow					O					
	RPM										

decomposition technique performed best for removing data noise in the heading parameter. From the result, it can be concluded that the combinations of data parameters and data noise filtering techniques mentioned above is the most effective combination for data noise filtering the given flight data.

5.5.4 Summary

As the role of flight data in aviation safety enhancement programs becomes increasingly important, ensuring clean flight data is also crucial to achieving the goal. However, the importance of flight data quality is often not considered an important factor that secures a reliable result. Especially when the number of data parameters is insufficient as in the flight data record in GA aircraft, the flight data quality should be considered more important because data parameter conversion process amplifies the power of data noise. Thus,

the primary goal of this study was to develop the most effective data cleaning method for GA flight data analysis with a limited number of flight data parameters. As the first step to achieve this goal, important data parameters are identified and grouped by six categories considering their measuring devices. Next, various data noise filtering techniques are surveyed in both time-domain and frequency-domain, then the filtering intensity ranges for each technique were set. Based on the selected parameters and data noise filtering techniques, noise filtering cases for the experiment were populated using a full factorial method to investigate all possible combinations. To select the best case in the developed combinations, noise filtering effectiveness metric, named FEV, was defined The FEV examines the errors between data-driven aerodynamic coefficients and modeled aerodynamic coefficients. The reason why the modeled values were selected as the reference data is that the modeled values can be considered as the true behavior of the aircraft and that should not be affected by the data noise filtering process. Thus, the case that resulted the minimum FEV were selected which means that this data noise filtering combination can remove the data noise most effectively in terms of the magnitude and variation of the error as well as noise power in the data set. It is also shown that data noise filtering process can worsen the result, so filtering techniques have to be properly selected. Finally, the optimal filtering case was identified, and this suggested technique can be applied to further flight data analysis and improve the credibility of the data analysis result.

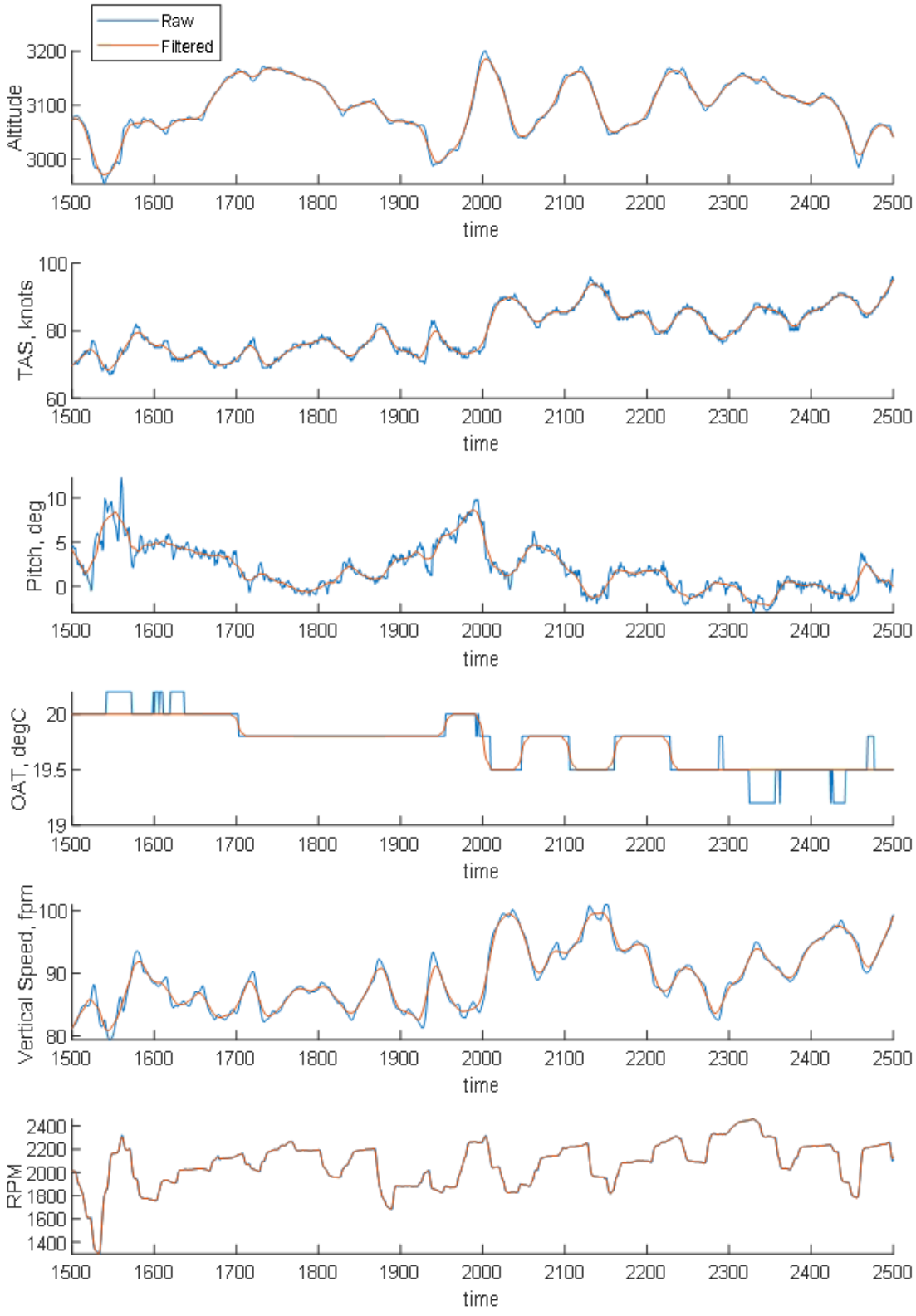

Figure 5.16: Sample Data Parameters: Comparison of Raw data and Filtered Data

Table 5.4: Input Parameters and Required Parameters for Calculating the Input Parameters

Parameter	**Description**	**Unit**	**Note**
T	Thrust	lbs	Given parameter (propulsion model)
- RPM	Engine RPM	$1/min$	Logged parameter
- $AltMSL$	Mean-sea-level altitude	$ftMSL$	Logged parameter
- OAT	Outside air temperature	$degC$	Logged parameter
- TAS	True airspeed	$knots$	Logged parameter
- ρ	Air density	$slug/ft^3$	Calculated parameter
W	Aircraft weight	lbs	Calculated parameter
- F_{Flow}	Fuel flow	gph	Logged parameter
- W_{TO}	Aircraft T/O weight	lbs	Given parameter
g	Gravity acceleration	ft/s^2	Calculated parameter
- $AltMSL$	Mean-sea-level altitude	$ftMSL$	Logged parameter
- OAT	Outside air temperature	$degC$	Logged parameter
ρ	Air Density	$slug/ft^3$	Calculated parameter
- $AltMSL$	Mean-sea-level Altitude	$ftMSL$	Logged parameter
- OAT	Outside air temperature	$degC$	Logged parameter
α	Angle-of-Attack	deg	Calculated parameter
- γ	Flight path angle	deg	Calculated parameter
- θ	Pitch angle	deg	Logged parameter
q	Pitch rate	rad/s	Calculated parameter
- ϕ	Roll angle	deg	Logged parameter
- θ	Pitch angle	deg	Logged parameter
- HDG	Heading angle	deg	Logged parameter
ϕ	Roll angle	deg	Direct parameter
γ	Path angle	deg	Calculated parameter
- V_{SpdG}	Vertical speed - GPS	fpm	Logged parameter
- $GndSpd$	Ground speed	$knots$	Logged parameter
V_{abs}	Absolute velocity	ft/s	Calculated parameter
- V_{SpdG}	Vertical speed - GPS	fpm	Logged parameter
- $GndSpd$	Ground speed	$knots$	Logged parameter
P_{dyn}	Dynamic pressure	lbf/ft^3	Calculated parameter
- IAS	Indicated airspeed	$knots$	Logged parameter
- ρ	Air density	$slug/ft^3$	Calculated parameter
S	Wing area	ft^2	Given parameter

CHAPTER 6
OPERATIONAL SAFETY ASSESSMENT

This research work is intended to show that the proposed data-driven aerodynamic modeling approach and the suggested flight data noise filtering method can contribute to GA safety enhancement efforts by providing more accurate aerodynamic characteristics during flight and better quality of flight data records. From the previous chapters, it was verified that the fidelity of the aerodynamic model had been improved and the quality of the flight data also has been enhanced. The first section of this chapter describes the methodology for operational safety assessment using the developed aerodynamic model and the cleaned flight data. The next section provides a statistical approach for developing operational envelopes for C172S aircraft using a large amount of flight data records. The last section discusses the practical usage of the suggested operational envelope by showing a detection process of abnormal flight operation.

6.1 Methodology Development

6.1.1 Overview

This chapter focuses on the operational safety evaluation process of fixed-wing GA aircraft. It is expected that incorporating the previously obtained aerodynamic model and clean flight data into the operational safety evaluation process will improve the validity of the data-driven GA safety assessment procedures. In other words, this chapter is intended to show that the benefits from the previous data-driven aerodynamic modeling method and the data-noise filtering method can practically affect the safety assessment process in a positive way. Therefore, the following research question was established, and the fundamental goal of the following sections is to provide answers to this question to support the research

goal of this study.

Research Question 3

How can flight performance safety of a fixed-wing GA aircraft be analyzed using a synthesis of an accurate aerodynamic performance model and clean flight data?

- How can operational performance limits or flight envelopes for a fixed-wing GA aircraft be identified using performance models and flight data?
- How can the generated performance envelopes be used for quantitatively judging or determining that an aircraft is in a dangerous or safe state?

In order to address the research question, this study utilizes a large amount of flight data records of C172S GA aircraft which are provided in courtesy of a research partner school. Among thousands of the available flight data records, a subset of the data set was chosen for the scope of this research considering operating regions, flight profiles, and data quality. For example, in the original dataset, some of the data were not fully logged from the beginning to the end, and some flights were logged while conducting multiple go-around practices. Also, the flights operated in multiple airports and take off and landed on various runways. Since such factors may affect the consistency of the results, this study focused on the flights landed on the runway that has the most operations were involved. After this pre-processing of the flight data records, the number of flight data records given by the research partner school was reduced to around 1,400 flights, and they were the primary resources of this data-driven safety assessment effort.

Given the data records, operational flight envelopes during approach and landing phases are examined by statistically analyzing common behaviors of the aircraft during that phases of flight. As discussed earlier, approach and landing is highly risky phases of flight. Among various flight operations, this study focuses on the approach and landing safety of GA. By

concentrating on these high risky phases, the safety assessment method suggested in this study can improve the efficiency of the hazard identification process. That being said, this study suggests a GA safety assessment methodology that enhances the safety management system which can have a positive impact on overall GA safety. Thus, the flight data record that corresponds to approach and landing are extracted for the statistical analysis. Once the flight data records are processed for further analysis, they are analyzed in terms of approach safety and landing safety. To assess the flight safety in both the approach and landing phases, the critical data parameters that represent approach and landing safety performances are selected and explained in the next section. Using these parameters, standard operating ranges of the parameters are identified for determining any abnormal activities of the aircraft. This operational safety analysis uses both raw flight data and noise-removed flight data to compare and examine the effect of the noise removal step on the results.

The next step in this flight safety assessment work is to detect abnormal flights in the data set using both raw and noise-filtered data. In this step, operational flight safety is reviewed using a statistical metric that represents how the flights are far from "normal" operations. After abnormal events are detected among the flights in approach and landing phases, the corresponding flights are reviewed and examined in the end to provide the answer to the research question stated above.

6.1.2 Experiment Setup

This section provides plans of the experiment designed to support the research question established in the previous section. The goal of this research is to suggest a methodology for developing standard operational envelopes that can be used for enhancing GA fixed-wing aircraft flight safety. The standard flight envelope is somewhat ambiguous to be determined because of the variety of GA aircraft characteristics and operational procedures. Thus, considering safety as normality can be more helpful for establishing its operational performance envelopes. Also, it is necessary to measure the operational safety using a

quantitative metric for the assessment work to be more consistent. This research, therefore, demonstrates the following hypothesis to provide solutions to satisfy the requirements that are essential for a more reliable and steadier GA flight safety assessment procedure.

Hypothesis 3

Using a synthesis of a realistic aircraft performance model and clean flight data will reduce the chance of misidentifying or failing to identify abnormal flight operations.

In order to prove the hypothesis mentioned above, it is required to have the two primary elements: Reference performance envelopes and a quantitative safety metric for the flight safety assessment. As discussed earlier, the reference performance envelopes can be defined in a statistical way using the flight data records. By looking at their ordinary and general operations in the flight data, standard operational limits are obtained in this study. Among many other phases of flight, this study mainly focuses on approach and landing phases because these are considered as more safety-critical phases of flight. In the suggested process of developing standard flight performance envelopes, key flight data parameters of interest are selected for both approach and landing phases considering safety events related to each phase. While some parameters are selected for both phases of flight, some parameters are chosen for landing or approach phase only. The selected parameters will be discussed in the following section. Using the selected flight parameters that can represent the safety behavior of the aircraft, ordinary operational ranges are set and they are used in this safety assessment experiment.

After the standard flight performance envelopes that define ordinary flight performances are developed, a quantitative metric is developed for measuring the aircraft's operational safety based on the performance envelopes. The developed metric takes the most important role in this experiment by quantifying how far the flight is from the ordinary flight. The definition of the developed metric is elaborated in the following section. Using this quan-

titative safety metric, this experiment attempts to detect abnormal flights among the given set of flight data records.

Given the standard operation envelopes and the quantitative safety assessment metric, this experiment performs safety assessment works on the entire flight records using both raw data and noise-filtered data. Finally, the result of this experiment proves that a synthesis of the data-driven aircraft performance model and noise-filtered flight data provides more reliable results of GA flight safety assessment procedures.

6.2 Standard Flight Performance Envelopes

As discussed in the previous section, this study focuses on approach and landing phases which are considered as one of the safety-critical phases of flight due to the proximity to the ground. The following sections explain the suggested steps of developing standard flight performance envelopes for both the approach and landing phases. The flight data parameters selected for assessing each phase of flight are listed and explained first. Next, standard flight performance envelopes for the selected flight data parameters are shown.

6.2.1 Landing Phase

Parameter Selection

The representative safety events that are relevant to the landing phase are a hard landing, runway over-run, and runway veer off. The definitions of the landing safety events are explained as follows.

- **Hard Landing**: The event when an aircraft hits the runway with higher force and speed than that in normal touch-down.
- **Runway Over-run**: The event when an aircraft on takeoff or landing roll extends beyond the end of the runway.

- **Runway Veer-off**: The event when an aircraft on takeoff or landing roll extends the side line of the runway.

Multiple facts can cause the explained safety events during landing. One of the facts that can lead to poor landing is the high energy at touch-down. The total energy of aircraft consists of potential energy and kinetic energy, and they can be calculated using Equation 6.1 and 6.2 respectively, where W is the aircraft weight, h is the altitude, V is the airspeed, and g is the gravity acceleration.

$$PE = Wh \tag{6.1}$$

$$KE = \frac{WV^2}{2g} \tag{6.2}$$

The total energy of the aircraft is the sum of both potential energy and kinetic energy. When the total energy is normalized by the aircraft weight, it becomes the specific total energy, STE which can be calculated using Equation 6.3. This metric is also known as the total energy height and it is independent of aircraft weight. Poor management of this total energy height at landing can cause the undesired safety events mentioned above.

$$STE = h + \frac{V^2}{2g} \tag{6.3}$$

Another factor that can cause an unsafe event at landing is the abnormal aircraft speed. Aircraft speed can be divided into longitudinal and lateral speed with respect to the ground surface. Vertical speed and ground speed are the two airspeed components of an aircraft and the two parameters at touch-down are examined in this study for the landing safety assessment. Aircraft attitude at touch-down is also the data parameter that can be considered as one of the contributing factors to the safety event at landing. Poor management of pitch can cause both hard landing and runway over-run, and poor roll angle at touch-down can lead the aircraft to the runway veer-off.

The location on the runway where the aircraft hits at touch-down is also an important factor for landing safety. Since the runway where the aircraft landed in the flight data is long enough not to worry about the runway over-run. Thus, this study examines the center-line deviation of the touch-down point only.

Finally, this research utilizes the contributing factors for aircraft landing performance mentioned above and examines the operational safety of the landing phase using the selected flight data parameters at the touch-down moment. The selected flight data parameters for the landing safety assessment effort are listed in Table 6.1. Thus, this study intends to develop standard operational envelopes for each parameter and the developed operational envelopes are explained in the next section.

Table 6.1: Flight Data Parameters for Landing Performance Assessment

Flight Data Parameter	**Flight Data Name**	**Unit**
Total Energy Height	TE	ft
Total Energy Height Rate	TER	ft/sec
Vertical Speed	V_{Spd}	fpm
Ground Speed	$GndSpd$	knots
Pitch Angle	$Pitch$	degree
Roll Angle	$Roll$	degree
Center-Line Deviation	$CDev$	ft

Performance Envelopes

The fundamental concept of the performance envelopes to be developed in this study is to provide the range of normal operations for GA fixed-wing aircraft. The normal operations can be defined by observing a large number of flight data records. Mean and standard deviation are the primary drivers for developing the standard operational envelope in this research. For the parameters that are selected for the safety assessment, mean and standard

deviation of the parameter are obtained at the moment of the touch-down. Assuming that the number of the flight records are large enough so the data follows a normal distribution, the abnormality level can be defined by the standard deviation which is a measure for quantifying the amount of variation of the data. The abnormality levels can be defined using following equations where X is the data parameter of interest, μ is the mean of the dataset, and σ is the standard deviation of them.

$$\mu - \sigma \leq X \leq \mu + \sigma \tag{6.4}$$

$$\mu - 2\sigma \leq X \leq \mu + 2\sigma \tag{6.5}$$

Equation 6.4 defines the boundaries for the abnormality level 1, and Equation 6.5 defines the boundaries for the abnormality level 2. The abnormality level 1 boundaries form the range where the data parameter is in the condition of a normal operation. In other words, the range within one standard deviation from the mean can be considered as a standard operating range. Similarly, the parameters located outside of the one-standard-deviation boundaries (level 1), and within the two-standard-deviation boundaries, (level 2), are considered as in the "warning" condition. When the parameter is outside of the level 2 boundaries, it is detected as a "severe" situation. In statistics, the three-sigma rule of thumb explains that nearly all data points are located within three standard deviations of the mean. Figure 6.1 depicts this three-sigma rule. As shown in the figure, approximately 4.5% of the dataset are outside of the level 2 range when the dataset follows a normal distribution. Thus, this study considers any parameters of the flight data records are lies outside of the two-standard-deviation range, defined as the abnormality level 2, as "abnormal" events during the flight.

Applying this statistical approach in the development of standard flight performance envelopes, the range of normal and abnormal operations for the selected parameters are

defined. The rest of this section provides the defined performance envelopes for the touch-down safety assessment work.

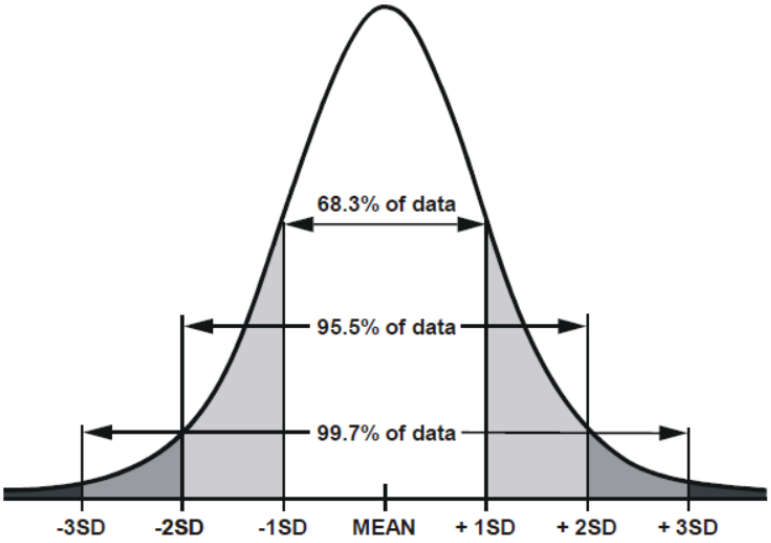

Figure 6.1: Normal Distribution Curve with Mean and Standard Deviation [83]

• *Energy Parameters*

The energy parameters at the touch-down points are collected to provide the operational envelopes for each energy metric. As defined in Figure 6.2, the abnormality level-one-boundaries for the total energy height are 112.22 ft and 171.46 ft while the abnormality level-two-boundaries for the total energy height are 82.59 ft and 201.08 ft. The mean of total energy height is 141.84 ft.

The total energy height rate is also one of the informative data parameters for evaluating touch-down performance. As shown in Figure 6.2, the mean, the abnormality level-1 boundaries, and the abnormality level 2 boundaries are defined and summarized in Table 6.2.

• *Speed Parameters*

The speed parameters that can be used for the safety assessment at touch-down are the vertical speed and the ground speeds. The collected data points of the vertical speed (sink

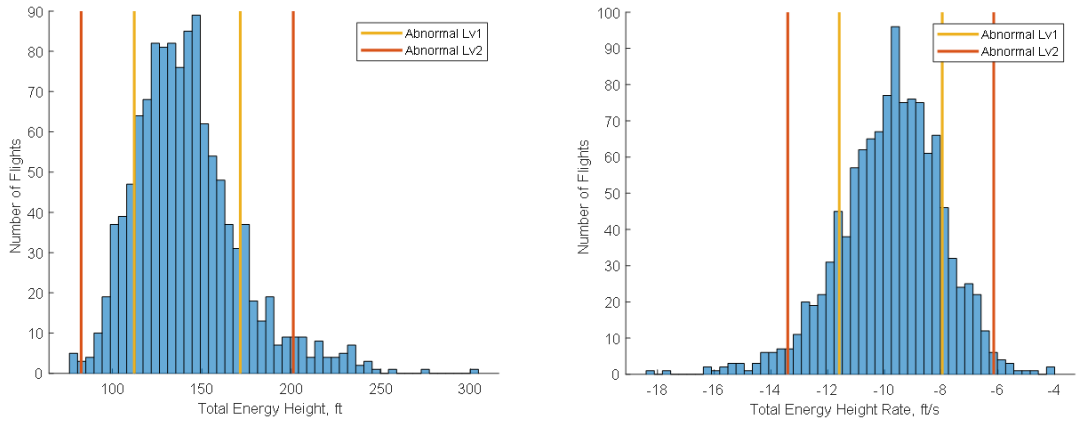

(a) Total Energy Height (b) Total Energy Height Rate

Figure 6.2: Energy Parameters at Touch-Down

rate) and the ground speeds are distributed in Figure 6.3. Using these parameters at the touch-down moment, the boundaries for normal operation ranges are defined as shown in Figure 6.4. The detailed information of the boundaries are summarized in Table 6.2 in the following section.

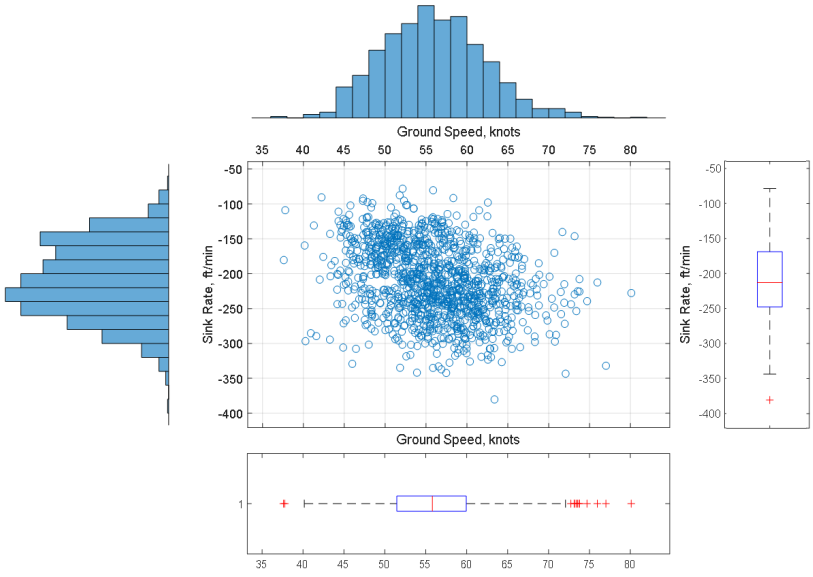

Figure 6.3: Touchdown Speed (Sink Rate and Ground Speed)

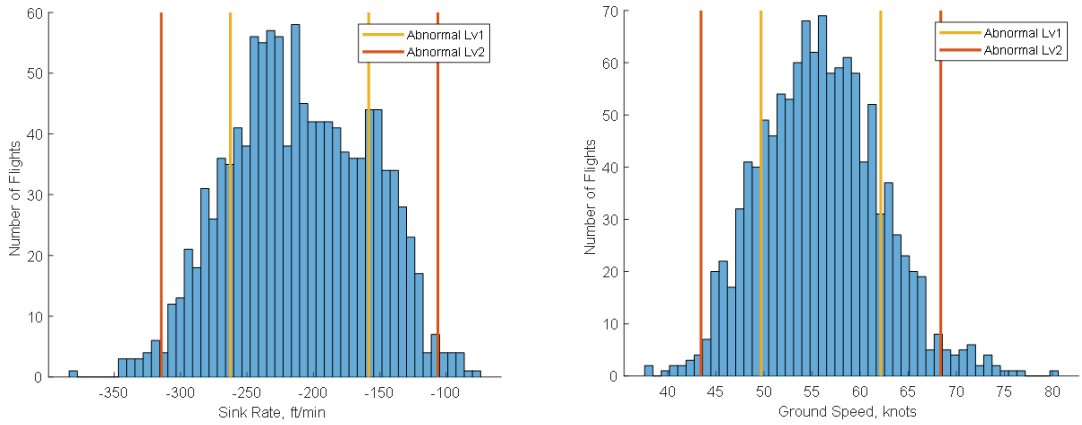

(a) Vertical Speed

(b) Ground Speed

Figure 6.4: Speed Parameters at Touch-Down

• *Attitude Parameters*

When an aircraft hits the ground during landing, its attitudes have to be managed accordingly to avoid undesired safety events such as hard landing or runway excursion. Thus, the aircraft attitude parameters, pitch and roll, are evaluated at touch-down and shown in Figure 6.5. From the distribution of them, the abnormality levels are set as described in Figure 6.6 and they are listed in Table 6.2.

• *Location Parameter*

Touch-down location on runways is highly relevant to runway over-run or runway veer-off events. When the runway where an aircraft operates is sufficiently long, the pilot may not pay attention to the longitudinal position of its touchdown. The selected runway in this study is sufficiently long, so longitudinal points of the flights are not concerned in this study. Instead, the centerline deviation of each flight was measured to evaluate its touch-down performance regarding the location. The measured touch-down locations for the flights are depicted in Figure 6.7 (a), and the defined standard operation ranges are described in Figure 6.7 (b). The detailed information about the specified ranges are shown

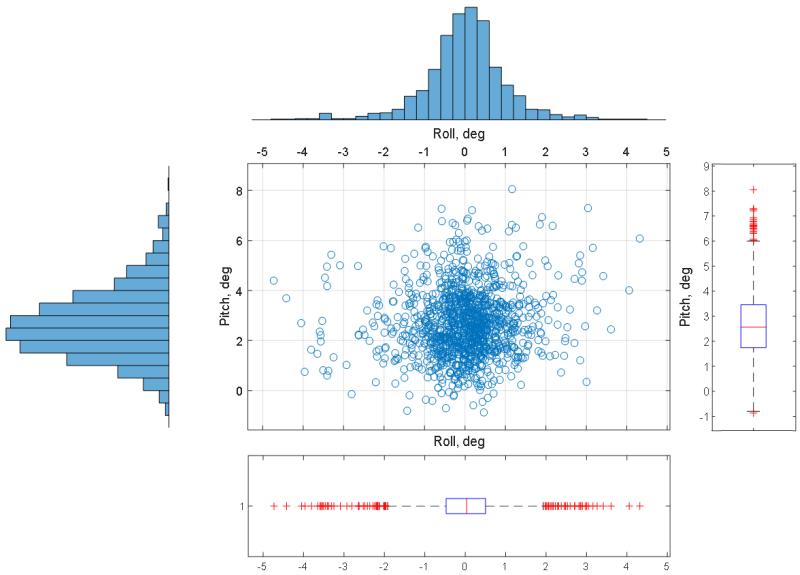

Figure 6.5: Touchdown Attitude (Pitch and Roll)

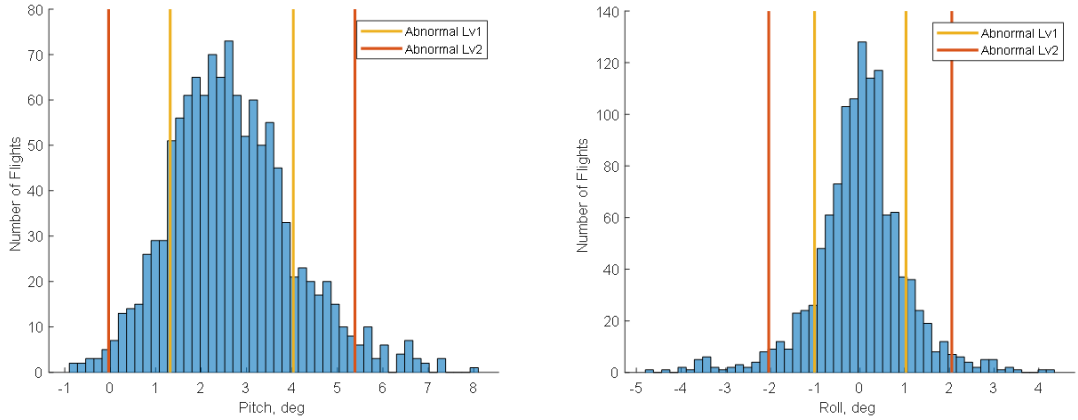

(a) Pitch Angle

(b) Roll Angle

Figure 6.6: Attitude Parameters at Touch-Down

in Table 6.2 in the next section.

Summary

As discussed previously, aircraft landing performance can be evaluated using specific parameters that have significant impacts on its touch-down performance. Therefore, the key data parameters for the landing performance assessment are selected and elaborated in

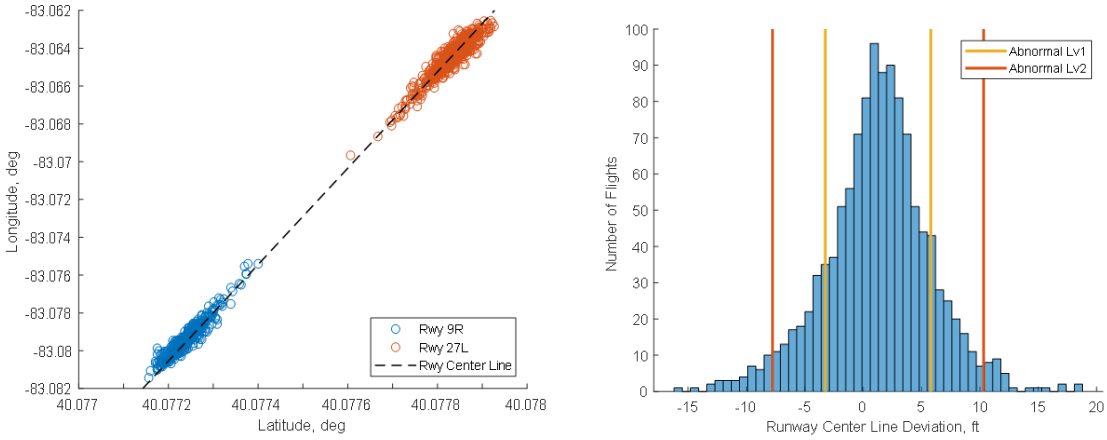

(a) Touch-Down Location (Runway 9R and 27L)

(b) Runway Center-line Deviation

Figure 6.7: Touch-Down Location and Center-Line Deviation

previous sections. For each selected parameter, normal operation ranges in two different levels were defined using its mean and standard deviation at touch-down. Finally, the standard performance envelopes were developed for all the selected parameters, and they are summarized in Table 6.2. This values will be used for the landing safety assessment work for a specific flight in later part in this chapter.

Table 6.2: Standard Safe Performance Envelopes for Touch-Down

Parameter	Unit	Center	Abnormal Lv1		Abnormal Lv2	
		Mean	Lower	Upper	Lower	Upper
Total Energy	ft	141.84	112.22	171.46	82.59	201.08
Total Energy Rate	ft/s	-9.78	-11.59	-7.96	-13.41	-6.15
Vertical Speed	fpm	-210.42	-262.51	-158.34	-314.59	-106.25
Ground Speed	Knots	55.92	49.70	62.15	43.47	68.38
Pitch	deg	2.67	1.32	4.03	-0.04	5.38
Roll	deg	0.01	-1.02	1.03	-2.04	2.05
Centerline Deviation	ft	1.28	-3.25	5.80	-7.77	10.32

6.2.2 Approach Phase

Parameter Selection

Approach phase is the last portion of the flight prior to landing. During the approach phase, an aircraft loses altitude and the pilot pay attention to the aircraft attitude, speed, and alignment with the runway while descending. For example, it is desired to maintain 3 degrees of descent angle in a stable approach. In addition, the normal approach requires constant airspeed and a constant energy loss during the flight. In this phase of flight, the flap setting is one of the main contributing factors that affect the aircraft stability during approach, and this information is essential for evaluating its safety in terms of airspeed because the exceedance limits are often defined in a specific flap setting. Also, the aerodynamic coefficients information that can be obtained from the aerodynamic model is crucial indicators for the aircraft's approach performance. Therefore, the following parameters in Table 6.3 are selected for the development of standard performance envelope during the approach phase.

As shown in Table 6.3, the selected parameters for this phase of flight shares the same parameters for the landing performance assessment work. For location indicating parameters, altitude above ground level is selected instead of center-line deviation compared to the landing performance parameters. Furthermore, aerodynamic-related parameters such as lift coefficient, drag coefficient, and angle-of-attack parameters are added for the assessment of the flight safety in the approach phase. Similar to the previous touch-down performance parameters, these approach performance parameters are used for the development of the standard operational envelopes for the approach phase of flight. While the basic definition of the suggested approach performance envelopes remains the same as the previously explained landing performance envelopes, the normal operating range of the approach phase are not for one specific moment. The suggested approach performance envelopes vary according to the distance remaining to the touch-down point.

Table 6.3: Flight Data Parameters for Approach Performance Assessment

Flight Data Parameter	Flight Data Name	Unit
Total Energy Height	TE	ft
Total Energy Height Rate	TER	ft/sec
Vertical Speed	V_{Spd}	fpm
Ground Speed	$GndSpd$	knots
Pitch Angle	$Pitch$	degree
Roll Angle	$Roll$	degree
Altitude above Ground Level	Alt_{AGL}	ft
Lift Coefficient	C_L	
Drag Coefficient	C_D	
Angle-of-Attack	AOA	degree
Indicated Airspeed	IAS	knots

Performance Envelopes

The methodology of developing performance envelopes for the approach phase is almost the same as the methodology that is explained in the landing phase performance envelope. The biggest difference is that the performance envelope for the approach phase is for observing the flight performance from a reference point to the touch-down point based on the distance left until the runway. The reason why the remaining distance is set as reference information is this is the only parameter that does not change depending on different flights, so it provides objective information about each flight parameter. Thus, the selected data parameters are observed with respect to the distance remaining. The distance left for each flight can be calculated using its latitude and longitude information when the touch-down point is obtained. Again, as discussed in the operational envelope development step for the landing phase, the same statistical approach is applied using its mean and standard

deviation. Eventually, normal operating ranges for each selected parameter are defined in two abnormality levels. The subset of the developed standard operation envelopes is shown as follows. This section intends to focus on the flight data parameters that are not discussed in the landing performance envelopes.

• *Aircraft Altitude and Speed*

Altitude and airspeed are the most representative parameters that provide intuitive information about the status of the flight. As discusses earlier, the flight parameters are compared with respect to the distance remaining until the touch-down location. Figure 6.8 shows the overall flight profiles of the altitude and the indicated airspeed. As shown in the figures, the variance of the parameters forms the normal operating ranges and the ranges are varying when the aircraft approaches the touch-down point. If a specific distance is selected, the developed boundaries of the abnormality levels are defined using the mean and the standard deviation of that point. This instantaneous information about the performance envelopes will be discussed later.

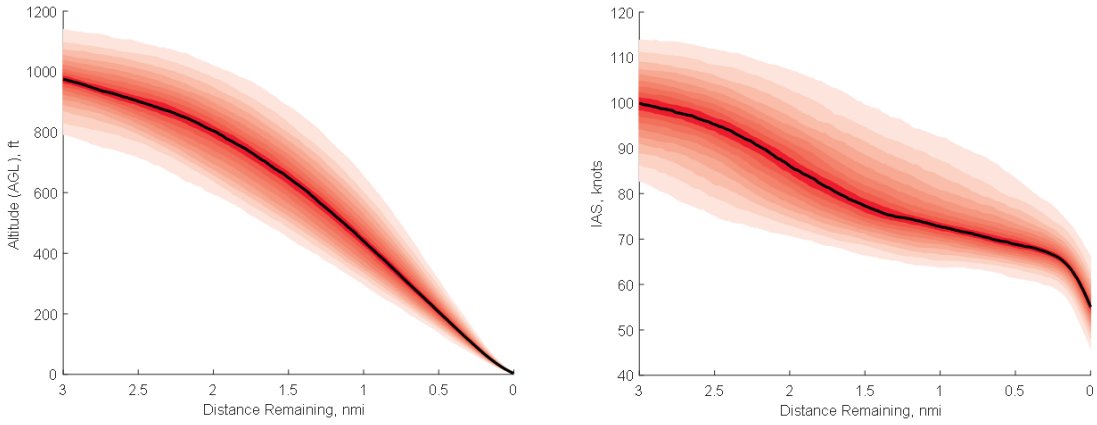

(a) Altitude

(b) Indicated Airspeed

Figure 6.8: Altitude and Indicated Airspeed Envelopes during Approach Phase

• *Aerodynamic Parameters*

The aerodynamic parameters of an aircraft during flight such as lift and drag coefficients are another set of parameters that can be used for determining if the aircraft is in a stable and safe condition. The parameters can be obtained using the aerodynamic model that was developed in the previous chapter. This aerodynamic model requires two inputs: Angle-of-attack and flap settings. The angle-of-attack information can be calculated using the other flight data parameters such as flight path angle and pitch angle. The quality of these parameters can be assured when the proposed data-noise filtering technique is applied to them. Also, the flap settings can be estimated using the aerodynamic model and other data parameters as discussed in the previous chapter. This flap information is very important because that flap setting defines several exceedance events for airspeed [23]. Since the flap setting is not often logged for GA aircraft, clean flight data and accurate aerodynamic performance model that are previously obtained can provide an essential information for the approach safety analysis. The following figures are the identified operating envelopes for the flap setting, angle-of-attack, and aerodynamic coefficients.

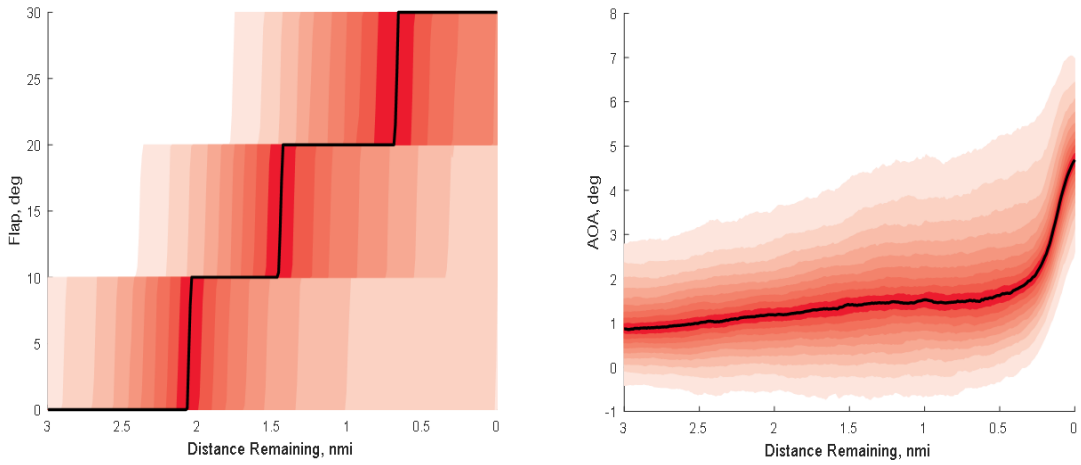

(a) Flap Setting

(b) Angle-of-Attack

Figure 6.9: Aerodynamic Inputs Envelopes during Approach and Landing

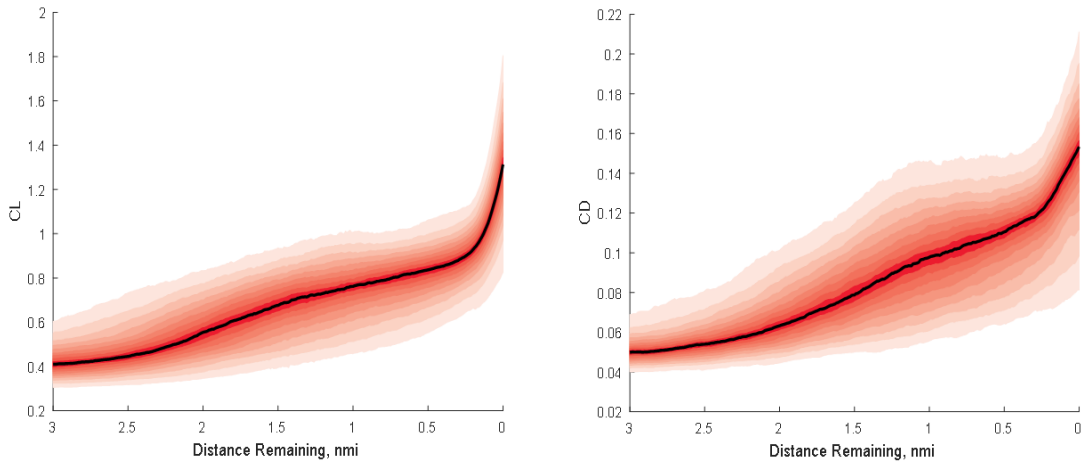

(a) Lift Coefficient (b) Drag Coefficient

Figure 6.10: Aerodynamic Coefficients Envelopes during Approach and Landing

• *Energy Parameters*

The energy parameters are universal parameters that can be examined in any phases of flight for any aircraft. Especially when the energy parameters are normalized by the aircraft weight, they can provide general information about the aircraft's energy state during flight. As discussed in the section about the landing performance envelope, same energy parameters are examined in approach phase again. The energy parameters with varying values of distance remaining are gathered to provide the operational envelopes for each energy metric during the approach phase, and they are shown in Figure 6.11.

• *Instantaneous Envelopes*

From the continuous operating envelopes defined in the previous section, instantaneous envelopes also can be defined when a reference distance left is fixed. Previously, normal operating envelopes for the final thee nautical mile of flight has been developed but the scope can be defined by safety analyzers or users. Also, instantaneous performance envelopes can be obtained when the remaining distance is set as a specific point of interest. For example, the abnormality limits at the moment when the distance remaining is 0.5 nautical miles

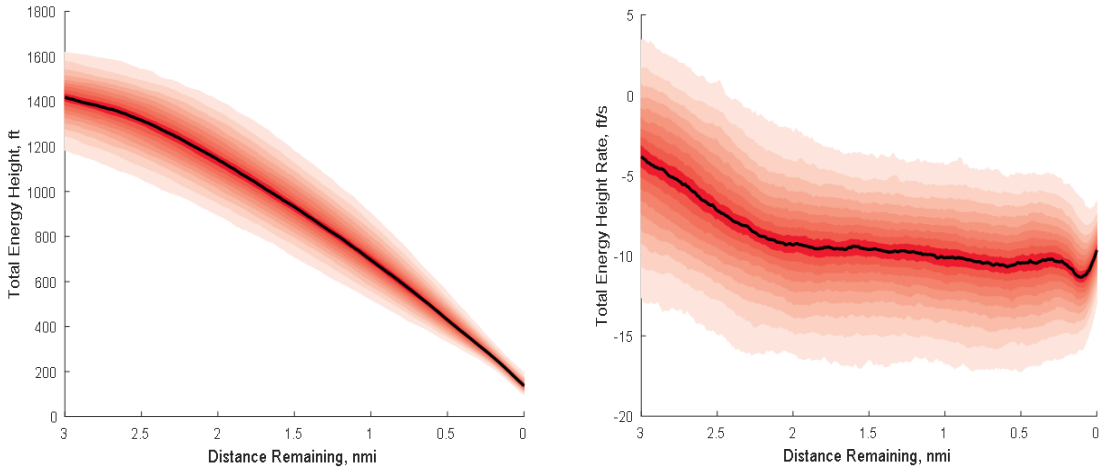

(a) Lift Coefficient

(b) Drag Coefficient

Figure 6.11: Aerodynamic Coefficients Envelopes during Approach and Landing

can be identified by looking at the previously defined approach operating envelopes. Some examples of the identified abnormality limits for this case are shown in Figure 6.12. The boundaries for the other approach performance parameters are also obtained in the same way and summarized in Table 6.4.

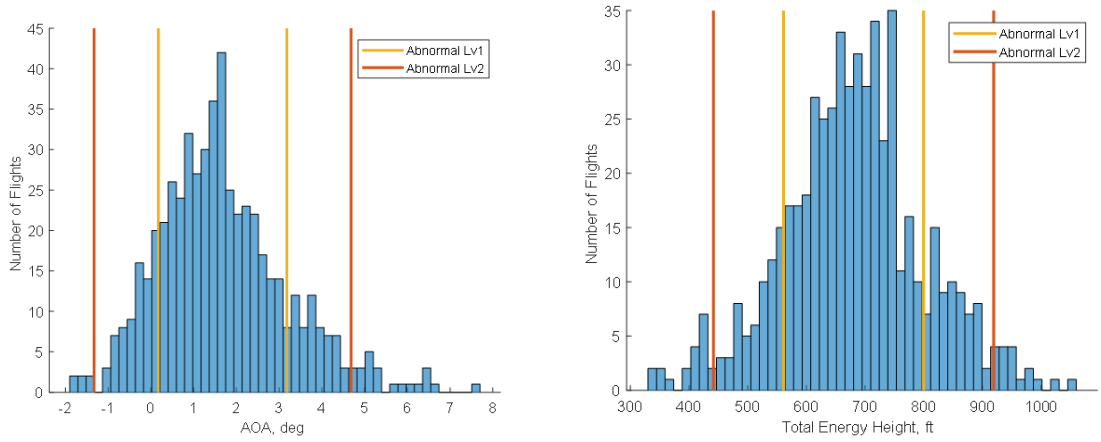

(a) Angle-of-Attack at 0.5 nmi left

(b) Total Energy Height at 0.5 nmi left

Figure 6.12: Sample Instantaneous Envelopes during Approach and Landing

Table 6.4: Standard Normal Performance Envelopes (0.5 nmi left) - Approaching Phase

Parameter	Unit	Center	Abnormal Lv1		Abnormal Lv2	
		Mean	Lower	Upper	Lower	Upper
Total Energy	ft	680.38	560.95	799.80	441.53	919.23
Total Energy Rate	ft/s	-10.42	-14.33	-6.50	-18.24	-2.59
Vertical Speed	fpm	-519.03	-704.95	-333.12	-890.87	-147.20
Ground Speed	Knots	71.45	61.39	81.50	51.34	91.55
Pitch Angle	deg	-2.49	-4.48	-0.50	-6.47	1.49
Roll Angle	deg	-1.63	-8.34	5.09	-15.06	11.81
Altitude (AGL)	ft	422.42	309.11	535.72	195.80	649.03
Lift Coeff.		0.73	0.56	0.90	0.38	1.07
Drag Coeff.		0.10	0.07	0.12	0.04	0.15
Agle-of-Attack	deg	1.68	0.17	3.18	-1.33	4.68
Indicated Airspee	Knots	75.70	66.02	85.38	56.33	95.06

6.2.3 Summary

In this section, approach performance envelopes for various flight data parameters are developed in a statistical method. It is shown that the suggested method for developing normal operating envelopes provided answers to the following research question.

Reserach Question 3.1

How can operational performance limits or flight envelopes for a fixed-wing GA aircraft be identified using performance models and flight data?

As mentioned prevouisly, this study focuses on safety-critical performance parameters so operational performance limits for the certain parameters have been created in this sec-

tion. The flight data parameters that can provide useful information for determining the aircraft's safety or stability during approach were selected. Among the parameters chosen, aerodynamic coefficients offer beneficial information to the safety assessment procedure by making the flap activity information available using the aerodynamic model and other flight data parameters. Using the selected parameters, the standard performance envelopes for each parameter are defined for the approach and landing phases of flight. Finally, it is demonstrated that instantaneous flight envelopes can be specified when a reference distance is set and the specified flight envelopes when the distance remaining is 0.5 nautical miles are summarized.

6.3 Safety Assessment using Safety Score

The primary purpose of this section is to suggest a quantitative metric that can be used for GA flight safety assessment with given standard performance envelopes for approach and landing phases. As explained earlier, the developed standard performance envelopes are based on the common behaviors of the aircraft operated at a specific runway. By looking at how a particular flight is operating within the normal operating ranges obtained above, the flight can be judged if it is in a safe or normal operational region or not. In other words, the safety of a specific flight at a certain moment can be examined by looking at its position in the normality range, which is the standard performance envelopes, constructed from the information of other aircraft's behaviors at the moment. It has to be noted here that not every abnormal flight detected by this method cannot be considered as unsafe flight because GA aircraft operations may contain many variabilities in their operations. However, abnormal operations or flights are likely to become unsafe operations when the normality is quantitatively defined with a sufficient number of reference datasets. when it is required to examine the flight safety in a certain period of operation, the normality test mentioned above has to be performed differently. Thus, this section is devoted to providing the answers to the research question 3.2. To be more concrete, the following sections explains

quantitative metrics that can be utilized in the flight safety assessment procedure using the previously obtained standard performance envelopes.

Research Question 3.2

How can the generated performance envelopes be used for quantitatively judging or determining that an aircraft is in a dangerous or safe state?

6.3.1 Abnormality Test

In statistics, the z-score is the number that indicates the normality of the data. When the mean and the standard deviation are calculated, the Z-score can also be calculated using Equation 6.6, where μ is the mean, and σ is the standard deviation of the data set. x is the specific data point and Equation 6.6 calculates its z-score of the data point x.

$$z = \frac{x - \mu}{\sigma} \tag{6.6}$$

By the definition of the z-score shown in the equation above, this metric can be useful for assessing the abnormality of the flight for an instantaneous point. For example, at the moment of the touch-down of an aircraft, the center-line deviation of the specific flight can be examined using the z-score. When the absolute value of the calculated z-score of the center-line deviation is greater than one and less than two, it means that this specific touch-down performance falls into the abnormality level 1, "warning", by the definition of the developed performance envelope for the center-line deviation. Similarly, if the z-score of the center-line deviation at touch-down is greater than 2, it means that the touch-down performance in terms of its location was poor and this event is assigned to the level 2, "Severe". Using this metric, it is possible to examine how a specific data parameter at a certain instantaneous moment is abnormal. In other words, the Z-score can be used to test abnormality of any particular flight at a specific moment.

6.3.2 Cumulative Landing and Approach Safety Score (CLASS)

It is explained that the Z-score is a good quantitative metric for an instantaneous event. However, when evaluating flight safety analysis, it is not sufficient to evaluate the overall flight profile for a specific parameter by looking at the momentary events only. Thus, this study proposes a new quantitative metric that can satisfy the following requirements.

- The metric should be able to test abnormality of a flight with given data set and performance envelopes.
- The metric should be able to measure how long the flight has crossed the normal operating boundaries.
- The metric should be able to reflect how far away the abnormal event of the flight occurred from the touchdown, and should be able to weight based on the remaining distance.
- The metric should be able to compare the operational safety of a specific data parameter among different flights.

Having a quantitative metric that satisfies the above-mentioned requirements is essential for GA operational safety performance during the approach and landing phase. Thus, this study proposes a quantitative safety evaluation metric named "Cumulative Landing and Approach Safety Score (CLASS)." The quantitative metric, CLASS, can be defined through the following procedure which consists of four steps.

CLASS Calculation Step 1

A sample flight is shown in Figure 6.13 (a) for a selected parameter x. When a data parameter x is given at a point with the distance left $D(i)$, the Z-score at this point can be

calculated using Equation 6.7. From the flight data records, the mean $\mu(i)$ and standard deviation $\sigma(i)$ of the parameter x at the point i are given.

$$Z_x(i) = \frac{x(i) - \mu_x(i)}{\sigma_x(i)} \tag{6.7}$$

By the definition of the z-score, the obtained z-score is the score that shows how far the data point is from the mean value normalized by the standard deviation at the moment. The calculated z-score is also a dataset that varies with the distance left as shown in Figure 6.13 (b).

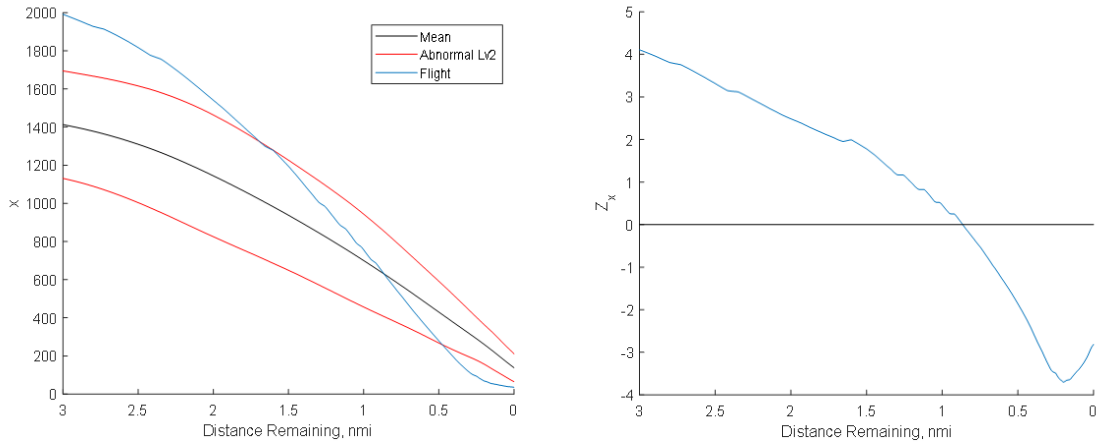

(a) A Parameter and its Envelope

(b) Abnormality Score

Figure 6.13: A Sample Flight for CLASS Calculation - Part 1.

CLASS Calculation Step 2

Now, it is intended to detect any data points that exceed both the upper or lower boundaries of the pre-defined abnormality level 2. Thus, the calculated z-scores are converted to absolute values first, then subtracted by two as shown in Equation 6.8. The result of this step of calculation is shown in Figure 6.14 (a).

$$Z_x^*(i) = |Z_x(i)| - 2 \tag{6.8}$$

If the value ${Z^*}_x(i)$ is a negative value here, that means the point where ${Z^*}_x(i)$ is within the abnormality level 2 range. Thus, safety score of the points with negative ${Z^*}_x(i)$ values need to be set as zero. In other words, the safety score does not intend to detect any points that is within normal operating ranges, so the safety score of the points are neglected.

CLASS Calculation Step 3

Then, the current safety score, ${Z^*}_x(i)$ is normalized by the distance left added by a weighting factor w. It is important to note that events that occur near the touchdown point are riskier than events that occur farther from that point. In other words, even if the exceeded area in two different points with different distance remaining, it cannot be considered as the two results have the same degree of risk. The importance of its proximity to the touch-down point can be weighted using the weighting factor. When the weighting factor is selected as a higher number, it means that the distance left has less impact on the safety score. Conversely, a low weighting factor is chosen, the effect that the remaining distance has on the safety score becomes high. Also, the safety score is converted into a negative value for more intuitive interpretation of the metric, since "safety" is often considered as a positive concept. In this way, higher CLASS value indicates safer or more ordinary condition and lower CLASS value indicate that the parameter is in more abnormal condition. Therefore, the weighted safety score at the moment, $\overline{{Z^*}}_x(i)$ can be expressed as Equation 6.9, and the result of the sample flight is depicted in Figure 6.14 (b).

$$\overline{{Z^*}}_x(i) = \begin{cases} -\frac{Z^*_x(i)}{D(i)+w}, & \text{if } Z^*_x(i) \geq 0 \\ 0, & \text{otherwise.} \end{cases} \tag{6.9}$$

CLASS Calculation Step 4

Finally, the CLASS for the data parameter x can be obtained by integrating all the data points in the series using Equation 6.10. The CLASS of this parameter x during the

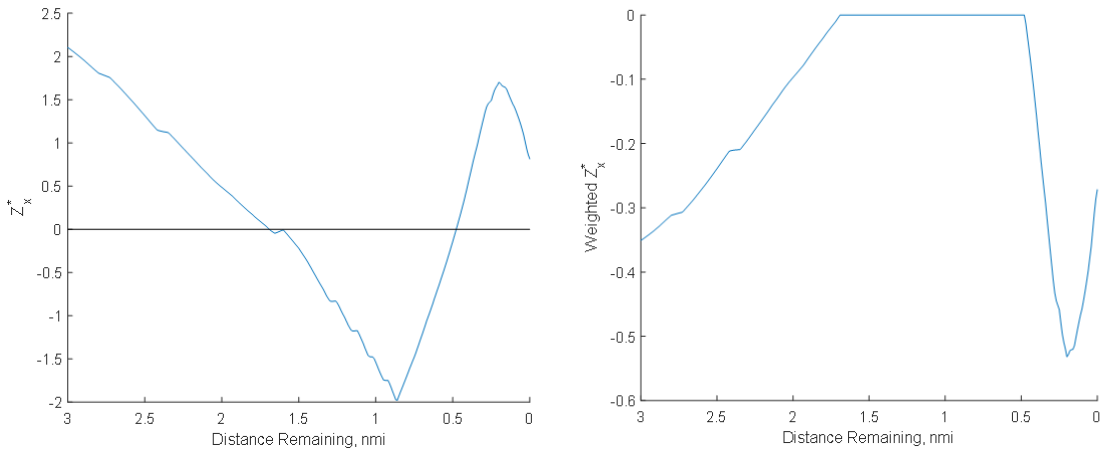

(a) Exceeded Abnormality Score (b)

Figure 6.14: A Sample Flight for CLASS Calculation - Part 2.

approach and landing phases is -0.42 when the weighting factor is selected as 3. By the definition of CLASS, the maximum value of this score is zero. When the CLASS is closer to zero, it means that the parameter evaluated by this metric has never exceeded the normal operating range during the flight.

$$CLASS_x = \sum_i \overline{Z^*}_x(i) \tag{6.10}$$

By the definition of the CLASS, this value indicates the weighted area of the exceedances happened during flight normalized by distance. Thus, this metric is a dimensionless quantity, so this safety score can be used for any data parameters in the flight data. In summary, this safety metric can provide information about how big, how long, and when the data parameter during approach and landing phase exceed the abnormality level 2. The next section demonstrates how this metric can be utilized for a specific flight data record to quantitatively evaluate the flight safety during the approach and landing phase.

6.4 Experiment and Result

The primary focus of this study is to improve GA safety by combining aerodynamic models with clean data. As the last step to achieve the overarching goal of this study, this section performs several experiments using the aerodynamic model and noise-filtered flight data. In the earlier section of this chapter, a methodology for determining the standard operational envelopes has been introduced, and the methodology has been utilized using a large number of actual flight data. Furthermore, a quantitative metric that can measure not only the magnitude of safety exceedance events but also the duration of the events has been developed. The following experiments in this next chapter will demonstrate the process of evaluating the operational safety of the GA aircraft by combining the standard performance envelope and the safety assessment metric mentioned above.

6.4.1 Unstable Approach Detection

Among various phases of flight, this experiment focuses on quantitatively measuring the operational safety during approach and landing phase. The suggested safety assessment metric, CLASS, can be used for any metrics if its mean and standard deviation are provided from the populated data points from the flight data records. Using the previously defined performance envelopes, this experiment demonstrates the suggested flight safety assessment method on a certain flight record. The selected flight number has been investigated using the safety evaluation method.

In this experiment, the following eleven flight parameters are examined and their CLASS values are obtained. Among the mentioned parameters of interest, the total energy height will be discussed in this section.

- Total Energy Height (TE)
- Altitude AGL (ft)
- Total Energy Height Rate (TER)
- Indicated Airspeed (IAS)
- Vertical Speed (V_{Spd})
- Lift Coefficients (C_L)

- Ground Speed (GndSpd)
- Drag Coefficients (C_D)
- Pitch Angle (Pitch)
- Angle of Attack (AOA)
- Roll Angle (Roll)

The flight performances of the above parameters within the pre-defined performance envelopes are described in Figures 6.15 – Figure 6.20. As shown in the figures, some data parameters remained within the boundaries of abnormality level 2, while other parameters violated the boundaries multiple times. Instead of looking at the unsafe events shown in the figures intuitively, the exceedance events for each data parameter are required to be examined and compared quantitatively. Therefore, based on the criteria of calculating the CLASS elaborated in the previous section, the CLASS values for each parameter are calculated with both filtered data and raw data. Table 6.5 summarizes the CLASS for the approach and landing phase of the selected flight.

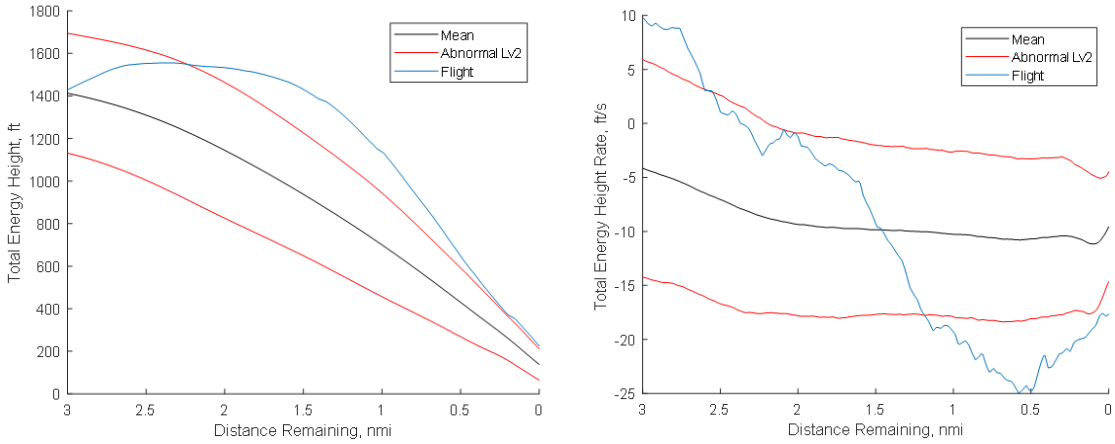

(a) Total Energy Height

(b) Total Energy Height Rate

Figure 6.15: Safety Assessment - Energy Parameters

As observed in Table 6.5, some parameters have the CLASS values of zero while other parameters have negative CLASS values. For example, the vertical speed has the lowest CLASS value compared to the other parameters. This low vertical-speed CLASS can

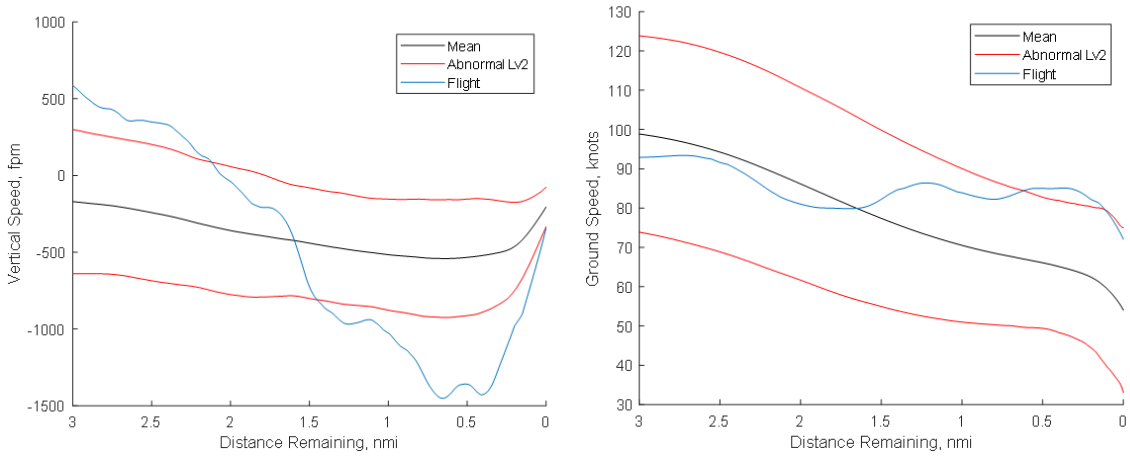

(a) Vertical Speed (b) Ground Speed

Figure 6.16: Safety Assessment - Speed Parameters

Table 6.5: Quantified Flight Safety Results using CLASS

Approach Stability Parameters	**CLASS (Filtered)**
Total Energy	-0.5195
Total Energy Rate	-0.3591
Vertical Speed	-0.7328
Ground Speed	-0.0404
Pitch Angle	-0.5134
Roll Angle	-0.2055
Altitude AGL	-0.6167
Lift Coefficient	0.0000
Drag Coefficient	0.0000
Angle-of-Attack	-0.0195
Indicated Airspeed	0.0000

be interpreted as that the aircraft had to sharply reduce its altitude in areas close to the touchdown point and this situation caused the vertical velocity to exceed the performance

envelope. Since the exceedance happened near the touch-down point, the safety score of this flight was worsened by the weighting factor. On the other hand, the aerodynamic parameters, the angle-of-attack, and the indicated airspeed have the safest score, which is zero, or relatively high scores. That means the aircraft was in a ordinary situation in terms of aerodynamic performance. Overall CLASS values for this particular flight indicate that this flight can be considered as a poor energy management flight.

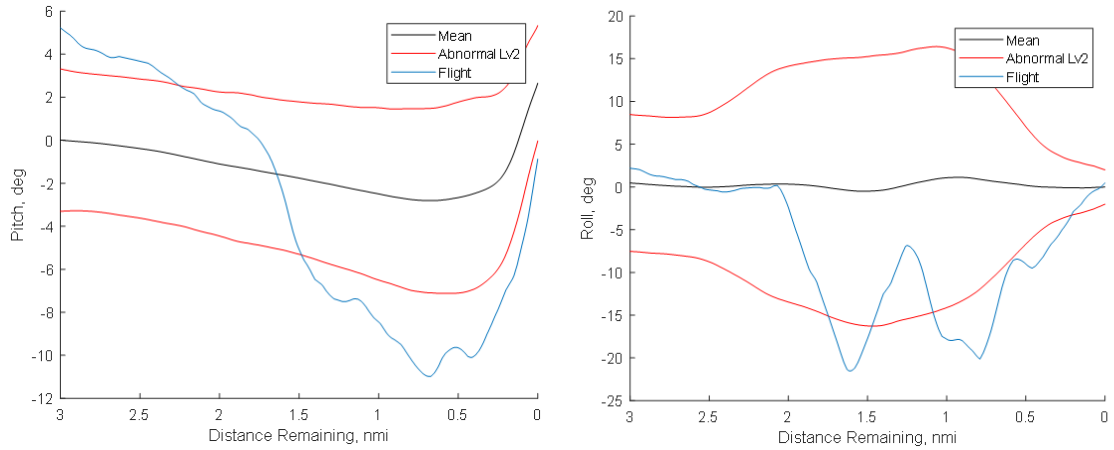

(a) Pitch Angle (b) Roll Angle

Figure 6.17: Safety Assessment - Attitude Parameters

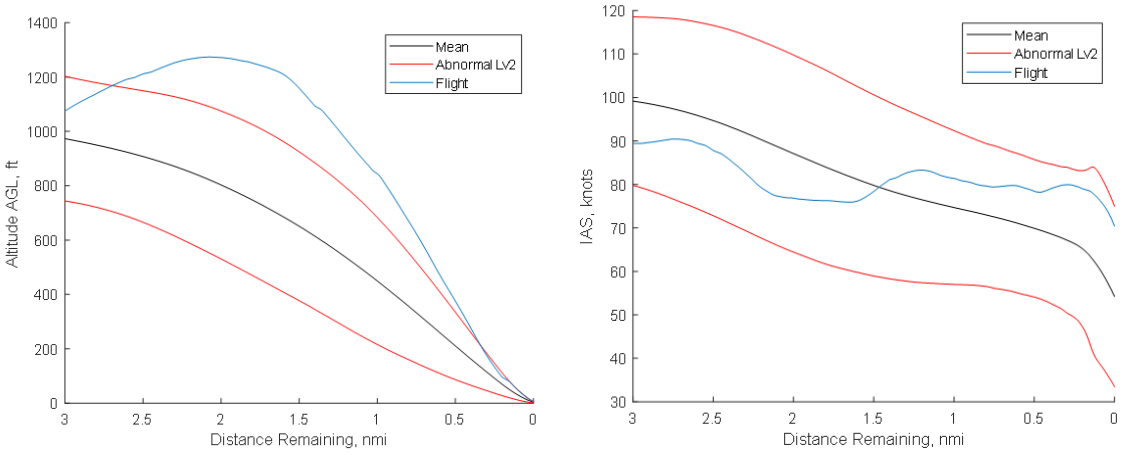

(a) Altitude AGL (b) Indicated Airspeed

Figure 6.18: Safety Assessment - Altitude and Speed

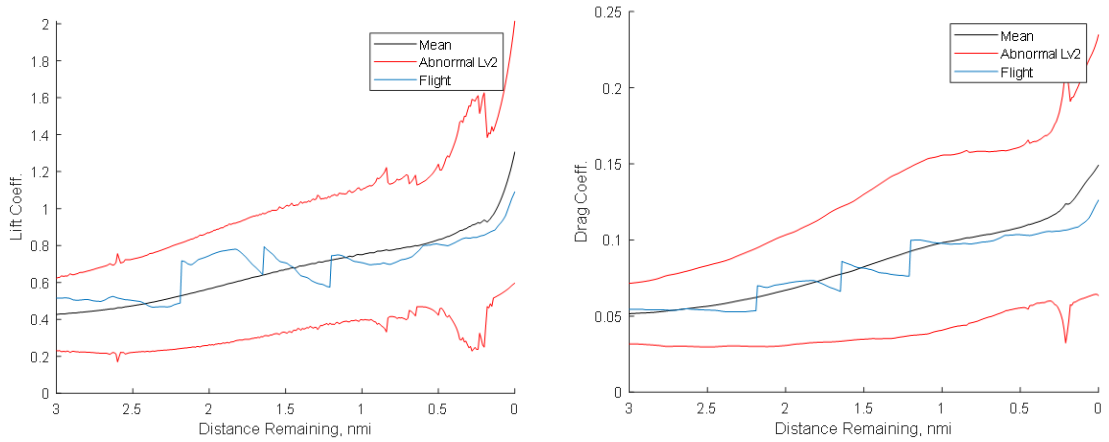

(a) Lift Coefficient (b) Drag Coefficient

Figure 6.19: Safety Assessment - Aerodynamic Parameters

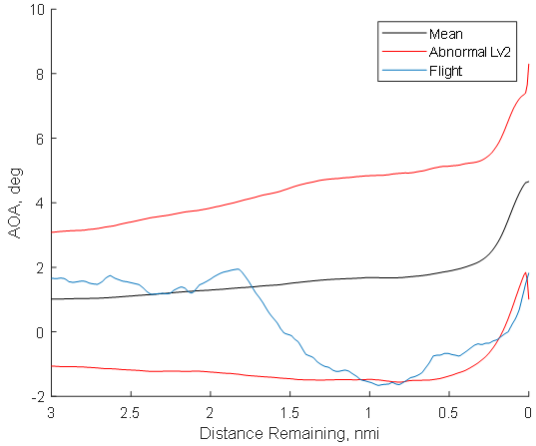

Figure 6.20: Safety Assessment - Angle-of-Attack

The quantified safety score of a particular parameter indicates how normal this parameter was during the flight. The selected performance parameters for evaluating approach and landing abnormality can be compared effectively using a spider chart as shown in Figure 6.21. This chart provides an overview of the flight using quantified safety performance using CLASS. This chart also shows the difference between filtered data result and raw data result. The next section discusses this noise effect on the safety assessment process. As shown in the figure, total energy, vertical speed, pitch angle, and altitude have lower CLASS values which means they performed abnormally during the flight. The spider chart

of CLASS can be used not only to compare different parameters of a flight but also to compare the overall operational performances between different flights. For example, Figure 6.21 and Figure 6.22 provide the quantified abnormality information for two different flights. By looking at these two charts together, the overall operational performance can be quantitatively compared. As shown in Figure 6.22, the flight number 98 was in more abnormal state in terms of its aerodynamic performance compared to the number flight 1,392 described in Figure 6.21. In this way, any flight performances in the dataset can be analyzed and compared each other.

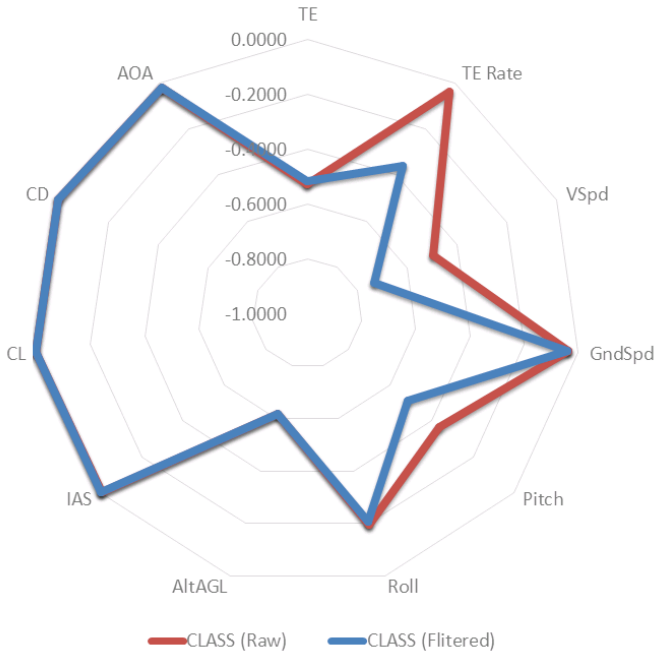

Figure 6.21: Safety Quantification using CLASS: Flight No. 1,392

To conclude that a certain flight operation was abnormal in terms of this specific parameter, other parameters and their circumstances must be considered together. For example, if the aircraft was approaching in a high-altitude condition, the pilot had to make the aircraft pitch-down so that the altitude of the aircraft can be in the normal range. In this case, the energy and pitch both can be detected as abnormal, but the abnormal pitch is the result of one of the pilot's corrective actions caused by the high altitude or high energy state. Thus, a comprehensive insight into the quantified safety scores is required for the flight

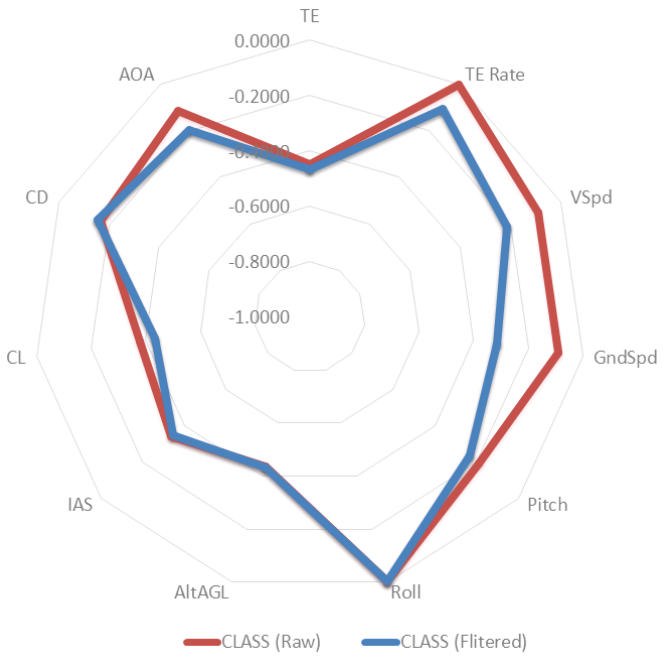

Figure 6.22: Safety Quantification using CLASS: Flight No. 98

safety assessment, and the developed CLASS metric provides beneficial information for the comprehensive safety assessment.

6.4.2 Data Noise and CLASS

In the previous section, it is shown that the CLASS metric can be utilized in the GA aviation safety assessment effort using a large number of flight data records. Also, the CLASS metric provides intuitive and useful information for safety measurement. The two fundamental elements of the safety assessment procedure are the standard performance envelopes and the quantitative metric, CLASS. Both elements are data-driven information so possibly existing data noise can affect the safety assessment result. The previous approach and landing safety assessment effort has been done with noise-filtered data obtained from Chapter 5. This experiment is designed for examining the effect of data noise on the GA approach and landing safety assessment result using CLASS. The result of this experiment can support the following hypothesis that has been established for the safety assessment of GA operations.

Hypothesis 3

Using a synthesis of a realistic aircraft performance model and clean flight data will reduce the chance of misidentifying or failing to identify abnormal flight operations.

As the first step of the evaluation process, the safety assessment work conducted in the previous section was reproduced with raw flight data. The abnormality evaluation results of the same flight using both raw and filtered data cases are summarized in Table 6.6 and described in 6.23.

Table 6.6: CLASS Comparison between Filtered and Raw Data

Approach Stability Parameters	**CLASS (Filtered)**	**CLASS (Raw)**
Total Energy	-0.5195	-0.5307
Total Energy Rate	-0.3591	-0.4040
Vertical Speed	-0.7328	-0.4935
Ground Speed	-0.0404	-0.0380
Pitch	-0.5134	-0.3643
Roll	-0.2055	-0.1968
AltAGL	-0.6167	-0.6178
CL	0.0000	0.0000
CD	0.0000	0.0000
AOA	-0.0195	-0.0207
IAS	0.0000	-0.0049

As shown in both Table 6.6 and Figure 6.23, while many parameters have the similar CLASS result, the difference of the vertical speed and the pitch CLASS results is reflectively large. Also, it was detected that the indicated airspeed was in the safe operational envelope during the entire approach phase when the noise-filtered data is used for the evaluation. However, when the raw data was used in the process, the CLASS of indicated

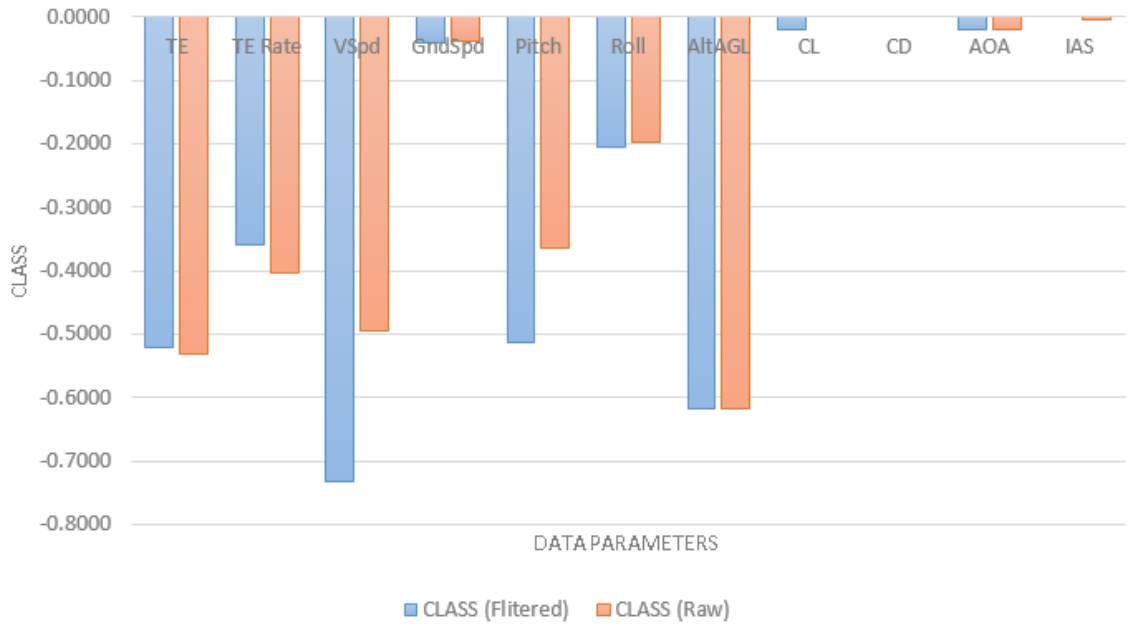

Figure 6.23: CLASS Result Comparison between Raw Data and Filtered Data Utilized

airspeed shows that it has exceeded the boundary even if it was a small period of time. The lift coefficient is also a similar example of this difference, but in this case, the CLASS of lift coefficient shows oppositely. This difference can be caused by different boundaries defined because of data noise. Also, even if the boundaries are similarly defined when noise-filtered or raw data parameters are utilized, the flight data parameter itself being observed in the safety assessment process may show different behaviors. The result of the suggested safety assessment method can have less false-positive detections using the filtered data. In order to have a better observation on the causes of discrepancy, the total energy rate of the previously evaluated flight was chosen because this parameter has the highest discrepancy of raw data or filtered data-driven CLASS results. As shown in Figure 6.24, both data-driven boundaries of performance envelopes and the flight parameter being examined have a non-negligible discrepancy. From this observation, it is confirmed again that a data noise reduction process is absolutely necessary in the data-driven analysis because it is shown that data noise may have a significant impact on the result in a specific case. This can be supported by comparing how many flights in the entire flight data records are perceived

as the events that exceeded the boundaries of the performance envelope. In this study, the total energy height and vertical speed are selected as sample parameters for observing the effect of data noise on the abnormality detection results.

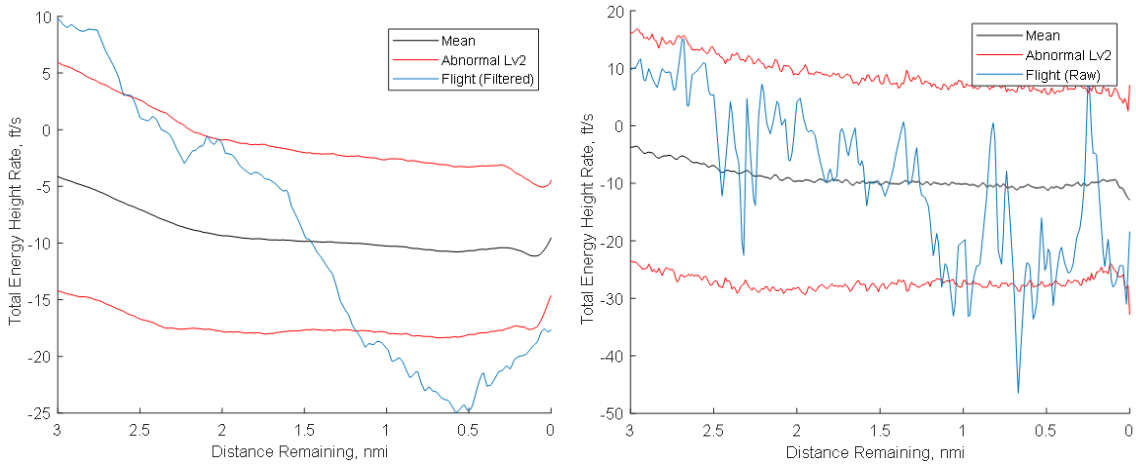

(a) Total Energy Rate from Filtered Data

(b) Total Energy Rate from Raw Data

Figure 6.24: Total Energy Rate Comparison : Raw data and Filtered Data

Total Energy Height

For 1,447 flight records, total energy height of each flight was calculated for this research. Also, the CLASS value for the total energy height was also obtained from the data by measuring its variation from the mean. The total energy height CLASS are derived using both raw and noise-filtered data and gathered to examine the differences between them.

Figure 6.25 shows the differences between raw-data-driven CLASS and filtered-data-driven CLASS. The differences between them are explicitly shown in Figure 6.26. Overall, the filtered data detected the abnormal events with the more lower CLASS value which means raw data observed the exceedances as more severe events. The result is summarized in Figure 6.27. Among the entire flights, the filtered data detected 255 flights that exceeded the total energy height boundaries while the raw data detected 310 flights as the case. The number of flights that were detected by both raw and filtered data is 251. Only four flights

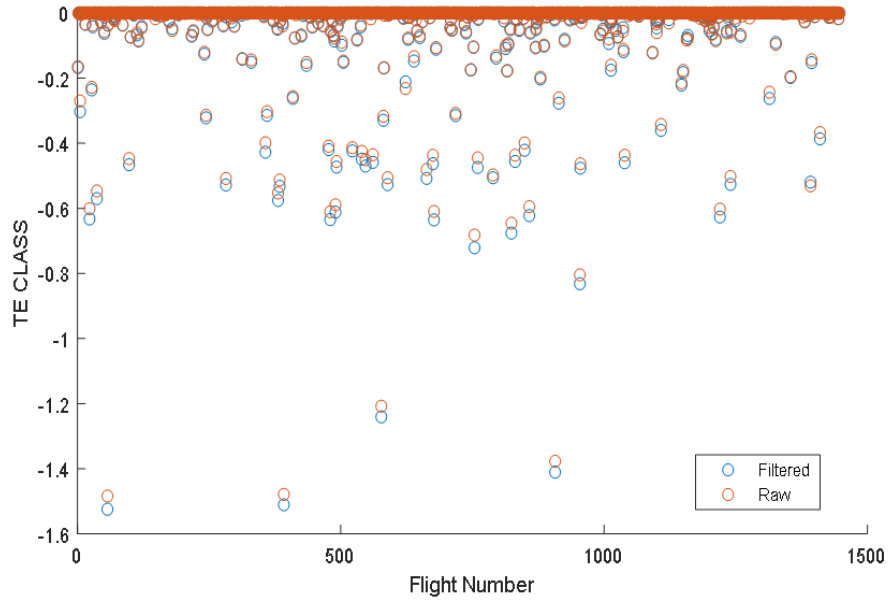

Figure 6.25: Total Energy Height CLASS - All Flights

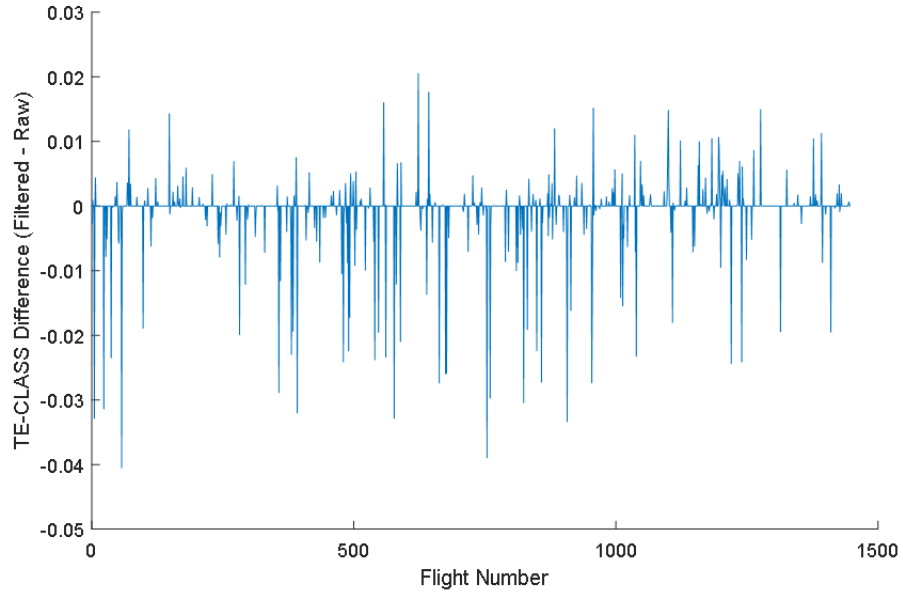

Figure 6.26: Total Energy Height CLASS Difference - All Flights

were detected only by the filtered data, and 59 flights are detected only by raw data. When the result of the filtered-data-driven assessment is considered true, utilizing raw data in the process false-positively detects 59 events out of 1,447 flights.

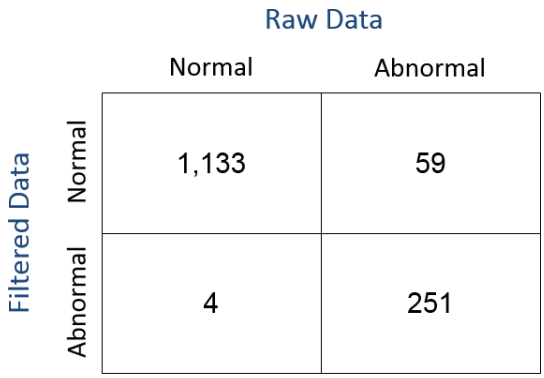

Figure 6.27: Total Energy Abnormality Detection

Vertical Speed

The same experiment was conducted on the vertical speed parameter. As discussed earlier, this vertical speed parameter has the biggest discrepancies between raw-data-driven CLASS and filtered-data-driven CLASS. Figure 6.28 and Figure 6.29 visualizes the discrepancy as below.

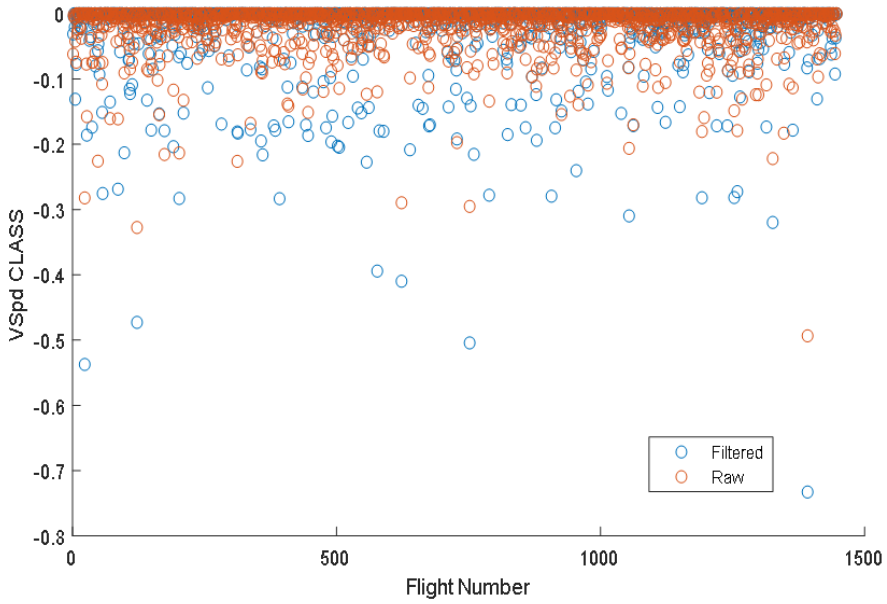

Figure 6.28: Total Energy Height Rate CLASS - All Flights

According to the CLASS calculated using the filtered data, 546 flights were detected as the flight that has exceeded that given normal operating performance envelopes at least once

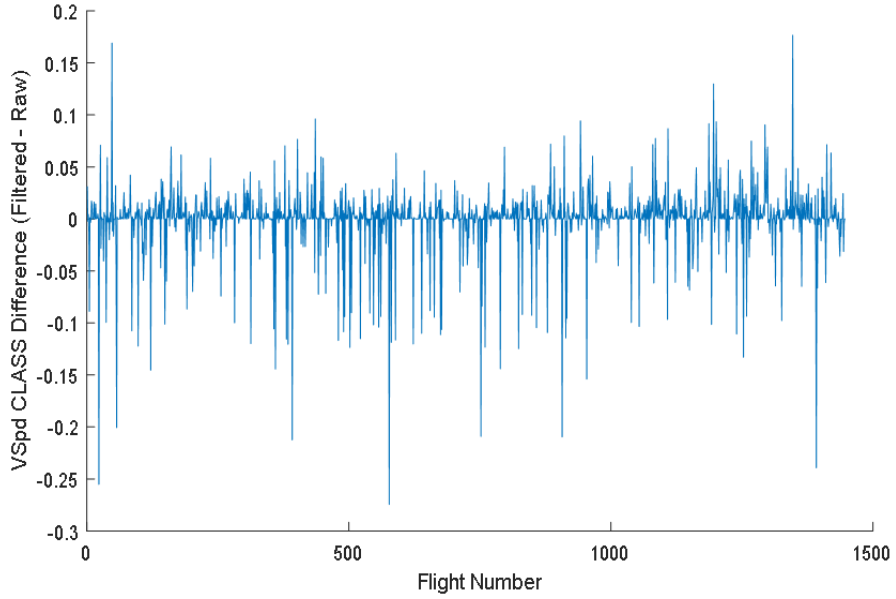

Figure 6.29: Total Energy Height Rate CLASS Difference - All Flights

during the flight. On the other hand, 1,057 flights out of 1,447 flights were detected by the raw-data-driven CLASS. Among them, 534 flights are detected as abnormal flights by both filtered and raw-data-driven CLASS valuse. The quantitatively assessed abnormality result for vertical speed parameter of entire flights are summarized in Figure 6.30. Overall, raw data detects more flights as abnormal exceedances, and that can be considered as driven by the data fluctuation caused by the data noise. As discussed earlier, the safety quantification result can be more reliable when the flight data parameters are filtered by a proper data noise removal technique because noise-filtered data can reduce false-positively detected abnormal events. Thus, it can be concluded that the previously established hypothesis has been proven through this experiment.

6.4.3 Summary

This study has shown that standard flight performance envelopes for a certain flight data parameter can be established by looking at a large number of flight data. The fundamental idea for this suggestion is that abnormality is the one that has to be avoided in terms

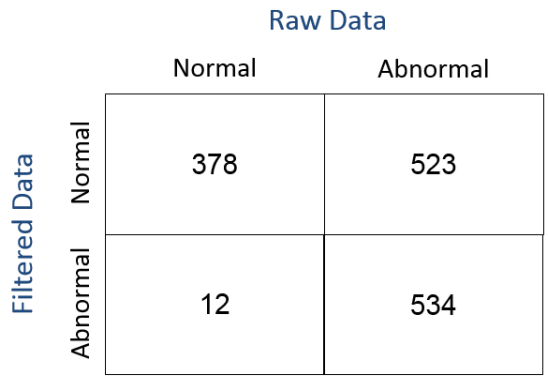

Figure 6.30: Vertical Speed Abnormality Detection

of safety. Thus, a quantitative metric, named CLASS, has been developed to measure the abnormality of the data parameter of interest. This experiment utilized the developed performance envelopes for the chosen parameters to detect any abnormal exceedances of the flight data parameters during approach and landing phases of flight. Also, it is proven that the CLASS can be used for detecting abnormal events for any parameters when normal operating range limits for the parameters are given. Finally, this study examined the difference between the safety assessment results driven by data noise by looking at the CLASS values obtained from raw and noise-filtered data. As a result, it is concluded that raw-data-driven CLASS values are more likely to detect abnormal events falsely and applying data-noise filtering techniques can reduce the chance of false-positively detecting any safety events.

CHAPTER 7
CONCLUSION

7.1 Summary

As air traffic demand is expected to increase significantly, aircraft safety has been a vital issue in the aviation community. However, the aviation aircraft accident statistics show that general aviation aircraft have relatively higher fatal accident rate compared to other classes of aircraft. Thus, the general aviation community has exerted great efforts to enhance the general aviation aircraft safety. Although extensive researches have been conducted to make the aircraft operations safe, most of the safety enhancement techniques are for large commercial aircraft. Also, safety enhancement techniques for GA requires additional cost for acquiring additional devices such as flight data recorder. To bring the benefits of the aircraft safety enhancement system to the GA field, it is essential to have a good understanding of the uniqueness of the GA. The benefits of aviation safety management and enhancement programs can be maximized when the programs are flexible enough to reflect the uniqueness of GA operations adequately. Given the requirements for GA aircraft safety, this study established a research goal that is to provide more effective methods for evaluating the operational safety of a fixed-wing GA aircraft using an aerodynamic performance model and flight data noise removal techniques. This fundamental goal leads to the following sub-goals. First, this research aims to develop a realistic and accurate aerodynamic performance model that is computationally affordable and compositionally flexible so that this modeling method can be utilized by any GA aircraft users capturing the characteristics of each aircraft. Also, this study proposes an effective noise removal technique for the purpose of obtaining clean and credible flight information for the operational safety assessment process. Finally, using the developed reliable aerodynamic

performance model and filtered clean flight data, this work suggests an idea of evaluating flight performance safety of a GA fixed-wing aircraft using flexible standard performance envelopes and a quantitative safety assessment metric.

To achieve the first research goal which is to develop a realistic and accurate aerodynamic performance model, this study provides a flexible aerodynamic modeling methodology for a GA fixed-wing aircraft considering the nature of GA operations. The necessary fidelity level of the aerodynamic model is defined as the capability of predicting its flap activity during flight. As the first step for developing an aerodynamic model that meets the necessary level of fidelity, this study introduces an improved theoretical modeling approach not only using a single theoretical modeling method but also evaluating, comparing, and combining all the possible modeling methods. Based on the developed theoretical model, this study enhances the accuracy of the aerodynamic model by optimizing the shape of the model curves with shape modification factors and actual flight data. For generating realistic flight data for the data-driven modeling process, this study suggests several strategic flight maneuvers, then utilizes the flight data obtained from the suggested flight maneuvers. It is proven that using the final outcome of this data-driven modeling process, the developed aerodynamic model can estimate the flap activity during flight with high accuracy. Given the accurate aerodynamic model, it is tested that the discrepancy between modeled aerodynamic coefficients and data-driven calculated aerodynamic coefficient can indicate the proximity to stall. Finally, this study provides an aircraft performance modeling method that can generate a not only flexible but also accurate performance model, which can predict and capture the aircraft aerodynamic behavior in any operational conditions.

The second goal of this study is to develop a methodology that can effectively remove any data noise and improve the quality of the flight data records for flight data-driven GA safety enhancement programs. As the role of flight data in aviation safety enhancement programs becomes increasingly important, this study ensures clean flight data to achieve the goal of the programs. When the number of data parameters is insufficient as in the flight

data record in GA aircraft, the flight data quality should be considered more important because data parameter conversion process amplifies the power of data noise. To solve this problem, this study introduces the HADaR (Hybrid Approach for Data-noise Reduction) method which is designed for filtering data noise in flight data records. The first process of the HADaR method is identifying important flight data parameters and grouping the parameters by six categories considering their measuring devices. It is assumed here that data noise characteristics are dependent on their measuring types. The next step of this method is to survey and investigate various data noise filtering techniques in both time-domain and frequency-domain. In this study, three techniques in the time domain, and two techniques in the frequency domain are utilized with two different levels of filtering intensity factors for each technique. Based on the selected parameters and data noise filtering techniques, this method populates the noise filtering cases using the full factorial method to investigate all possible combinations. To select the best case in the developed combinations, this method uses the noise filtering effectiveness metric, named FEV, which examines the errors between data-driven aerodynamic coefficients and modeled aerodynamic coefficients considering the magnitude of the error, the variation of the error and noise power in the dataset. This method considers the modeled values as the reference data because the modeled values can be considered as the true behavior of the aircraft, and that should not be affected by the data noise filtering process. In the end, this method selects the case that yields the minimum FEV, and it means that the selected data noise filtering combination can remove the noise most effectively with less probability of losing true behavior of the aircraft. After the experiment, it is shown that data noise filtering process can worsen the result, so noise filtering techniques have to be utilized appropriately. Finally, this study suggests that the HADaR method can be applied to further flight data analysis to improve the credibility of the data-driven analysis result.

The ultimate goal of this study to develop a safety enhancement methodology for a GA fixed-wing aircraft using the developed reliable aerodynamic performance model and the

clean flight data. Thus, the last part of this study suggests a procedure for flight safety assessment that utilizes flexible standard performance envelopes and a quantitative safety assessment metric for the safety evaluation. First of all, this study provides a way of establishing the flexible standard performance envelopes for a particular flight data parameter by observing a large number of flight data records. The basic foundation of the flexible standard performance envelopes is that any abnormal flight or event within the large dataset can be considered as an event that has a higher possibility of being unsafe. Besides, this study suggests a quantitative safety evaluation metric, the Cumulative Landing and Approach Safety Score (CLASS), to measure the abnormality of the data parameters of the flight compared to the other flights that have contributed to forming the standard envelope. The CLASS provides intuitive and useful information for the safety evaluation process because direct comparisons between different parameters are available with this metric. Using the developed performance envelope and the CLASS metric, this study demonstrates that a specific flight and their flight data parameters can be quantitatively determined if the flight has any abnormal exceedances during the flight during its approach and landing phases of flight. The quantitative analysis is available due to the CLASS that can detect risky events for any parameters when the performance envelopes and their boundaries for the parameters are given. Also, this study examines how data noise can affect the flight safety assessment results by comparing the CLASS values obtained from raw and noise-filtered data. Finally, this experiment demonstrates that applying the HADaR method can provide more reliable safety assessment results and this can be quantitatively judged using the CLASS metric.

In summary, this study reveals that the suggested data-driven aerodynamic modeling method and the HADaR method are capable of providing more credible information toward the GA safety assessment work. For the aviation safety enhancement efforts to be flexible, precise aircraft performance models and clean flight data have to be appropriately obtained and used. Furthermore, a proper data noise filtering method that is specific to GA flight data and an appropriate data collection procedure is required for improving the relia-

bility of data-driven safety analysis programs. Finally, this study provides a way to satisfy the above-mentioned requirements for the GA safety enhancement programs by harmonizing the accurate performance model and the cleaned flight data Therefore, this research is expected to positively contribute to GA safety enhancement by introducing a quantitative safety assessment and monitoring methodology to the GA safety field.

7.2 Contributions

The primary contribution of this research is the quantitative flight safety assessment and monitoring methodology for GA operations. In particular, this study allows GA safety analysts or GA users to develop the standard flight performance envelopes that are most appropriate for their operational condition or the aircraft they utilize. The standard flight performance envelopes developed by the method provided in this study serve as a criterion for judging or assessing the GA flight safety. This study provides a quantitative safety assessment metric, the CLASS. The quantitative metric suggested by this study provides a means of objectively determining the safety of not only a GA aircraft but also any other type of aircraft. Therefore, this study contributes to the evaluation of GA flight safety using the suggested performance envelopes and the quantitative safety assessment metric.

Furthermore, this study contributes to more precise and flexible information at the flight planning stage. One of the most important information used in the flight planning stage is the aerodynamic performance information of the aircraft. The aerodynamic model developed using the proposed data-driven aerodynamic modeling process can provide the information reflecting the characteristics of a particular aircraft. Because this information reflects the characteristics of a particular aircraft, the flight plan established with this information will further ensure the safety of the flight. A possible outcome of this research contribution can be a form of smart device applications that enables GA stakeholders or GA aircraft users to have more reliable flight data monitoring results and more accurate flight operation plans.

Finally, the HADaR method suggested in this study contributes to improving the reliability of the results from data-driven GA safety enhancement programs. It is evident that the results from data-driven analysis programs are highly dependent on the quality of the data being utilized in the process. Considering the importance of the aviation safety-related result, the reliability of the result should be improved by enhancing the quality of the data. Thus, this study provides GA safety stakeholders a methodology for incorporating appropriate data noise filtering techniques into their safety assessment process.

To sum up, the ultimate contribution of this study is the formulation and demonstration of a quantitative data-driven GA safety assessment methodology. The flexible and reliable aircraft performance model and the accuracy-enhanced flight data records support the proposed safety assessment methodology. Eventually, this research will contribute to improving GA aircraft safety by closing the existing gap that current safety enhancement programs have such as lack of reliable flight data and absence of flexible aircraft performance information.

7.3 Recommendations

This study suggested a methodology for improving the safety of GA and provided a way to satisfy the requirements for achieving this goal, then successfully demonstrated its applicability. The suggested GA safety enhancement methodology can be further improved when the predictive capability is incorporated in the GA safety assessment work. As discussed earlier, the crucial parameters that represent the aircraft's flight safety are selected and investigated using the CLASS metric. Revealing the relation between landing performance indicators and approach performance indicators can maximize the benefit of the suggested assessment methodology. Appropriate machine learning techniques are expected to reveal the relation, and approach and landing simulation experiments can be used to obtain data necessary for machine learning techniques. Once machine running techniques reveal the relationship between the approach parameters and the touch-down parameters,

the GA safety assessment method will be more useful because of its predictability obtained from the knowledge about the relationship.

Furthermore, the advantages of the data-driven aerodynamic modeling suggested in this study can provide benefits to GA aircraft users as a flexible flight planning tool. The existing flight planning tools are widely used in the GA community, but these tools utilize the aircraft performance tables provided by the aircraft manufacturer. In this study, it is shown that the suggested data-driven modeling methodology can provide more flexibility to the aerodynamic performance models. Thus, the data-driven aerodynamic models developed through the proposed methodology in this study can practically benefit the GA users if the advantages of the developed model in this study are transformed into a user-specific performance table or a flight planning tool. If this user-specific flight planning tool is practically realized as a type of mobile applications, it is one example of the case in which this study actually contributes to improving aviation safety.

Also, the developed quantitative safety evaluation metric, the CLASS, can be used for educational purposes. Since the CLASS is a metric that can measure how safely the aircraft performed within the normal operating range, it is another form of the scores that can be used to asses student pilots performance at pilot training schools. In addition, the safety or abnormality assessment method for GA operation suggested in this study can be connected with the performance models and cleaned flight data to investigate and mitigate the actual causes of the abnormal events detected by this method. This effort to find the exact causes of the detected abnormal performances requires more information about unknown pilot inputs. Thus, a flight simulator environment supported by accurate and realistic performance models can provide useful information for further improvement of this method.

Appendices

APPENDIX A

THEORETICAL AERODYNAMIC MODELING EQUATIONS

A.0.1 Overview

The aerodynamic model consists of lift and drag models for flap-up condition and flap-down condition. Thus, the theoretical aerodynamic modeling process can be divided into four parts: lift curve modeling for clean configuration, lift curve modeling for flap-deployed configuration, drag polar for clean configuration, and drag polar for flap-deployed configuration. For clean configuration of an aircraft, the lift curve can be modeled in three steps: 2-d airfoil, 3-d wing, and complete aircraft. For flap-deflected configuration of an aircraft, variation of lift caused by the flap deflection can be estimated using three parameters: lift increment, lift-curve slope change, and maximum lift-coefficient increment. For the drag polar of an aircraft in clean configuration, total drag of an aircraft consists of parasite drag and induced drag that can be modeled in several theoretical methods. For the drag variation caused by flap settings can be modeled considering profile drag increment, induced drag increment, and interference drag increment. The following sections summarizes all the equations for estimating lift curve and drag polar components. Chapter 4 explains provides detailed information on the equations summarized in this section.

A.0.2 Lift Equations

Flaps-Up

• *Zero Lift Angle-of-Attack*

- 2-D Airfoil (α_{0l})

$$\alpha_{0l} = k(\alpha_i - \frac{57.3}{2\pi} C_{l_i}) \tag{A.1}$$

- 3-D Wing (α_{0L_W})

$$\alpha_{0L_W} = \left\{ \alpha_{0l} + \left(\frac{\Delta\alpha_0}{\varepsilon_t} \right) \varepsilon_t \right\} \left\{ \frac{(\alpha_{0l})_{atM}}{(\alpha_{0l})_{atM=0.3}} \right\} \tag{A.2}$$

- Aircraft (α_{0L_A})

$$\alpha_{0L_A} = -\frac{C_{L_{0A}}}{C_{L_{\alpha A}}} \tag{A.3}$$

$$C_{L_{0_A}} = C_{L_{0_{Wf}}} + C_{L_{\alpha_h}} \eta_h \frac{S_h}{S} \left(i_h - \varepsilon_{0_h} \right) \tag{A.4}$$

• *Lift Curve Slope*

- 2-D Airfoil (C_{l_α})

$$C_{l_\alpha} = \frac{1.05}{\beta} \left(\frac{C_{l_\alpha}}{(C_{l_\alpha})_{theory}} \right) (C_{l_\alpha})_{theory} \tag{A.5}$$

- 3-D Wing ($C_{L_{\alpha_W}}$)

$$C_{L_{\alpha_W}} = \frac{2\pi AR}{2 + \sqrt{(\frac{AR\beta}{\kappa})^2 (1 + \frac{(\tan\Lambda_{C/2})^2}{\beta^2}) + 4}} \tag{A.6}$$

$$C_{L_{\alpha_W}} = \frac{C_{l_\alpha}}{\sqrt{1 + \frac{C_{l_\alpha}}{(\pi AR)^2}} + \frac{C_{l_\alpha}}{\pi AR}} \tag{A.7}$$

- Aircraft ($C_{L_{\alpha_A}}$)

$$C_{L_{\alpha_A}} = C_{L_{\alpha_{Wf}}} + C_{L_{\alpha_h}} \eta_h \left(\frac{S_h}{S} \right) \left(1 - \left(\frac{d\varepsilon}{d\alpha} \right) \right) \tag{A.8}$$

$$C_{L_{\alpha_A}} = C_{L_{\alpha_W}} + C_{L_{\alpha_h}} \left(\frac{S_h}{S} \right) \left(1 - \left(\frac{d\varepsilon}{d\alpha} \right) \right) \tag{A.9}$$

$$C_{L_{\alpha_A}} = C_{L_{\alpha_W}} \left(\frac{S_{exposed}}{S_{ref}} \right) F \tag{A.10}$$

• *Angle-of-Attack Limit for Linear Range*

- 2-D Airfoil (α^*) & 3-D Wing ($\alpha^*{}_W$)

$$\alpha^* = \alpha^*{}_W = \alpha_0 + \frac{C_{l_{max}} - 0.3}{C_{l_\alpha}} \left(\frac{180}{\pi} \right) \tag{A.11}$$

- Aircraft ($\alpha^*{}_A$)

$$\alpha^*_A = \alpha^*_W - i_W \tag{A.12}$$

• *Angle-of-Attack for Maximum Lift Coefficient*

- 2-D Airfoil ($\alpha_{C_{l_{max}}}$)

$$\alpha_{C_{l_{max}}} = \alpha^* + \frac{0.39}{C_{l_\alpha}} \left(\frac{180}{\pi} \right) \tag{A.13}$$

- 3-D Wing ($(\alpha_{C_{Lmax}})_W$)

$$(\alpha_{C_{Lmax}})_W = \frac{C_{L_{max_W}}}{C_{L_{\alpha_W}}} + \alpha_{0L_W} + \Delta\alpha_{stall} \tag{A.14}$$

- Aircraft ($(\alpha_{C_{Lmax}})_A$)

$$(\alpha_{C_{Lmax}})_A = (\alpha_{C_{Lmax}})_W - i_W - \Delta\alpha_{W/C} \tag{A.15}$$

• *Maximum Lift Coefficient*

- 2-D Airfoil ($C_{l_{max}}$)

$$C_{l_{max}} = C_{l_{max_{base}}} + C_{l_{max_{camber}}} + C_{l_{max_{thickness}}} + C_{l_{max_{Reynolds}}} + C_{l_{max_{roughness}}} + C_{l_{max_{Mach}}} \tag{A.16}$$

- 3-D Wing ($C_{L_{max_W}}$)

$$C_{L_{max_W}} = \frac{C_{L_{max_W}}}{C_{l_{max}}} C_{l_{max}} + \Delta C_{L_{max_W}} \tag{A.17}$$

- Aircraft ($C_{L_{max_A}}$)

$$C_{L_{max_A}} = C_{L_{max_W}} - C_{L_{\alpha_{Wf}}} \Delta\alpha_{W/C} + C_{L_{\alpha_h}} \left(\frac{s_h}{s}\right) \left\{ \left(\alpha_{C_{L_{max}}}\right)_A \left(1 - \frac{d\varepsilon}{d\alpha} - \varepsilon_{0_h}\right) + i_h \right\} \tag{A.18}$$

Flaps-Down

• *Lift Increment*

- 2-D Airfoil (ΔC_l)

$$\Delta C_l = C_{l_\alpha} \alpha_\delta \delta_f \tag{A.19}$$

- 3-D Wing (ΔC_{L_W})

$$\Delta C_{L_W} = k_b \Delta C_l \left(\frac{C_{L_{\alpha_W}}}{C_{l_\alpha}}\right) \left(\frac{\alpha_{\delta_{C_L}}}{\delta_{C_l}}\right) \tag{A.20}$$

- Aircraft (ΔC_{L_A})

$$\Delta C_{L_A} = \Delta C_{L_W} + k_{Wh} \frac{S_h}{S} \Delta C_{L_h} - C_{L_{\alpha_h}} \eta_h \frac{S_h}{S} \Delta\varepsilon_f \tag{A.21}$$

• *Lift Curve Slope Change*

- 2-D Airfoil ($(C_{l_\alpha})_\delta$)

$$(C_{l_\alpha})_\delta = \frac{c'}{c} C_{l_\alpha} \tag{A.22}$$

- 3-D Wing ($(C_{L_{\alpha_W}})_\delta$)

$$(C_{L_{\alpha_W}})_\delta = C_{L_{\alpha_W}} \left\{ 1 + \left(\frac{c^{'}}{c} - 1 \right) \frac{S_{W_f}}{S} \right\} \tag{A.23}$$

- Aircraft ($(C_{L_{\alpha_A}})_\delta$)

$$(C_{L_{\alpha_A}})_\delta = k_{Wh}(C_{L_{\alpha_W}})_\delta + C_{L_{\alpha_h}} \eta_h \frac{S_h}{S} \left\{ 1 - (\frac{d\varepsilon}{d\alpha})_\delta \right\} \tag{A.24}$$

• *Maximum Lift Coefficient Increment*

- 2-D Airfoil ($\Delta C_{l_{max}}$)

$$\Delta C_{l_{max}} = k_1 k_2 k_3 (\Delta C_{l_{max}})_{base} \tag{A.25}$$

- 3-D Wing ($\Delta C_{L_{max_W}}$)

$$\Delta C_{L_{max_W}} = \Delta C_{l_{max}} \frac{S_{W_f}}{S} k_\Delta \tag{A.26}$$

- Aircraft ($\Delta C_{L_{max_A}}$)

$$\Delta C_{L_{max_A}} = (\Delta C_{L_{max_W}}) + C_{L_{\alpha_h}} \frac{S_h}{S} \left\{ (1 - \frac{d\varepsilon}{d\alpha}) + i_h - \Delta\varepsilon_f \right\} \tag{A.27}$$

A.0.3 Drag Equations

Flaps-Up

• *Parasite Drag (Zero-Lift Drag)*

- Equivalent Skin-Friction Method

$$C_{D_0} = C_{D_{min}} = C_{f_e} \left(\frac{S_{wet}}{S_{ref}} \right) \tag{A.28}$$

- Component Buildup Method

$$C_{D_0} = C_{D_{min}} = \frac{\sum \left(C_{f_c} F F_c Q_c S_{wet_c} \right)}{S_{ref}} + C_{D_{misc}} + C_{D_{L\&P}} \tag{A.29}$$

- Extracting Drag from L/D_{max} Information

$$C_{D_0} = C_{D_{min}} = \frac{C_{L_{BG}}}{(L/D)_{max}} - \frac{(C_{L_{BG}})^2}{\pi ARe} \tag{A.30}$$

• *Induced Drag*

- Oswald Span Efficiency Method

$$K = \frac{1}{\pi ARe} \tag{A.31}$$

- Leading Edge Suction Method

$$K = S_C K_{100} + (1 - S_C) K_0 \tag{A.32}$$

Flaps-Down

• *Drag Increment*

- Flap Profile Drag Increment

$$\Delta C_{D_p} = \Delta C_{d_p} \cos(\Lambda_{c/4}) \left(\frac{S_{wf}}{S} \right) \tag{A.33}$$

- Induced Drag Increment

$$\Delta C_{D_i} = K^2 \left(\Delta C_{L_{flap}} \right)^2 \cos(\Lambda_{c/4}) \tag{A.34}$$

- Interference Drag Increment

$$\Delta C_{D_{int}} = K_{int} \Delta C_{D_p} \tag{A.35}$$

- Total aircraft Drag Increment

$$\Delta C_{D_{flap}} = \Delta C_{D_p} + \Delta C_{D_i} + \Delta C_{D_{int}} \tag{A.36}$$

APPENDIX B

FLIGHT MANEUVER CARDS FOR FLIGHT DATA COLLECTION

One of the advantages of GA operation is that generating data is relatively easy. In order to obtain realistic and use-specific information, this study suggests a set of flight maneuvers which consists of five different phases: low altitude cruise, climb, high altitude cruise, slow flight and stall recovery, and simulated go-around flight. The suggested flight comprised two complete cycles of the flap (0-10-20-30-20-10-0 deg) at two distinct altitudes separated by a full-power climb. Thereafter, the flaps were used during a transition to slow flight followed by a simulated rectangular pattern entry at altitude. The Garmin G1000 data log corresponding to this flight has been verified to ensure that the test flight is acceptable. Flap operation during the flight was noted by the flight crew using the NAV1 frequency, which is logged by the G1000 system. The following figures are the flight test cards that describe the suggested flight maneuvers. Based on this flight cards, a partner school has generated a flight data record. This study has utilized this flight data in the data-drive aerodynamic modeling process and the data-noise filtering process.

Flight Card	Testing Time (Approx.)
1. Flap cycle test during cruise at 3,000ft	~ 15 min
2. Climb test from 3,000ft to 5,500ft	~ 7-10 min
3. Flap cycle test during cruise at 5,500ft	~ 15 min
4. Slow flight test (stall recovery)	~ 3 min
5. Rectangular pattern and go-around test	~ 3 min
	Total Net Testing Time: ~ 43-46 min

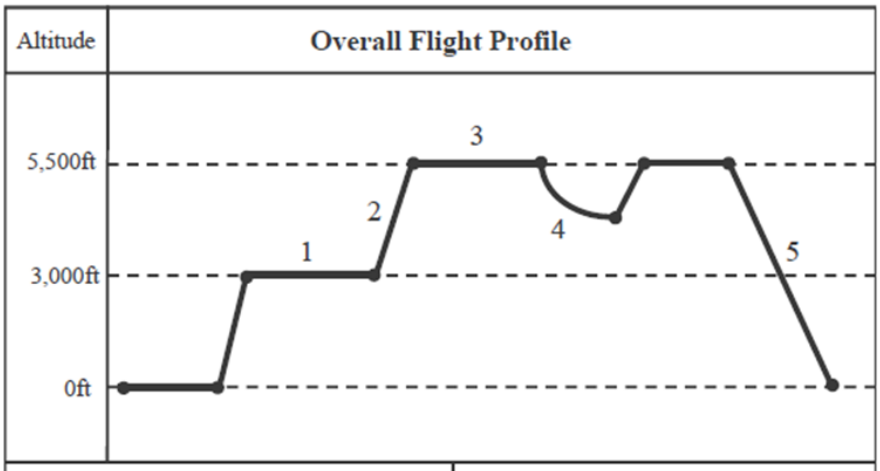

Takeoff Weight (lb)	
Landing Weight (lb)	
Takeoff Fuel (gal)	
Landing Fuel (gal)	

Flight Cards
1: Flap cycle (Cruise)
2: Climb
3: Flap cycle (Cruise)
4: Slow flight and stall recovery
5: Simulated pattern and go-around

Important Notes:

- When moving flaps while flying straight, mark start of flap movement with Wing-Wag (WW) — Flight card 1, 3, and 4
- When moving flaps while turning, commence turn coinciding with start of flap movement — Flight card 5

Figure B.1: Flight Card - Overview of the Flight

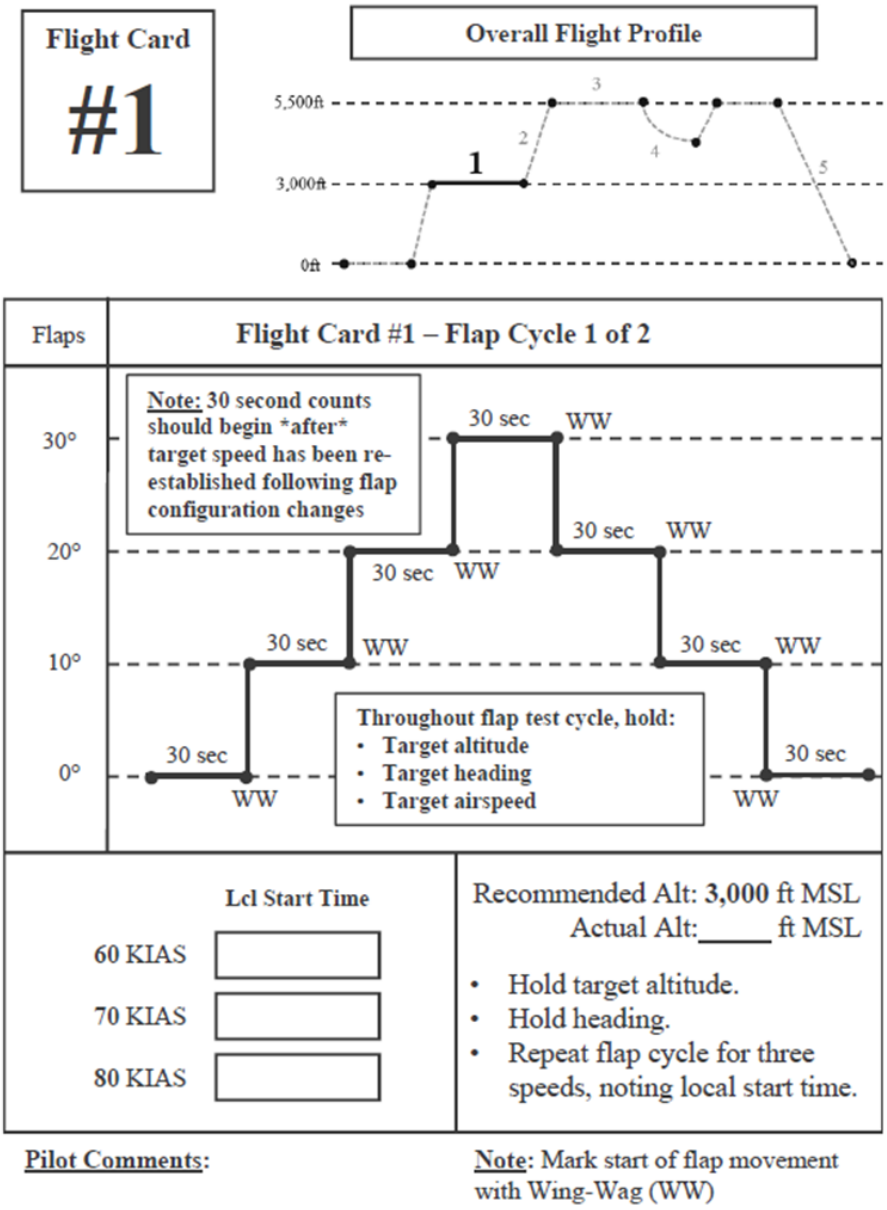

Figure B.2: Flight Maneuver 1 - Flap Cycle Test during Cruise at 3,000 ft

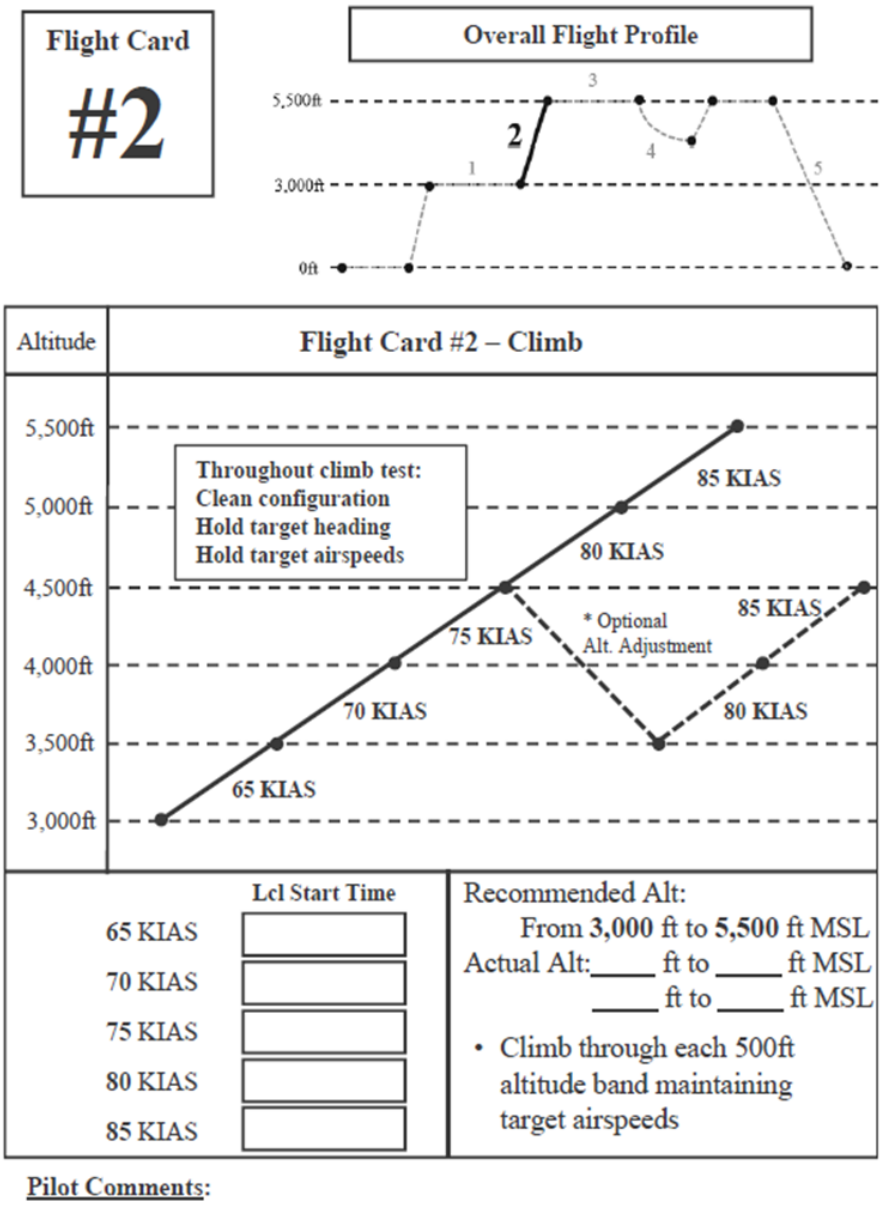

Figure B.3: Flight Maneuver 2 - Climb Test from 3,000 ft to 5,500 ft

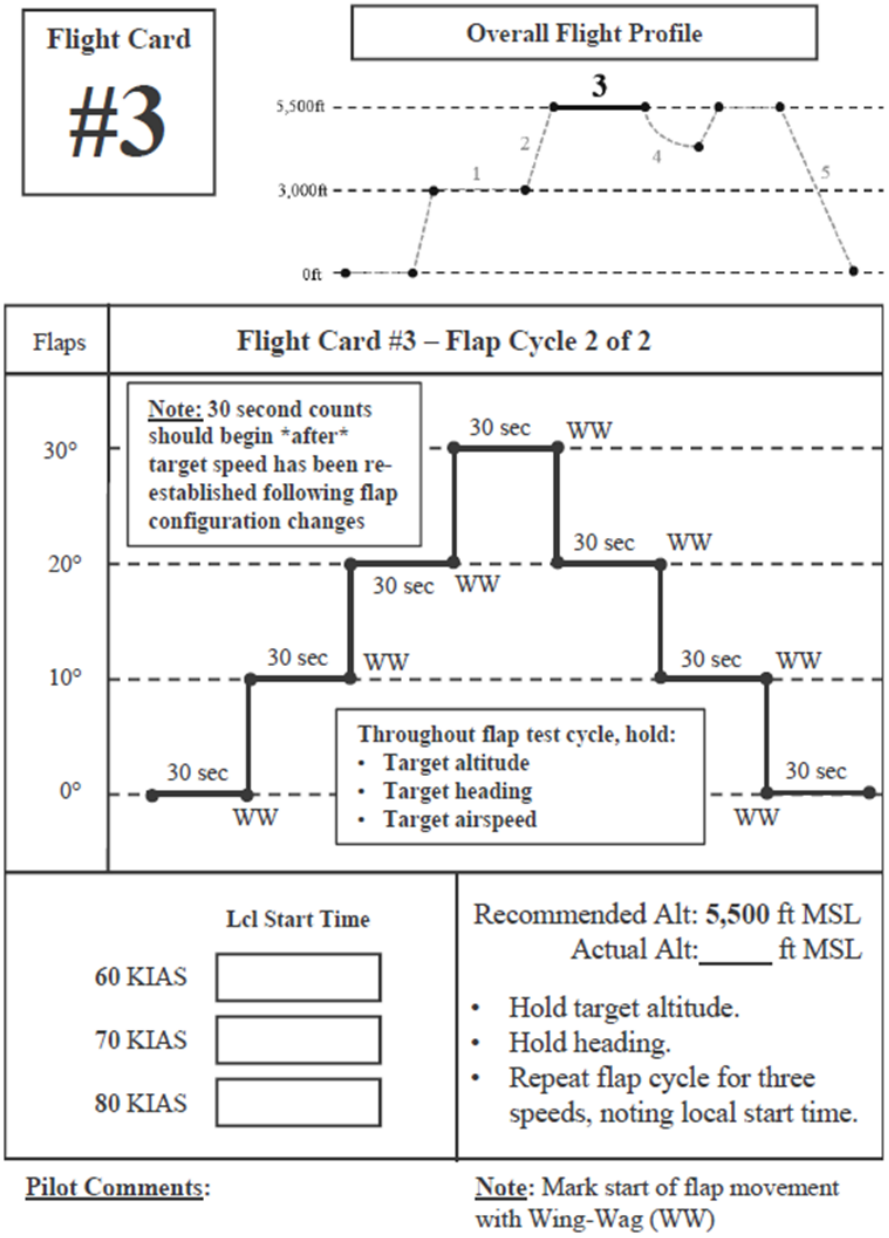

Figure B.4: Flight Maneuver 3 - Flap Cycle Test during Cruise at 55,000 ft

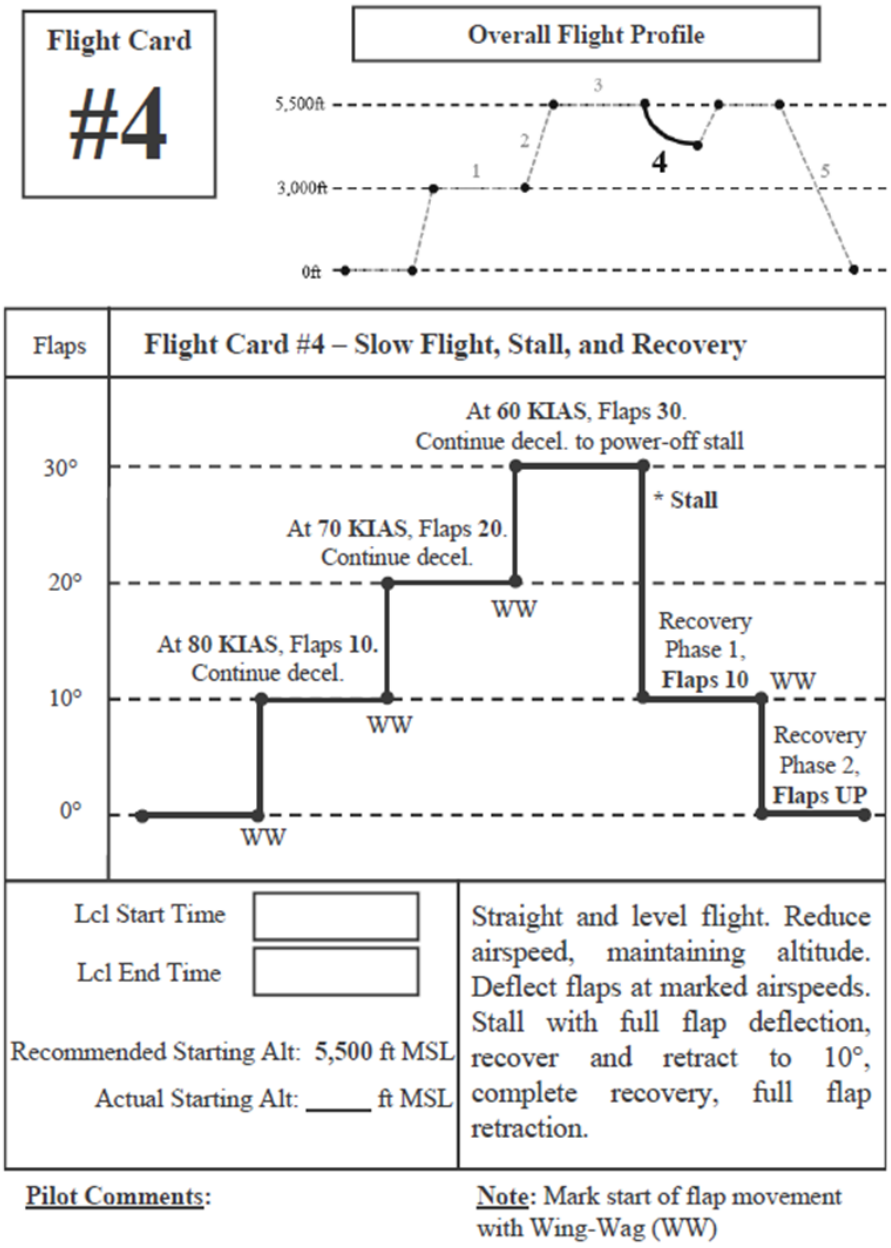

Figure B.5: Flight Maneuver 4 - Slow Flight Test (Stall Recovery)

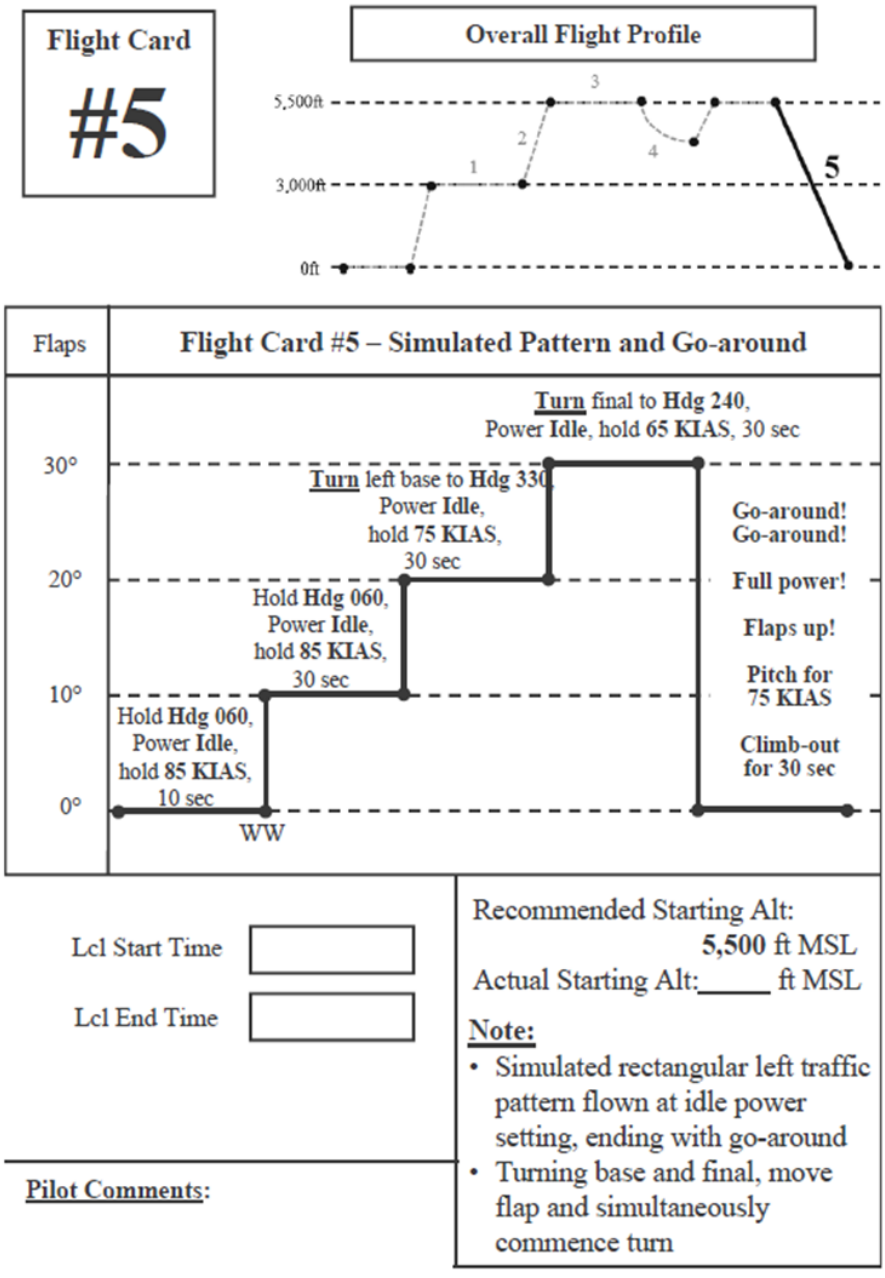

Figure B.6: Flight Maneuver 5 - Rectangular Pattern and Go-Around Test

REFERENCES

[1] *Pilot/Controller Glossary*, 11th ed., Federal Aviation Administration (FAA), 2016.

[2] *2017 Annual Report*. 1400 K Street NW, Suite 801 Washington, DC 20005: General Aviation Manufacturers Association (GAMA), 2018, www.GAMA.aero.

[3] "Review of the Classification and Definitions Used for Civil Aviation Activities," International Civil Aviation Organization, Montreal, Canada, SAT/10-WP/7, 2009.

[4] G. Perry, "The 25th Joseph T. Nall Report: General Aviation Accident in 2013," The Aircraft Owners and Pilots Association (AOPA) Air Safety Institute, 421 Aviation way Frederic, MD 21701, 2016.

[5] *What is General Aviation?* Aircraft Owners and Pilots Association, `https://www.aopa.org/-/media/files/aopa/home/advocacy/what_ga.pdf`, 2017.

[6] "General Aviation Airports: A National Asset," U.S. Department of Transportation Federal Aviation Administration, Washington D.C., May 2012.

[7] "FAA Aerospace Forecast: Fiscal Years 2016-2036," Federal Aviation Administration, The Forecasts, Performance Analysis Division (APO-100), Office of Aviation Policy, and Plans, 2017.

[8] *Fact Sheet - General Aviation Safety*, Federal Aviation Administration, `https://www.faa.gov/news/fact_sheets/`, Accessed: October, 2018.

[9] *Safety Management Manual (SMM)*, 3rd ed., Doc 9859 AN/474, International Civil Aviation Organization (ICAO), 2013.

[10] A. J. Stolzer and J. J. Goglia, *Safety Management Systems in Aviation*, 1st ed. 110 Cherry Street Suite 3-1, Burlington, VT 05401-3818: Ashgate, 2015.

[11] "Advisory Circular - Flight Operational Quality Assurance," U.S. Department of Transportation and Federal Aviation Administration, Tech. Rep. AC-120-82, Apr. 2004.

[12] *Aviation Safety Action Program*, Federal Aviation Administration, `https://www.faa.gov/about/initiatives/asap/`, Accessed: October, 2018.

[13] *Fact Sheet - viation Safety Information Analysis and Sharing Program*, Federal Aviation Administration, https://www.faa.gov/news/fact_sheets/, Accessed: October, 2018.

[14] *National Transportation Statistics*, United States Department of Transportation, Bureau of Transportation Statistics, Air Carrier and General Aviation Safety Data, Apr. 2016.

[15] J. Borghese, "NASA Advisory Council Aeronautics Committee Report," NASA Johnson Space Center, Dec. 2015.

[16] "FAA Performance and Accountability Report," Federal Aviation Administration, 2016.

[17] *The General Aviation Joint Steering Committee - Safety Enhancements*, http://www.gajsc.org/safety-enhancements/, Accessed: October, 2018.

[18] *General Aviation Air Safety Investigators (GA-ASI) Workshop*, http://www.gama.aero/public-view-events/ga-asi-workshop, Accessed: October, 2018.

[19] *Air Safety Institute - Aircraft Owners and Pilots Association*, https://www.aopa.org/training-and-safety/air-safety-institute, Accessed: October, 2018.

[20] *PEGASAS Center of Excellence for General Aviation Safety*, Federal Aviation Administration PEGASAS Factsheet, Oct. 2015.

[21] "Approach Hazards Overview," Flight Safety Foundation, Tech. Rep., Oct. 2000, https://flightsafety.org/wp-content/uploads/2016/09/alar_bn5-1-apprhazard.pdf.

[22] A. T. S. Branch, *Airplane Flight Handbook*, FAA-H-8083-3A. Oklahoma City, OK 73125: U.S. Department of Transportation, Federal Aviation Administration, 2004.

[23] N. Fala and K. Marais, "Detecting Safety Events during Approach in General Aviation Operations," in *Proceedings of the 16th AIAA Aviation Technology, Integration, and Operations Conference*, Washington, D.C.: American Institute of Aeronautics and Astronautics, June 2016.

[24] A. Rao and T. Puranik, "Retrospective Analysis of Approach Stability in General Aviation Operations," in *Proceedings of the 2018 Aviation Technology, Integration, and Operations Conference, AIAA Aviation Forum*, Atlanta, Georgia: American Institute of Aeronautics and Astronautics, June 2018.

[25] "Stabilized Approach," Flight Safety Foundation, Tech. Rep., Aug. 2000, https://flightsafety.org/wp-content/uploads/2016/09/alar_bn7-1stablizedappr.pdf.

[26] A. Campbell, P. Zaal, J. Schroeder, and S. Shah, "Development of Possible Go-Around Criteria for Transport Aircraft," in *Proceedings of the 2018 Aviation Technology, Integration, and Operations Conference, AIAA Aviation Forum*, Atlanta, Georgia: American Institute of Aeronautics and Astronautics, June 2018.

[27] *Administrator's Fact Book*, FAA Office of Communications, FAA Office of Communications, Sep. 2018.

[28] M. McCollum, *General Aviation Pilots Get Their GAARD Up with New App*, https://www.mitre.org/publications/project-stories/general-aviation-pilots-get-their-gaard-up-with-new-app, Accessed: October, 2018.

[29] "General Aviation Airports: A National Asset," U.S. Department of Transportation and Federal Aviation Administration, 800 Independence Ave, SW. Washington, DC 20591, Tech. Rep., May 2012.

[30] "Advisory Circular, 120-82 - Flight Operational Quality Assurnace," Tech. Rep., 4, https://www.faa.gov/regulations_policies/advisor.

[31] "Laying Down Common Requirements for the Provision of Air Navigation Services," Tech. Rep., 10.

[32] *ASIAS - Aviation Safety Information Analsysis and Sharing*, ASIAS Homepage, https://portal.asias.aero/web/guest, Accessed: October, 2018.

[33] "Fact Sheet – Aviation Safety Information Analysis and Sharing Program," U.S. Department of Transportation and Federal Aviation Administration, Tech. Rep., Dec. 2017.

[34] *PEGASAS - The Partnership to Enhance General Aviation Safety, Accessibility and Sustainability*, PEGASAS Homepage, https://www.pegasas.aero/, Accessed: October, 2018.

[35] "Guidance on the Establishment of a Flight Data Analysis Program (FDAP) - Safety Management Systems (SMS)," Australian Government Civil Aviation Safety Authority, Aug. 2011.

[36] L. Li, S. Das, R John Hansman, R. Palacios, and A. N. Srivastava, "Analysis of Flight Data Using Clustering Techniques for Detecting Abnormal Operations," *Journal of Aerospace Information Systems*, vol. 12, pp. 1–12, 2015.

[37] T. G. Puranik, E. Harrison, S. Min, H. Jimenez, and D. Mavris, "Energy-Based Metrics for General Aviation Flight Data Record Analysis," in *Proceedings of the 16th AIAA Aviation Technology, Integration, and Operations Conference*, Washington, D.C.: American Institute of Aeronautics and Astronautics, June 2016.

[38] P. Zarchan and H. Musoff, *Fundamentals of Kalman Filtering - A Practical Approach*, 4th ed. American Institute of Aeronautics and Astronautics/Aerospace Press, 2015, Progress in Astronautics and Aeronautics, Volume 246.

[39] D. Simon, *Optimal State Estimation: Kalman, H Infinity, and Nonlinear Approache*. Hoboken, New Jersey: John Wiley and Sons, Inc., 2006.

[40] A. Vretblad, *Fourier Analysis and Its Applications*. New York, New York: Springer-Verlag New York, Inc., 2003.

[41] T. A. Gallagher, A. J. Nemeth, and L. Hacein-Bey, "An introduction to the Fourier transform: relationship to MRI.," *American Journal of Roentgenology*, vol. 190, no. 5, pp. 1396–1405, 2008.

[42] J. Roskam, *Airplane Design, Part VI: Preliminary Calculation of Aerodynamic, Thrust and Power Characteristics*. Kansas: Roskam Aviation and Engineering corporation, 1987.

[43] J. D. Anderson, *Aircraft Performance and Design*, 1st ed. New York City, NY: McGraw-Hill Education, 2010.

[44] D. P. Raymer, *Aircraft Design: A Conceptual Approach*, 5th ed. 1801 Alexander Bell Drive, Reston, Virginia 20191-4344: American Institute of Aeronautics and Astronautics, Inc., 2012.

[45] J. T. Lowry, *Performance of Light Aircraft*. 1801 Alexander Bell Drive, Reston, Virginia 20191-4344: American Institute of Aeronautics and Astronautics, Inc., 1999.

[46] J. T. Lowry, *Computing Airplane Performance with The Bootstrap Approach: A Field Guide*, Flight Physics, Sep. 1995.

[47] J. T. Lowry, "The Bootstrap Approach to Predicting Airplane Flight Performance," *Journal of Aviation/Aerospace Education and Research*, vol. 6, pp. 25–33, 1995.

[48] R. V. Jategaonkar, *Flight Vehicle System Identification: A Time-Domain Methodology*, 2nd ed., ser. Progress in Astronautics and Aeronautics. 1801 Alexander Bell Drive, Reston, VA 20191-4344: American Institute of Aeronautics and Astronautics, Inc., 2015, vol. 245.

[49] L. A. Zadeh, "From circuit theory to system theory," *Proceedings of the IRE*, vol. 50, no. 5, pp. 856–865, 1962.

[50] *Wind Tunnel Testing, NASA Glenn Research Center*, https://www.grc.nasa.gov/WWW/K-12/airplane/tuntest.html, Accessed: October, 2018.

[51] A. Turnbull, "The Typical General Aviation Aircraft," NASA Langley Research Center, Hampton, Virginia, Tech. Rep. NASA/CR-1999-209550, Sep. 1999.

[52] "2014-2015 GA Accident Scorecard," Aircraft Owners and Pilots Association (AOPA), Josepph T. Nall Report, 2016.

[53] *2001 Cessna 172S N3547L Aircraft Details*, Journeys Aviation, Boulder, Colorado, https://www.journeysaviation.com/N3547L.php, Accessed: October, 2018.

[54] *Information Manual: Cessna Skyhawk SP*, 1st ed., Pilot's Operating Handbook, Model 172S NAV III GFC 700 AFCS, Cessna Aircraft Company, 2007.

[55] *Garmin G1000 Integrated Flight Deck Pilot's Guide*, 10th ed., Cessna Nav III, Garmin Ltd., 2011.

[56] I. H. Abbott, A. E. VonDoenhoff, and L. S. Stivers, "Summary of Airfoil Data," National Advisory Committee for Aeronautics (NACA), Tech. Rep. NACA TR-824, 1945.

[57] R. D. Finck, "USAF Stability and Control DATCOM," McDonnell Douglas Corporation, Long Beach, California, Tech. Rep. AFWAL-TR-83-3048, Apr. 1978.

[58] S. Gudmundsson, *General Aviation Aircraft Design: Applied Methods and Procedures*. 225 Wyman Street, Waltham, MA 02451: Butterworth-Heinemann, 2013.

[59] "Maximum Lift of Wings with Trailing-Edge Flaps at Low Speeds," Engineering Sciences Data Unit (ESDU), IHS Inc., London, Tech. Rep. ESDU 91014, Aug. 1995.

[60] M. Selig, *Aircraft Dynamics Models for Use with Flight Gear*, UIUC Applied Aerodynamics Group, Urbana, IL, 2002.

[61] P. Jackson, *Janes All The World's Aircraft*. United Kingdom: Jane's Information Group, 2004-2005.

[62] M. Nita and D. Scholz, "Estimating the Oswald Factor from Basic Aircraft Geometrical Parameters," German Society for Aeronautics and Astronautics (DGLR) German Aerospace Congress, Berlin, Germany, Document ID 281424, 2012.

[63] L. K. Loftin, *Quest for Performance: The Evolution of Modern Aircraft*. Washington, D.C.: NASA Scientific and Technical Information Branch, 1985.

[64] M. Saarlas, *Aircraft Performance*. Hoboken, New Jersey: John Wiley and Sons, Inc., 2009.

[65] E. Harrison, "A Methodology for Predicting and Mitigating Loss of Control Incidents for General Aviation Aircraft," PhD thesis, Georgia Institute of Technology, Nov. 2018.

[66] M. H. J. Amelink, M. Mulder, M. M. Passen, and J. Flach, "Theoretical Foundations for a Total Energy-Based Perspective Flight-Path Display," *The International Journal of Aviation Psychology*, vol. 15, no. 3, pp. 205–231, 2005.

[67] J. R. Merkt, "Flight energy management training: Promoting safety and efficiency," *Journal of Aviation Technology and Engineering*, vol. 3, no. 1, pp. 24–36, 2013.

[68] A. T. S. Branch, *Pilot's Handbook of Aeronautical Knowledge*, FAA-H-8083-25B. Oklahoma City, OK 73125: U.S. Department of Transportation, Federal Aviation Administration, 2016.

[69] J. C. Jacob Benesty, *Optimmal Time-Domain Noise Reduction Filters - A Theoretical Study*, 1st. Heidelberg, Berlin, Germany: Springer, 2011.

[70] S. W. Smith, *The Scientist and Engineer's Guide to Digital Signal Processing*, 2nd ed. San Diego, California: California Technical Publishing, 2009.

[71] *Moving Average Filters*, Motor Behaviour - Cognitive Psychology and Neuroscience Perspectives, 2011 `https://motorbehaviour.wordpress.com/2011/06/11/moving-average-filters/`, Accessed: October, 2018.

[72] R. V. Garimella, "A Simple Introduction to Moving Least Squares and Local Regression Estimation," vol. 6, 2017.

[73] T. Hastie, *Statistical Models in S - Local regression models*. Routledge, CRC Press, 2017, ISBN: 9781351414227.

[74] *Matlab Online Documentation*, MathWorks, `https://www.mathworks.com/help/matlab/`, Accessed: October, 2018.

[75] *Smoothing Splines, Local Regression, and GAMs*, Data Mining and Analysis Class Note, Stanford University, Nov. 2017.

[76] Q. Mary and D. o. E. Westfield College, *Smoothing with Cubic Splines*. Pollock, D.S.G., Queen Mary, and Westfield College. Department of Economics, 1993.

[77] A. G. Jaime Rubio-Hervas and Y.-S. Ong, "Data-driven risk assessment and multi-criteria optimization of UAV operations," *Aerospace Science and Technology*, vol. 77, pp. 510 –523, 2018.

[78] *What is a Fourier Transfporm?* Quesntions and Answers in MRI, https://http://mriquestions.com/fourier-transform-ft.html, Accessed: October, 2018.

[79] K. Wallis, G. Akers, P. Collins, R. Davis, A. Frazier, M. Oxley, and A. Terzuoli, "Complex empirical mode decomposition, hilbert-huang transform, and fourier transform applied to moving objects," in *2012 IEEE International Geoscience and Remote Sensing Symposium*, 2012, pp. 4395–4398.

[80] N. E. Huang, Z. Shen, S. R. Long, M. C. Wu, H. H. Shih, Q. Zheng, N.-C. Yen, C. C. Tung, and H. H. Liu, "The empirical mode decomposition and the hilbert spectrum for nonlinear and non-stationary time series analysis," *Proceedings of the Royal Society of London A: Mathematical, Physical and Engineering Sciences*, vol. 454, no. 1971, pp. 903–995, 1998.

[81] J. Daintith, *A Dictionary of Physics*, ser. Oxford Paperback Reference. OUP Oxford, 2009, ISBN: 9780199233991.

[82] *Signal-to-Noise Ratio*, Don H. Johnson, Scholarpedia, 2006, https://http://mriquestions.com/fourier-transform-ft.html, Accessed: October, 2018.

[83] *Summary Measures for Quantitative Data*, Ilinois State University, Lecture Notes, Lesson Five, https://www.aopa.org/-/media/files/aopa/home/advocacy/what_ga.pdf, 2017.